ORNL/SPR-2022/2497

Nuclear Software Validation for 7% Enriched UO_2 Fuel Lattices

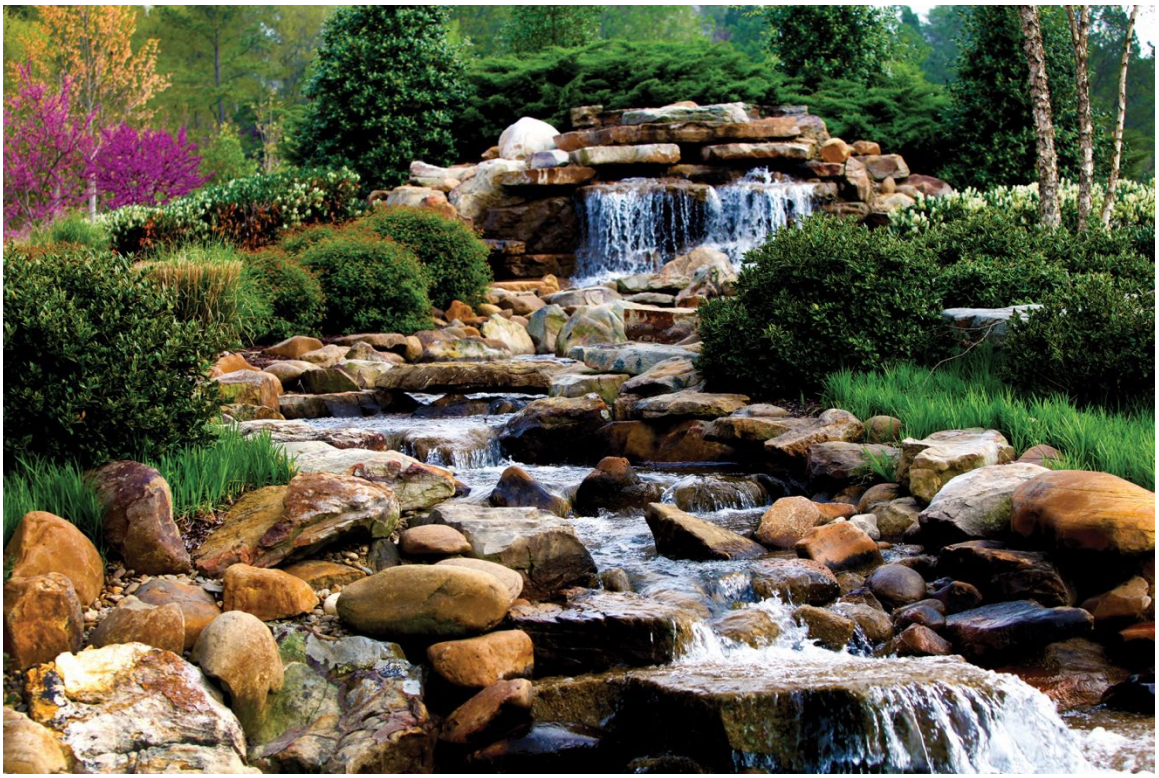

Andrew Godfrey

July 2022

OAK RIDGE National Laboratory

ORNL IS MANAGED BY UT-BATTELLE LLC FOR THE US DEPARTMENT OF ENERGY

ORNL/SPR-2022/2497

Nuclear Energy and Fuel Cycle Division

NUCLEAR SOFTWARE VALIDATION FOR 7% ENRICHED UO_2 FUEL LATTICES

Andrew Godfrey

July 2022

Prepared by
OAK RIDGE NATIONAL LABORATORY
Oak Ridge, TN 37831
managed by
UT-BATTELLE LLC
for the
US DEPARTMENT OF ENERGY
under contract DE-AC05-00OR22725

CONTENTS

LIST OF FIGURES

*Note: Figures in Appendices are not included.

LIST OF TABLES

ABBREVIATIONS

1D	One-dimensional (typically axial)
2D	Two-dimensional (typically radial)
7uPCX	Seven Percent Critical Experiment
CE	continuous energy (cross sections)
DOE	US Department of Energy
HALEU	high-assay low-enriched uranium
ICSBEP	International Handbook of Evaluated Criticality Safety Benchmark Experiments
MG	Multigroup (energy cross sections)
NNSA	National Nuclear Security Administration
ORNL	Oak Ridge National Laboratory
pcm	percent mille of reactivity
PNNL	Pacific Northwest National Laboratory
PWR	pressurized water reactor
SNL	Sandia National Laboratory
TTP	Tritium Technology Program
VERA	Virtual Environment for Reactor Applications

ABSTRACT

This analysis performs validation for the Virtual Environment for Reaction Application's (VERA's) neutronics codes MPACT and Shift against measured data from the Seven Percent Critical Experiment (7uPCX) at Sandia National Laboratory. The benchmarking supports the future application of VERA for analysis of high-assay low-enriched uranium (HALEU) fuel in commercial pressurized water reactors (PWRs). VERA demonstrates very good agreement with measured data, and the deterministic code MPACT also agrees very well with higher-fidelity stochastic methods KENO-VI and Shift in both total neutron flux and fission rate distribution comparisons. Despite some significant differences between the 7uPCX and existing commercial PWRs that challenge the neutron cross section data and transport solver methods used by MPACT, all of the results are excellent. The agreement increases the confidence in the applicability and accuracy of VERA for reactor analysis of HALEU fuels in commercial reactors.

ACKNOWLEDGMENTS

This research was supported by ORNL staff members Aaron Graham, Tara Pandya, and Mark Baird, who provided invaluable assistance with access and use of the nuclear analysis software documented in this activity.

This research was funded by the Tritium Technology Program at Pacific Northwest National Laboratory, operated by Battelle for the U.S. Department of Energy, for the National Nuclear Security Administration (NNSA) Tritium Sustainment Subprogram, through Work Order 566126 Amendment 2.

This research made use of the resources of the High-Performance Computing Center at Idaho National Laboratory, which is supported by the Office of Nuclear Energy of the U.S. Department of Energy and the Nuclear Science User Facilities under Contract No. DE-AC07-05ID14517. The SCALE calculations were performed on the Artemis computing cluster at Oak Ridge National Laboratory.

1. PURPOSE

Throughout the history of the US commercial nuclear power industry, nuclear fuel enrichment has been limited to 5.0% ^{235}U by heavy metal weight. Interest in high-assay low-enriched uranium (HALEU) fuel has recently increased as one option to improve nuclear power efficiency, as it can decrease fuel batch sizes and storage requirements, offset discrete poison usage, and increase fuel cycle lengths. This analysis seeks to validate the nuclear software in the Virtual Environment for Reactor Applications (VERA) for HALEU fuel by simulation of the Seven Percent Critical Experiment (7uPCX) at Sandia National Laboratory [1]. This experiment includes 15 near-critical configurations of approximately 1,000 6.90% enriched fuel rods placed in a cylindrical square-pitched array inside a tank of water.

This analysis uses the VERA codes MPACT and Shift to compare calculated eigenvalues to estimated measured values for each tank configuration. Furthermore, the SCALE stochastic code KENO-VI is also utilized for comparison purposes. Evaluation of energy group structures and ENDF data versions are also included. Finally, code-to-code comparisons of neutron flux and fission rate distributions are performed.

2. MODEL DESCRIPTION

The 7uPCX experiment is described in detail in the report by Harms and Miller [1]. The experiment was designed to represent HALEU fuel for light-water reactors. The critical assembly is a water-moderated and reflected array of aluminum-clad square-pitched 6.90% enriched UO_2 fuel rods. Fifteen different tests provide various fuel configurations that include empty positions and solid aluminum rods for moderator displacement. Burnable poisons are not included, and experiment control elements are designed such that they are fully withdrawn from the assembly during the testing. A cutaway view of the critical assembly core tank from Harms and Miller [1] is shown in Figure 1.

In the 7uPCX experiment, fuel rods were added to the cylindrical fuel array in an approach-to-critical manner. Inverse count rate measurements provided an extrapolated critical number of rods, but the assembly never achieves criticality. The subcritical eigenvalue for the system is derived based on calculated incremental fuel rod reactivity worths as the inverse count rate approaches 0.0. Unlike other critical experiments, the water level in the tank is maintained sufficiently above the active fuel such that it does not affect the criticality of the system.

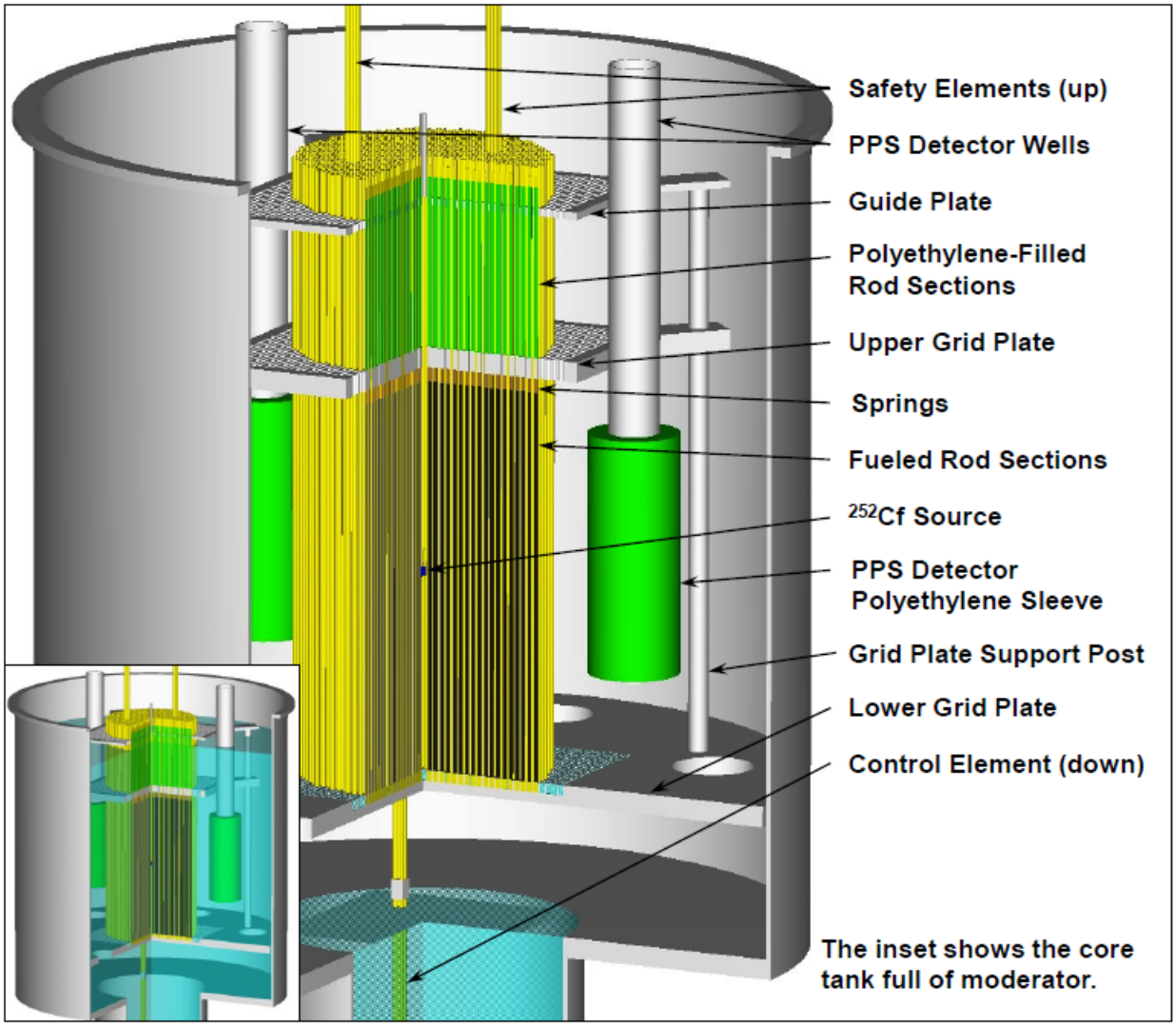

Figure 1: Cut-away view of the critical assembly [1].

KENO-V models for the 15 tests were developed and documented as part of the original experiment documentation [1]. These models ignore several features of the experiment geometry that are assumed to not impact the calculated results, including the following:

- The core tank and outside ambient air are not modeled.
- The control elements and safety elements are not modeled since they are fully removed/withdrawn from the experiment when approaching criticality.
- The lower tank projection below the tank is not modeled.
- The lower and upper grid plates are modeled, but the upper guide plate is not.
- The californium neutron source is not modeled.

Only 19 cm of axial reflector materials are modeled above and below the active fuel. These regions include moderator below the fuel and the fuel rod polyethylene regions above the fuel. Beyond these regions, neutrons are assumed to fully escape (non-reentrant boundary). Sensitivity studies were performed to verify adequacy of the axial reflector thicknesses. Adding an additional 20 cm to both the top and bottom thicknesses of water resulted in a difference of 13 pcm, a difference between two cases that each had 10 pcm of estimated uncertainty.

Figure 2 provides a radial layout of the original KENO-V model for Case 8 from Harms and Miller [1]. Here, the detector drywells are clearly visible outside of the fuel rods, as well as the cylindrical arraignment of the fuel itself.

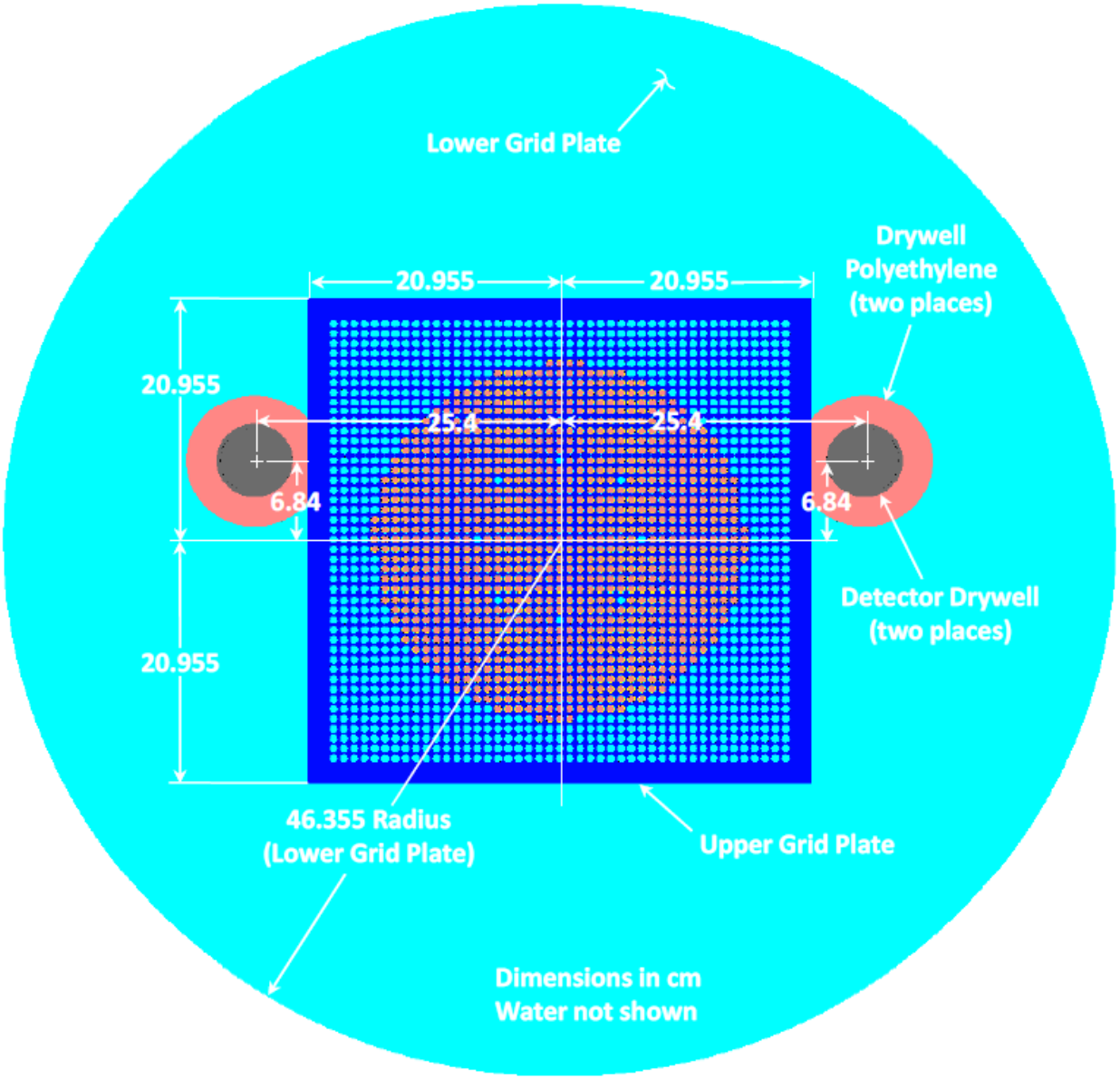

Figure 2: Radial layout of the KENO-V benchmark model of Case 8 [1].

The axial layout of the fuel rods in the original KENO-V model is shown in Figure 3. The fuel rods and solid aluminum rods rest in cutouts in the lower grid plate and are held in place by through-holes in the upper grid plate. The fuel rods consist of end caps (only the bottom cap is modeled), the fuel region, stainless-steel compression spring, an aluminum spacer that is assumed to align with the upper grid plate, and a polyethylene spacer region. The top of the fuel rod extends beyond the top of the KENO-V model.

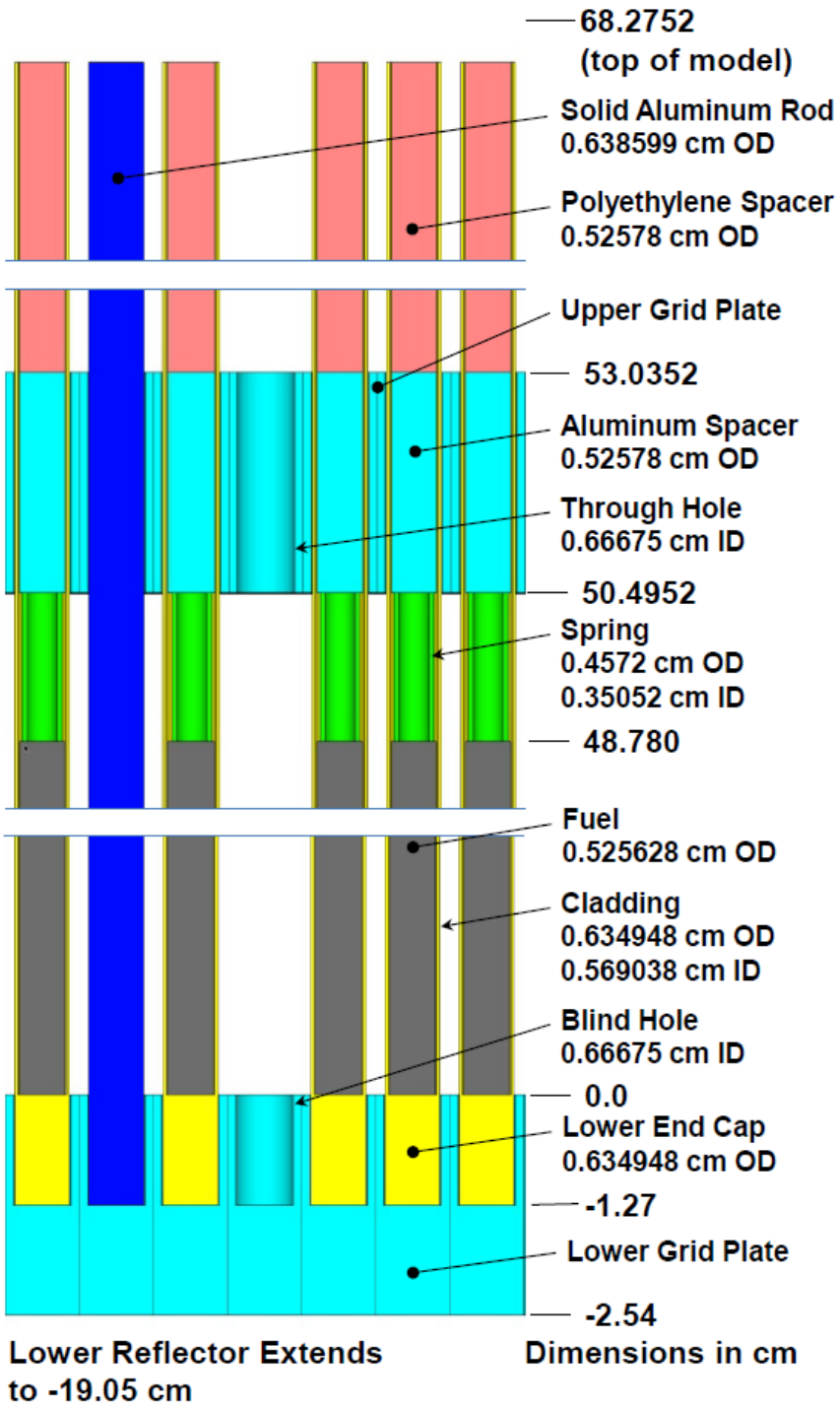

Figure 3: Axial layout of the KENO-V benchmark model of Case 8 [1].

The 15 configurations pf the 7uPCX experiment are shown in Table 1, along with the experimental k-effective values derived from extrapolations to delayed critical (Ref. 1, Table 30), which have been further adjusted for sensitivity and uncertainty analyses performed by Harms and Miller [1] to account for variation in multiple experiment parameters, such as temperature, fuel mass, and fuel rod diameter. The final experimental uncertainty is reported in Table 46 of Harms and Miller [1] as 100 percent mille (pcm). See Figures 15–29 of that document for the detailed fuel layout for each test configuration.

Table 1: 7uPCX Experiment Configurations and Measured k-effective

Case Number	Description	Number of Fuel Rods	Number of Al Rods	k-effective (±0.0010)[1]
1	All fuel rods and no empty locations	1057	—	0.9995
2	Neutron source in center location	1056	—	0.9999
3	4 empty locations – 8 pin pitches apart	1041	—	0.9990
4	4 empty locations – 16 pin pitches apart	1041	—	0.9986
5	4 empty locations – 24 pin pitches apart	1041	—	0.9980
6	4 empty locations – 32 pin pitches apart	1041	—	0.9974
7	8 empty locations – 8 pin pitches apart	1029	—	0.9994
8	8 empty locations – 16 pin pitches apart	1029	—	0.9987
9	8 empty locations – 24 pin pitches apart	1029	—	0.9978
10	8 empty locations – 32 pin pitches apart	1029	—	0.9969
11	8 aluminum rods – 8 pin pitches apart	1049	8	0.9994
12	8 aluminum rods – 16 pin pitches apart	1049	8	0.9993
13	8 aluminum rods – 24 pin pitches apart	1049	8	0.9993
14	8 aluminum rods – 32 pin pitches apart	1049	8	0.9991
15	Various empty locations resembling PWR fuel assembly lattices	872	—	0.9996

3. SOFTWARE AND METHODS

3.1 KENO-VI

Harms and Miller documented KENO-V.a results for the 7uPCX experiment using SCALE 6.1.1. In this analysis, the newer KENO-VI is utilized from both SCALE 6.2 and 6.3.

KENO is a well-known 3D Monte Carlo (MC) particle transport code [2]. It has been utilized for decades for a wide variety of critical safety applications and has an extensive validation base. KENO-V.a and KENO-VI produce equivalent eigenvalues within the range of calculated uncertainty. KENO-VI contains the same features as KENO-V.a, in addition to a more complex geometry package. In this work, KENO-VI is used with both continuous-energy (CE) and multigroup (MG) cross section data libraries. CE KENO-VI applications provide the most accurate neutron transport results in the SCALE code system, given enough computational resources to sample a sufficient number of particle histories.

3.2 MPACT

MPACT is the deterministic neutron transport capability in VERA. It is an advanced pin-resolved whole-core multigroup transport solver based on the 2D/1D synthesis method, on the frame of a 3D coarse mesh finite difference method, for which radial and axial correction factors are obtained from 2D method-of-characteristics and 1D P_N, respectively. The neutron transport is performed using 51 energy-group cross sections, based on the subgroup method of on-the-fly resonance self-shielding. The discretization of the core is typically three radial and eight azimuthal flat source regions per fuel pellet, with non-uniform axial

plane thickness ranging from 2 to 15 cm. Fuel assembly features such as spacer grids, fuel and absorber plena, and end plugs can be modeled explicitly. MPACT performs the same neutron transport calculations in the upper, lower, and radial reflector regions of the reactor core, explicitly modeling most ex-core structures, requiring no a priori approximations of the core boundary conditions, as is needed for nodal diffusion methods. MPACT also controls the functional application features of the VERA core simulator, such as critical boron search, equilibrium xenon calculations, predictor–corrector depletion, in-core detector response calculations, reading and writing restart files, and performing fuel shuffling, decay, and discharge [3-6].

MPACT has been extensively validated for a wide variety of commercial pressurized water reactor (PWR) types, fuel assembly types, and burnable absorber types. Through a direct coupling with the SCALE depletion and decay code ORIGEN—and a direct coupling with the subchannel thermal hydraulics code COBRA-TF—MPACT has simulated hundreds of fuel cycles and produced good agreement with measured data, such as those for critical boron concentrations, control rod reactivity worths, isothermal temperature coefficients, and in-core detector reaction rate distributions. In addition, extensive code-to-code comparisons to MC-based software such as KENO-VI, Shift, MCNP, MC21, and Serpent have demonstrated excellent agreement in both reactivity and power distribution. Therefore, for commercial PWR problems, MPACT provides accuracy very close to MC methods, but with much reduced computational requirements, enabling many more calculations on much less computing resources.

3.3 SHIFT

Shift is a massively parallel, CE MC radiation transport code available within VERA and SCALE that employs a high-speed internal geometry package for PWRs and solves both MG and CE neutron, photon, and coupled neutron–photon transport problems [3,7]. Shift provides novel transport algorithms and hybrid methods tailored for leadership-class computing platforms, in addition to multiple geometries, tallies, and physics methods. Shift has the following additional characteristics:

- Flexible, high-performance MC radiation transport framework
- Physics agnostic – ability to perform calculations with either MG or CE cross section data
- Geometry agnostic – supports four different types of geometry specifications, including SCALE geometry, Exnihilo Reactor ToolKit geometry (for VERA in-core), general geometry, and MCNP geometry
- Fixed-source and eigenvalue solvers
- Fixed-source solution acceleration and variance reduction via hybrid methods (CADIS and FW-CADIS)
- Multiple parallel decompositions and concurrency models
- Highly scalable – designed to scale from laptops to supercomputers

Shift uses predominantly the same CE ENDF/B-VII.1 data library as that provided for KENO-VI in SCALE. Other libraries can also be utilized, including MG and ENDF/B-VIII.0. Therefore, Shift can be expected to produce similar results for criticality safety problems as KENO-VI, yet Shift's parallelization permits far more particle histories; therefore, it can obtain much smaller local uncertainty for parameters such as flux of fission distributions in reactor cores.

Shift has been benchmarked extensively against the large number of criticality safety cases used for validation of KENO-VI [8]. Shift has also been used in eigenvalue mode to simulate the initial criticality of at least four different commercial PWRs. Finally, Shift has been validated for ex-core fluence applications by comparison to ex-core coupons irradiated in a commercial reactor, in a VERA application

in which MPACT provides the neutron source term, and Shift provides the fixed-source ex-core neutron flux through its variance reduction techniques. For more details on these applications, please contact the author.

4. ANALYSES

This benchmark analysis is divided into multiple sections. First, a summary and comparison of previously generated results are collected and presented to quantify and understand any additional significant biases in new results. Second, new results are generated with KENO-VI using models and inputs consistent with previous results. These results help to understand differences resulting from improved code versions and nuclear data. Finally, results are generated with VERA codes MPACT and Shift and are compared to values in the previous sections.

4.1 PREVIOUSLY GENERATED RESULTS

Several sets of results for the 7uPCX experiments have already been publicized:

1. The original publication for the *International Handbook of Evaluated Criticality Safety Benchmark Experiments* (ICSBEP) [1] included results from KENO-V.a (SCALE 6.1.1), MCNP 5, APOLLO2 (2.8.3), and MORET 5.

2. The SCALE Verified, Archived Library of Inputs and Data (VALID) database is regularly utilized for software testing and validation for new SCALE versions and releases. The 7uPCX experiment, being part of the ICSBEP, is included in this dataset (called LEU-COMP-THERM-078). SCALE 6.1.2 and SCALE 6.2.2 results were located for these cases, from both KENO-V.a and KENO-VI [8].

3. A new SCALE sequence in version 6.3 called *CSAS-Shift* has been developed and validated. This sequence is like CSAS6, but KENO-VI is replaced with the new Shift MC transport code. This is the same Shift used in VERA, but it has different interfaces and implementation. CSAS-Shift is designed to read a CSAS6 (KENO-VI) input with minimal modifications. This validation has is document in Pandya et al. [9].

These previously generated results from KENO-V.a, KENO-VI, and Shift, using both CE and MG cross sections have been collected and are provided in Table 2. Also included are the ENDF-B data versions utilized, the type of user input file, and the maximum one-sigma statistical uncertainty reported for the results. Then, the eigenvalue difference from the measured value recorded in Harms and Miller [1] is provided in pcm.

Table 2: Previously Calculated Eigenvalues and Differences from Measurement (pcm)

Code	Meas	KENO-V.a	KENO-V.a	KENO-V.a	KENO-V.a	KENO-V.a	KENO-V.a	KENO-V.a	KENO-VI	Shift	Shift	Shift
SCALE		6.1.1	6.1.1	6.1.2	6.2.2	6.2.2	6.2.2	6.2.2	6.2.2	6.3.0	6.3.0	6.3.0
ENDF/B		7.0	7.0	7.0	7.0	7.1	7.1	7.1	7.1	7.1	7.1	7.1
Groups		CE	238g	CE	CE	CE	252g	56g	CE	CE	252g	CE
Input		KENO-V.a	KENO-V.a	KENO-V.a	KENO-V.a	KENO-V.a	KENO-V.a	KENO-V.a	KENO-VI	KENO-V.a	KENO-V.a	KENO-VI
Source		Ref. 1	Ref. 1	—	Ref. 8	Ref. 8	Ref. 8	Ref. 8	Ref. 8	Ref. 9	Ref. 9	Ref. 9
Sigma	<0.001	<0.0002	<0.0002	<0.0001	<0.0001	<0.0001	<0.0001	<0.0001	<0.0001	<0.0001	<0.0001	<0.0001
1	0.9995	0.9973	0.9963	0.99772	0.99804	0.99829	0.99681	0.99676	0.99815	0.99791	0.99714	0.99802
2	0.9999	0.9981	0.9965	0.99822	0.99843	0.99861	0.99714	0.99734	0.99872	0.99835	0.99739	0.99831
3	0.9990	0.9968	0.9958	0.99711	0.99782	0.99756	0.99619	0.99623	0.99766	0.99750	0.99663	0.99732
4	0.9986	0.9968	0.9955	0.99678	0.99732	0.99713	0.99603	0.99606	0.99725	0.99694	0.99604	0.99722
5	0.9980	0.9963	0.9950	0.99636	0.99691	0.99688	0.99557	0.99548	0.99692	0.99669	0.99590	0.99669
6	0.9974	0.9956	0.9938	0.99581	0.99633	0.99615	0.99499	0.99497	0.99620	0.99600	0.99522	0.99596
7	0.9994	0.9974	0.9960	0.99730	0.99807	0.99813	0.99674	0.99670	0.99797	0.99760	0.99717	0.99792
8	0.9987	0.9969	0.9955	0.99679	0.99728	0.99725	0.99617	0.99610	0.99731	0.99714	0.99625	0.99714
9	0.9978	0.9958	0.9945	0.99603	0.99630	0.99642	0.99507	0.99506	0.99634	0.99624	0.99548	0.99619
10	0.9969	0.9947	0.9935	0.99480	0.99540	0.99521	0.99401	0.99407	0.99531	0.99498	0.99431	0.99522
11	0.9994	0.9976	0.9962	0.99744	0.99799	0.99806	0.99665	0.99686	0.99797	0.99776	0.99683	0.99780
12	0.9993	0.9977	0.9966	0.99746	0.99798	0.99787	0.99676	0.99661	0.99786	0.99768	0.99703	0.99769
13	0.9993	0.9973	0.9959	0.99729	0.99798	0.99775	0.99667	0.99655	0.99809	0.99783	0.99673	0.99758
14	0.9991	0.9972	0.9957	0.99726	0.99780	0.99786	0.99644	0.99630	0.99751	0.99754	0.99662	0.99748
15	0.9996	0.9982	0.9978	0.99819	0.99872	0.99873	0.99782	0.99802	0.99876	0.99850	0.99821	0.99857
1	–	−220	−320	−178	−146	−121	−269	−274	−135	−159	−236	−148
2	–	−180	−340	−168	−147	−129	−276	−256	−118	−155	−251	−159
3	–	−220	−320	−189	−118	−144	−281	−277	−134	−150	−237	−168
4	–	−180	−310	−182	−128	−147	−257	−254	−135	−166	−256	−138
5	–	−170	−300	−165	−109	−112	−243	−252	−108	−131	−210	−131
6	–	−180	−360	−159	−107	−125	−241	−243	−120	−140	−218	−144
7	–	−200	−340	−210	−133	−127	−266	−270	−143	−180	−223	−148
8	–	−180	−320	−191	−142	−145	−253	−260	−139	−156	−245	−156
9	–	−200	−330	−177	−150	−138	−273	−274	−146	−156	−232	−161
10	–	−220	−340	−210	−150	−169	−289	−283	−159	−192	−259	−168
11	–	−180	−320	−196	−141	−134	−275	−254	−143	−164	−257	−160
12	–	−160	−270	−184	−132	−143	−254	−269	−144	−162	−227	−161
13	–	−200	−340	−201	−132	−155	−263	−275	−121	−147	−257	−172
14	–	−190	−340	−184	−130	−124	−266	−280	−159	−156	−248	−162
15	–	−140	−180	−141	−88	−87	−178	−158	−84	−110	−139	−103
Average	–	**−188**	**−315**	**−182**	**−130**	**−133**	**−259**	**−259**	**−133**	**−155**	**−233**	**−152**
St Dev	–	**23**	**43**	**19**	**18**	**19**	**26**	**30**	**20**	**19**	**30**	**18**

The CE results in Harms and Miller [1] have an average difference of −188 ± 23 pcm (SCALE 6.1, ENDF/B-VII.0), where 23 pcm is one standard deviation for the population of the 15 cases. This result improved to −133 ± 19 pcm with SCALE 6.2 and ENDF/B-VII.1. The improvement (58 ± 19 pcm) comes from use of SCALE 6.2, compared to the original results with SCALE 6.1. The CE ENDF/B-VII.1 data library does not produce a significant difference from the previous libraries, with a difference over the 15 cases of only −3 ± 16 pcm. The results from KENO-VI are approximately the same as KENO-V.a, as expected. The results from the new SCALE 6.3 CSAS-Shift sequence are slightly worse at −155 ± 19 pcm, but within about two standard deviations, and the results are very similar between both formats of input files. The overall results are very good, though with a negative bias (i.e., calculated reactivity is lower than measured), especially considering the reported uncertainty for the measurements in Harms and Miller [1] is 100 pcm.

In the results from all three sources, those for MG are somewhat worse than those for CE, as expected. The 238-group library in SCALE 6.1 produced results 127 pcm worse than the CE result. The 252-group library in SCALE 6.2 performed about the same; likewise, the newer 56-group library performed similarly to the 252-group library, as did the 252-group library with Shift.

In the previously calculated results, the KENO parameter to end the calculation when a user-input statistical uncertainty is reached was employed (sig). This resulted in a statistical uncertainty of approximately 10 pcm for most of these cases. Using 40,000 particles per generation, skipping 50 generations, the typical KENO calculation progressed to about 2,114 generations, on average, before the calculation was ended. This means that the typical calculation utilized approximately 8.3×10^7 active particle histories.

An approximation made in all the previous results is the lack of tungsten-180 in the fuel material. This isotope was not available in the SCALE ENDF/B-VII.0 data libraries, nor was natural tungsten. It will be included in all new results utilizing ENDF/B-VII.1 or later.

4.2 NEW SCALE RESULTS

The KENO-V.a models generated in previous analyses [1] and [8] were re-executed with the latest release of SCALE 6.2.4. The KENO-V.a model was run with the CE ENDF/B-VII.0 library for comparison to previous results. The KENO-V.a. models were converted to KENO-VI format using the SCALE sequence C5TOC6 and then used for all subsequent calculations. Only the following changes were made:

1. The tungsten limitation of the SCALE ENDF/B-VII.0-based data libraries does not exist in subsequent versions. Therefore, the natural tungsten number densities from the experiment specification [1] were used in all the ENDF/B-VII.1 and ENDF/B-VIII.0 calculations.

2. The cross section data libraries were updated for the various calculations, predominantly to the CE ENDF/B-VII.1 and ENDF/B-VIII.0 libraries, along with some MG libraries, as shown below.

3. The new SCALE sequence, CSAS6-Shift, was also utilized for comparison to the results from Shift in VERA. In this sequence, Shift replaces KENO-VI for the neutron transport calculation; other components of the CSAS6 sequence remain the same.

Though SCALE 6.2.4 was utilized for most calculations, a beta version of SCALE 6.3.0 was required for calculations using the ENDF/B-VIII.0 data library as well as the CSAS6-Shift sequence. These capabilities are new and unavailable in the current SCALE release version. A set of experiment cases was run for comparison of 6.2.4 and 6.3.0 results, and the eigenvalue differences over the 15 cases were

5 ± 18 pcm, in which both sets of cases had a reported statistical uncertainty of approximately 10 pcm. This test showed that SCALE 6.3.0 produces very similar results to SCALE 6.2.4 for these calculations.

Table 3 below provides all the results from newly executed SCALE models of the 7uPCX experiment.

Table 3: New SCALE Calculated Eigenvalues and Differences from Measurement (pcm)

Code	Meas	KENO-V.a	KENO-VI	KENO-VI	KENO-VI	KENO-VI	KENO-VI	Shift	Shift
SCALE		6.2.4	6.2.4	6.2.4	6.2.4	6.3.0	6.3.0	6.3.0	6.3.0
ENDF/B		7.0	7.1	7.1	7.1	7.1	8.0	7.1	8.0
Groups		CE	CE	252g	56g	CE	CE	CE	CE
Input		KENO-V.a	KENO-VI	KENO-VI	KENO-VI	KENO-VI	KENO-VI	KENO-VI	KENO-VI
Sigma	<0.00100	<0.0001	<0.0001	<0.0001	<0.0001	<0.0001	<0.0001	<0.00011	<0.00011
1	0.9995	0.99817	0.99795	0.99717	0.99663	0.99818	0.99748	0.99800	0.99736
2	0.9999	0.99855	0.99876	0.99751	0.99709	0.99866	0.99786	0.99860	0.99803
3	0.9990	0.99769	0.99754	0.99646	0.99613	0.99769	0.99695	0.99747	0.99691
4	0.9986	0.99748	0.99746	0.99629	0.99587	0.99708	0.99672	0.99712	0.99656
5	0.9980	0.99692	0.99693	0.99585	0.99536	0.99692	0.99616	0.99681	0.99617
6	0.9974	0.99629	0.99618	0.99516	0.99480	0.99612	0.99570	0.99597	0.99550
7	0.9994	0.99801	0.99801	0.99688	0.99672	0.99810	0.99734	0.99805	0.99735
8	0.9987	0.99739	0.99722	0.99633	0.99587	0.99727	0.99660	0.99727	0.99676
9	0.9978	0.99640	0.99626	0.99535	0.99509	0.99640	0.99582	0.99636	0.99556
10	0.9969	0.99545	0.99523	0.99429	0.99397	0.99531	0.99461	0.99516	0.99464
11	0.9994	0.99802	0.99782	0.99701	0.99662	0.99798	0.99743	0.99812	0.99728
12	0.9993	0.99796	0.99778	0.99697	0.99681	0.99817	0.99723	0.99809	0.99729
13	0.9993	0.99804	0.99793	0.99682	0.99653	0.99780	0.99717	0.99798	0.99721
14	0.9991	0.99768	0.99766	0.99650	0.99637	0.99770	0.99695	0.99759	0.99703
15	0.9996	0.99878	0.99872	0.99807	0.99770	0.99877	0.99808	0.99856	0.99827
1	—	−133	−155	−233	−287	−132	−202	−150	−214
2	—	−135	−114	−239	−281	−124	−204	−130	−187
3	—	−131	−146	−254	−287	−131	−205	−153	−209
4	—	−112	−114	−231	−273	−152	−188	−148	−204
5	—	−108	−107	−215	−264	−108	−184	−119	−183
6	—	−111	−122	−224	−260	−128	−170	−143	−190
7	—	−139	−139	−253	−268	−130	−206	−136	−205
8	—	−131	−148	−237	−283	−143	−210	−143	−194
9	—	−140	−154	−245	−272	−140	−198	−144	−224
10	—	−145	−167	−261	−293	−159	−229	−174	−226
11	—	−138	−158	−239	−278	−142	−197	−128	−212
12	—	−134	−152	−233	−249	−114	−207	−121	−201
13	—	−126	−137	−248	−277	−150	−213	−132	−209
14	—	−142	−144	−260	−273	−140	−215	−151	−207
15	—	−82	−88	−153	−190	−84	−152	−104	−134
Average	—	**−127**	**−136**	**−235**	**−269**	**−132**	**−199**	**−138**	**−200**
St Dev	—	**17**	**22**	**26**	**25**	**19**	**19**	**17**	**22**

The new SCALE results in Table 3 provide the following observations:

- The new KENO-V.a results with CE ENDF/B-VII.0 data and SCALE 6.2 agree well with the results found in Saylor et al. [8], with differences of 3 ± 9 pcm, where the maximum statistical uncertainties are 10 pcm for the two sets of cases.

- The new KENO-VI results with CE ENDF/B-VII.1 data and SCALE 6.2 agree well with the results found in Saylor et al. [8], with differences of −4 ± 11 pcm, where the maximum statistical uncertainties are 10 pcm for the two sets of cases.

- The new KENO-VI 252-group and 56-group results agree well with the comparable KENO-V.a results reported in Saylor et al. [8], with average differences from the original results of 24 ± 9 pcm and −10 ± 14 pcm, respectively. The MG biases from the new results are −99 ± 17 pcm for the 252-group calculation, and −133 ± 19 pcm for the 56-group calculation. Each of the comparison cases has a maximum statistical uncertainty of 10 pcm.

- The results from SCALE 6.3.0 are very similar to those from SCALE 6.2.4, based on CE ENDF/B-VII.1 KENO-VI calculations, with differences of 5 ± 18 pcm, where the maximum statistical uncertainties are 10 pcm for the two sets of cases.

- The SCALE 6.3.0 KENO-VI results using the CE ENDF/B-VIII.0 data library are somewhat worse than those using the CE ENDF/B-VII.1 data, with differences compared to the experiment measurements of −199 ± 19 pcm. Compared to the ENDF/B-VII.1 results, the differences are −67 ± 16 (i.e. use of ENDF/B-VIII.0 data results in worse agreement with measurement).

- The Shift results using CSAS6-Shift agree very well with the KENO-VI results, with differences of −7 ± 12 pcm with the CE ENDF/B-VII.1 data, and −1 ± 14 pcm with the CE ENDF/B-VIII.0 data library. The Shift statistical uncertainties are very slightly higher at 11 pcm. Likewise, the differences between ENDF/B-VII.1 and ENDF/B-VIII.0 results with Shift are very similar to those with KENO-VI, which ENDF/B-VIII.0 data producing larger differences from measurement.

In addition to eigenvalue results, both flux and fission tallies were computed using KENO-VI with CE ENDF/B-VII.1 data. The flux tally was performed over all energies. The fission tally capability was not available in SCALE 6.2.4, so version 6.3.0 was used instead. The results of the KENO-VI calculations were post-processed using the *mt2ascii* SCALE utility; subsequently, a Python script was used to convert the ASCII output to a VERA-formatted HDF5 binary file. Images of resulting radial and axial flux distributions are shown in Figure 4 and are discussed further in subsequent sections. Calculated neutron flux and fission rate distributions for all cases are provided in the appendices.

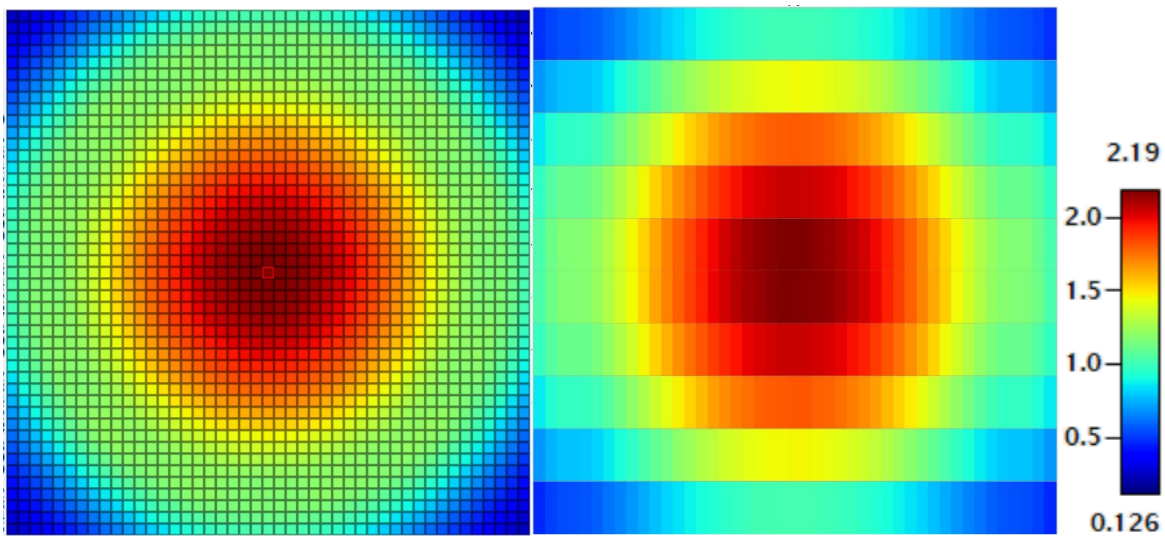

Figure 4: Radial (left) and axial (right) flux distributions from KENO-VI for Case 1.

4.3 VERA RESULTS

All of the previous results were generated with SCALE from inputs taken from the original specifications [1] or converted from those using SCALE utilities. In this section, new independent inputs are created for VERA using the ASCII common input format used in most VERA applications. This input format is designed for modeling commercial PWRs and is thus limited in modeling more generic critical experiments. However, this has been accomplished with some minor tricks and approximations, which are discussed below. An example of the VERA input is provided in Appendix E.

In addition to challenges with the VERA input, the MPACT 51-group cross section library based on the subgroup method of self-shielding [6] is designed and optimized for commercial PWR geometries and operating conditions. When developing VERA, as few energy groups as possible were used to reduce computational requirements while maintaining the desired level of fidelity and accuracy. VERA typically requires thousands of processors to run steady-state quarter-core calculations, so optimization of the cross section library was preferred over maintaining more energy groups to support a broader application set. For these reasons, it is crucial to understand the major difference between the 7uPCX experiment and a typical PWR, such as Watts Bar Nuclear Plant [10]. Table 4 provides comparison of some of the important parameters for these different reactors.

Table 4: Comparison of 7uPCX and Typical PWR Parameters

Parameter	7uPCX	Typical PWR
Moderator Temperature (°C)	25	312
Moderator Density (g/cc)	0.997	0.7
Soluble Boron (ppmB)	None	0–1,500
Pin Pitch (cm)	0.855	1.26
Fuel Rod Diameter (cm)	0.635	0.95
Fuel Rod Cladding	Aluminum	Zircaloy-4
Fuel Pellet Diameter (cm)	0.5256	0.8192
Active Fuel Height (cm)	48.78	365.76
Effective Core Diameter (cm)	29.92–31.63	322.5
Number of Fuel Rods	872–1,057	50,952
Excore Detectors	Two drywells near fuel	None within vessel
Radial Reflector Region	Moderator	Baffle plates, neutron pads

The VERA input is designed for cylindrical square-pitched LWR fuel rods grouped into square arrays of fuel assemblies. These assemblies utilize spacer grids for structural support for the fuel rods. For the 7uPCX experiment, the fuel, plenum springs, and aluminum and polyethylene spacers can be modeled explicitly. The upper and lower grid plates are modeled as homogenized spacer grids in the VERA input, in which an effective spacer grid mass is calculated to completely displace the coolant material that would normally exist within the spacer grid region in a normal LWR. The upper and lower reflector regions are also modeled consistent with the KENO model described previously [1]. The VERA input for Case 1 is provided in Appendix E.

Other approximations in the VERA model of the 7uPCX experiment are described below.

1. The lower grid plate is modeled as equivalent-mass spacer grids in the VERA input. These do not extend out to the core tank as in shown in Figure 1. Because the lower core plate is below the fuel and extends far radially from the active fuel, this approximation is not expected to impact the results.

2. The upper grid plate is modeled as an equivalent-mass spacer grid in the VERA input, which exists only around the locations where fuel rods can be placed. This does not include the slightly wider upper plate dimensions shown in Figure 2. This ~1.7 cm aluminum region around the upper grid plate is not expected to affect the results significantly.

3. The 7uPCX experiment is modeled in VERA as an array of 3×3 fuel assemblies (each with 15×15 fuel rod locations). By default, VERA will automatically create a radial reflector region with a width of one assembly pitch. Initial MPACT calculations using an assembly pitch of 38.475 cm (45 rods times 0.855 cm pin pitch) exhibited difficulty with convergence due to the large volume of low flux regions outside of the reactor core. Modeling the experiment as 3×3 assemblies (with no inter-assembly gap) reduces the assembly pitch to 12.825 cm and results in much better convergence behavior. In addition, 38.475 cm is a much thicker radial reflector than is needed. One problem with this approach is that it significantly complicates the input, because nine separate assemblies much be defined, each with unique axial regions, resulting in 45 distinct lattice inputs in the VERA ASSEMBLY block.

4. The largest approximation is the exclusion of the detector drywells in the VERA model. This was done simply because the VERA input is not flexible enough to model these geometric features shown in Figure 2. However, the detectors are several pin pitches away from the fuel, and the effect was calculated in Harms and Miller [1] (Section 3.1.7) to be 0.5 pcm, on average. The reactivity worth of the drywells was confirmed with new calculations using KENO-VI with CE ENDF/B-VII.1 data to be 2 ± 12 pcm; using CSAS6-Shift with CE ENDF/B-VII.1 data, the worth was confirmed to be 4 ± 14 pcm. Therefore, the detector drywells can be ignored, and the VERA input geometry is sufficient. The effect of the drywells on neutron flux or fission rate distribution was not evaluated. Radial neutron flux comparisons between KENO-VI (with the drywells) and Shift (without drywells) do not indicate any significant bias.

5. Due to the differences in the 7uPCX experiment and a typical LWR, particularly the size, moderator density, and pin pitch, MPACT exhibited difficulty with convergence for several of the initial cases. To resolve this, non-default nodal options—available in the more recent development version of the code (4.3RC7)—were utilized to obtain better convergence. This permitted successful solutions for all but Case 15 using the default transport-corrected P_0 (TCP_0) scattering treatment, and all cases using P_2 scattering. The nodal options used are shown below.

```
[MPACT]
 nodal_method p3
 nodal_group_loop 20
 nodal_group_start 1
 nodal_inners 20
 nodal_inner_tol 1e-5
 nodal_group_tol 1e-5
 nodal_relax_negative true
```

Figure 5 displays the MPACT radial geometry for Case 1 at the reactor mid-plane. Note that the various colors represent different unique materials in each of the nine ‘assemblies’ modeled, even though these materials are really the same. The inset region displays the meshing used for each pin cell. Note that only eight azimuthal angles were used rather than the 24 shown, which is an artifact of the method of visualization.

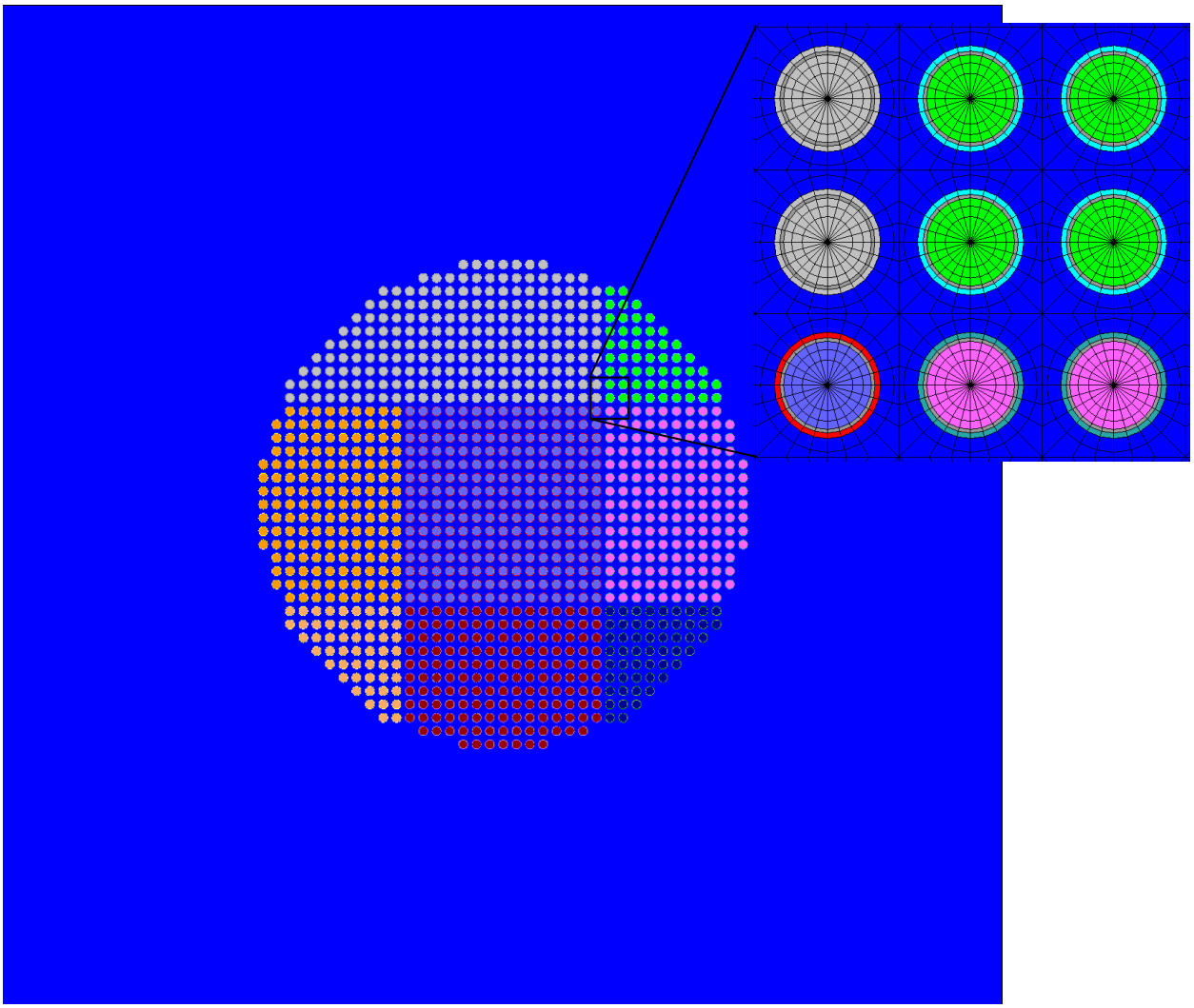

Figure 5: MPACT geometry for Case 1 – 2D slice at core midplane.

The VERA axial model (and the axial mesh for Shift tallies) was specified as ten uniform axial meshes in the active fuel, each 4.878 cm tall. This is slightly smaller than what would be typically used in a VERA PWR calculation. Outside of the fuel, thin axial planes are utilized for the upper and lower grid plates, and then four more axial planes are used for axial reflection beyond each grid plate, two 8.26 cm planes at the bottom and two 7.62 cm planes at the top. The total number of axial meshes is 18.

VERA 4.3RC7 was executed on Idaho National Laboratory's Sawtooth [11] supercomputer for all 15 cases of the experiment using the following six calculation types:

1. MPACT with TCP_0 scattering and 51 energy groups
2. MPACT with P_2 scattering and 51 energy groups
3. MPACT with P_2 scattering and 252 energy groups
4. Shift with CE ENDF/B-VII.1 data and 1 billion active particle histories
5. Shift with CE ENDF/B-VIII.0 data and 1 billion active particle histories
6. Shift with CE ENDF/B-VII.1 data and 10 billion active particle histories

The latter case with Shift was performed to improve the fission rate distribution statistics, discussed in a subsequent section of this report.

The eigenvalue results and their differences from the experiment are provided below.

Table 5: VERA Calculated Eigenvalues and Differences from Measurement (pcm)

Code	Meas	MPACT	MPACT	MPACT	Shift	Shift	Shift
Version		4.3RC7	4.3RC7	4.3RC7	4.2	4.2	4.2
ENDF/B		7.1	7.1	7.1	7.1	8.0	7.1
Groups		51g	51g	252g	CE	CE	CE
Scattering		TCP0	P2	P2	n/a	n/a	n/a
Sigma	<0.00100	n/a	n/a	n/a	<0.00005	<0.00005	<0.00002
1	0.9995	0.99955	0.99868	0.99401	0.99818	0.99784	0.99826
2	0.9999	1.00003	0.99916	0.99449	0.99878	0.99834	0.99873
3	0.9990	0.99899	0.99812	0.99345	0.99773	0.99726	0.99770
4	0.9986	0.99870	0.99785	0.99313	0.99744	0.99699	0.99739
5	0.9980	0.99828	0.99742	0.99273	0.99706	0.99645	0.99698
6	0.9974	0.99768	0.99682	0.99210	0.99642	0.99590	0.99636
7	0.9994	0.99935	0.99851	0.99378	0.99809	0.99763	0.99805
8	0.9987	0.99875	0.99789	0.99317	0.99740	0.99712	0.99742
9	0.9978	0.99785	0.99699	0.99227	0.99647	0.99609	0.99652
10	0.9969	0.99677	0.99590	0.99118	0.99548	0.99499	0.99541
11	0.9994	0.99938	0.99855	0.99387	0.99810	0.99771	0.99814
12	0.9993	0.99937	0.99854	0.99385	0.99808	0.99764	0.99811
13	0.9993	0.99932	0.99848	0.99378	0.99809	0.99760	0.99802
14	0.9991	0.99912	0.99825	0.99358	0.99786	0.99742	0.99783
15	0.9996	failed	0.99917	0.99457	0.99868	0.99845	0.99869
1	—	5	−82	−549	−132	−166	−125
2	—	13	−74	−541	−113	−156	−117
3	—	−1	−88	−555	−127	−174	−130
4	—	10	−75	−547	−116	−161	−121
5	—	28	−58	−527	−94	−155	−102
6	—	28	−58	−530	−98	−150	−104
7	—	−5	−89	−562	−131	−177	−135
8	—	5	−81	−553	−130	−158	−128
9	—	5	−81	−553	−133	−171	−128
10	—	−13	−100	−572	−142	−192	−149
11	—	−2	−85	−553	−130	−169	−126
12	—	7	−76	−545	−122	−166	−119
13	—	2	−82	−552	−121	−170	−128
14	—	2	−85	−552	−124	−168	−127
15	—	*failed*	−43	−503	−92	−115	−91
Average	—	**6**	**−77**	**−546**	**−120**	**−163**	**−122**
St Dev	—	**11**	**14**	**16**	**15**	**17**	**14**

The VERA results in Table 4 provide the following observations:

- Case 15 did not converge in MPACT with the specified input and TCP_0 scattering. It did converge with P_2 scattering. That case withstanding, the TCP_0 results are excellent with a difference from measurement of 6 ± 11 pcm. The P_2 results, which should be more accurate, are −77 ± 14 pcm. Therefore, it is concluded that because TCP_0 results are better that there is some small amount of cancellation of error. Both MPACT results are within the 100 pcm measurement uncertainty specified in Harms and Miller [1].

- The MPACT results using P_2 scattering and 252 energy groups performed much worse, with an average difference of −546 ± 16 pcm from the experiment. This MPACT subgroup library has not been employed for LWR problems and has not been validated. To improve this result, future work is needed to optimize the 252-group library for LWR-type problems.

- The Shift results using VERA input and CE ENDF/B-VII.1 data agree well with the experiment, with differences of −120 ± 15 pcm, where the maximum statistical uncertainty is 5 pcm. This also agrees extremely well with the CSAS6-Shift results using KENO-VI input with differences of only 18 ± 13 pcm, and it is approximately within the combined statistical uncertainty of the two codes. This validates the VERA input model against the more generic and flexible KENO-VI input format.

- The Shift results using the CE ENDF/B-VIII.0 data library are somewhat worse than using the CE ENDF/B-VII.1 data, with differences compared to the experiment measurements of −163 ± 17 pcm. Compared to the ENDF/B-VII.1 results, the differences are −43 ± 9 pcm. This difference in data versions is also very similar to the differences calculated with CSAS6-Shift (−62 ± 15 pcm).

- The Shift cases with the larger number of particle histories (10 billion) agree well with the smaller cases, with differences of only −2 ± 5 pcm. This demonstrates good convergence in the MC-calculated eigenvalue.

The average execution times and number of processors for these cases are shown below in Table 6. The Shift requirements for eigenvalue calculations are somewhat larger than those for MPACT, but for fission rate distribution, Shift requires approximately 10 times more resources to reduce the local statistical uncertainty to an acceptable level. This is discussed further in Appendix D.

Table 6: VERA Runtimes (min) and Computational Requirements

Code	MPACT	MPACT	MPACT	Shift	Shift	Shift
Version	4.3RC7	4.3RC7	4.3RC7	4.2	4.2	4.2
ENDF/B	7.1	7.1	7.1	7.1	8.0	7.1
Groups	51g	51g	252g	CE	CE	CE
Scattering	TCP_0	P_2	P_2	n/a	n/a	n/a
Particle Histories	n/a	n/a	n/a	1.25E9	1.25E9	1.25E10
Cores	162	162	162	480	480	960
Avg (min)	16.0	10.4	114.7	24.0	26.0	113.5
St Dev (min)	0.4	1.5	18.1	0.1	0.2	0.3
Total core-hours	43	28	310	192	208	1816

The neutron flux edits were enabled in the MPACT TCP_0 and P_2 cases so that comparison could be made to an MC-based reference solution. For this, the SCALE 6.2.4 version of KENO-VI was utilized using the CE ENDF/B-VII.1 data. The KENO-VI cases were rerun with 2 billion active particle histories, or about 24 times the original cases. This was needed to reduce the stochastic uncertainty in the local fuel rod fluxes. Additionally, a mesh tally (gfx) for the neutron flux was employed over all energy groups, using a discretization that matched the MPACT axial model described previously. Each of the cases was run on 320 cores on the ORNL Artemis computing cluster and required approximately six hours. The maximum local calculated uncertainty in the resulting flux distributions was approximately 1.0%. This is about the limit of what could reasonably be accomplished given limited computing resources. For results of particle history testing and calculated uncertainty, please see Appendix D.

The KENO-VI results were post-processed using a Python script into the VERA output HDF5 file format, and then a subsequent Python script was used to compare the normalized total neutron flux distributions between KENO-VI and MPACT. The results for Case 2 are shown below in Figures 6–8, and the results for subsequent cases are provided in Appendix A. In the figure, the radial slice on the left is taken near the core axial mid-plane (level 6), and the axial slice on the right is taken horizontally close to the center of the experiment. For each case, the normalized flux distribution differences are shown and used to calculate a root-mean-square (RMS) and maximum absolute difference. Only the values of flux in the fuel are used for the statistics.

In addition to the 3D normalized flux distribution statistics, a radial distribution (2D) is also calculated by axial integration of the 3D values in each fuel rod. This provides better MC statistics because the axial integration effectively increases the population size for the result. The 2D uncertainty is not calculated here but should be approximately reduced from the 3D values by the square root of ten (≈3.2×). The radial comparisons are provided in Figure 9.

The statistical results for the P_2 scattering cases are provided below in Table 7, and all results are included in Appendix A. The results are excellent, with a 3D RMS difference of 0.7% and a 2D RMS difference of 0.6%. This demonstrates very good agreement between MPACT and KENO-VI for total neutron flux distribution.

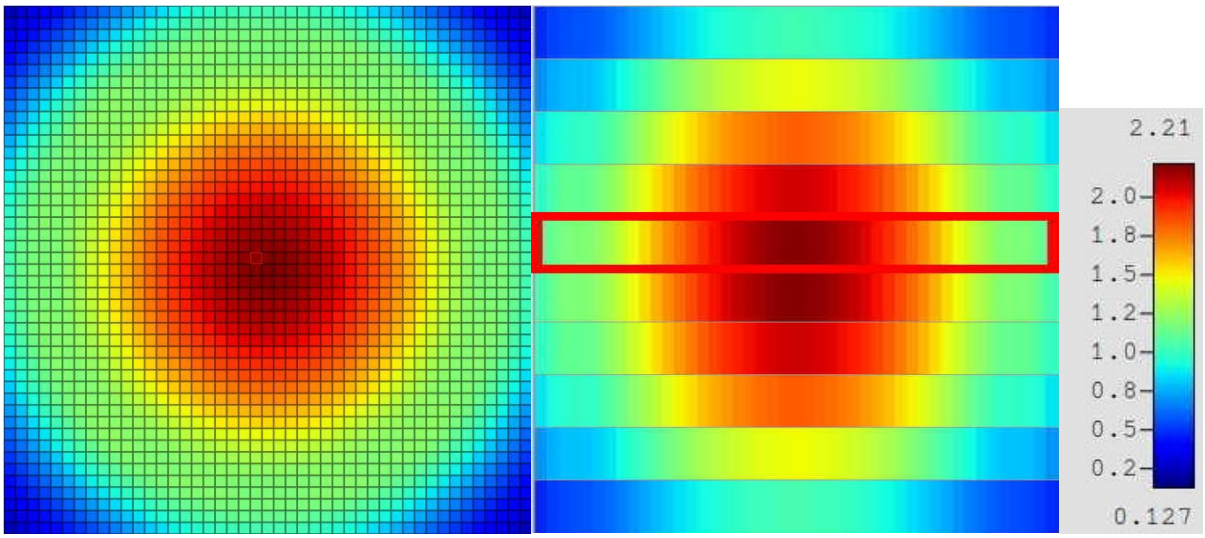

Figure 6: KENO-VI radial (left) and axial (right) flux distributions for Case 2.

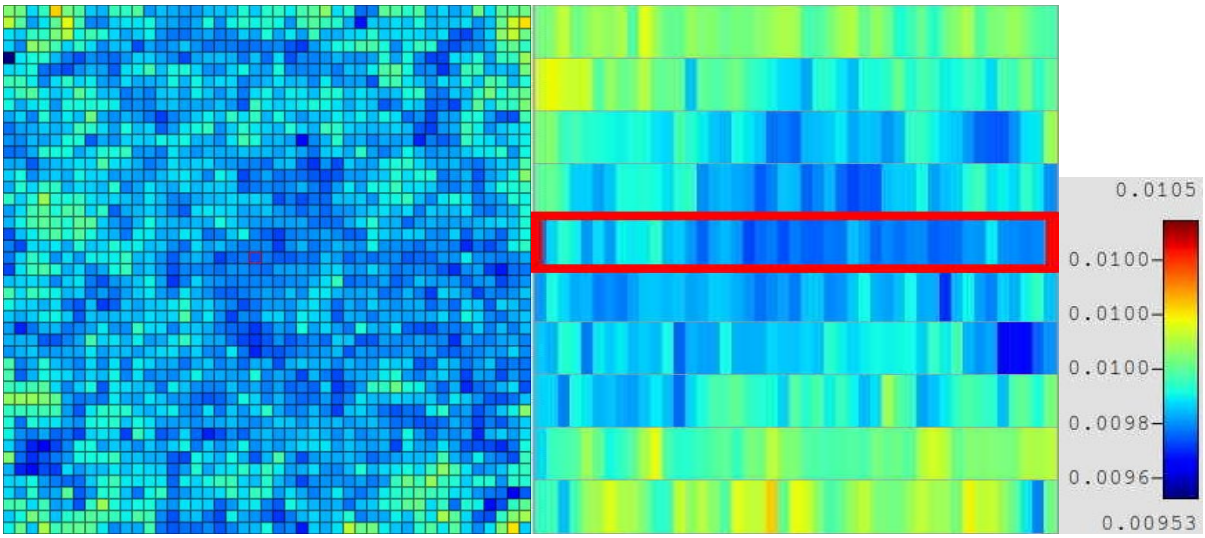

Figure 7: KENO-VI radial (left) and axial (right) fractional uncertainties for Case 2.

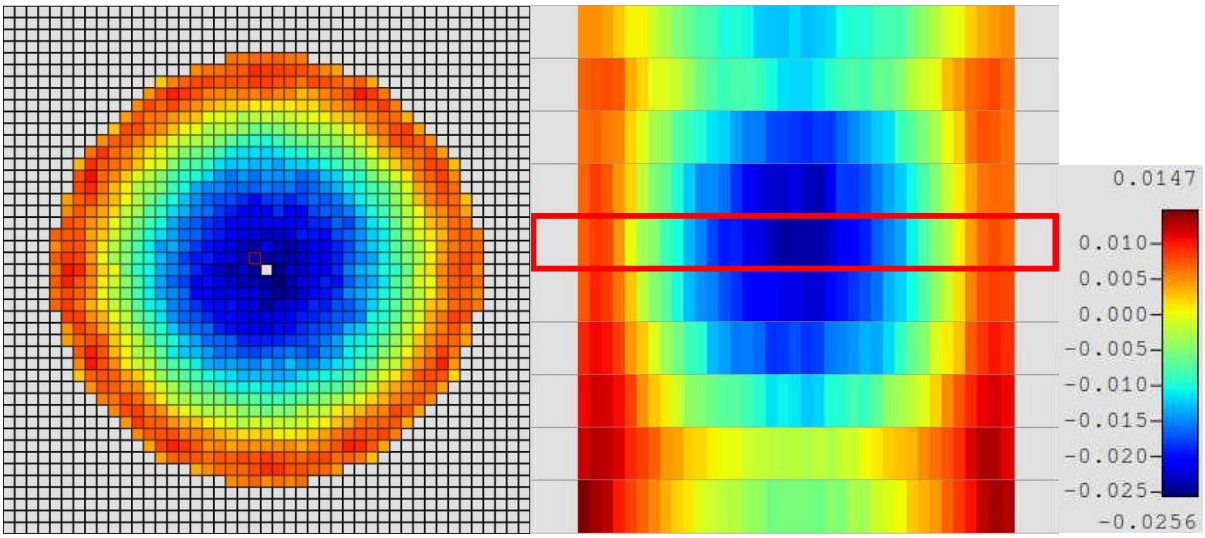

Figure 8: Radial (left) and axial (right) flux differences (MPACT-KENO-VI) for Case 2.

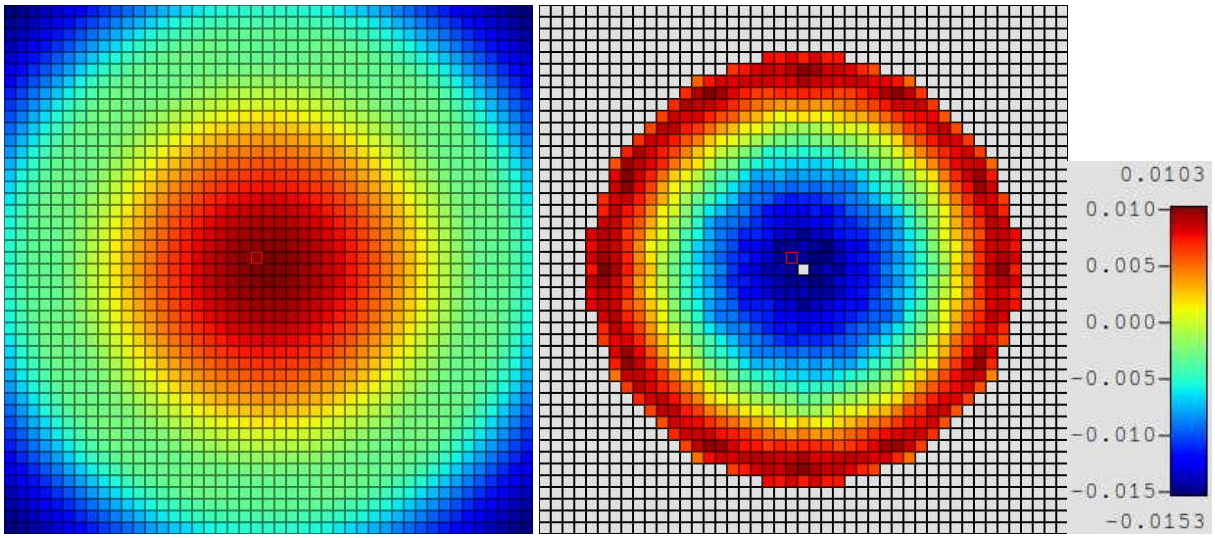

Figure 9: KENO-VI (left) radial flux distribution (left) and MPACT difference (right) for Case 2.

Table 7: Normalized Total Flux Distribution Statistics, MPACT-KENO-VI, P_2 Scattering

Case	k-eff Diff	3D RMS	3D Max	2D RMS	2D Max	AO Diff
1	50	0.73%	−1.97%	0.61%	−1.11%	−0.20%
2	56	0.73%	−2.08%	0.61%	−1.16%	−0.22%
3	55	0.72%	−2.03%	0.61%	−1.17%	−0.19%
4	53	0.74%	−2.02%	0.61%	−1.11%	−0.22%
5	58	0.73%	−1.95%	0.61%	−1.11%	−0.20%
6	54	0.72%	−1.86%	0.60%	−1.08%	−0.22%
7	57	0.72%	−1.99%	0.61%	−1.20%	−0.17%
8	55	0.73%	−1.95%	0.61%	−1.11%	−0.19%
9	57	0.73%	−2.02%	0.61%	−1.13%	−0.20%
10	58	0.72%	−1.95%	0.60%	−1.07%	−0.20%
11	56	0.74%	−2.11%	0.62%	−1.15%	−0.23%
12	53	0.73%	−1.94%	0.61%	−1.12%	−0.21%
13	58	0.73%	−1.93%	0.61%	−1.09%	−0.22%
14	59	0.72%	−1.93%	0.60%	−1.13%	−0.21%
15	48	0.72%	−2.15%	0.59%	−1.06%	−0.13%
Average	**55**	**0.73%**	**−1.99%**	**0.61%**	**−1.12%**	**−0.20%**
St Dev	**3**	**0.01%**	**0.08%**	**0.01%**	**0.04%**	**0.03%**

Neutron fission rate distributions were calculated and compared between KENO-VI (version 6.3) and Shift. As previously discussed, the number of particle histories was significantly increased in the KENO-VI calculation to reduce the local uncertainty of the stochastic calculations. All results are presented in Appendix B. Figures 10–13 below provide examples of the Shift results and differences from KENO-VI, with the total statistical results shown in Table 8.

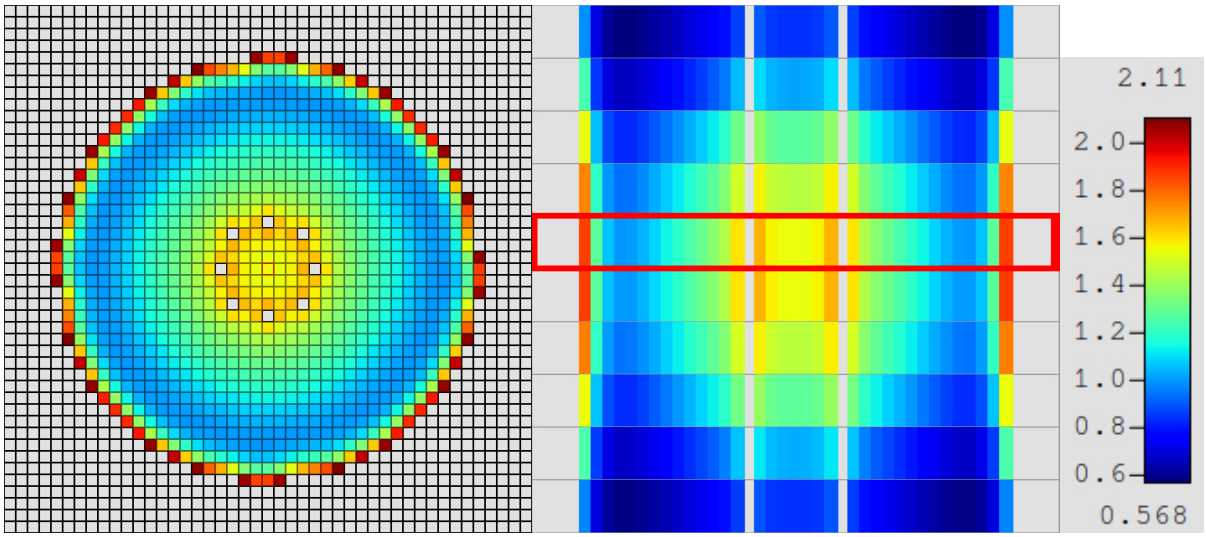

Figure 10: Shift Radial (left) and axial (right) fission rate distributions for Case 7.

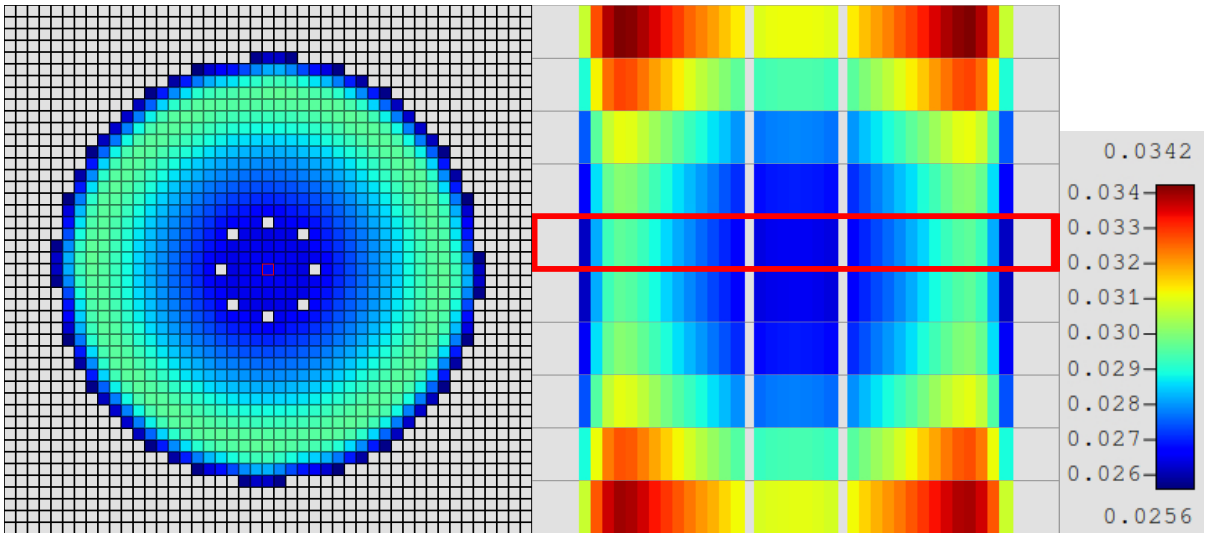

Figure 11: Shift radial (left) and axial (right) percent uncertainties for Case 7.

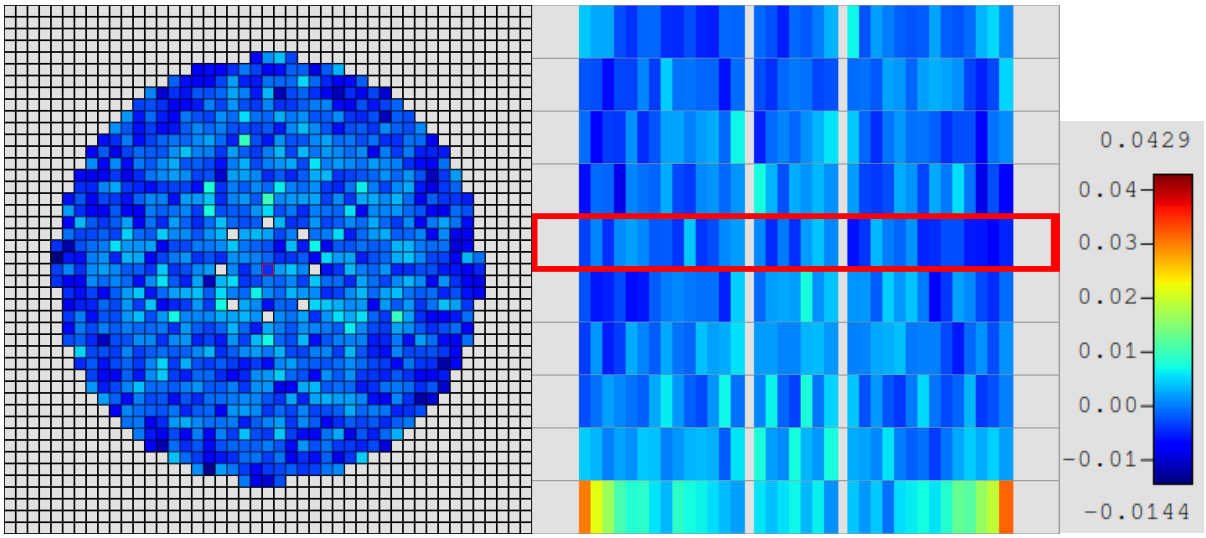

Figure 12: Radial (left) and axial (right) fission rate differences (Shift-KENO-VI) for Case 7.

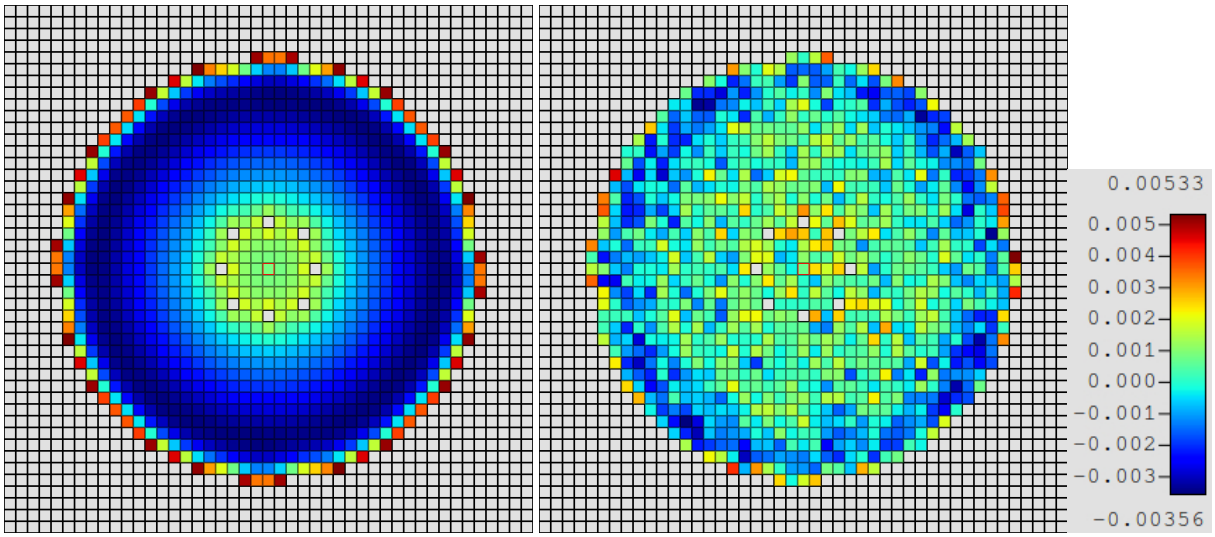

Figure 13: Shift (left) radial fission rates (left) and KENO-VI difference (right) for Case 7.

Table 8: Normalized Fission Rate Distribution Statistics, Shift-KENO-VI

Case	k-eff Diff	3D RMS	3D Max	2D RMS	2D Max	AO Diff
1	7	0.43%	3.70%	0.10%	0.57%	−0.18%
2	13	0.50%	4.12%	0.13%	0.62%	−0.19%
3	13	0.50%	3.87%	0.13%	0.55%	−0.21%
4	8	0.49%	3.59%	0.13%	0.55%	−0.20%
5	14	0.49%	4.02%	0.14%	0.64%	−0.19%
6	8	0.51%	4.00%	0.13%	0.70%	−0.22%
7	11	0.48%	4.29%	0.13%	0.53%	−0.18%
8	7	0.48%	3.84%	0.13%	0.62%	−0.18%
9	10	0.49%	4.27%	0.13%	0.52%	−0.19%
10	9	0.50%	4.19%	0.13%	0.76%	−0.20%
11	15	0.51%	4.07%	0.13%	0.53%	−0.23%
12	9	0.50%	3.63%	0.13%	0.50%	−0.19%
13	12	0.50%	4.28%	0.13%	0.49%	−0.20%
14	17	0.50%	4.02%	0.13%	0.51%	−0.21%
15	0	0.42%	2.82%	0.13%	0.45%	−0.18%
Average	**10**	**0.49%**	**3.91%**	**0.13%**	**0.57%**	**−0.20%**
St Dev	**4**	**0.03%**	**0.38%**	**0.01%**	**0.08%**	**0.01%**

Note that comparison of two stochastic codes includes non-trivial uncertainty, particularly when limited by computing resources. As shown in Appendix D, estimates of actual uncertainty in fuel rod fission rates are at least 0.1% (0.6% maximum) for Shift and 0.3% (1.4% maximum) for KENO-VI. The results indicate only a slightly larger 3D RMS difference at 0.5%, indicating extremely good observable agreement between the two high-fidelity MC codes. The 2D RMS difference is very low at 0.1%, benefiting from the variance reduction that occurs when the axial integration is performed.

Finally, the fission rate distributions were compared between Shift and MPACT, using both TCP_0 and P_2 scattering treatments. Due to the small size of the experiment and larger moderator density, the P_2

scattering case is expected to better match the MC results. Figures 14–16 provide examples of MPACT results and differences from Shift for Case 15, and Tables 9 and 10 provide the statistical summaries of the results for TCP_0 and P_2 scattering, respectively. For all the calculation results, please see Appendix C.

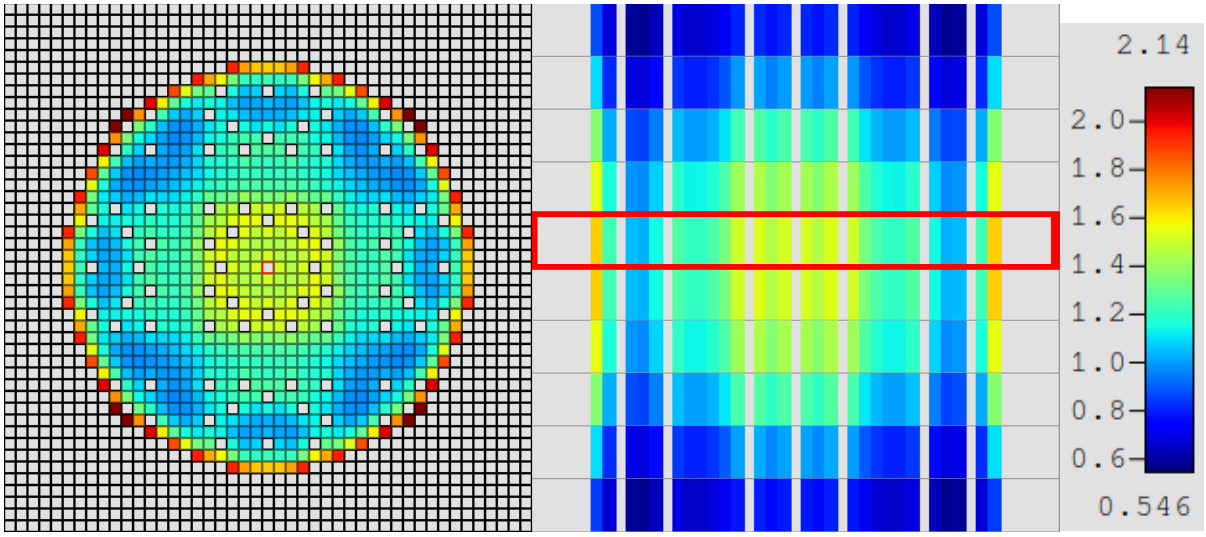

Figure 14: MPACT radial (left) and axial (right) fission rate distributions for Case 15 (P_2).

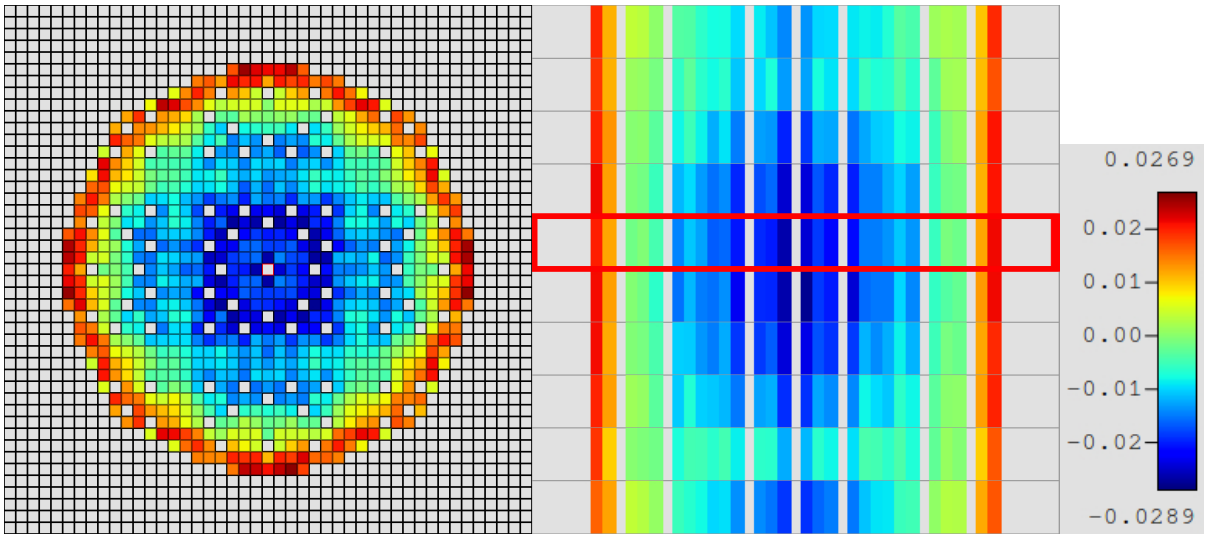

Figure 15: Radial (left) and axial (right) fission rate differences (MPACT-Shift) for Case 15 (P_2).

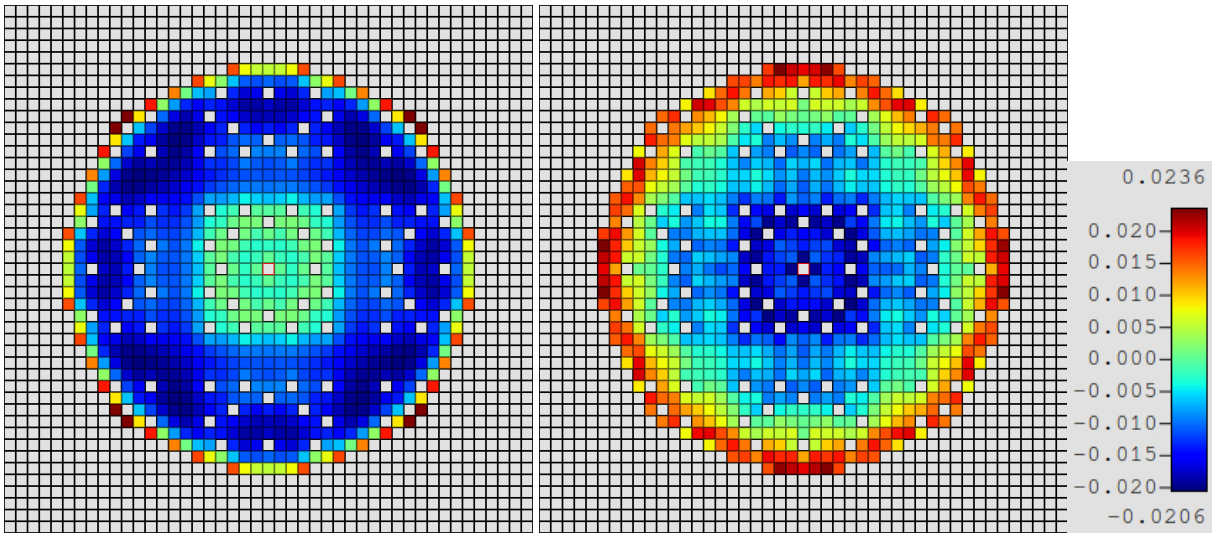

Figure 16: MPACT (left) radial fission rates (left) and Shift difference (right) for Case 15 (P_2).

Table 9: Normalized fission rate distribution statistics, MPACT-Shift, TCP_0 scattering.

Case	k-eff Diff	3D RMS	3D Max	2D RMS	2D Max	AO Diff
1	130	1.03%	−3.15%	0.99%	−2.47%	−0.07%
2	130	1.03%	−3.61%	1.00%	−2.68%	−0.06%
3	129	1.04%	−3.26%	1.00%	−2.51%	−0.05%
4	131	1.03%	−2.98%	0.99%	−2.31%	−0.05%
5	131	1.01%	−3.12%	0.98%	−2.34%	−0.05%
6	133	1.01%	−2.97%	0.98%	−2.31%	−0.04%
7	129	1.06%	−3.50%	1.02%	−2.55%	−0.05%
8	133	1.03%	−2.85%	0.99%	−2.23%	−0.04%
9	133	1.01%	−2.97%	0.97%	−2.31%	−0.05%
10	136	1.00%	−2.99%	0.96%	−2.30%	−0.05%
11	123	1.06%	−3.06%	1.02%	−2.45%	−0.05%
12	126	1.04%	−3.00%	1.00%	−2.33%	−0.05%
13	130	1.02%	−3.11%	0.99%	−2.33%	−0.05%
14	129	1.01%	−2.92%	0.98%	−2.34%	−0.06%
15	failed					
Average	**130**	**1.03%**	**−2.90%**	**0.99%**	**−2.23%**	**−0.05%**
St Dev	**5**	**0.02%**	**0.83%**	**0.02%**	**0.63%**	**0.01%**

Table 10: Normalized Fission Rate Distribution Statistics, MPACT-Shift, P_2 Scattering

Case	k-eff Diff	3D RMS	3D Max	2D RMS	2D Max	AO Diff
1	43	1.17%	3.06%	1.14%	2.55%	−0.07%
2	43	1.17%	−3.52%	1.15%	−2.57%	−0.06%
3	42	1.17%	−3.09%	1.14%	2.62%	−0.04%
4	45	1.18%	3.10%	1.15%	2.61%	−0.05%
5	45	1.17%	3.04%	1.14%	2.63%	−0.05%
6	46	1.17%	3.06%	1.14%	2.60%	−0.04%
7	46	1.20%	−3.20%	1.17%	2.69%	−0.04%
8	48	1.18%	3.04%	1.15%	2.67%	−0.04%
9	47	1.17%	3.30%	1.14%	2.71%	−0.05%
10	49	1.15%	3.07%	1.13%	2.74%	−0.05%
11	41	1.19%	2.95%	1.16%	2.54%	−0.05%
12	44	1.18%	3.01%	1.16%	2.60%	−0.06%
13	46	1.18%	−2.94%	1.15%	2.56%	−0.06%
14	42	1.16%	2.93%	1.13%	2.54%	−0.06%
15	48	1.14%	−2.89%	1.10%	2.36%	0.02%
Average	**45**	**1.17%**	**3.08%**	**1.14%**	**2.60%**	**−0.05%**
St Dev	**3**	**0.01%**	**0.16%**	**0.02%**	**0.09%**	**0.02%**

Though P_2 scattering should produce a better answer, in these results the fission rate distributions are slightly worse. The 3D RMS differences are 1.0% and 1.2% for TCP_0 and P_2 scattering, respectively. The 2D RMS differences are similar at 1.0% and 1.1% for TCP_0 and P_2 scattering, respectively. Both results demonstrate good agreement between the two codes. The similarity of the 2D and 3D values also indicate very good agreement in the axial direction (with 0.0% difference in axial offset on average).

5. CONCLUSIONS

This analysis demonstrates that neutronic methods in VERA can accurately predict the reactivity of the 7uPCX experiment conducted at Sandia National Laboratory. The Shift high-fidelity MC code produces results that are 120 pcm below measurements, which have a reported measurement uncertainty of 100 pcm. Shift also agrees very well (−16 pcm) with the KENO-VI MC code, which was also used in the benchmark specification.

The MPACT deterministic neutronics code in VERA, which is the workhorse for reactor simulation with thermal hydraulic coupling and depletion, predicts reactivity of the 7uPCX experiment within the 100 pcm uncertainty. Use of the default TCP_0 scattering option produces only a 6 pcm difference from measurement, although Case 15 failed to converge. The more rigorous P_2 scattering option converges for all cases, running faster than TCP_0, and it agrees well with measurement, with an average of 77 pcm difference. The standard deviation for all cases and codes is less than 15 pcm, indicating consistent accuracy across the variety of experiment configurations.

For neutron flux distribution, MPACT agreed very well with KENO-VI, with an RMS difference over all cases of 1.1% (TCP_0) and 1.2% (P_2). The radial distributions are slightly better, and the axial distributions are excellent. Likewise, MPACT agreed very well with Shift for fission rate distribution, with an RMS difference of 1.0% (TCP0) and 1.2% (P2). MPACT also used 65× fewer computing resources than Shift.

The fission rate distributions of the KENO-VI and Shift MC codes agree with a 0.5% RMS difference, which is estimated to be just larger than the statistically combined estimated uncertainty of the two codes.

The following additional conclusions are made based on observations of the analysis results:

- New results agree well with previously calculated results, based on older code versions and older ENDF data versions.
- KENO-VI results improved somewhat relative to the original specification [1] due to the use of SCALE 6.2.
- All of the MC-based codes (KENO-V.a, KENO-VI, and Shift) produce comparable results given the same data library.
- MG calculations have a negative bias compared to CE calculations. The 252-group results from KENO-VI are 99 pcm worse than the CE results, and the 56-group results are 133 pcm worse. However, these increased differences are not so large as to warrant development of a new MG library.
- Use of ENDF/B-VIII.0 has a slightly negative bias compared to ENDF/B-VII.1. In KENO-VI, use of ENDF/B-VIII.0 worsens the results by 67 pcm. In Shift, use of ENDF/B-VIII.0 worsens the results by 43 pcm. There is no indication from these results that ENDF/B-VIII.0 data are needed to model HALEU fuel.
- The results from the MPACT 252-group data library are not good and require more investigation and possibly library optimization. At this time this library should not be used.

For future work, the stability of the MPACT 2D/1D transport method should be evaluated for small experiments like this, and the use of P_2 scattering may be warranted under certain circumstances. Also, the fission rate distribution comparisons between MPACT and the MC-based codes may need to be further researched to understand why better agreement is not seen with P_2 scattering rather than TCP_0 scattering. Finally, if the MPACT 252-group data library is to be used for analyses, further evaluation and optimization is required.

6. REFERENCES

1. G. A. Harms and A. D. Miller, *Water-Moderated Square-Pitched U(6.90)O_2 Fuel Rod Lattices with 0.52 Fuel-to-Water Volume Ratio (0.855 cm pitch).* LEU-COMP-THERM-078. NEA/NSC/DOC/(95)03/IV Volume IV, SAND2013-1646P, Sandia National Laboratory, Albuquerque, NM (2103).
2. W. A. Wieselquist, R. A. Lefebvre, and M. A. Jessee, Eds., *SCALE Code System,* ORNL/TM-2005/39, Version 6.2.4, Oak Ridge National Laboratory, Oak Ridge, TN (2020). Available from Radiation Safety Information Computational Center as CCC-834.
3. M. Baird et al., *VERA 4.2 Release Notes*, CASL-U-2021-1977-000, CASL (September 2021), available online at https://vera.ornl.gov/wp-content/uploads/2021/09/VERA_4.2_Release_Notes.pdf
4. B. Collins, S. Palmtag, A. Godfrey, T. Downar, and K. Clarno, "Capabilities of VERA Version 4," *Proc. of the Consortium for Advanced Simulation of Light Water Reactors (CASL) Program*, 2020 ANS Virtual Winter Meeting, November 16–19, 2020, ANS, pp. 106–110 (2020).
5. MPACT Development Team, *MPACT Theory Manual, Version 2.0.0*, Oak Ridge National Laboratory and University of Michigan, CASL-U-2015-0078-000 (2015).
6. K. Kim, M. Williams, D. Wiarda, and A. Godfrey, "Development of a New 47-group Library for the CASL Neutronics Simulator," *Proc. ANS MC2015—Joint International Conference on Mathematics and Computation (M&C), Supercomputing in Nuclear Applications (SNA) and the Monte Carlo (MC) Method*, Nashville, Tennessee, April 19–23 (2015).
7. T. Pandya, S. Johnson, T. Evans, G. Davidson, S. Hamilton, and A. Godfrey, "Implementation, Capabilities, and Benchmarking of Shift, a Massively Parallel Monte Carlo Radiation Transport Code," *Journal of Computational Physics*, **308**, 239–272 (2015).
8. E. M. Saylor, W. J. Marshall, J. B. Clarity, Z. Clifton, and B. T. Rearden, *Criticality Safety Validation of SCALE 6.2.2*. ORNL/TM-2018/884, ORNL (September 2018). Web. doi:10.2172/1479759.
9. T. Pandya, S. Johnson, B. Langley, R. Lefebvre, and B. J. Marshall, *Verification and Validation of New SCALE Sequence: CSASSHIFT*, ORNL/SR-2016/401, ORNL (August 2016).
10. A. Godfrey, *VERA Core Physics Benchmark Progression Problem Specifications*, CASL-U-2012-0131-004, Revision 4, CASL (August 2014).
11. "NCRC INL's Nuclear Computational Resource Center," INL, available online at https://inl.gov/ncrc/

APPENDIX A. Neutron Flux Comparisons between MPACT and KENO-VI

APPENDIX A. NEUTRON FLUX COMPARISONS BETWEEN MPACT AND KENO-VI

The following results are comparisons of normalized total neutron flux distributions calculated for the 7uPCX experiment. The reference solutions are from KENO-VI mesh tally calculations using CE ENDF/B-VII.1 data in SCALE 6.2.4. The KENO-VI results are derived from the original models [1] and were generated with 2 billion active particle histories. The MPACT results are from VERA version 4.3RC7 using the default transport-corrected P_0 and the higher-order P_2 scattering treatments. Tables A-1 and A-2 provide the overall statistical summary, whereas Figures A-1 through A-74 provide 2D color plots of the relevant results. For each case, the following are provided:

- KENO-VI normalized total flux distribution, presented as radial and axial slices through the center of the experiment.
- KENO-VI calculated fractional uncertainty in the total flux distribution, presented as radial and axial slices through the center of the experiment.
- Differences between MPACT and KENO-VI normalized total flux distributions, presented as radial and axial slices through the center of the experiment, where the MPACT result is using TCP_0 scattering.
- Differences between MPACT and KENO-VI normalized total flux distributions, presented as radial and axial slices through the center of the experiment, where the MPACT result is using P_2 scattering.
- Differences between MPACT and KENO-VI radial (axially integrated) normalized total flux distributions for both TCP_0 and P_2 MPACT results.

Table A-1: Normalized Total Flux Distribution Statistics, MPACT-KENO-VI, TCP_0 Scattering

Case	K-eff Diff	3D RMS	3D Max	2D RMS	2D Max	AO Diff
1	137	0.85%	−2.50%	0.75%	−1.51%	−0.21%
2	143	0.85%	−2.56%	0.74%	−1.53%	−0.23%
3	142	0.84%	−2.53%	0.74%	−1.59%	−0.20%
4	138	0.85%	−2.48%	0.75%	−1.48%	−0.22%
5	144	0.84%	−2.42%	0.74%	−1.49%	−0.20%
6	141	0.84%	−2.37%	0.73%	−1.43%	−0.22%
7	140	0.84%	−2.52%	0.74%	−1.61%	−0.18%
8	140	0.85%	−2.41%	0.74%	−1.45%	−0.19%
9	143	0.85%	−2.46%	0.75%	−1.50%	−0.20%
10	145	0.84%	−2.42%	0.73%	−1.45%	−0.20%
11	139	0.86%	−2.56%	0.76%	−1.57%	−0.23%
12	135	0.85%	−2.43%	0.75%	−1.48%	−0.21%
13	142	0.85%	−2.46%	0.74%	−1.47%	−0.22%
14	146	0.84%	−2.39%	0.74%	−1.51%	−0.21%
15				*failed*		
Average	**141**	**0.85%**	**−2.30%**	**0.74%**	**−1.40%**	**−0.21%**
St Dev	**3**	**0.01%**	**0.64%**	**0.01%**	**0.39%**	**0.01%**

Table A-2: Normalized Total Flux Distribution Statistics, MPACT-KENO-VI, P_2 Scattering

Case	k-eff Diff	3D RMS	3D Max	2D RMS	2D Max	AO Diff
1	50	0.73%	−1.97%	0.61%	−1.11%	−0.20%
2	56	0.73%	−2.08%	0.61%	−1.16%	−0.22%
3	55	0.72%	−2.03%	0.61%	−1.17%	−0.19%
4	53	0.74%	−2.02%	0.61%	−1.11%	−0.22%
5	58	0.73%	−1.95%	0.61%	−1.11%	−0.20%
6	54	0.72%	−1.86%	0.60%	−1.08%	−0.22%
7	57	0.72%	−1.99%	0.61%	−1.20%	−0.17%
8	55	0.73%	−1.95%	0.61%	−1.11%	−0.19%
9	57	0.73%	−2.02%	0.61%	−1.13%	−0.20%
10	58	0.72%	−1.95%	0.60%	−1.07%	−0.20%
11	56	0.74%	−2.11%	0.62%	−1.15%	−0.23%
12	53	0.73%	−1.94%	0.61%	−1.12%	−0.21%
13	58	0.73%	−1.93%	0.61%	−1.09%	−0.22%
14	59	0.72%	−1.93%	0.60%	−1.13%	−0.21%
15	48	0.72%	−2.15%	0.59%	−1.06%	−0.13%
Average	**55**	**0.73%**	**−1.99%**	**0.61%**	**−1.12%**	**−0.20%**
St Dev	**3**	**0.01%**	**0.8%**	**0.01%**	**0.04%**	**0.03%**

Note that the MPACT result for Case 15 with TCP_0 scattering is not included because it did not successfully converge.

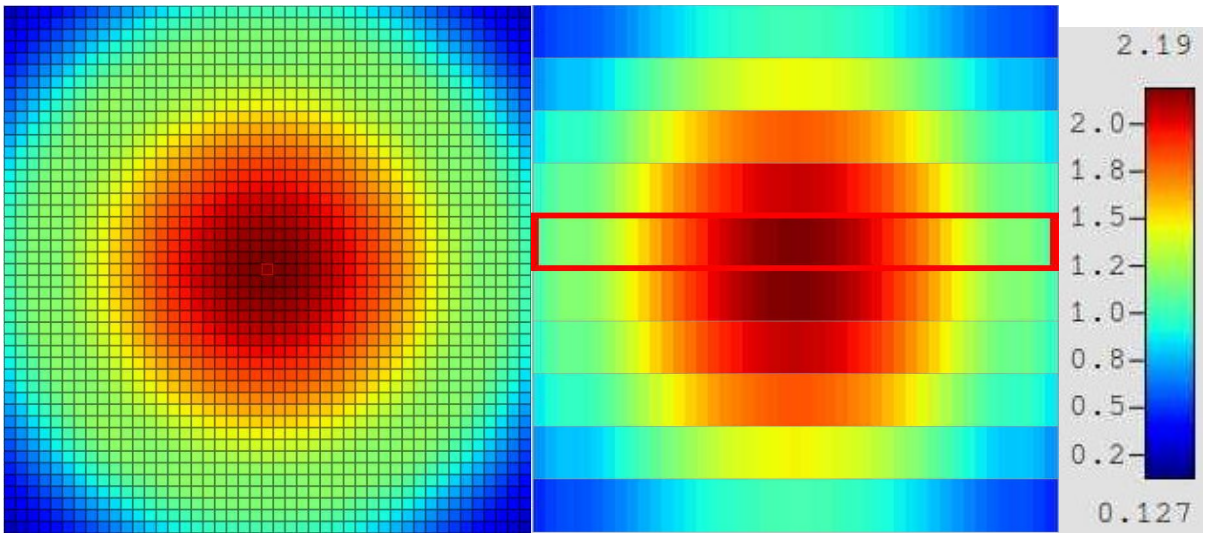

Figure A-1: KENO-VI radial (left) and axial (right) slices of flux distributions for Case 1.

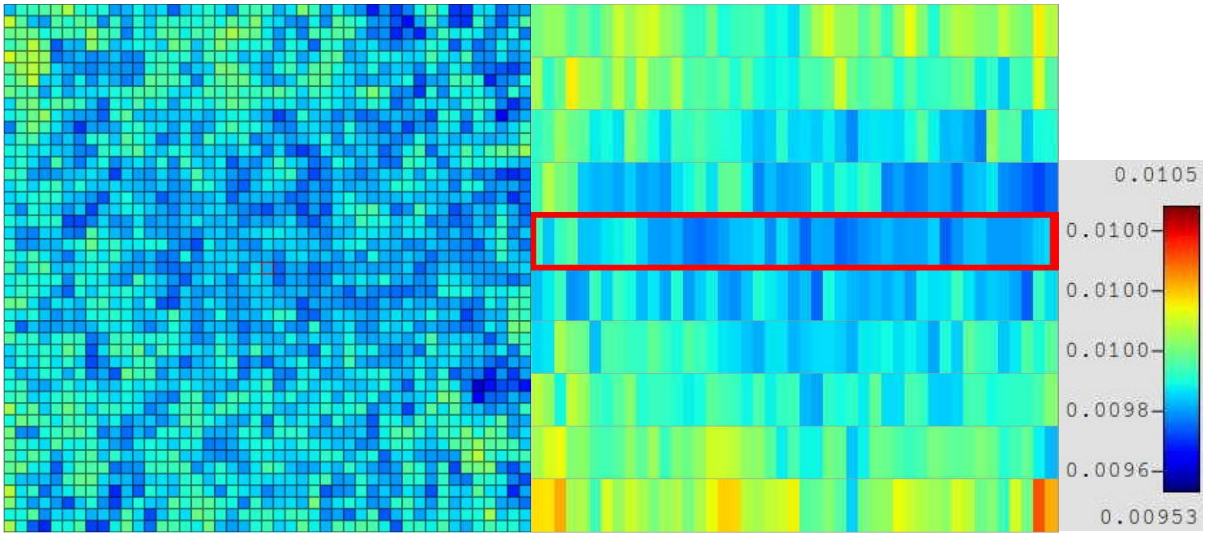

Figure A-2: KENO-VI radial (left) and axial (right) slices of fractional uncertainties for Case 1.

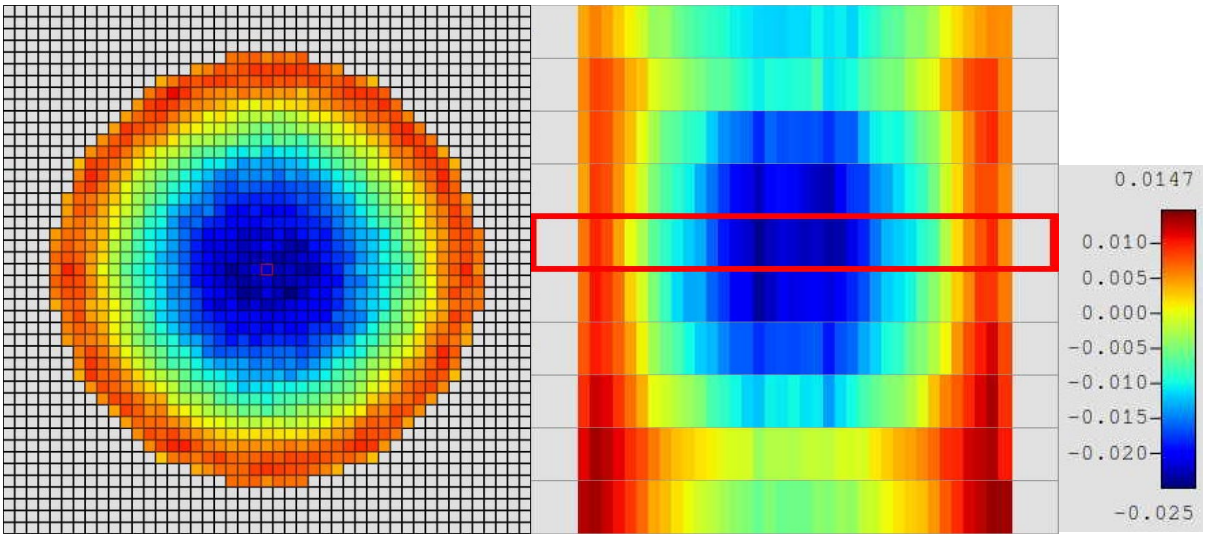

Figure A-3: MPACT radial (left) and axial (right) slices of flux distribution differences (TCP0) for Case 1.

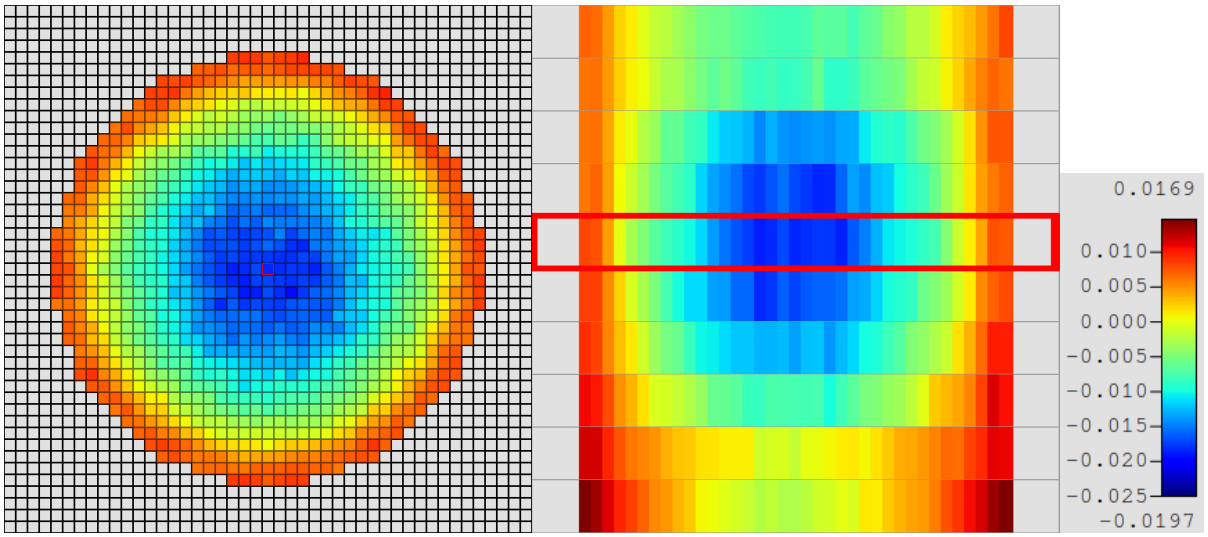

Figure A-4: MPACT radial (left) and axial (right) slices of flux distribution differences (P2) for Case 1.

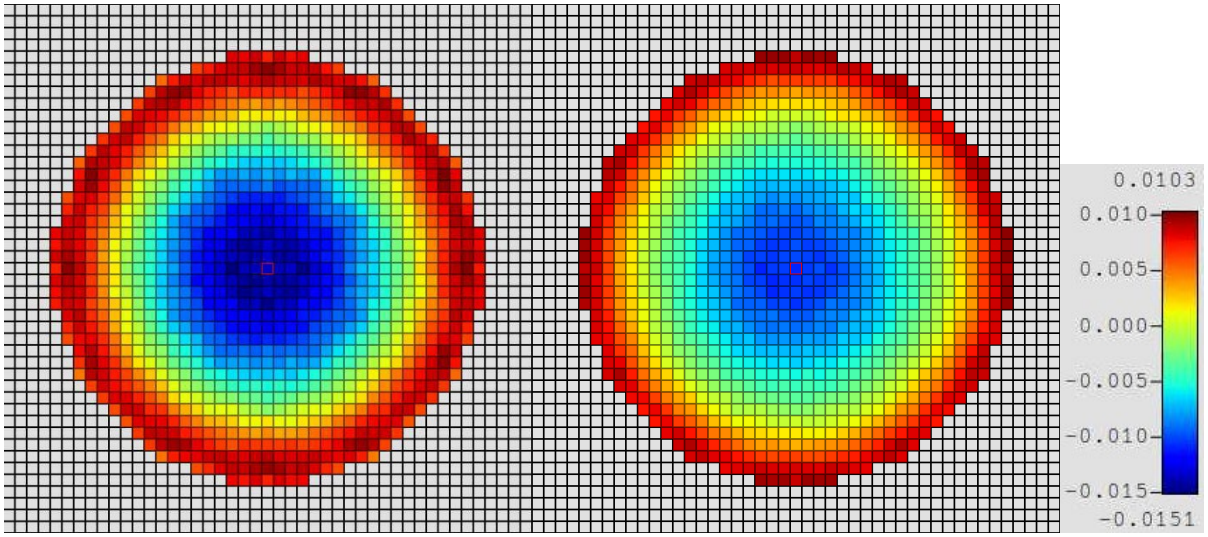

Figure A-5: MPACT radial flux distribution differences for TCP0 (left) and P2 (right) for Case 1.

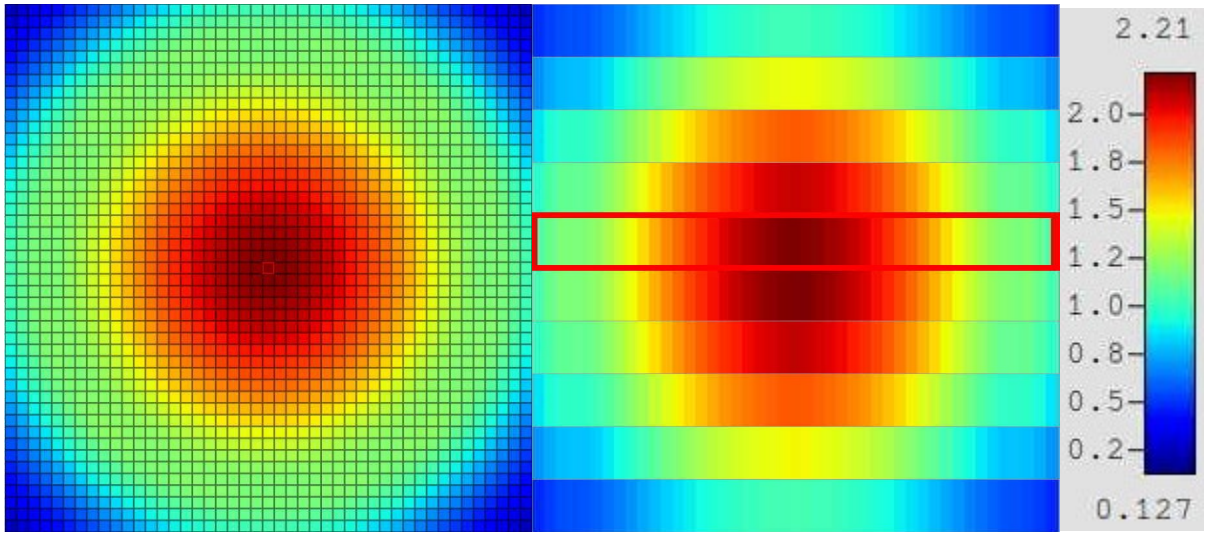

Figure A-6: KENO-VI radial (left) and axial (right) slices of flux distributions for Case 2.

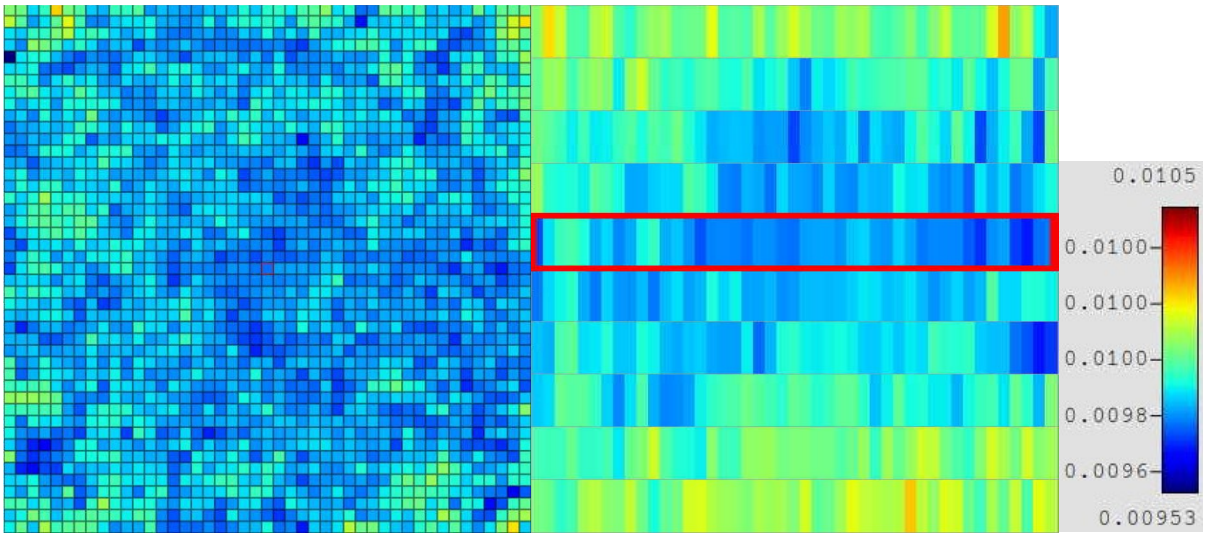

Figure A-7: KENO-VI radial (left) and axial (right) slices of fractional uncertainties for Case 2.

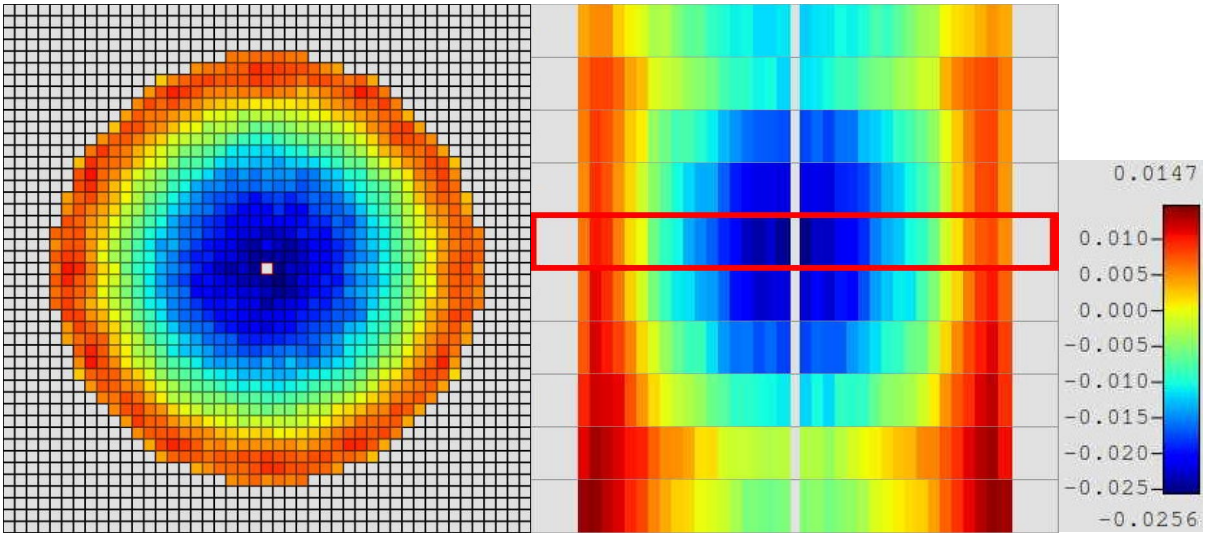

Figure A-8: MPACT radial (left) and axial (right) slices of flux distribution differences (TCP0) for Case 2.

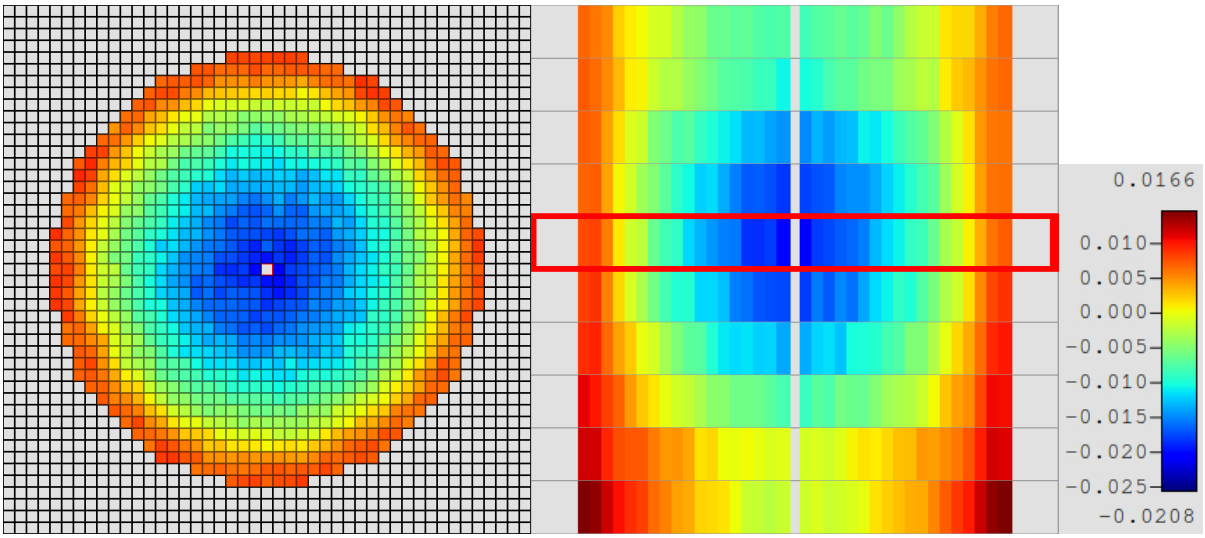

Figure A-9: MPACT radial (left) and axial (right) slices of flux distribution differences (P2) for Case 2.

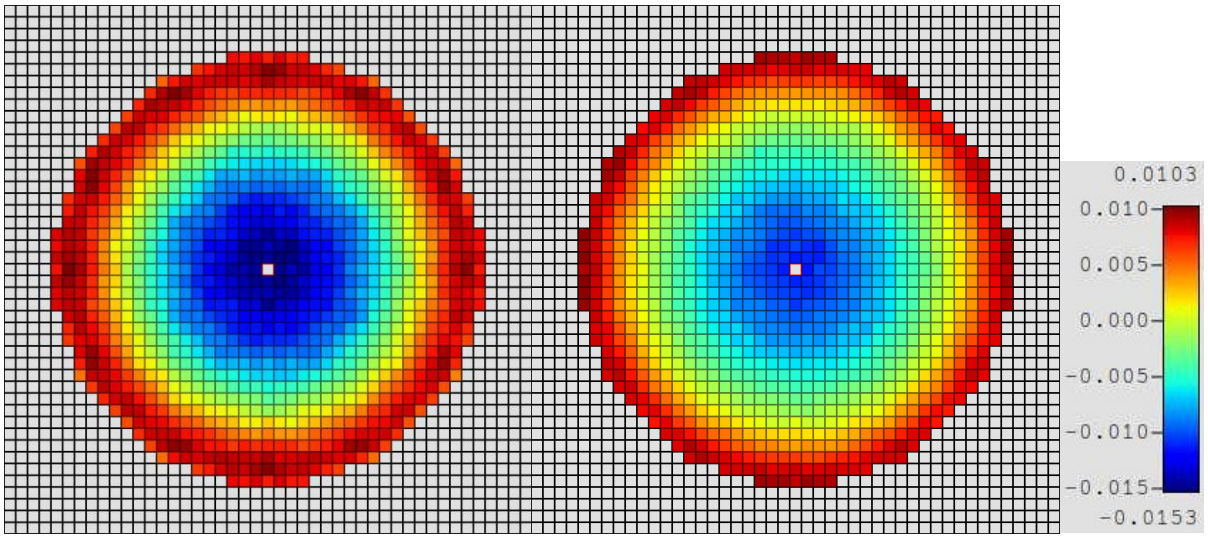

Figure A-10: MPACT radial flux distribution differences for TCP0 (left) and P2 (right) for Case 2.

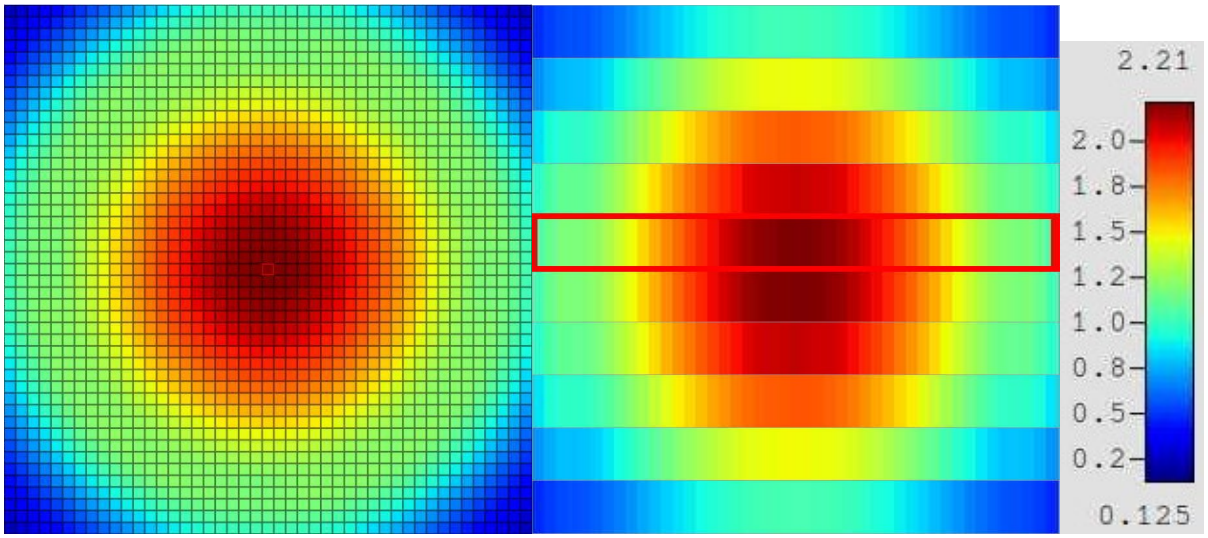

Figure A-11: KENO-VI radial (left) and axial (right) slices of flux distributions for Case 3

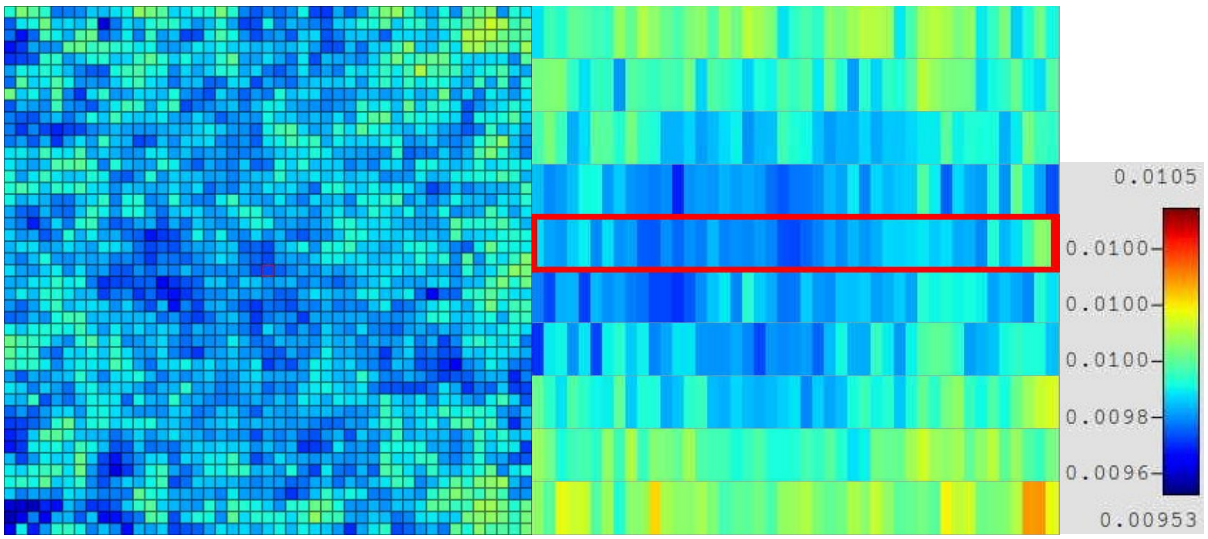

Figure A-12: KENO-VI radial (left) and axial (right) slices of fractional uncertainties for Case 3.

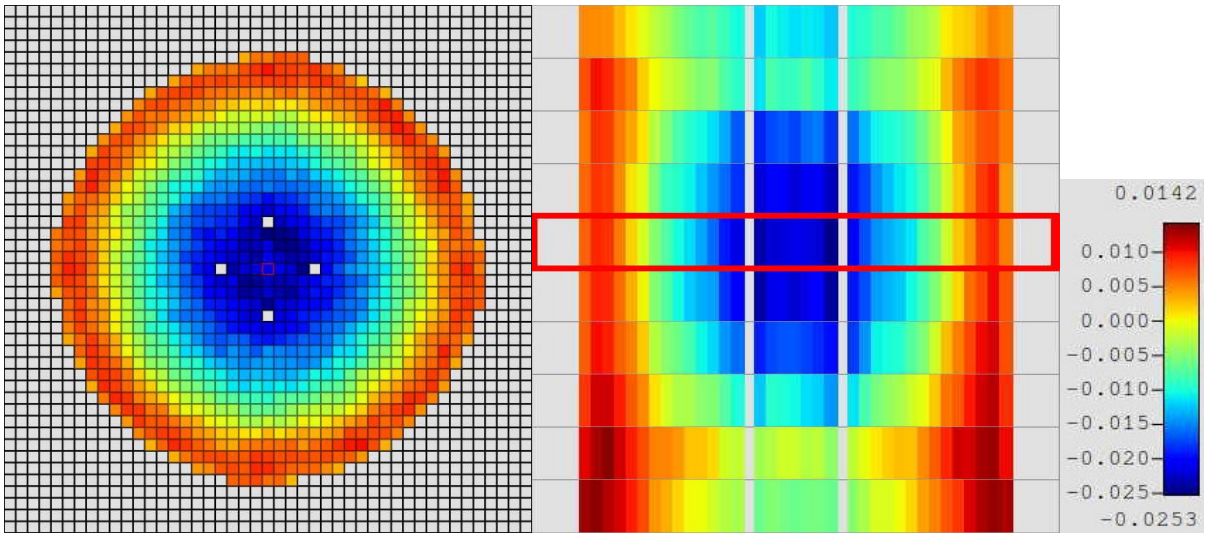

Figure A-13: MPACT radial (left) and axial (right) slices of flux distribution differences (TCP0) for Case 3.

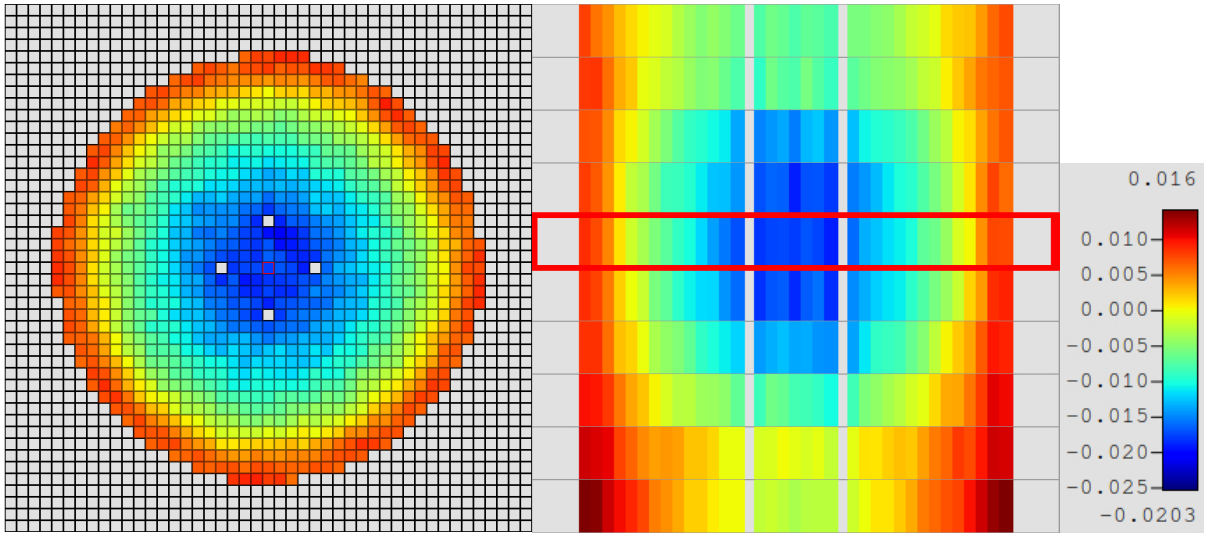

Figure A-14: MPACT radial (left) and axial (right) slices of flux distribution differences (P2) for Case 3.

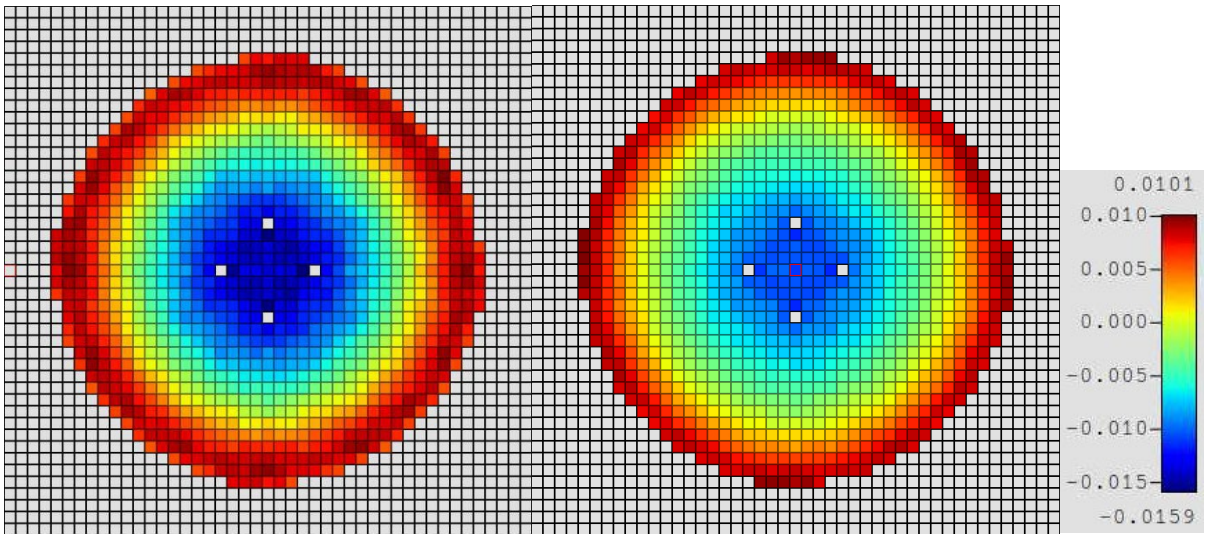

Figure A-15: MPACT radial flux distribution differences for TCP0 (left) and P2 (right) for Case 3.

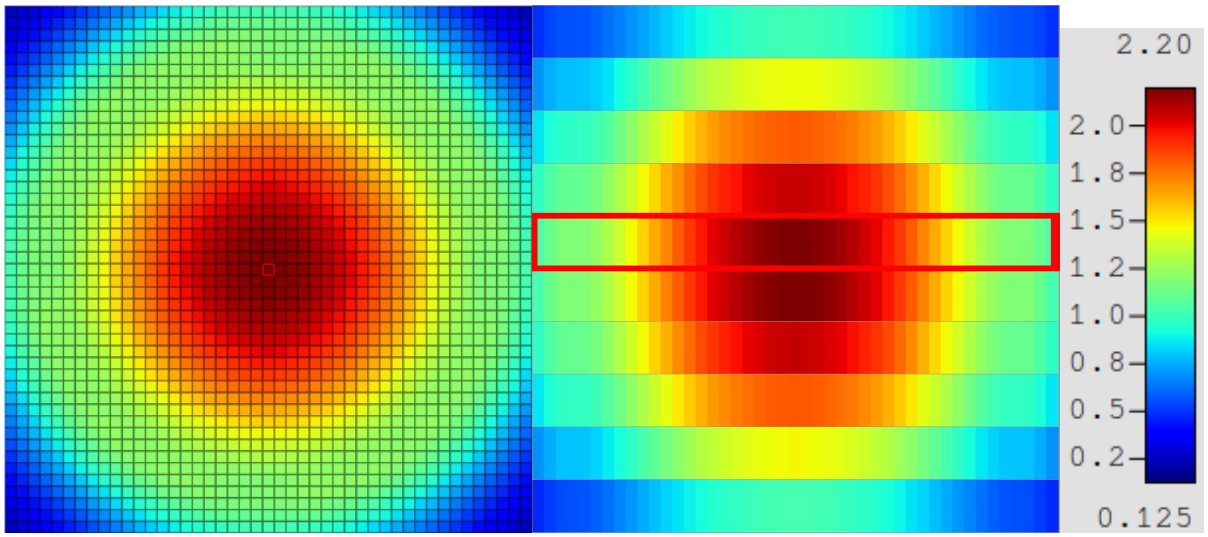

Figure A-16: KENO-VI radial (left) and axial (right) slices of flux distributions for Case 4.

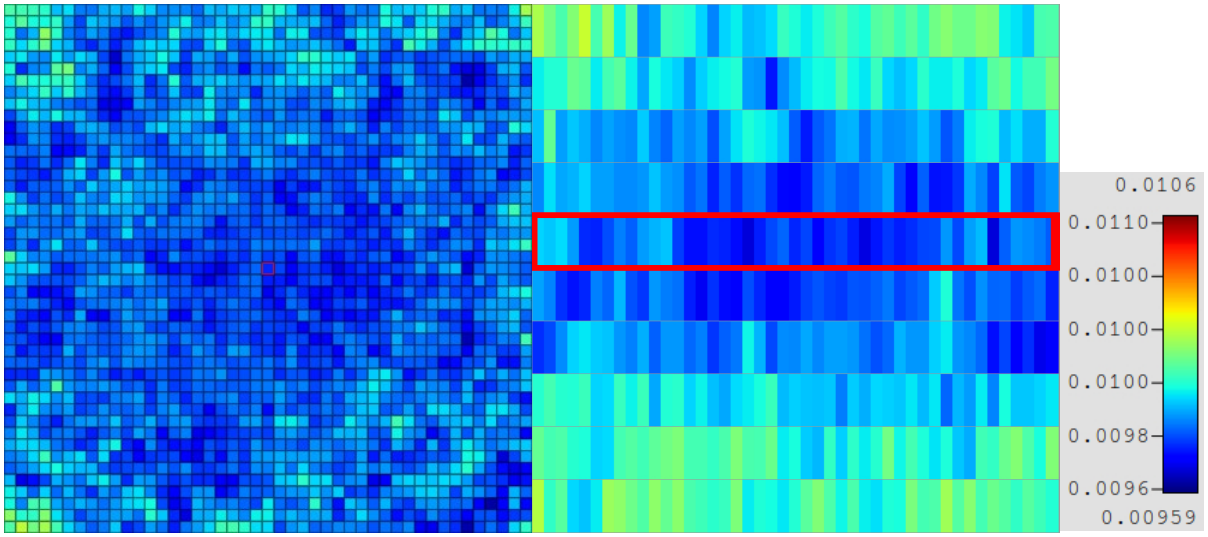

Figure A-17: KENO-VI radial (left) and axial (right) slices of fractional uncertainties for Case 4.

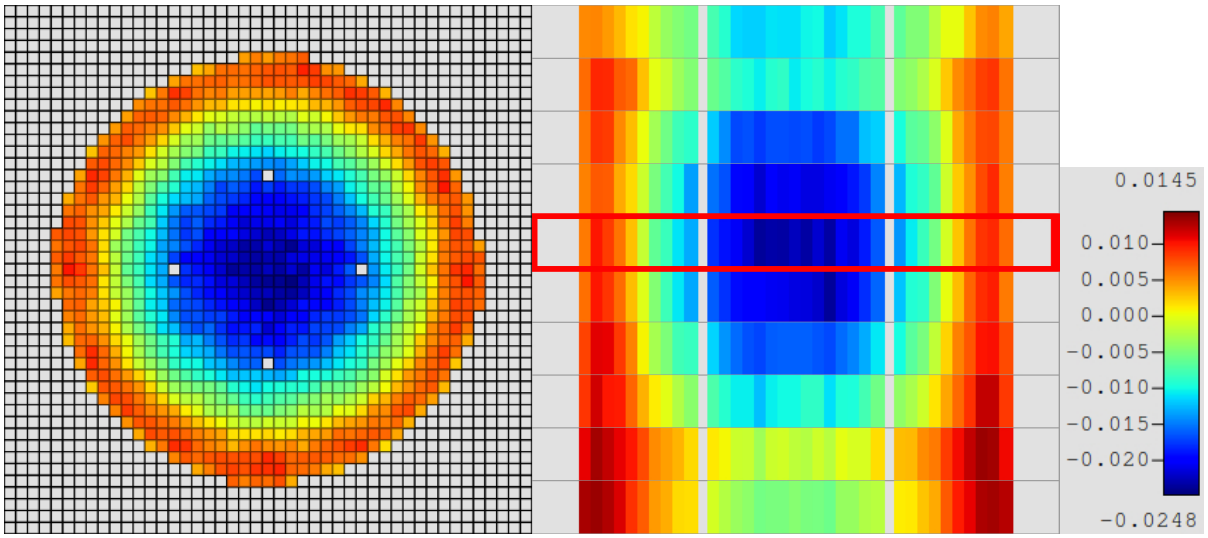

Figure A-18: MPACT radial (left) and axial (right) slices of flux distribution differences (TCP0) for Case 4.

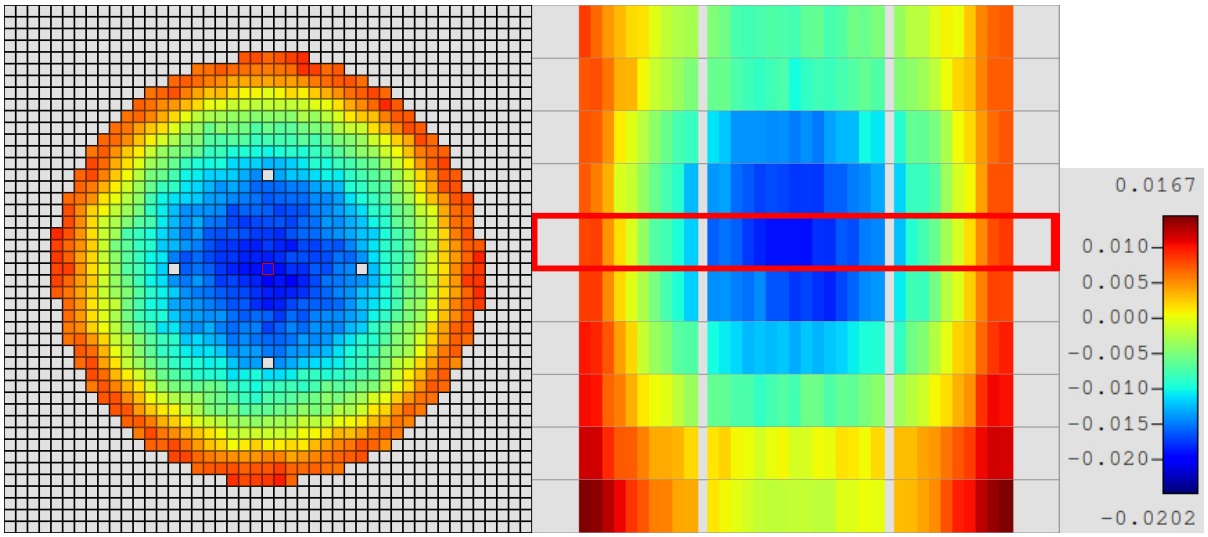

Figure A-19: MPACT radial (left) and axial (right) slices of flux distribution differences (P2) for Case 4.

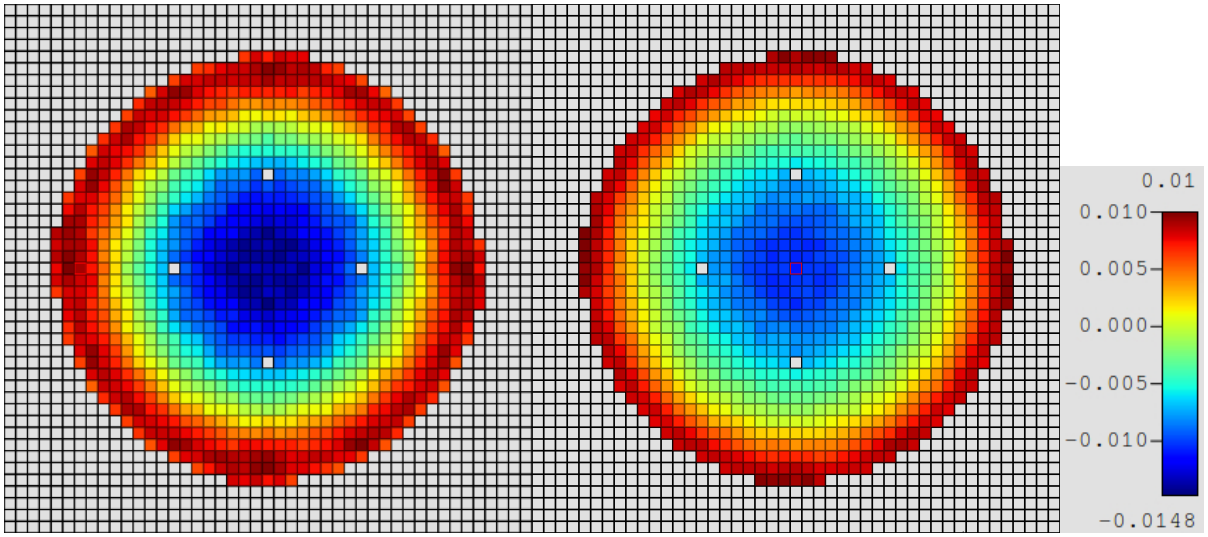

Figure A-20: MPACT radial flux distribution differences for TCP0 (left) and P2 (right) for Case 4.

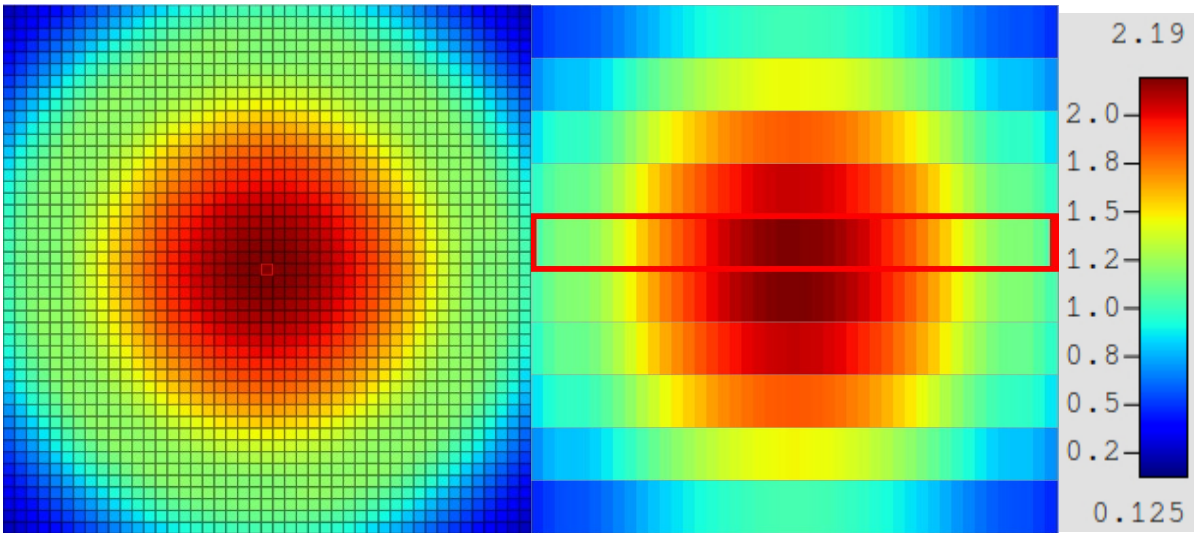

Figure A-21: KENO-VI radial (left) and axial (right) slices of flux distributions for Case 5.

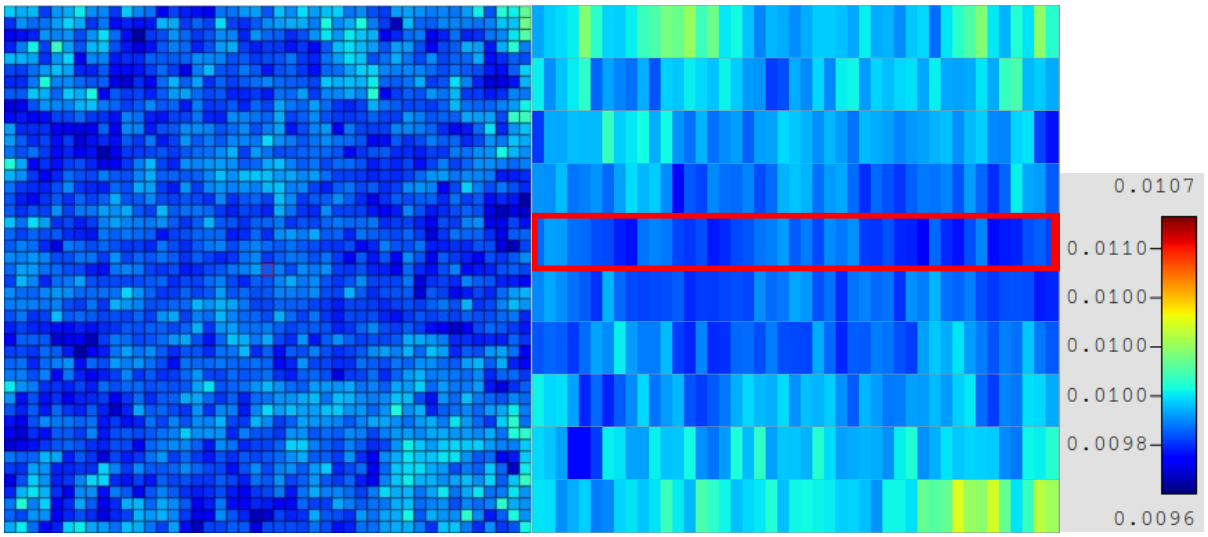

Figure A-22: KENO-VI radial (left) and axial (right) slices of fractional uncertainties for Case 5.

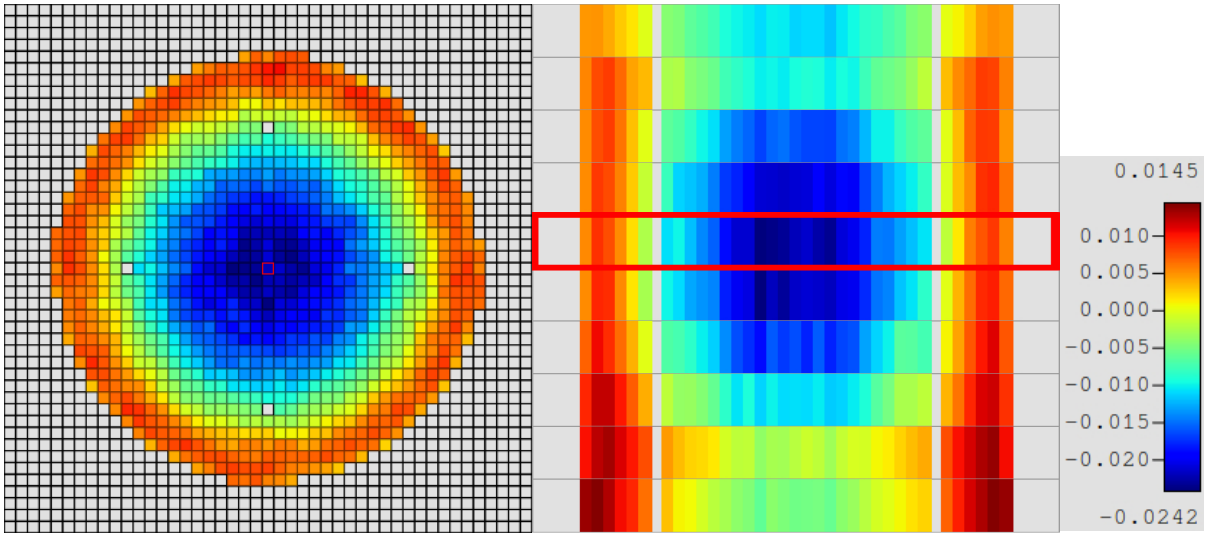

Figure A-23: MPACT radial (left) and axial (right) slices of flux distribution differences (TCP0) for Case 5.

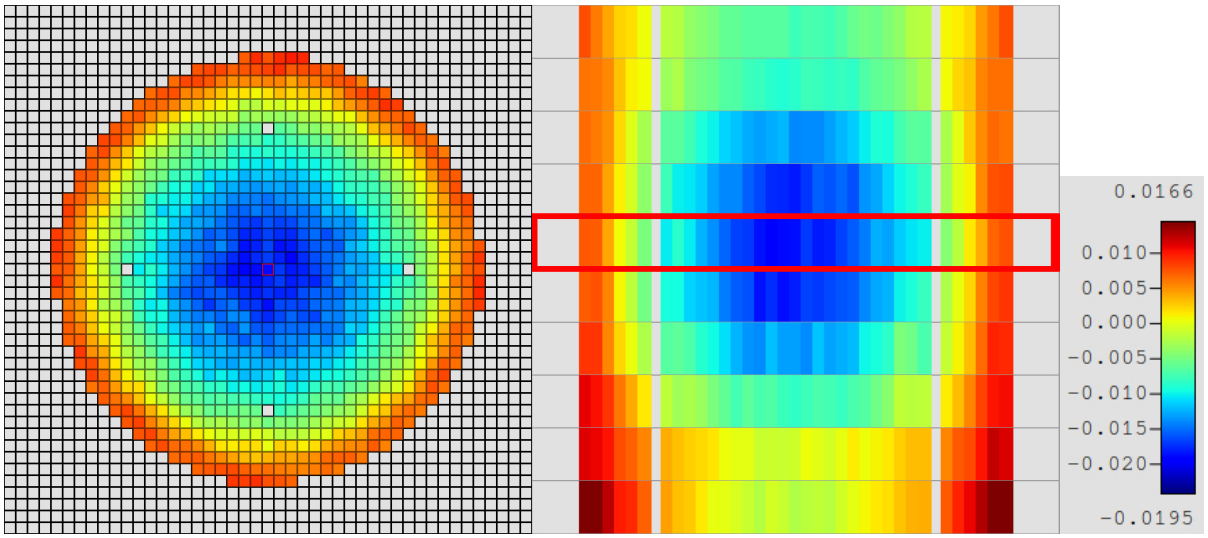

Figure A-24: MPACT radial (left) and axial (right) slices of flux distribution differences (P2) for Case 5.

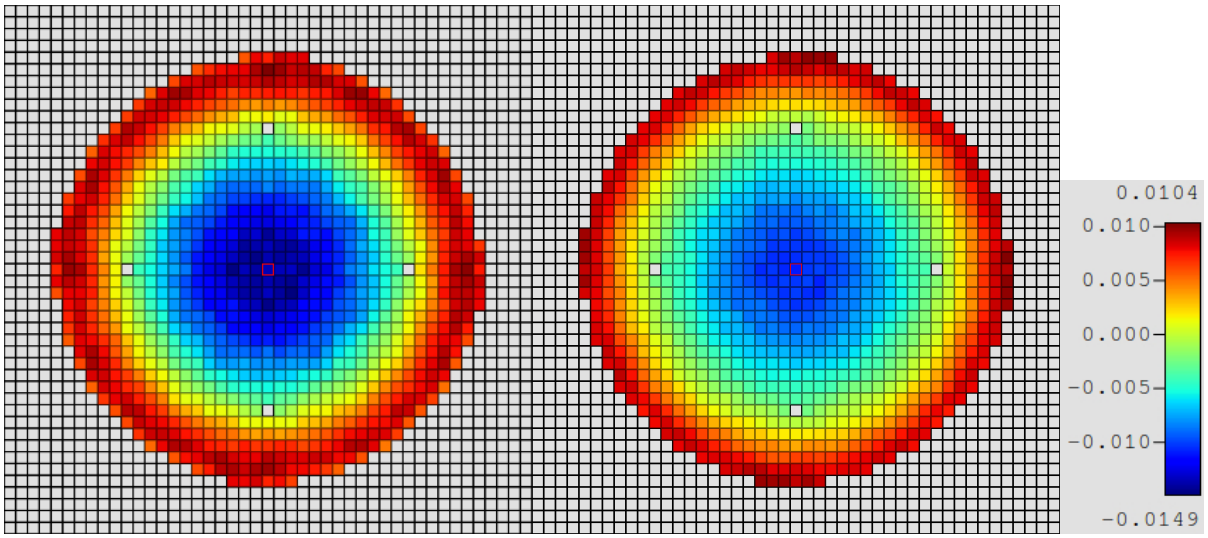

Figure A-25: MPACT radial flux distribution differences for TCP0 (left) and P2 (right) for Case 5.

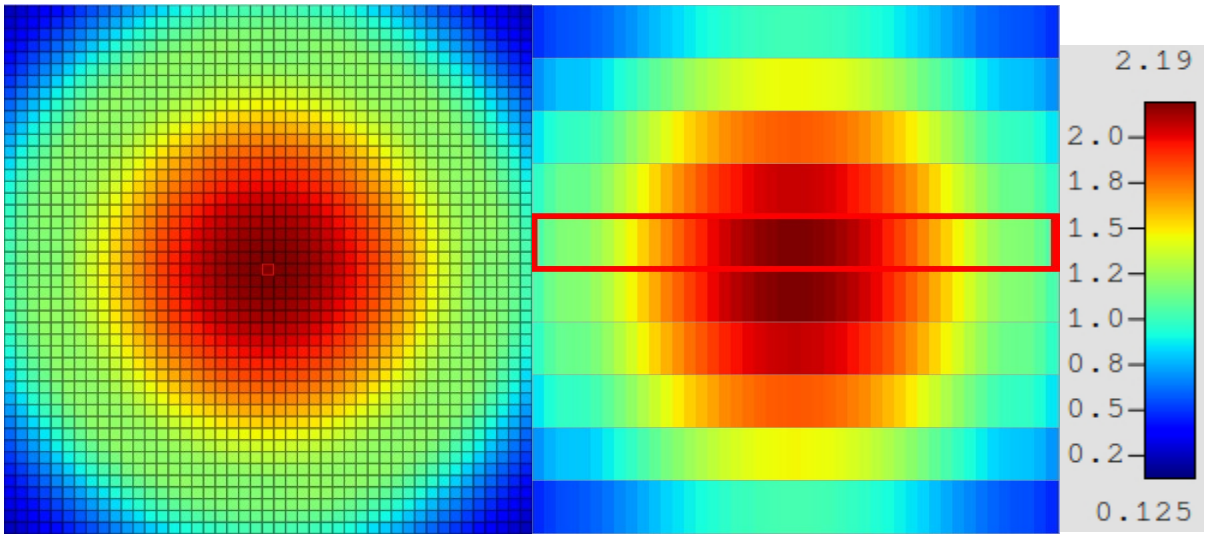

Figure A-26: KENO-VI radial (left) and axial (right) slices of flux distributions for Case 6.

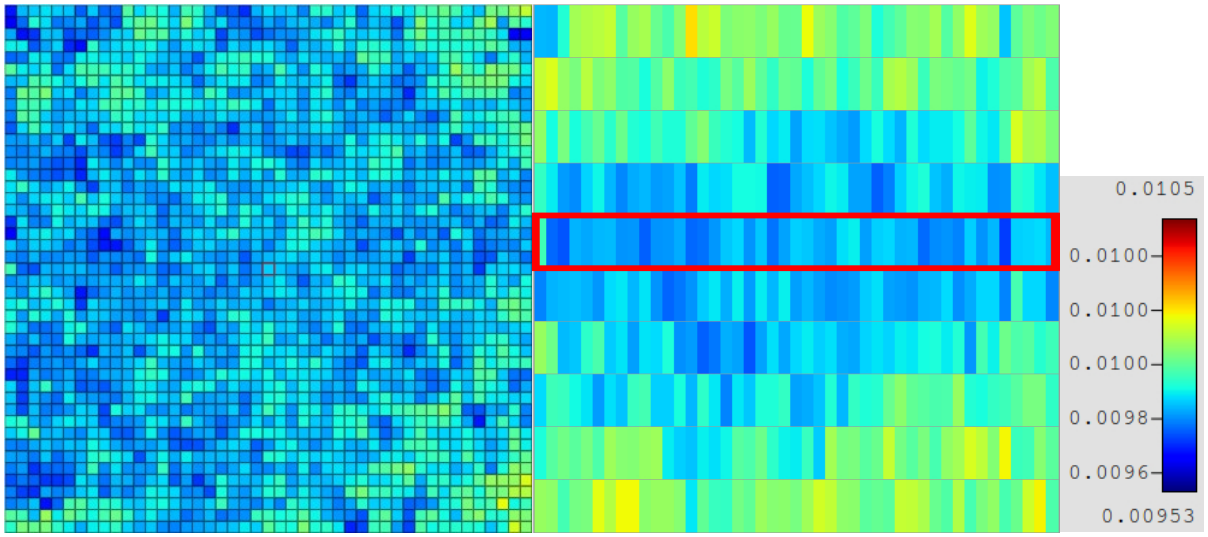

Figure A-27: KENO-VI radial (left) and axial (right) slices of fractional uncertainties for Case 6.

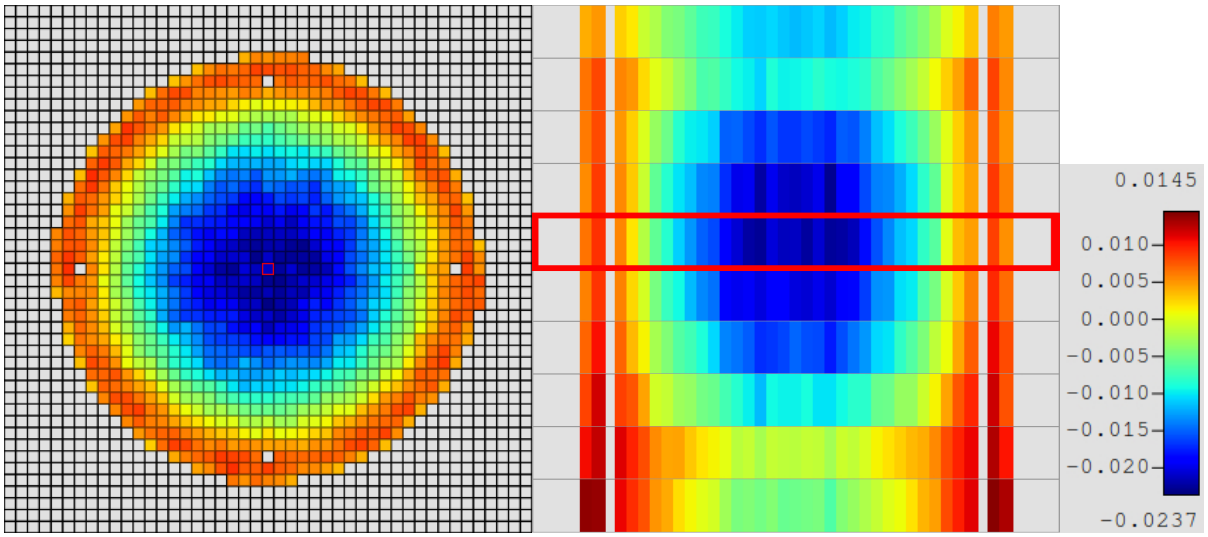

Figure A-28: MPACT radial (left) and axial (right) slices of flux distribution differences (TCP0) for Case 6.

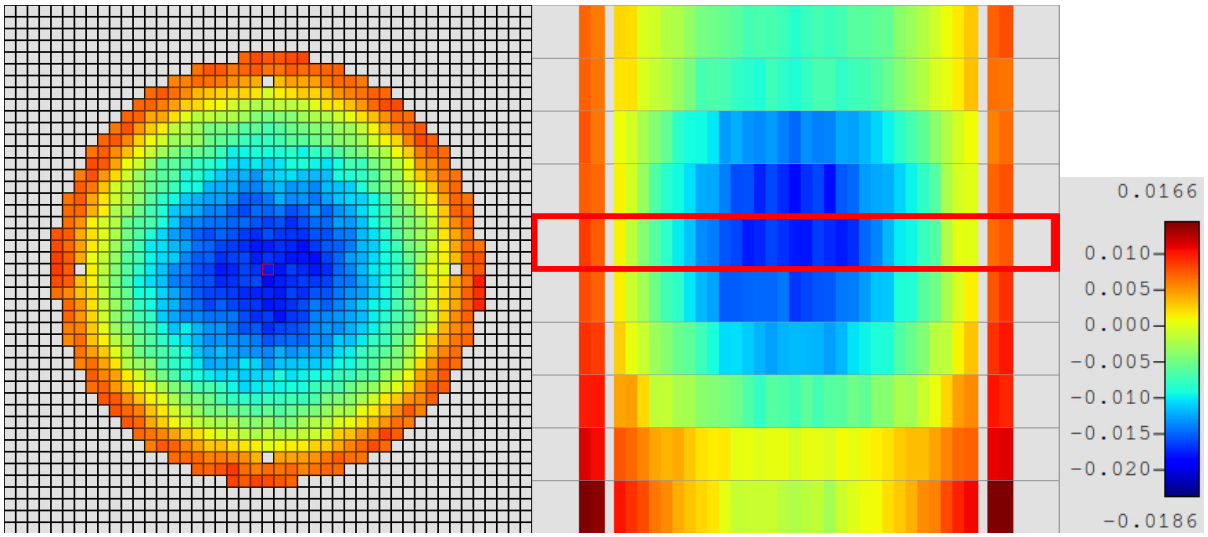

Figure A-29: MPACT radial (left) and axial (right) slices of flux distribution differences (P2) for Case 6.

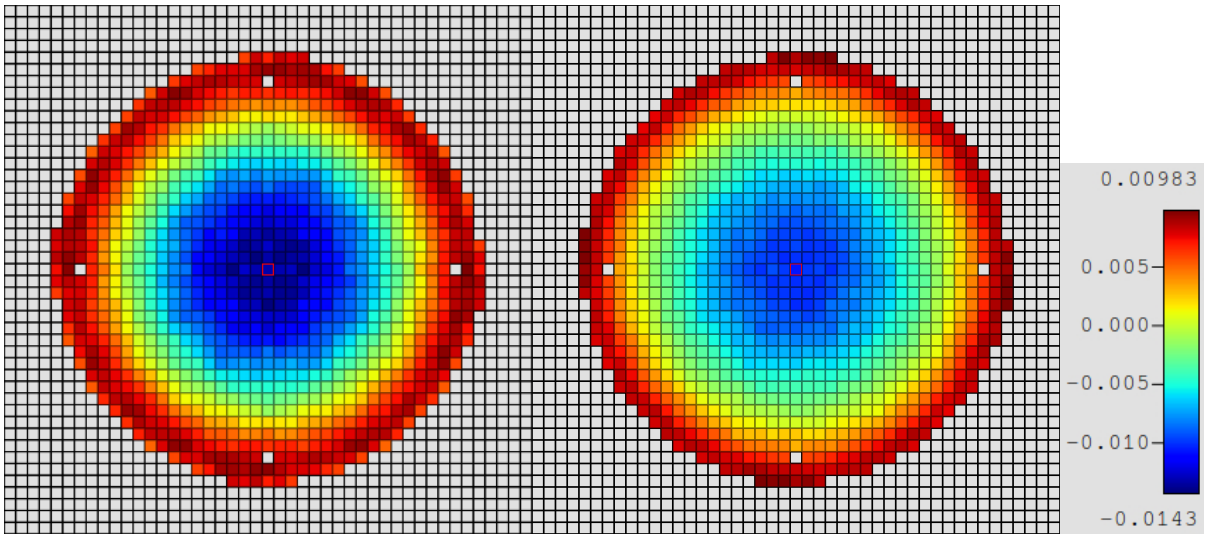

Figure A-30: MPACT radial flux distribution differences for TCP0 (left) and P2 (right) for Case 6.

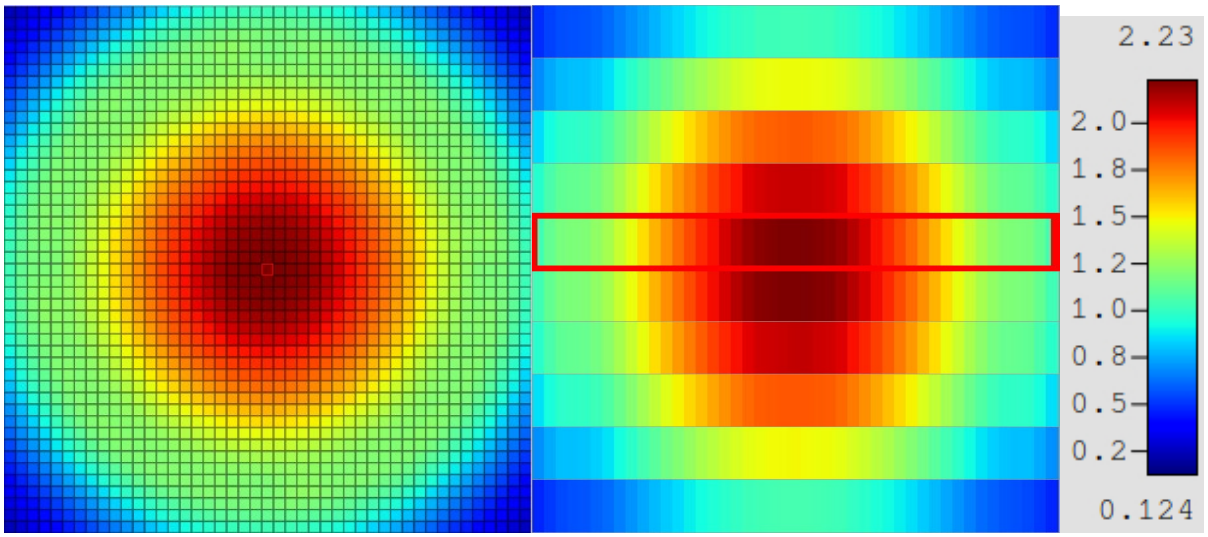

Figure A-31: KENO-VI radial (left) and axial (right) slices of flux distributions for Case 7.

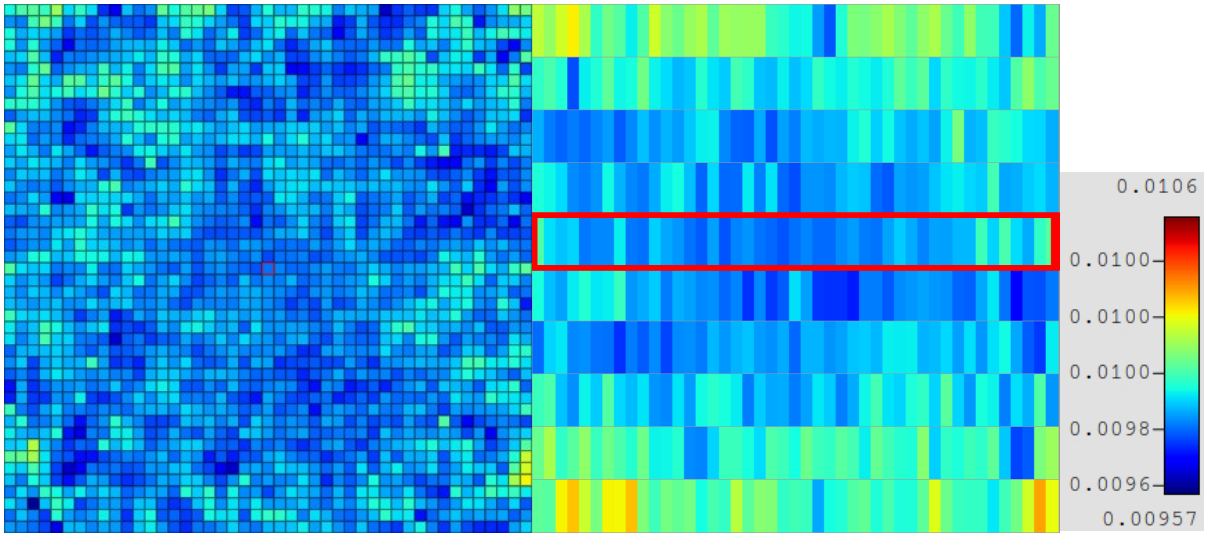

Figure A-32: KENO-VI radial (left) and axial (right) slices of fractional uncertainties for Case 7.

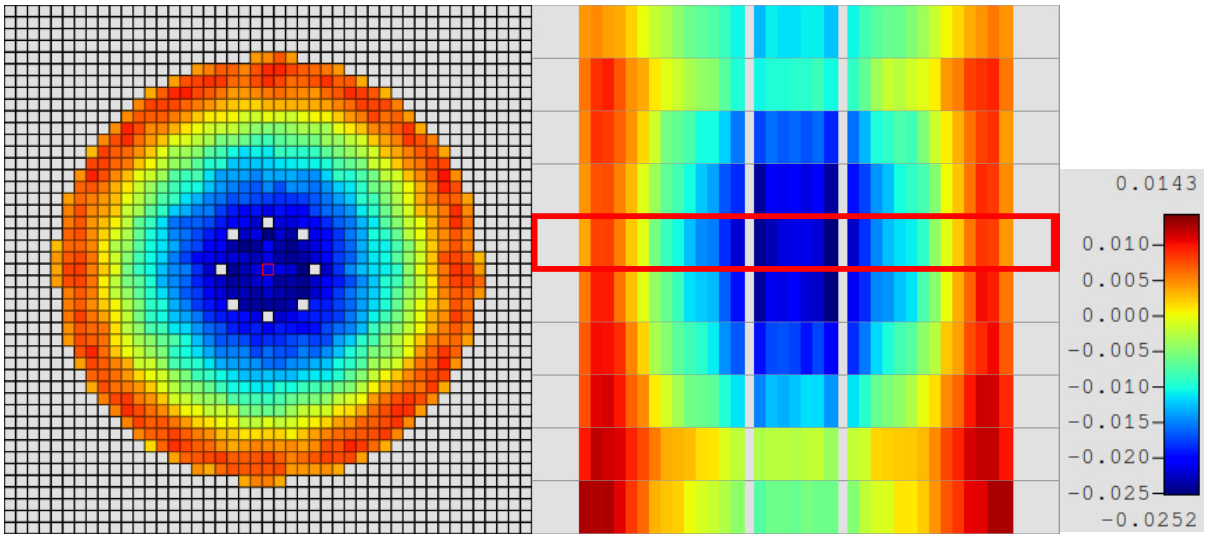

Figure A-33: MPACT radial (left) and axial (right) slices of flux distribution differences (TCP0) for Case 7.

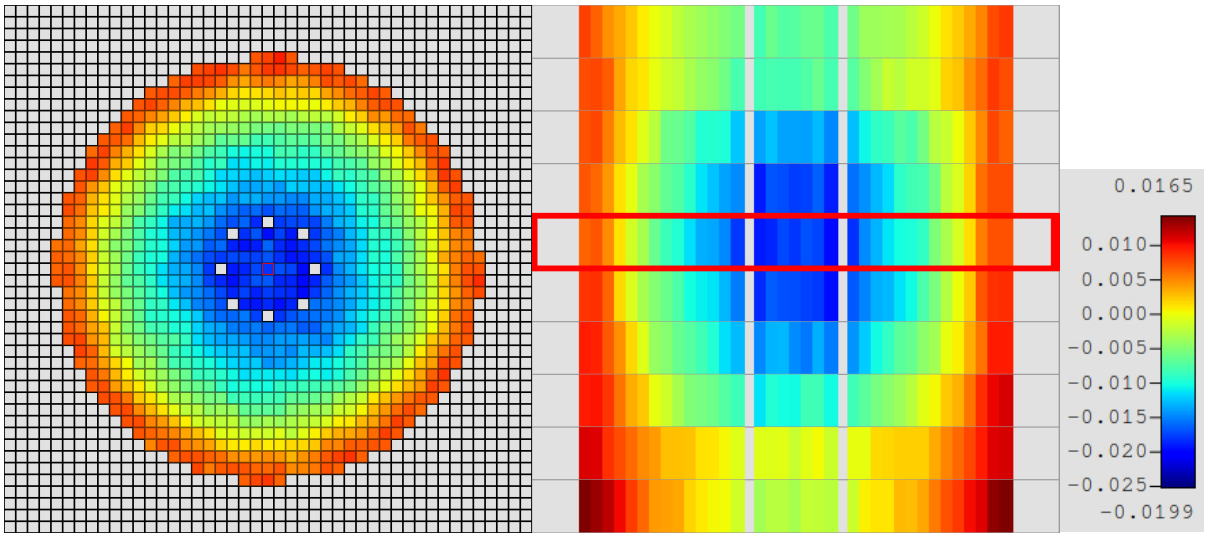

Figure A-34: MPACT radial (left) and axial (right) slices of flux distribution differences (P2) for Case 7.

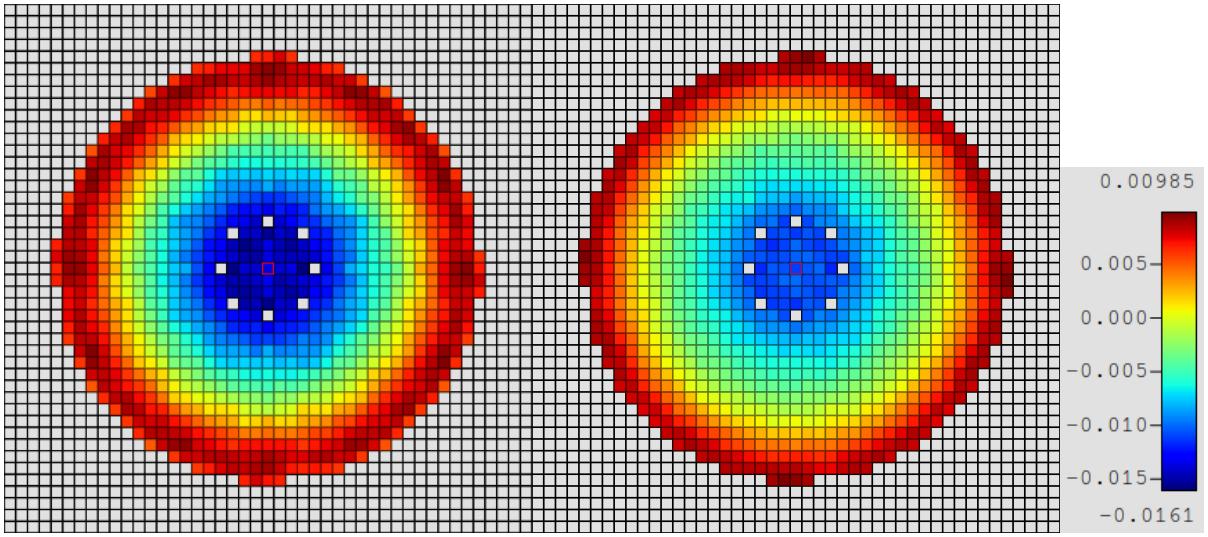

Figure A-35: MPACT radial flux distribution differences for TCP0 (left) and P2 (right) for Case 7.

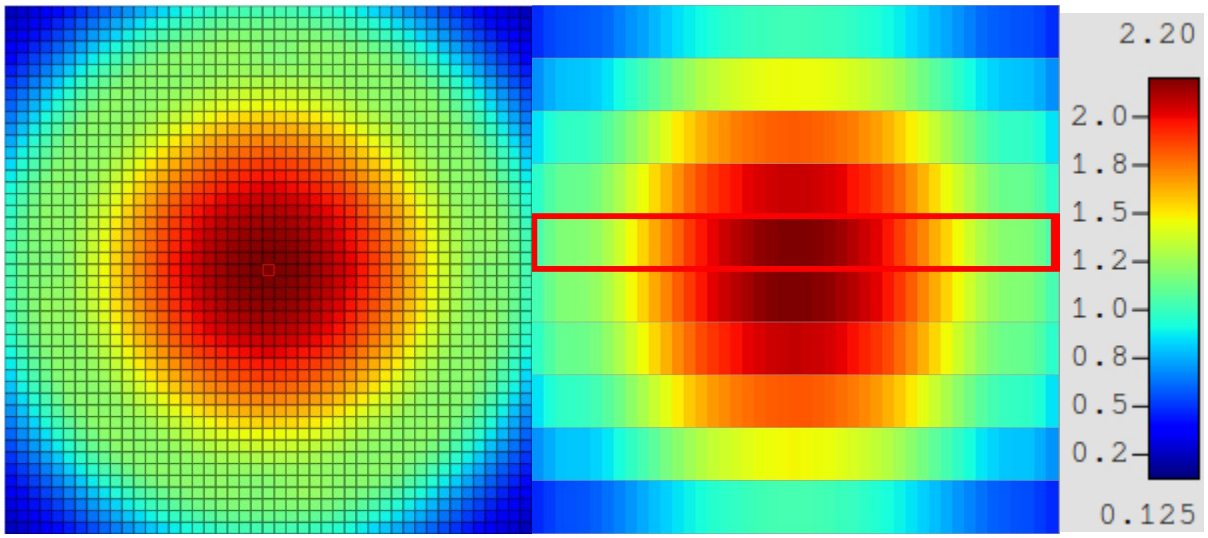

Figure A-36: KENO-VI radial (left) and axial (right) slices of flux distributions for Case 8.

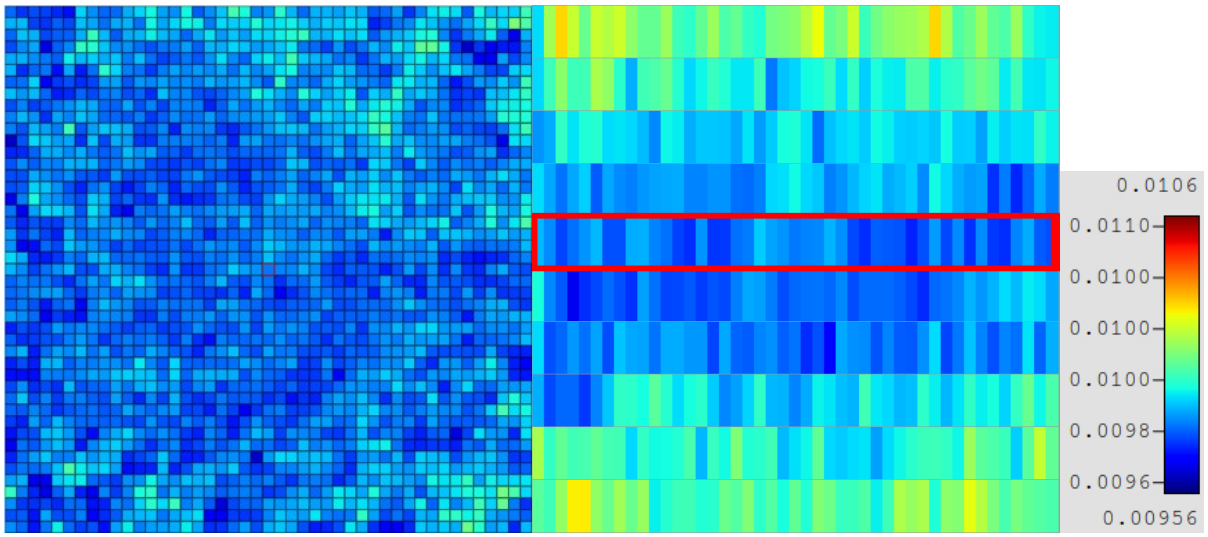

Figure A-37: KENO-VI radial (left) and axial (right) slices of fractional uncertainties for Case 8.

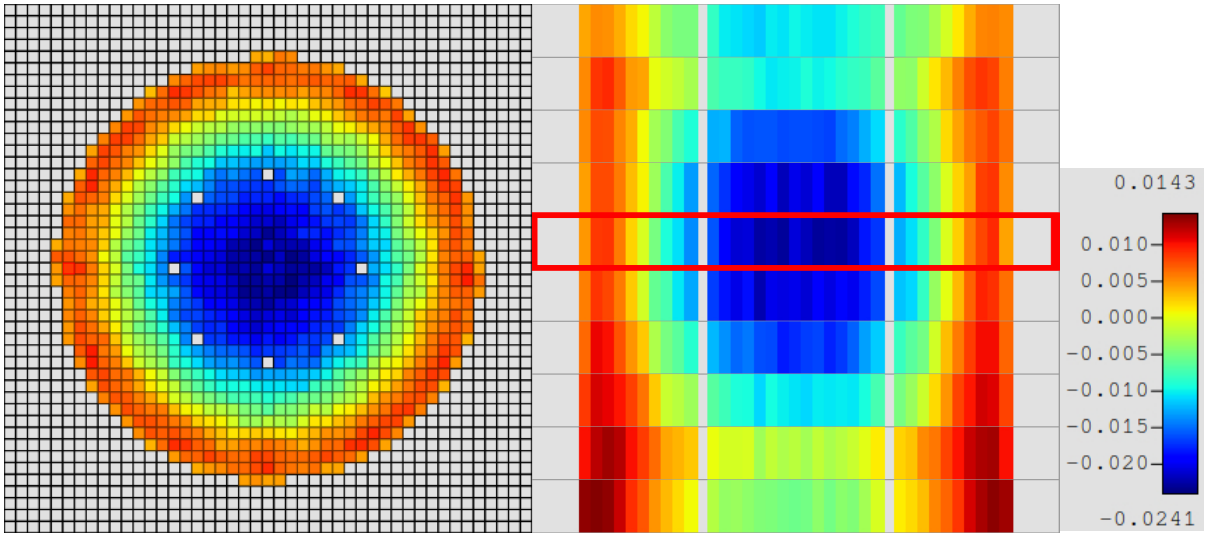

Figure A-38: MPACT radial (left) and axial (right) slices of flux distribution differences (TCP0) for Case 8.

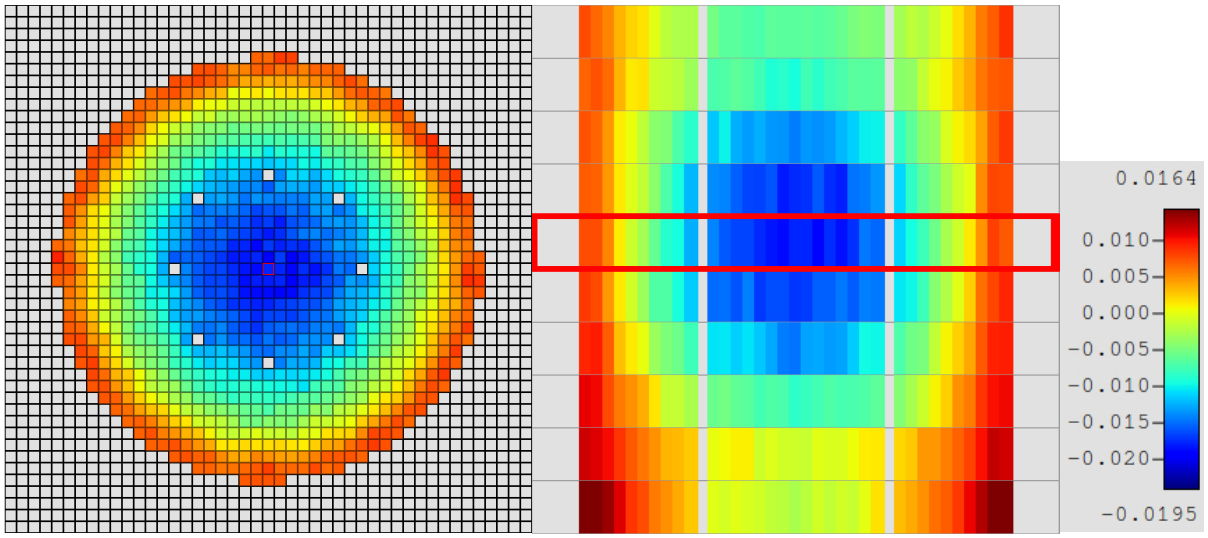

Figure A-39: MPACT radial (left) and axial (right) slices of flux distribution differences (P2) for Case 8.

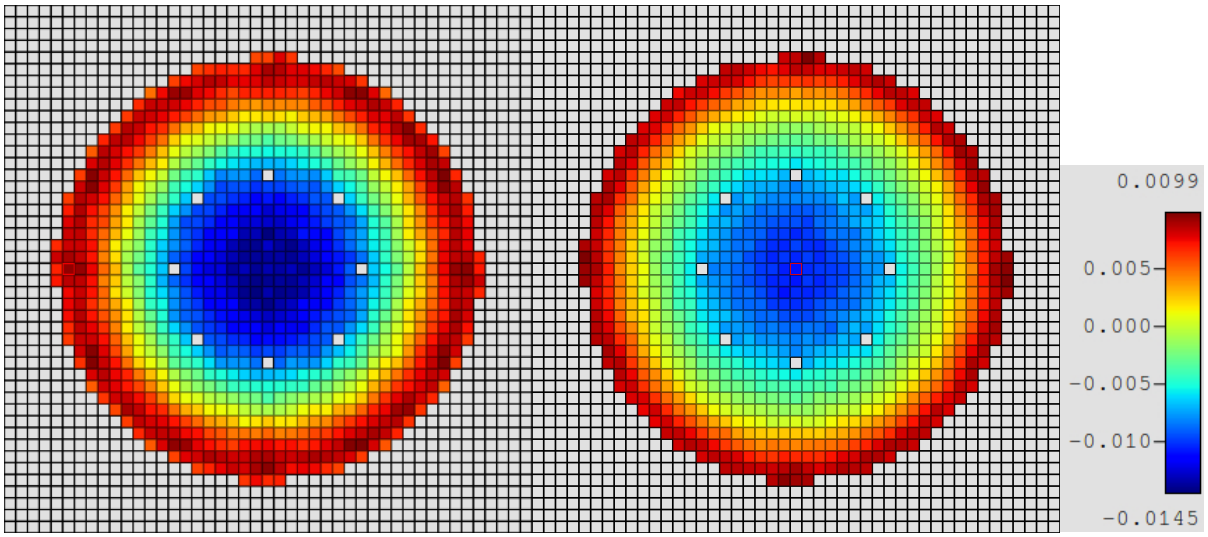

Figure A-40: MPACT radial flux distribution differences for TCP0 (left) and P2 (right) for Case 8.

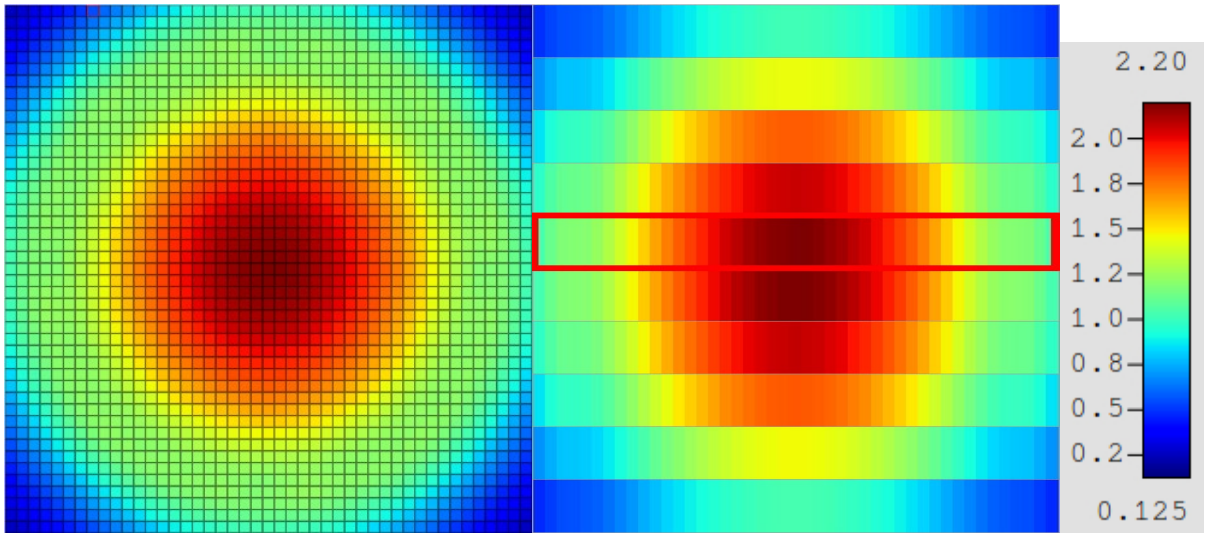

Figure A-41: KENO-VI radial (left) and axial (right) slices of flux distributions for Case 9.

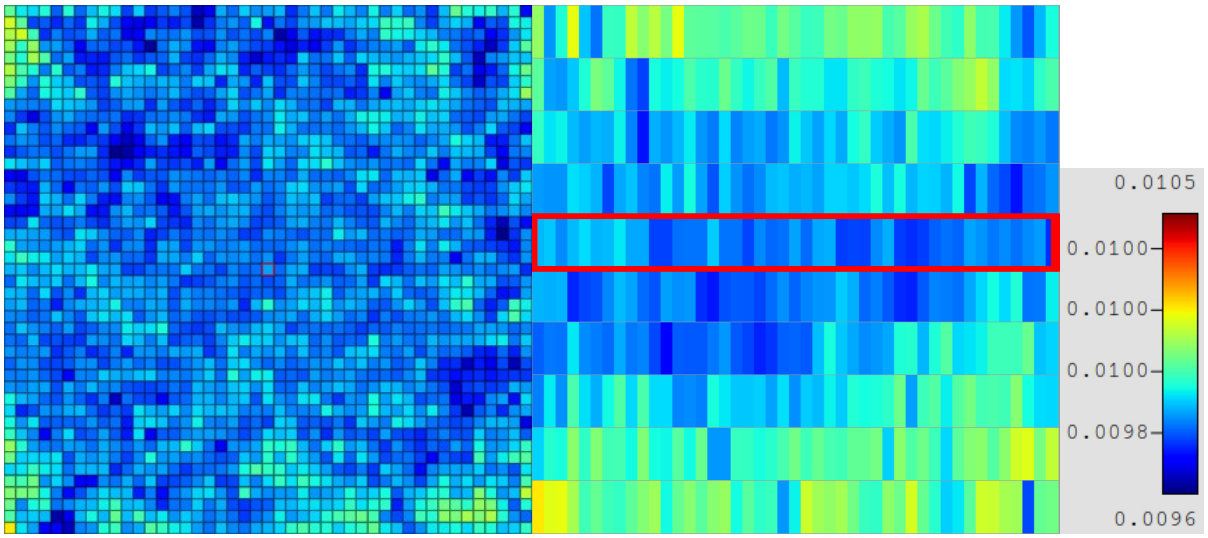

Figure A-42: KENO-VI radial (left) and axial (right) slices of fractional uncertainties for Case 9.

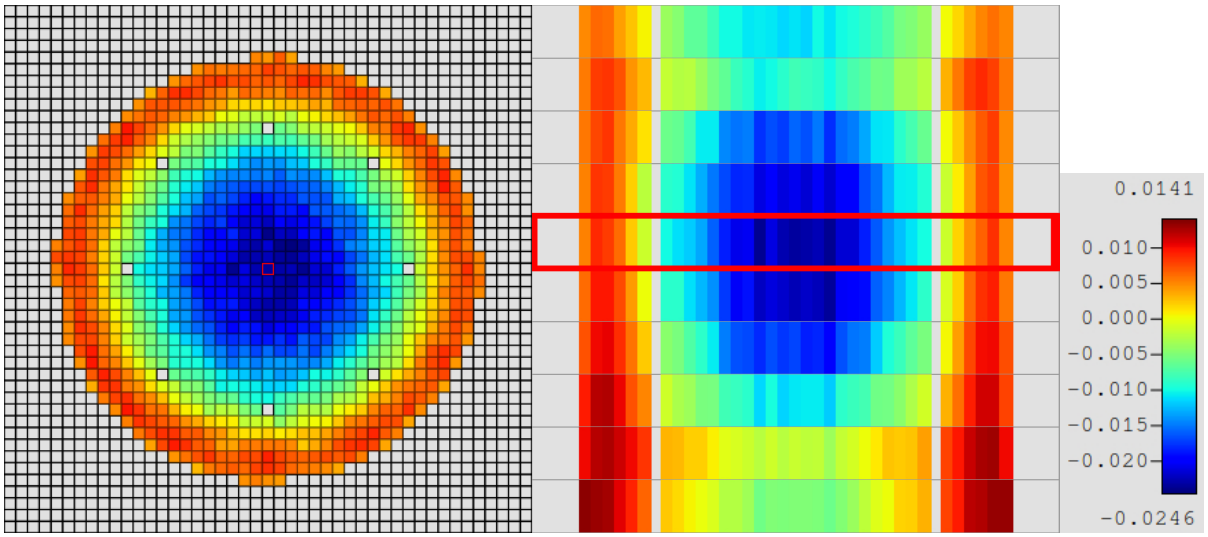

Figure A-43: MPACT radial (left) and axial (right) slices of flux distribution differences (TCP0) for Case 9.

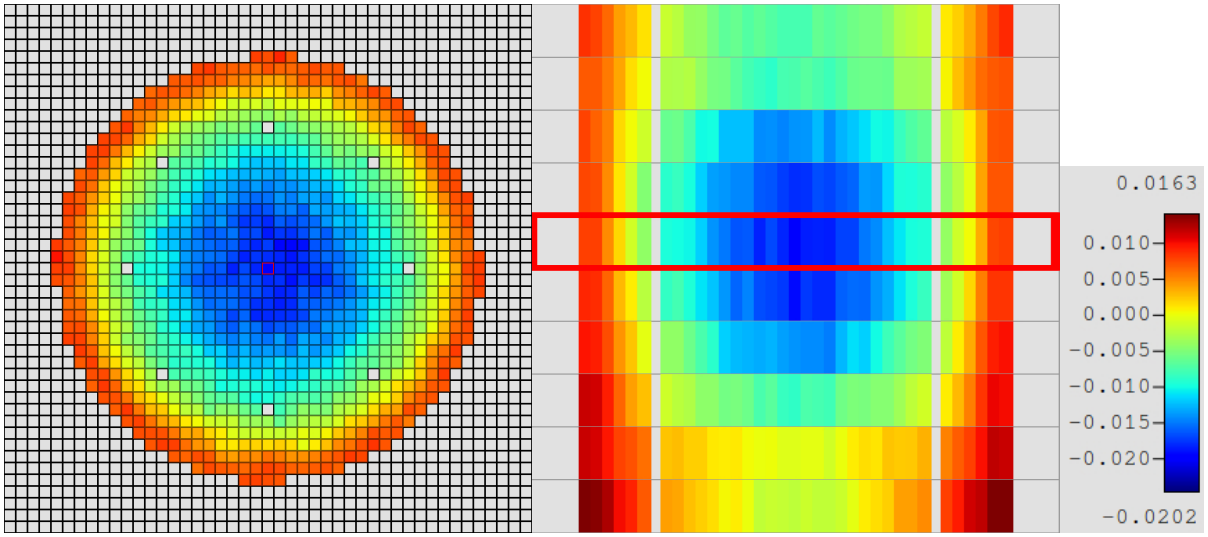

Figure A-44: MPACT radial (left) and axial (right) slices of flux distribution differences (P2) for Case 9.

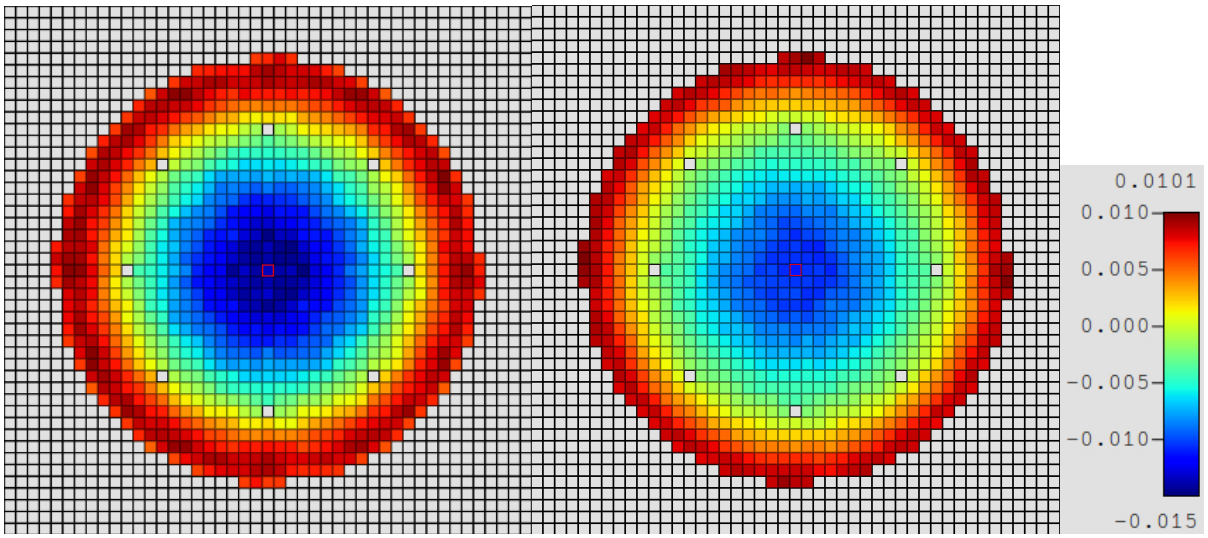

Figure A-45: MPACT radial flux distribution differences for TCP0 (left) and P2 (right) for Case 9.

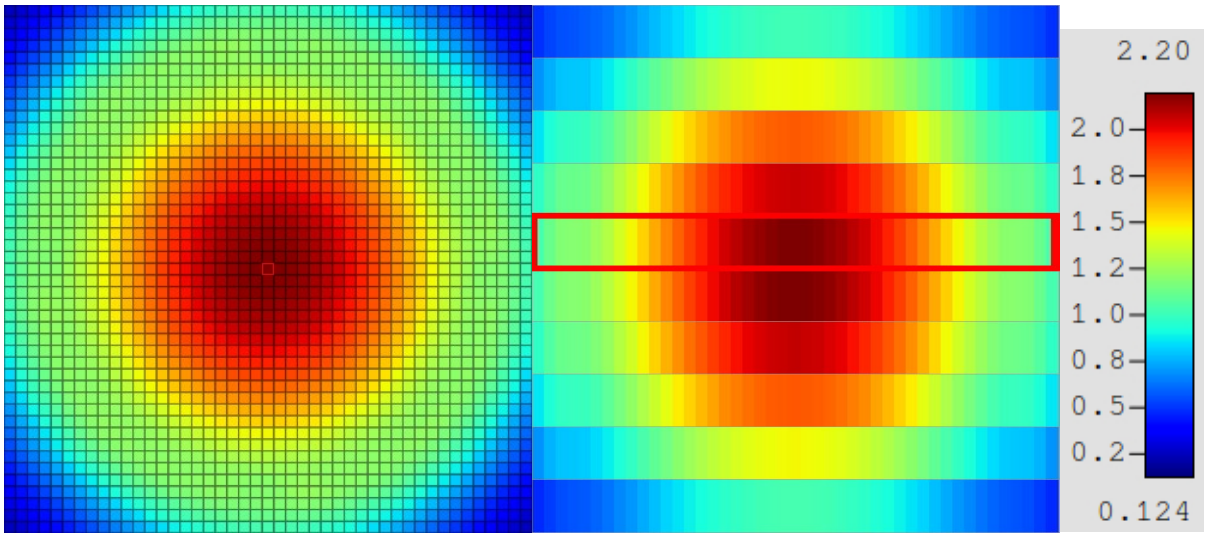

Figure A-46: KENO-VI radial (left) and axial (right) slices of flux distributions for Case 10.

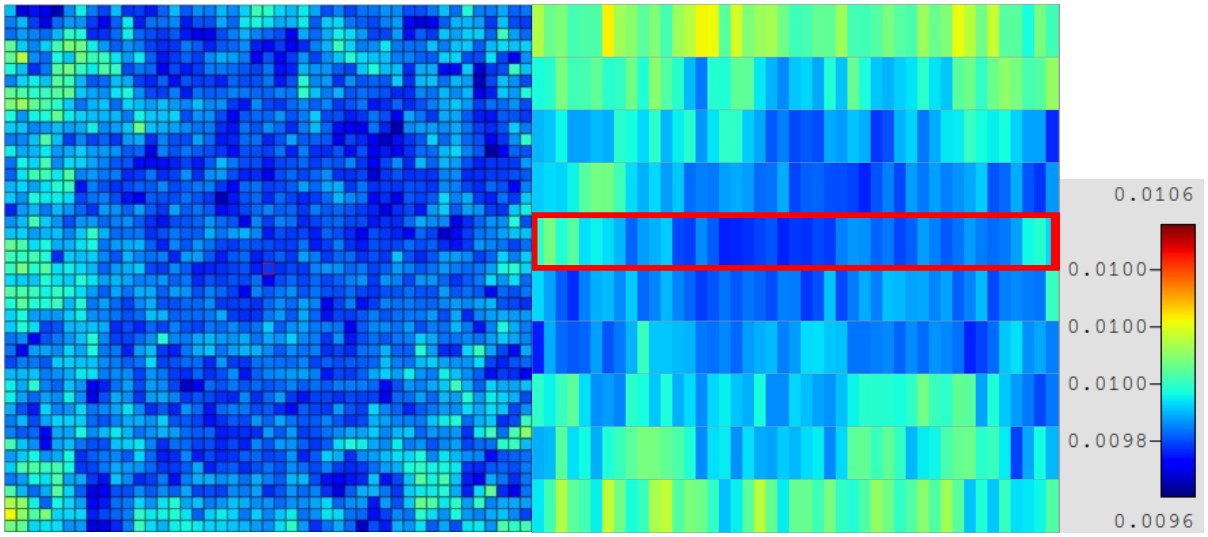

Figure A-47: KENO-VI radial (left) and axial (right) slices of fractional uncertainties for Case 10.

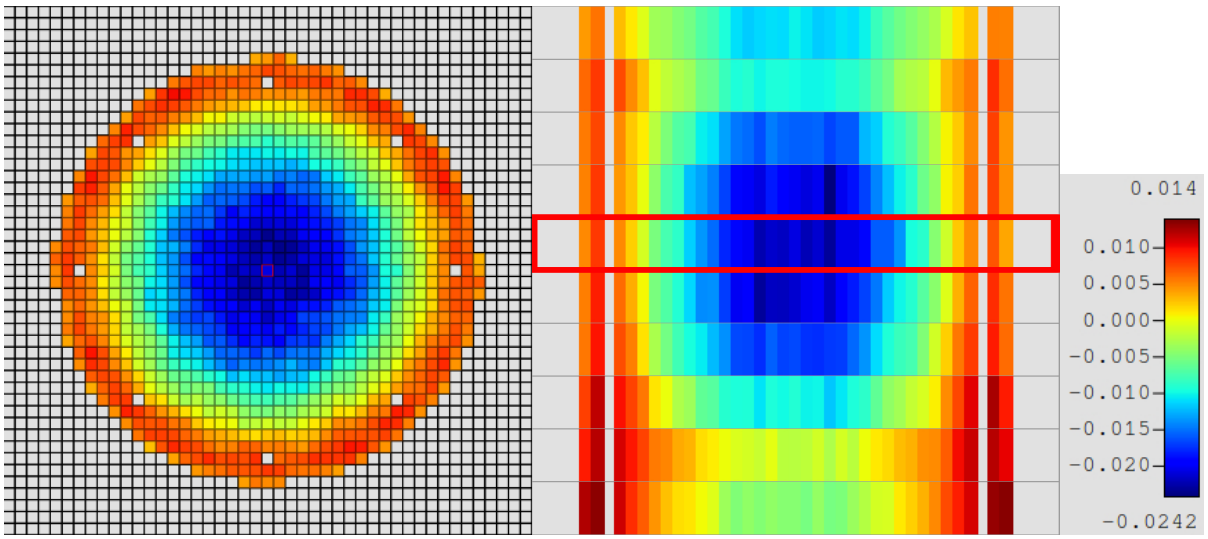

Figure A-48: MPACT radial (left) and axial (right) slices of flux distribution differences (TCP0) for Case 10.

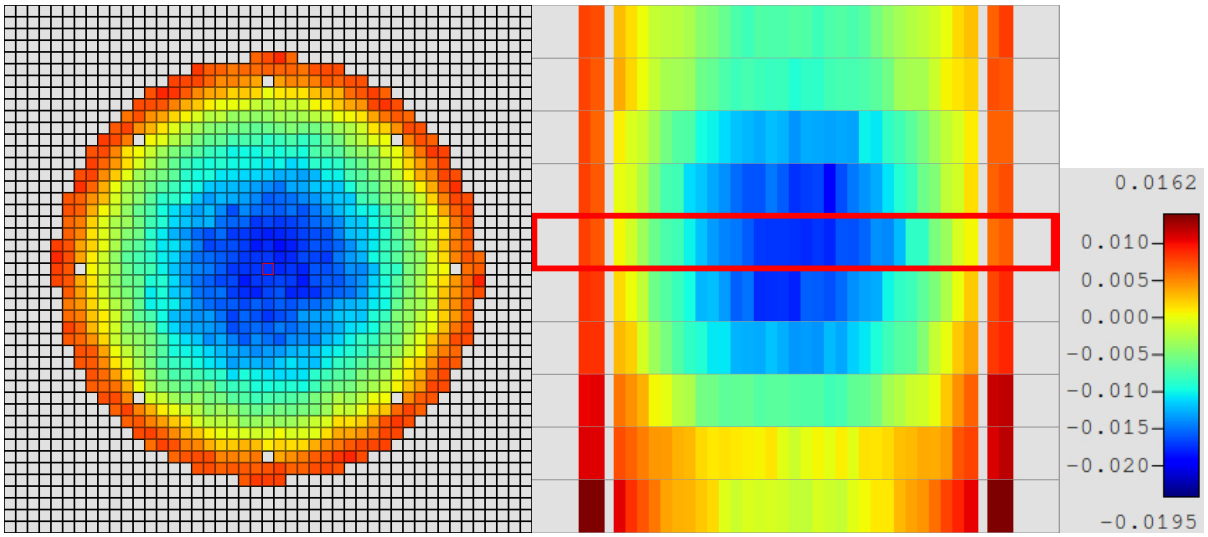

Figure A-49: MPACT radial (left) and axial (right) slices of flux distribution differences (P2) for Case 10.

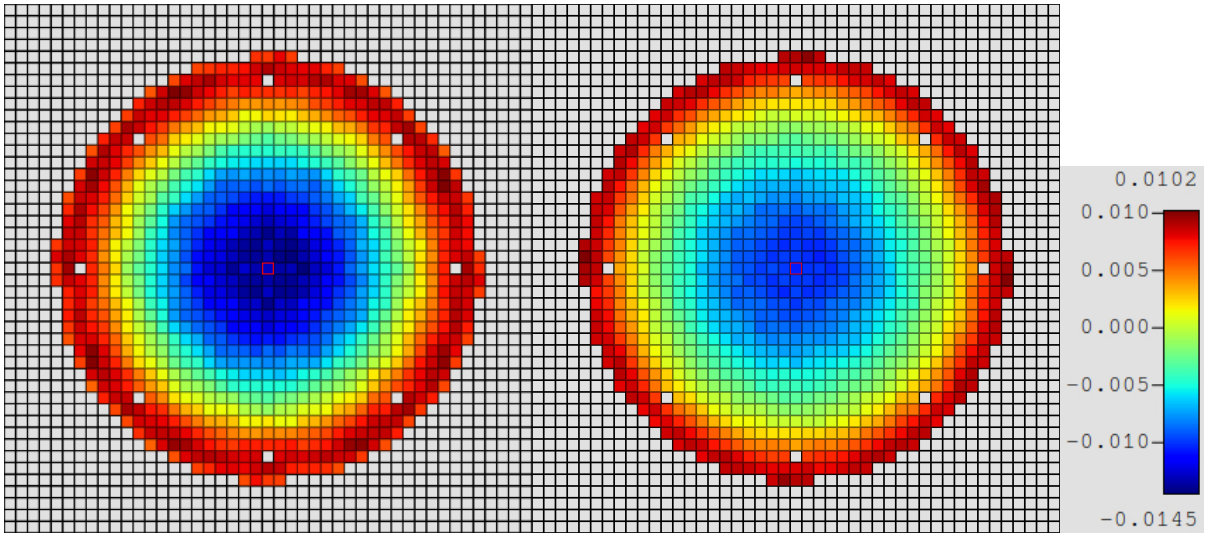

Figure A-50: MPACT radial flux distribution differences for TCP0 (left) and P2 (right) for Case 10.

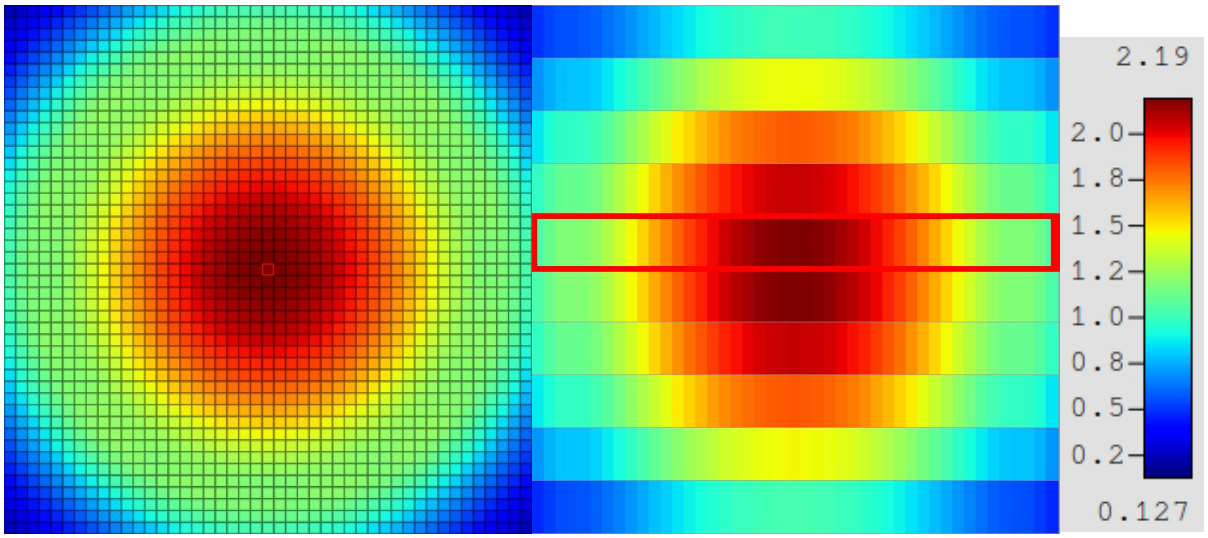

Figure A-51: KENO-VI radial (left) and axial (right) slices of flux distributions for Case 11.

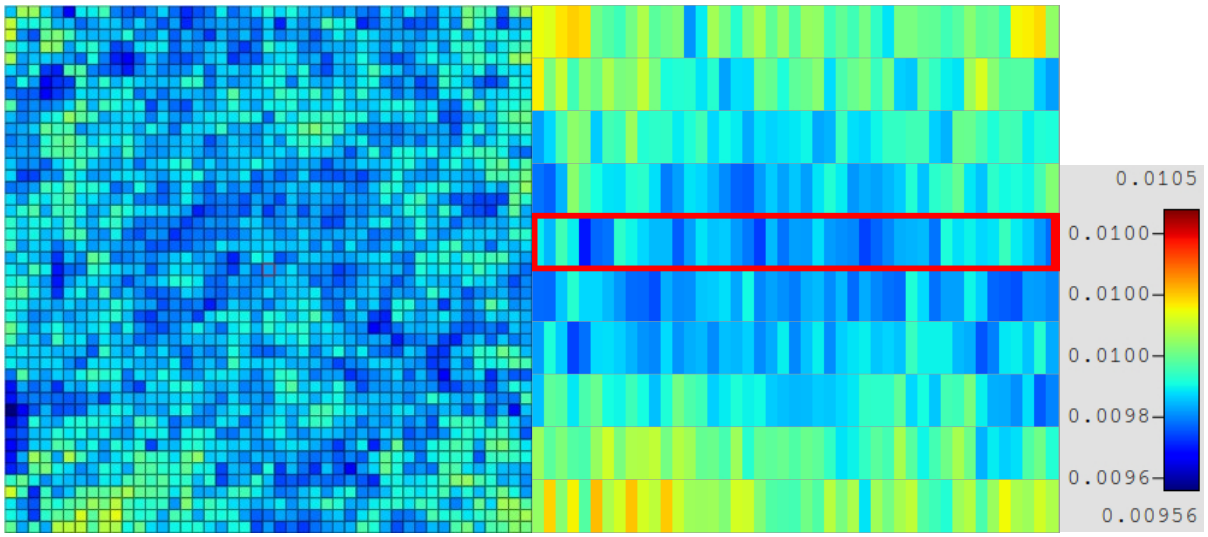

Figure A-52: KENO-VI radial (left) and axial (right) slices of fractional uncertainties for Case 11.

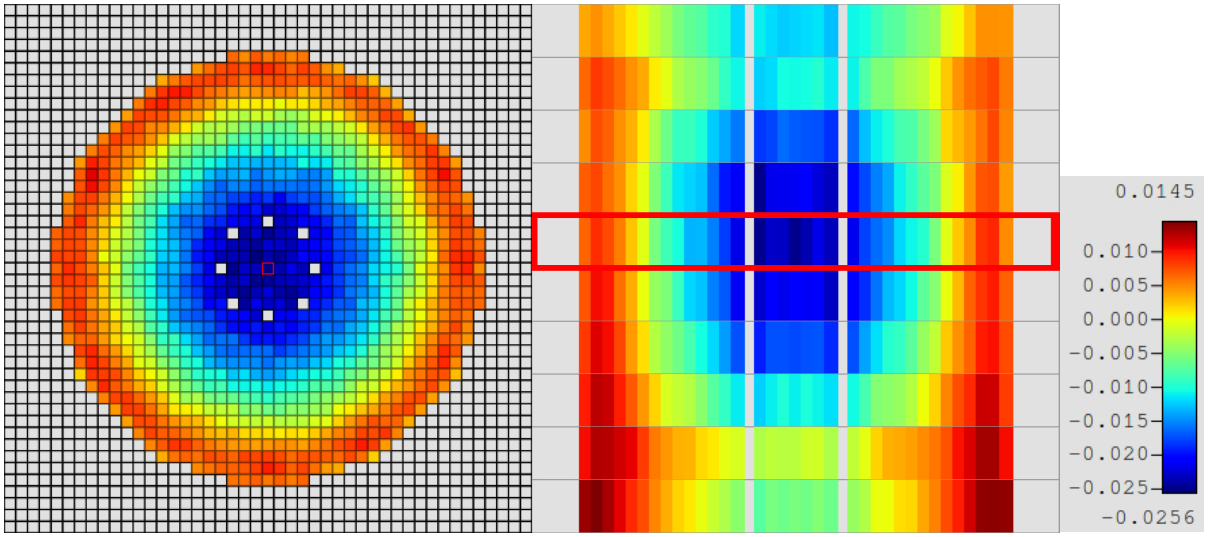

Figure A-53: MPACT radial (left) and axial (right) slices of flux distribution differences (TCP0) for Case 11.

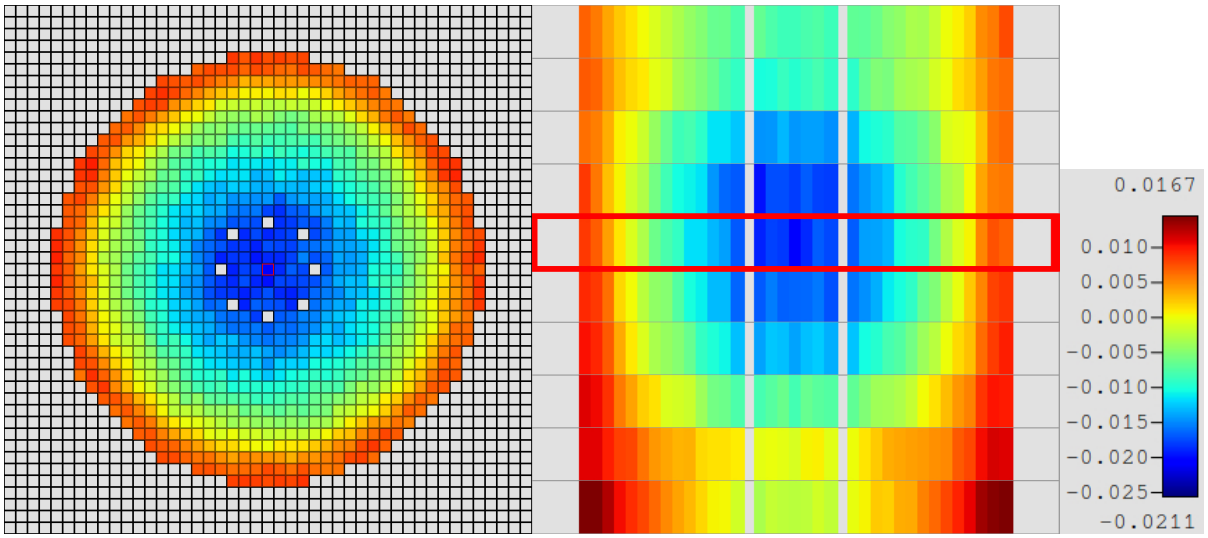

Figure A-54: MPACT radial (left) and axial (right) slices of flux distribution differences (P2) for Case 11.

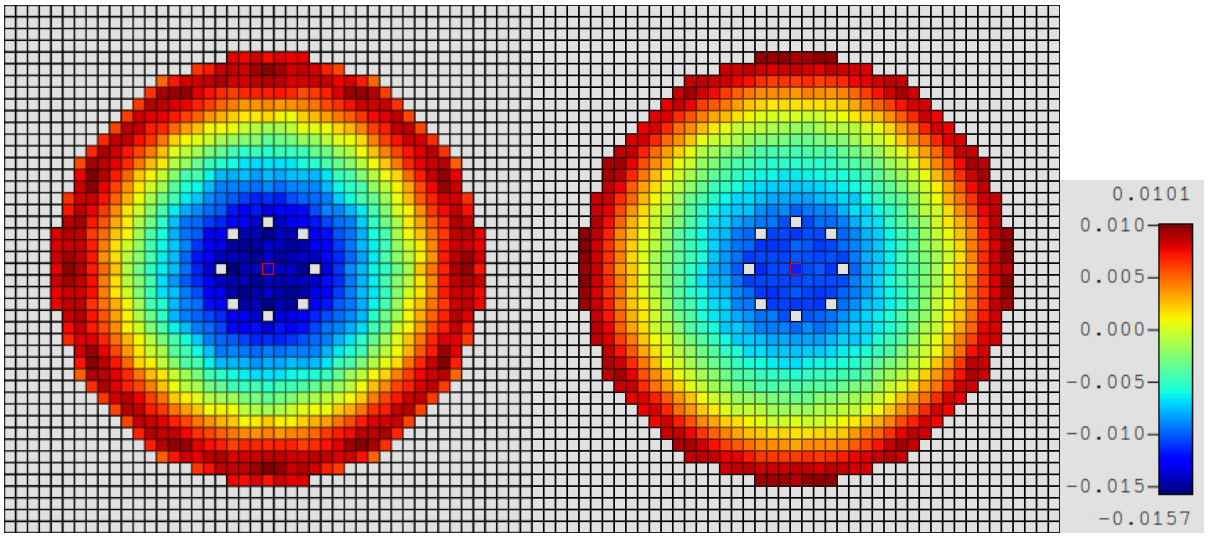

Figure A-55: MPACT radial flux distribution differences for TCP0 (left) and P2 (right) for Case 11.

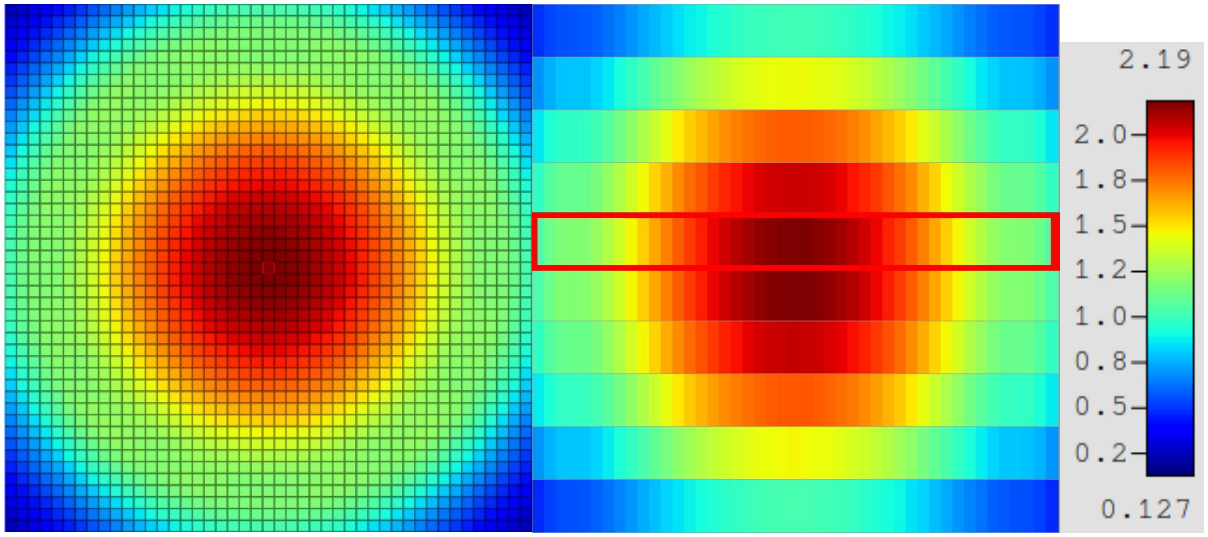

Figure A-56: KENO-VI radial (left) and axial (right) slices of flux distributions for Case 12.

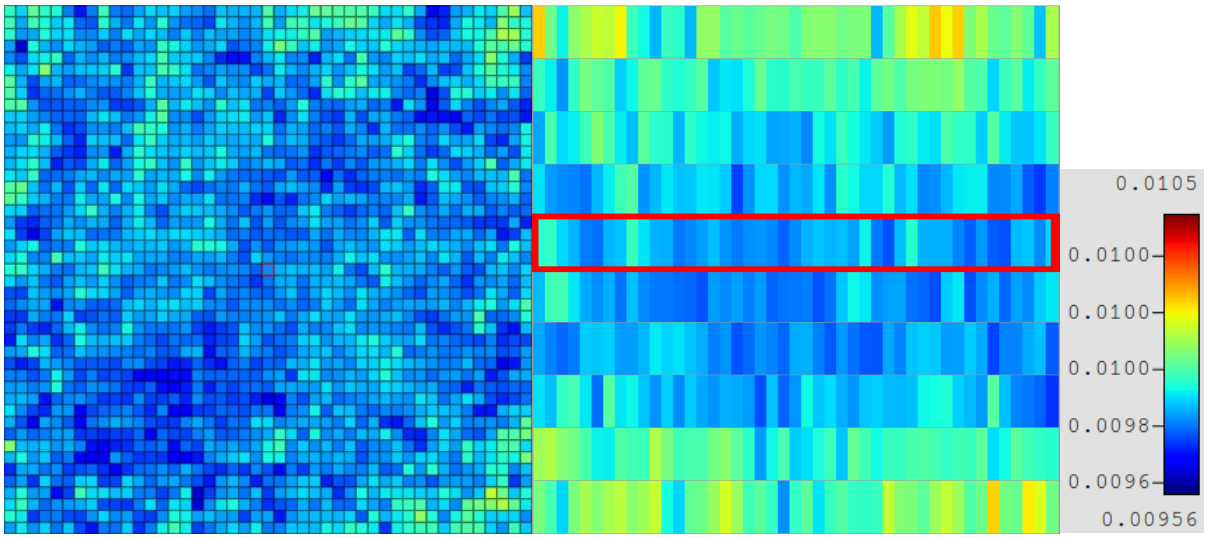

Figure A-57: KENO-VI radial (left) and axial (right) slices of fractional uncertainties for Case 12.

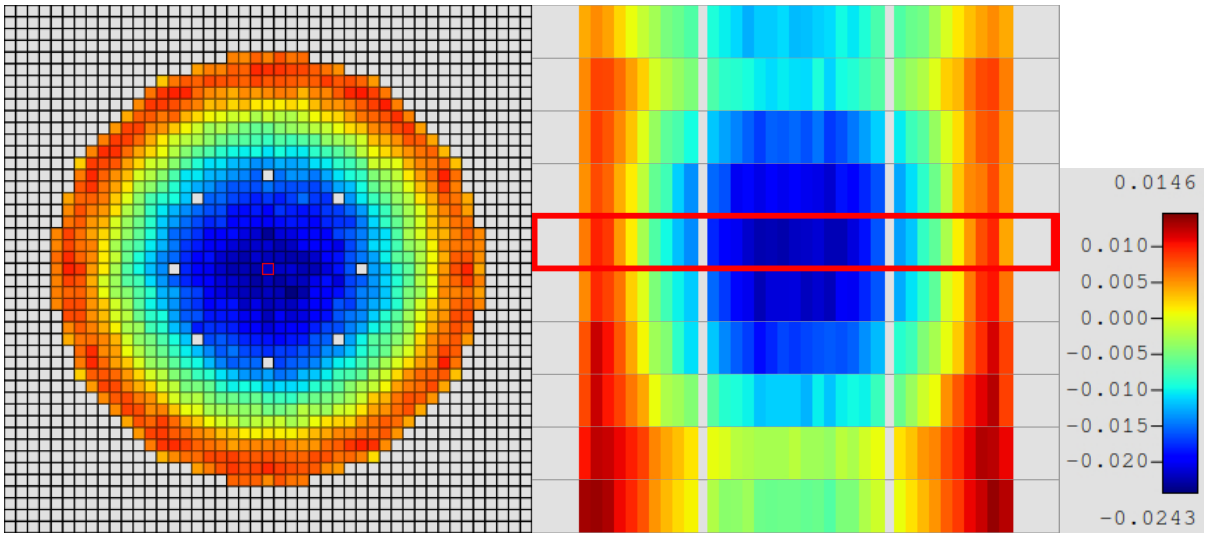

Figure A-58: MPACT radial (left) and axial (right) slices of flux distribution differences (TCP0) for Case 12.

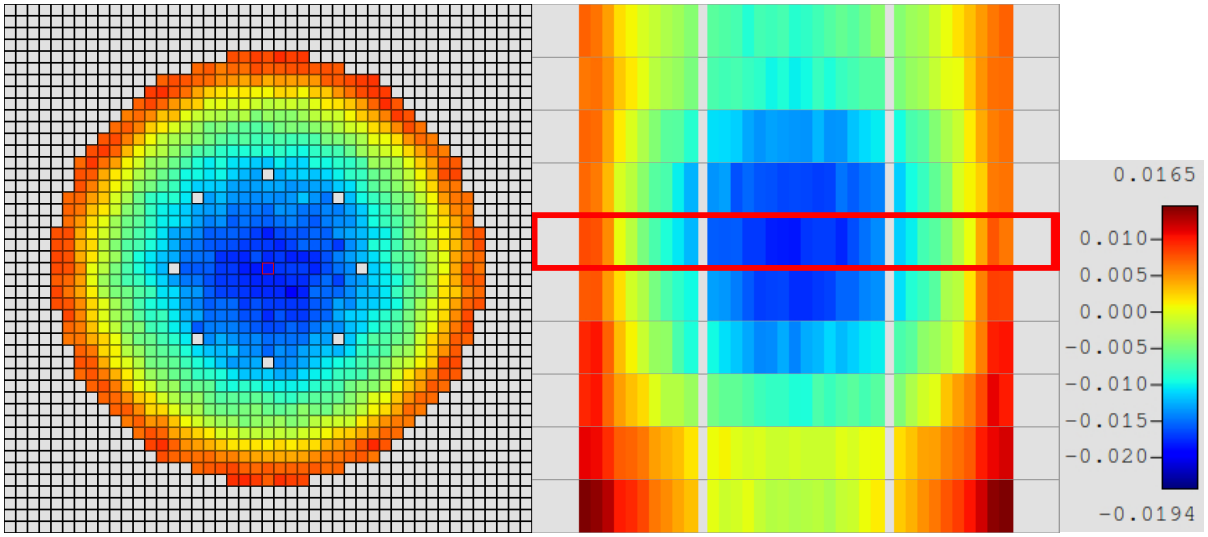

Figure A-59: MPACT radial (left) and axial (right) slices of flux distribution differences (P2) for Case 12.

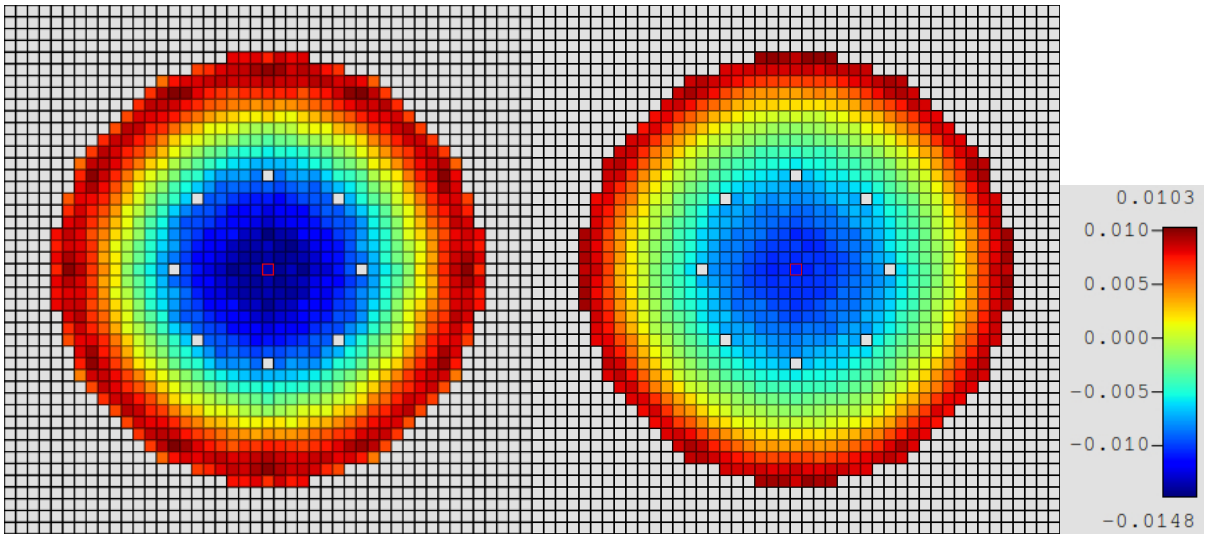

Figure A-60: MPACT radial flux distribution differences for TCP0 (left) and P2 (right) for Case 12.

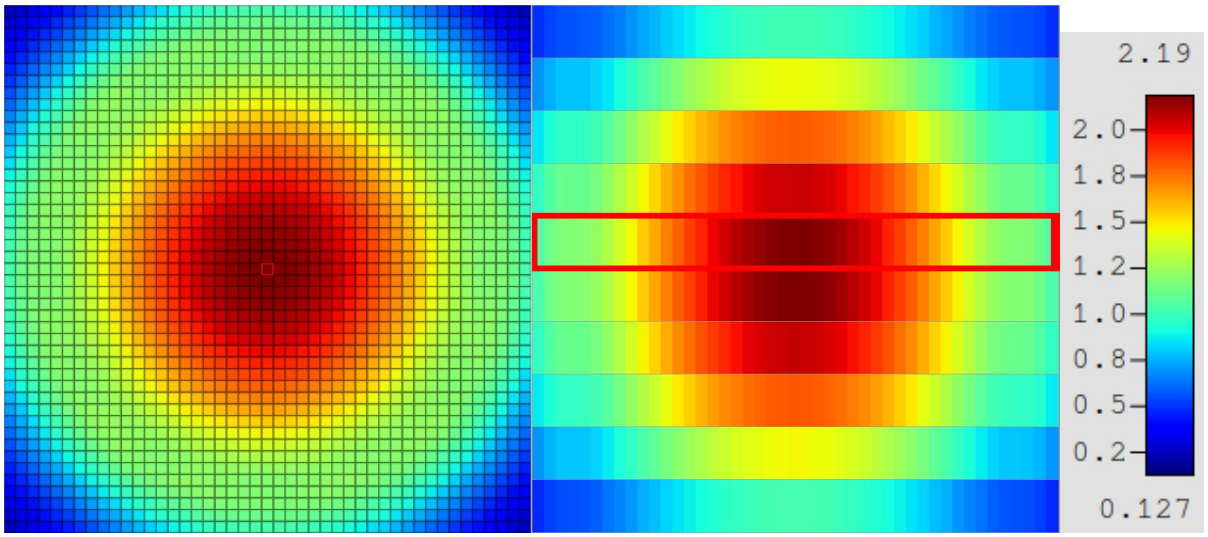

Figure A-61: KENO-VI radial (left) and axial (right) slices of flux distributions for Case 13.

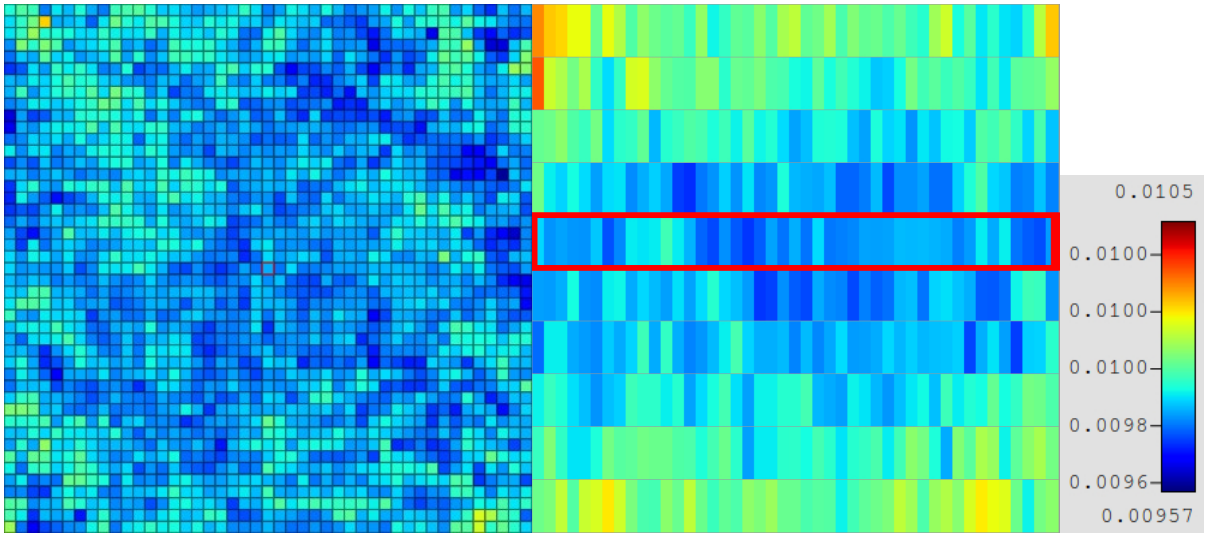

Figure A-62: KENO-VI radial (left) and axial (right) slices of fractional uncertainties for Case 13.

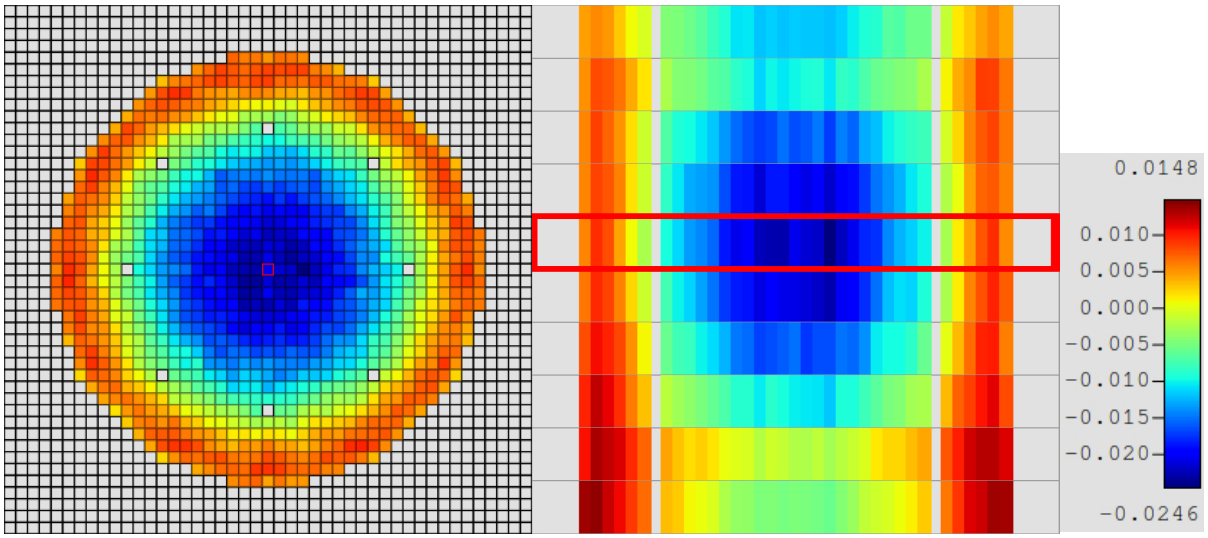

Figure A-63: MPACT radial (left) and axial (right) slices of flux distribution differences (TCP0) for Case 13.

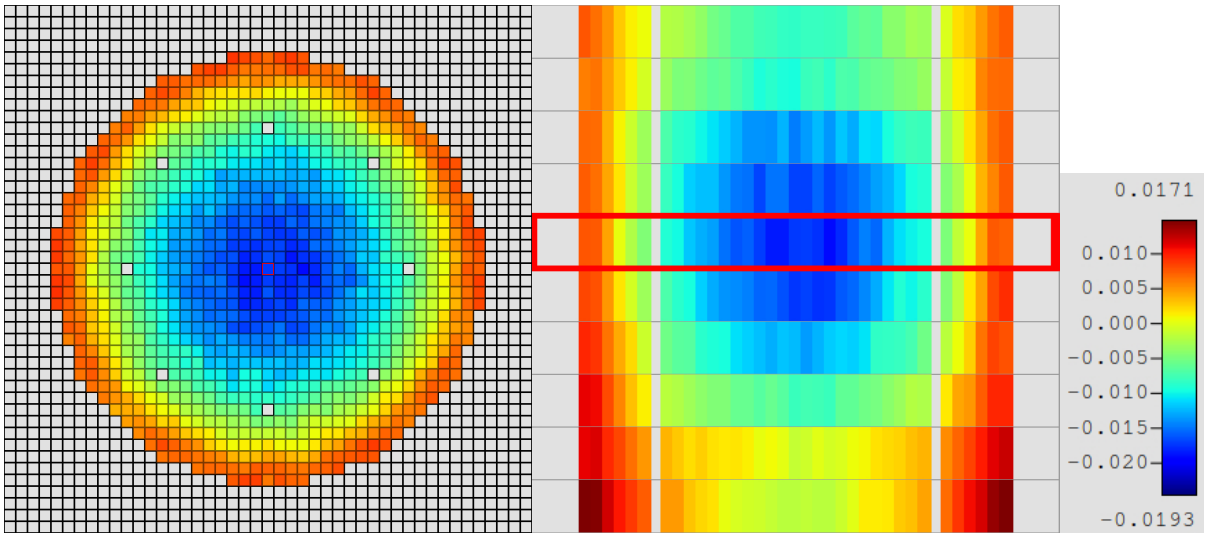

Figure A-64: MPACT radial (left) and axial (right) slices of flux distribution differences (P2) for Case 13.

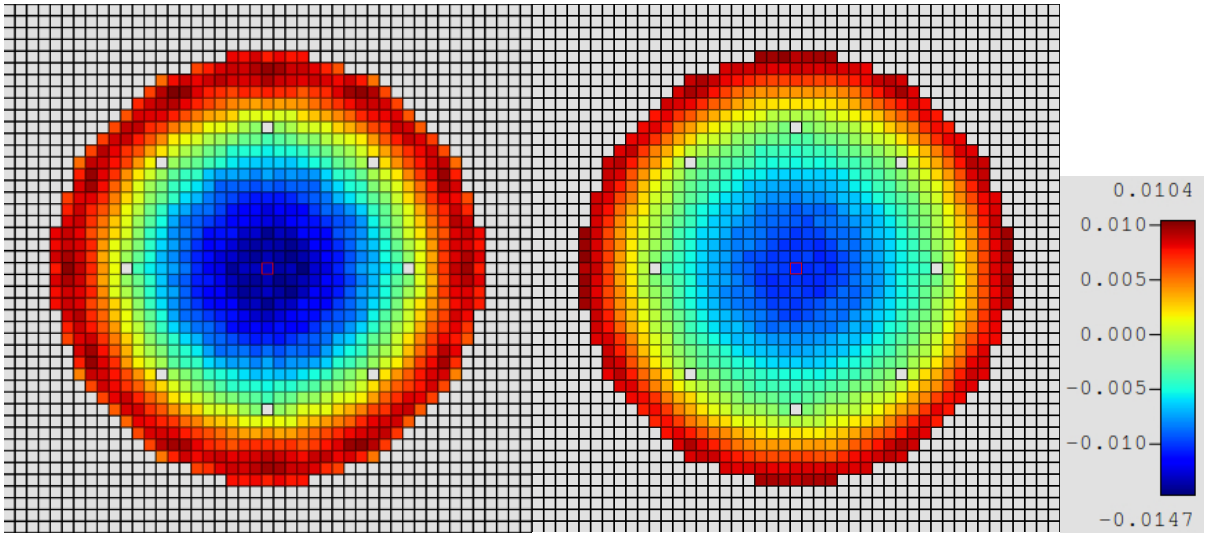

Figure A-65: MPACT radial flux distribution differences for TCP0 (left) and P2 (right) for Case 13.

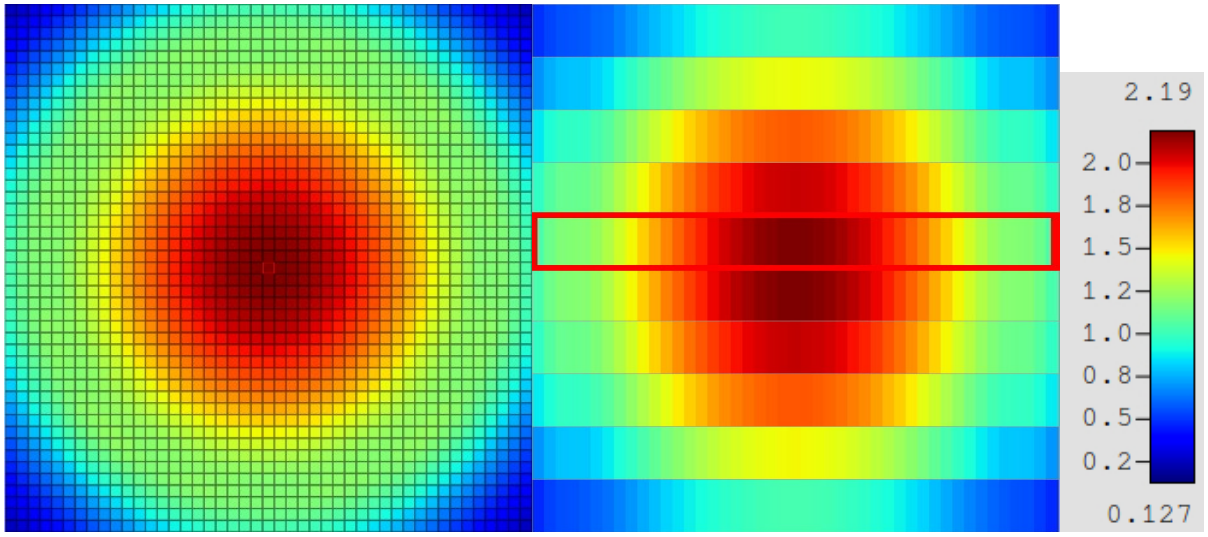

Figure A-66: KENO-VI radial (left) and axial (right) slices of flux distributions for Case 14.

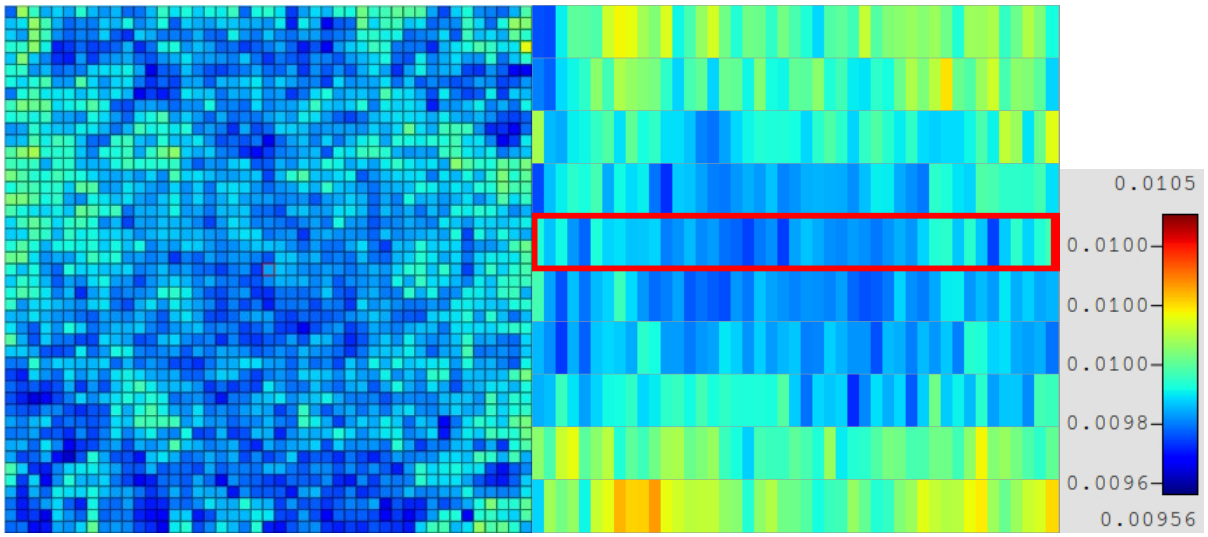

Figure A-67: KENO-VI radial (left) and axial (right) slices of fractional uncertainties for Case 14.

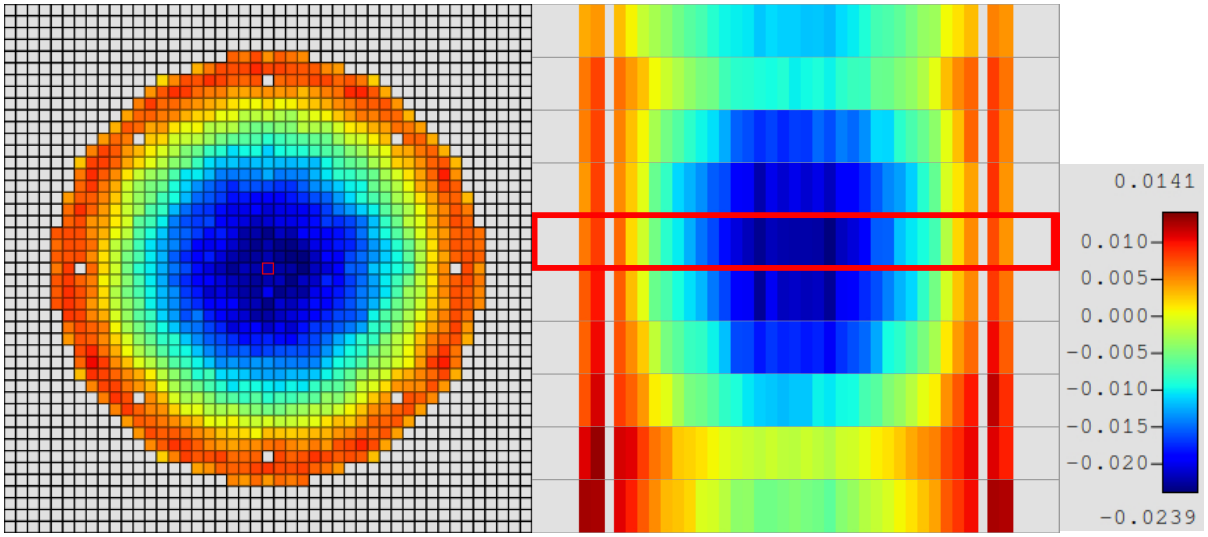

Figure A-68: MPACT radial (left) and axial (right) slices of flux distribution differences (TCP0) for Case 14.

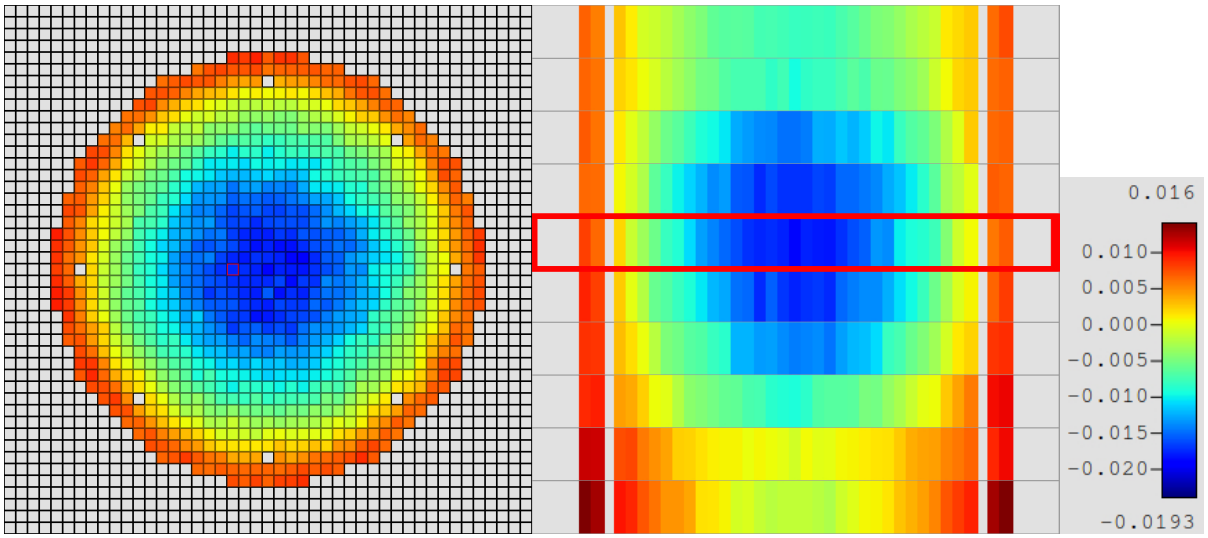

Figure A-69: MPACT radial (left) and axial (right) slices of flux distribution differences (P2) for Case 14.

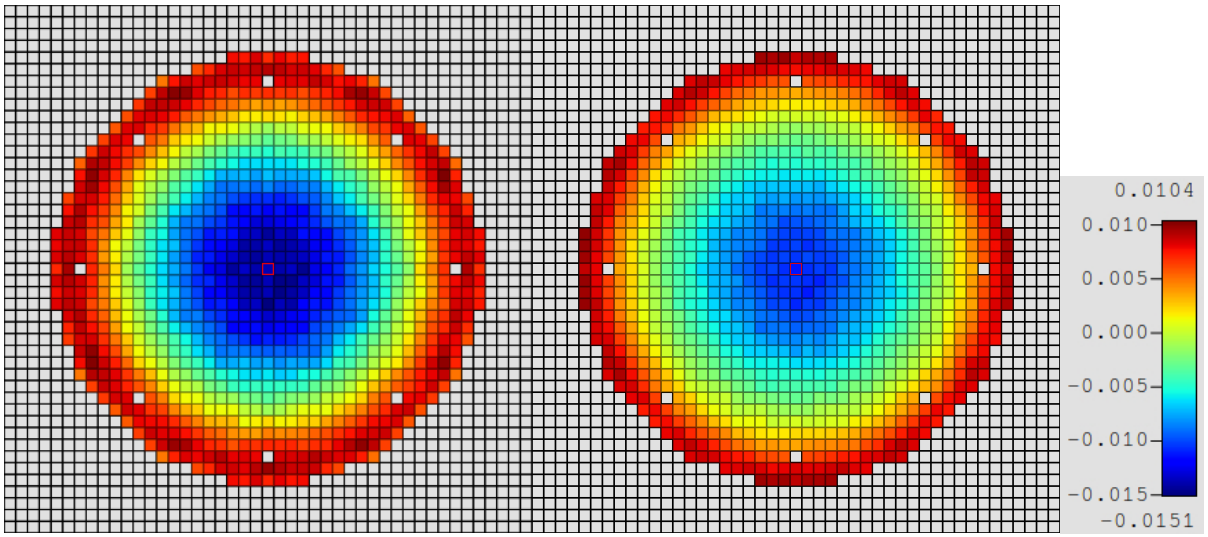

Figure A-70: MPACT radial flux distribution differences for TCP0 (left) and P2 (right) for Case 14.

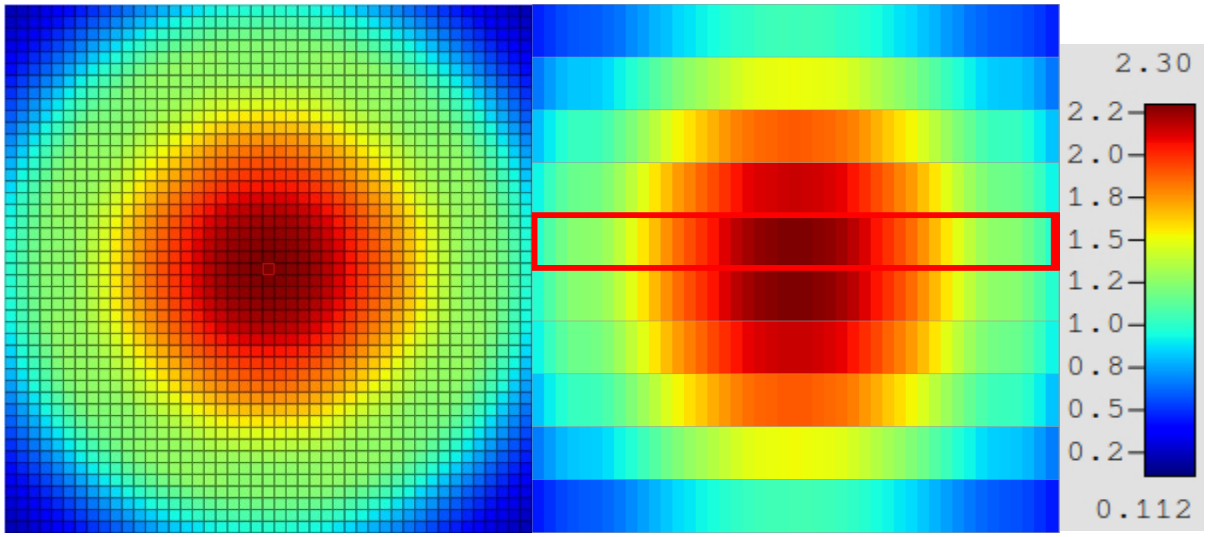

Figure A-71: KENO-VI radial (left) and axial (right) slices of flux distributions for Case 15.

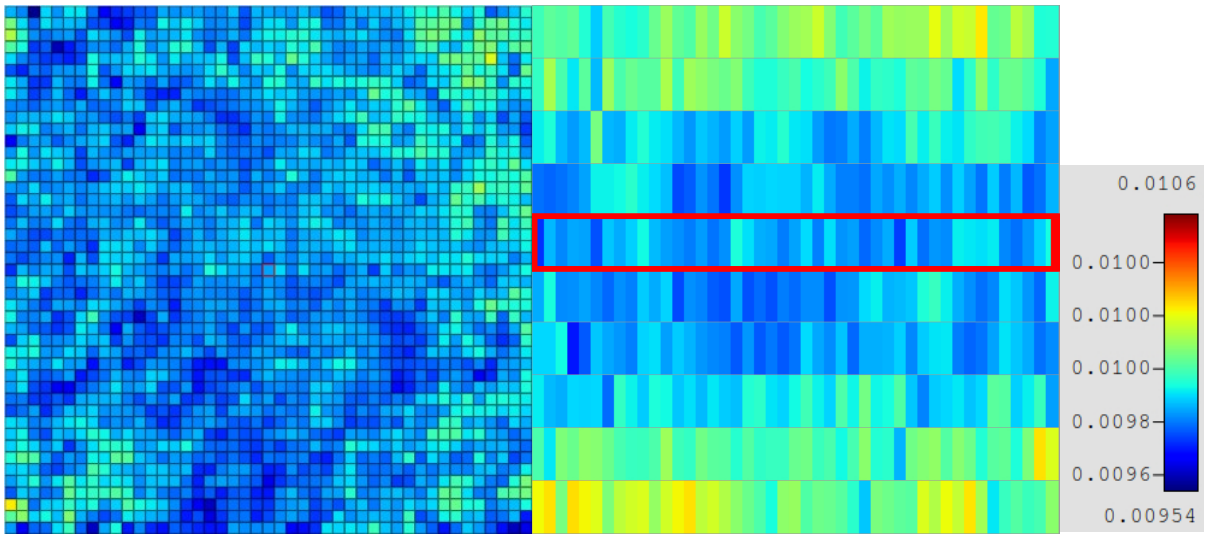

Figure A-72: KENO-VI radial (left) and axial (right) slices of fractional uncertainties for Case 15.

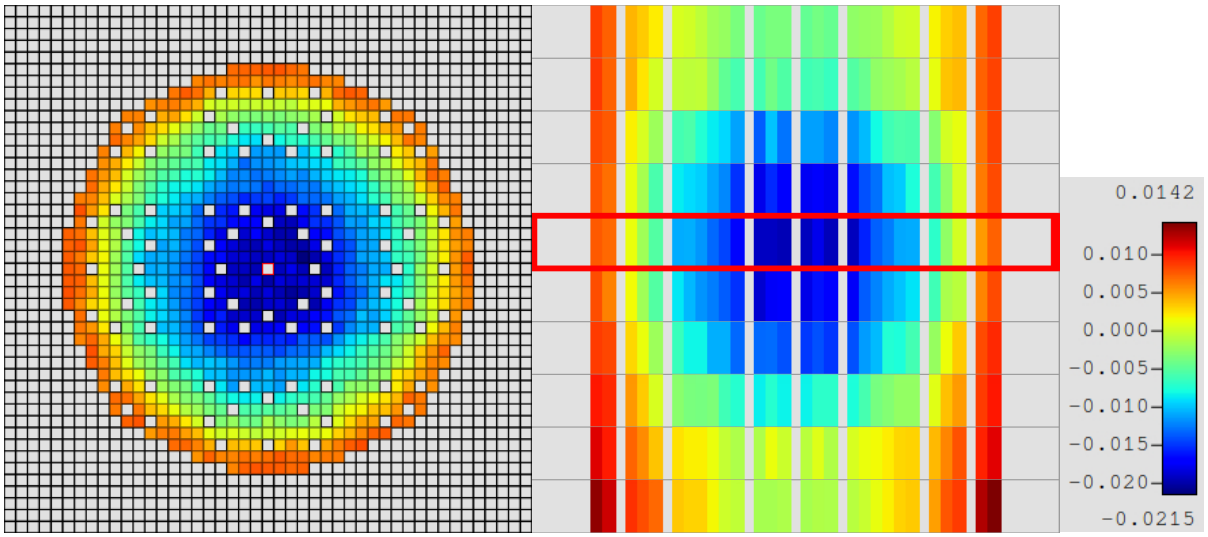

Figure A-73: MPACT radial (left) and axial (right) slices of flux distribution differences (P2) for Case 15.

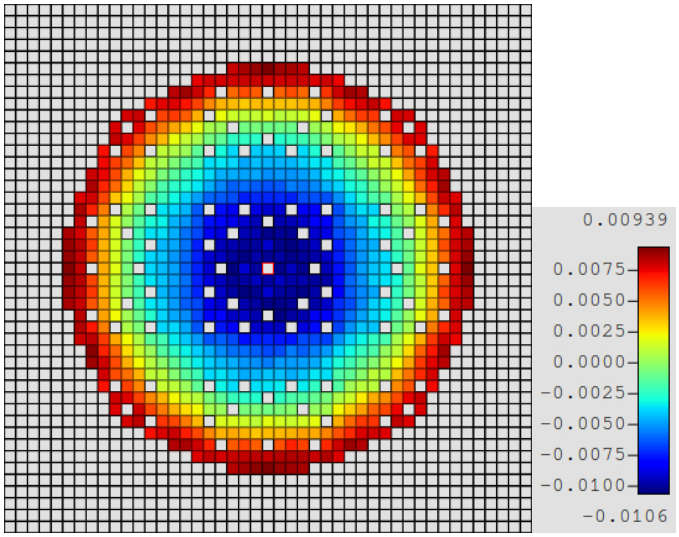

Figure A-74: MPACT radial flux distribution differences for P2 for Case 14.

APPENDIX B. Fission Rate Distribution Comparisons between Shift and KENO-VI

APPENDIX B. FISSION RATE DISTRIBUTION COMPARISONS BETWEEN SHIFT AND KENO-VI

The following results are comparisons of normalized fission rate distributions calculated for the 7uPCX experiment. The reference solutions are from KENO-VI mesh tally calculations using CE ENDF/B-VII.1 data in SCALE 6.3.0. The KENO-VI results are derived from the original models [1] and were generated with 2 billion active particle histories. The Shift results are from VERA version 4.2 and were generated with 10 billion active particle histories. Table B-1 provides the overall statistical summary; Figures B-1 through B-60 provide 2D color plots of the relevant results. For each case, the following are given:

- KENO-VI normalized fission rate distribution, presented as radial and axial slices through the center of the experiment.
- KENO-VI calculated fractional uncertainty in the fission rate distribution, presented as radial and axial slices through the center of the experiment.
- Differences between Shift and KENO-VI normalized fission rate distributions, presented as radial and axial slices through the center of the experiment.
- Differences between Shift and KENO-VI radial (axially integrated) normalized total fission rate distributions.

Note that the Shift results use five times the number of active particle histories as the KENO-VI calculations. This should result in approximately half of the local statistical uncertainty calculated by KENO-VI. The Shift fission rate distributions and uncertainties are shown in Appendix C. For more discussion of particle histories and local uncertainties, see Appendix D.

Table B-1: Normalized Fission Rate Distribution Statistics, Shift-KENO

Case	k-eff Diff	3D RMS	3D Max	2D RMS	2D Max	AO Diff
1	7	0.43%	3.70%	0.10%	0.57%	−0.18%
2	13	0.50%	4.12%	0.13%	0.62%	−0.19%
3	13	0.50%	3.87%	0.13%	0.55%	−0.21%
4	8	0.49%	3.59%	0.13%	0.55%	−0.20%
5	14	0.49%	4.02%	0.14%	0.64%	−0.19%
6	8	0.51%	4.00%	0.13%	0.70%	−0.22%
7	11	0.48%	4.29%	0.13%	0.53%	−0.18%
8	7	0.48%	3.84%	0.13%	0.62%	−0.18%
9	10	0.49%	4.27%	0.13%	0.52%	−0.19%
10	9	0.50%	4.19%	0.13%	0.76%	−0.20%
11	15	0.51%	4.07%	0.13%	0.53%	−0.23%
12	9	0.50%	3.63%	0.13%	0.50%	−0.19%
13	12	0.50%	4.28%	0.13%	0.49%	−0.20%
14	17	0.50%	4.02%	0.13%	0.51%	−0.21%
15	0	0.42%	2.82%	0.13%	0.45%	−0.18%
Average	**10**	**0.49%**	**3.91%**	**0.13%**	**0.57%**	**−0.20%**
St Dev	**4**	**0.03%**	**0.38%**	**0.01%**	**0.08%**	**0.01%**

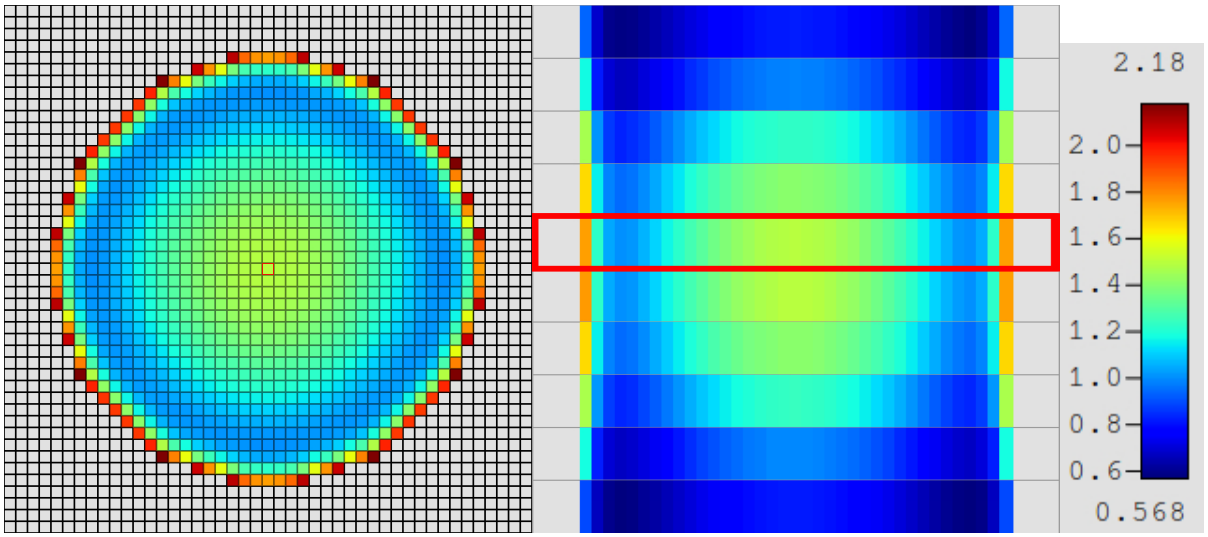

Figure B-1: KENO-VI radial (left) and axial (right) slices of fission rate distributions for Case 1.

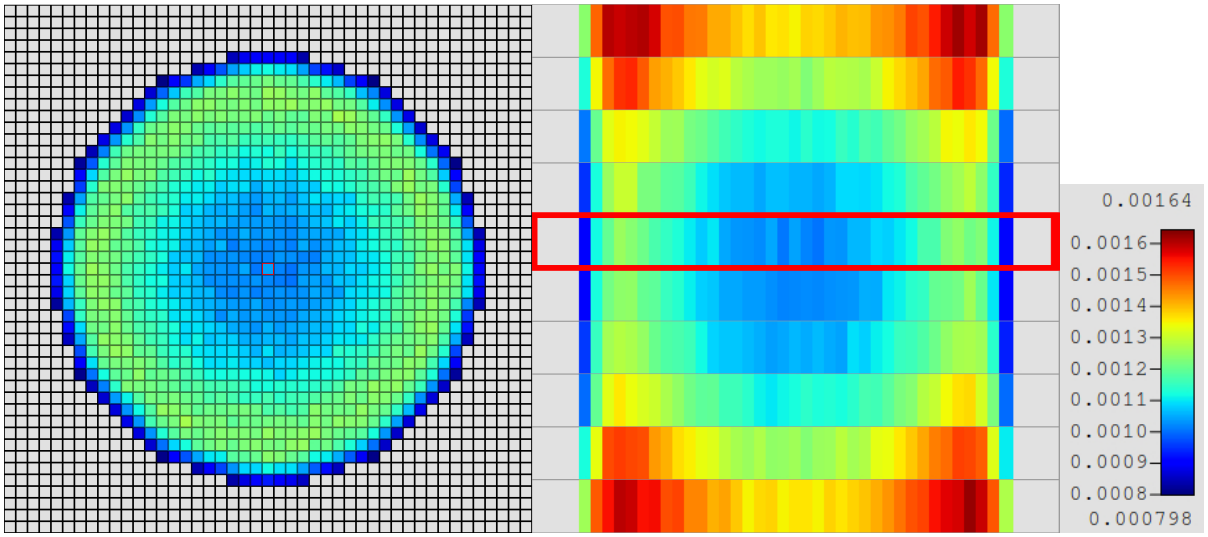

Figure B-2: KENO-VI radial (left) and axial (right) slices of fractional uncertainties for Case 1.

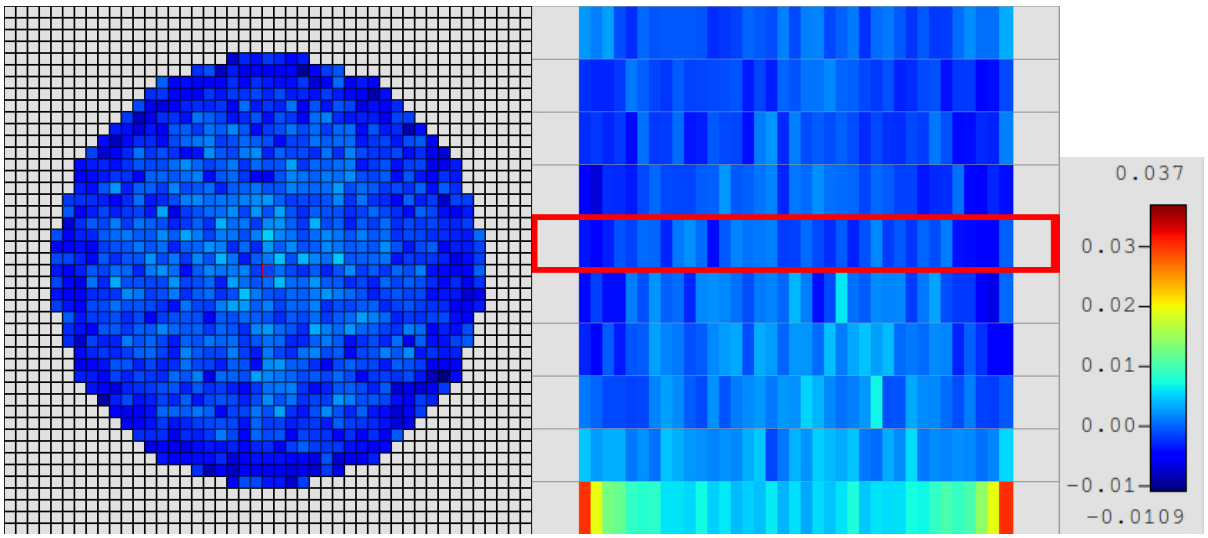

Figure B-3: Shift radial (left) and axial (right) slices of fission rate distribution differences for Case 1.

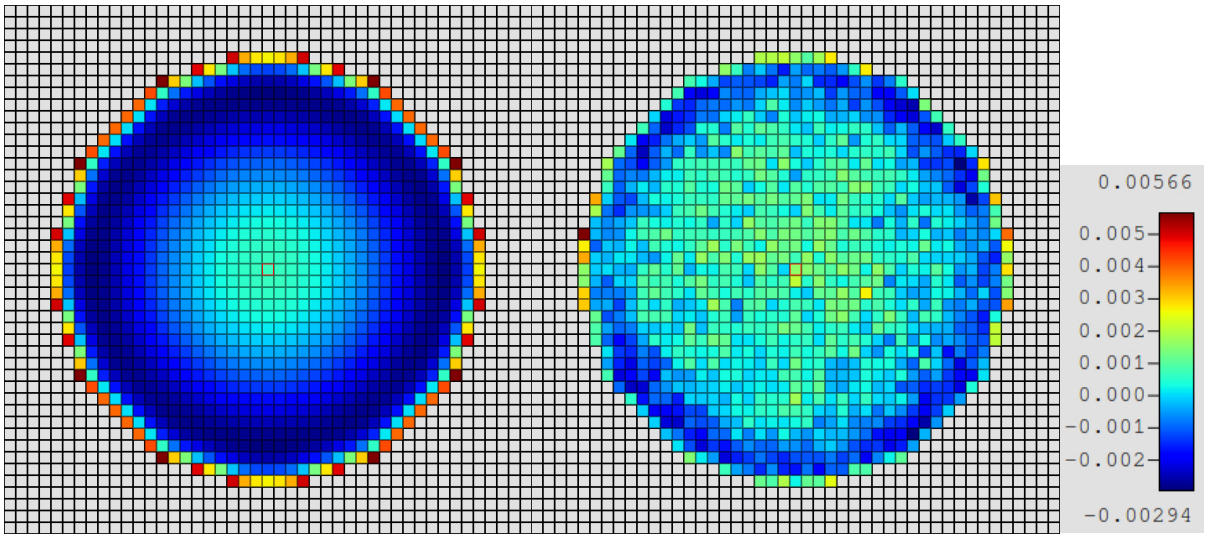

Figure B-4: KENO-VI radial fission rate distribution (left) and Shift Differences (right) for Case 1.

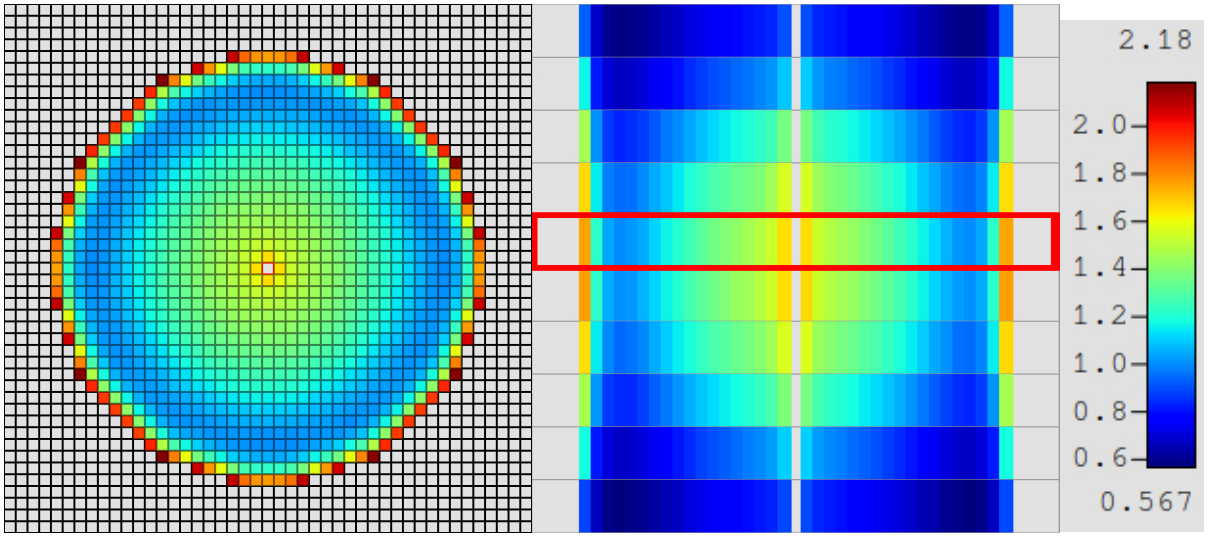

Figure B-5: KENO-VI radial (left) and axial (right) slices of fission rate distributions for Case 2.

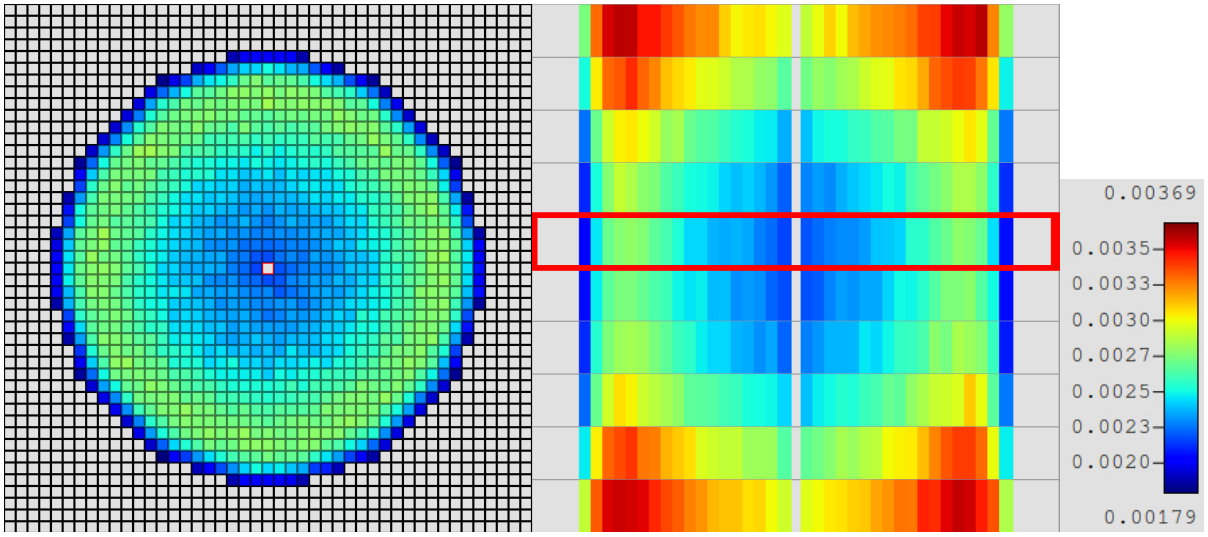

Figure B-6: KENO-VI radial (left) and axial (right) slices of fractional uncertainties for Case 2.

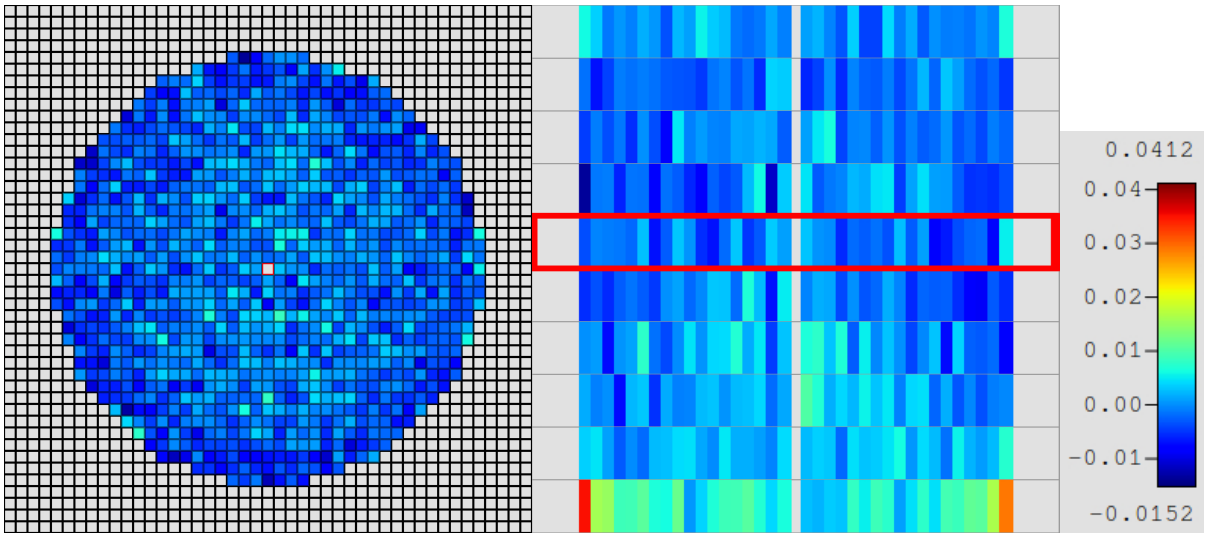

Figure B-7: Shift radial (left) and axial (right) slices of fission rate distribution differences for Case 2.

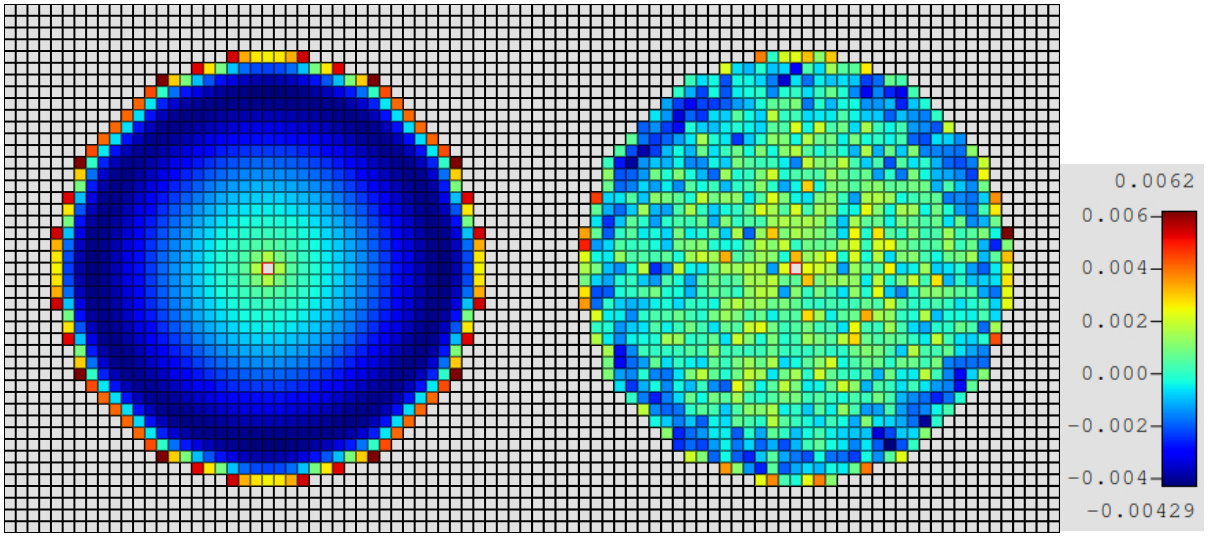

Figure B-8: KENO-VI radial fission rate distribution (left) and Shift Differences (right) for Case 2.

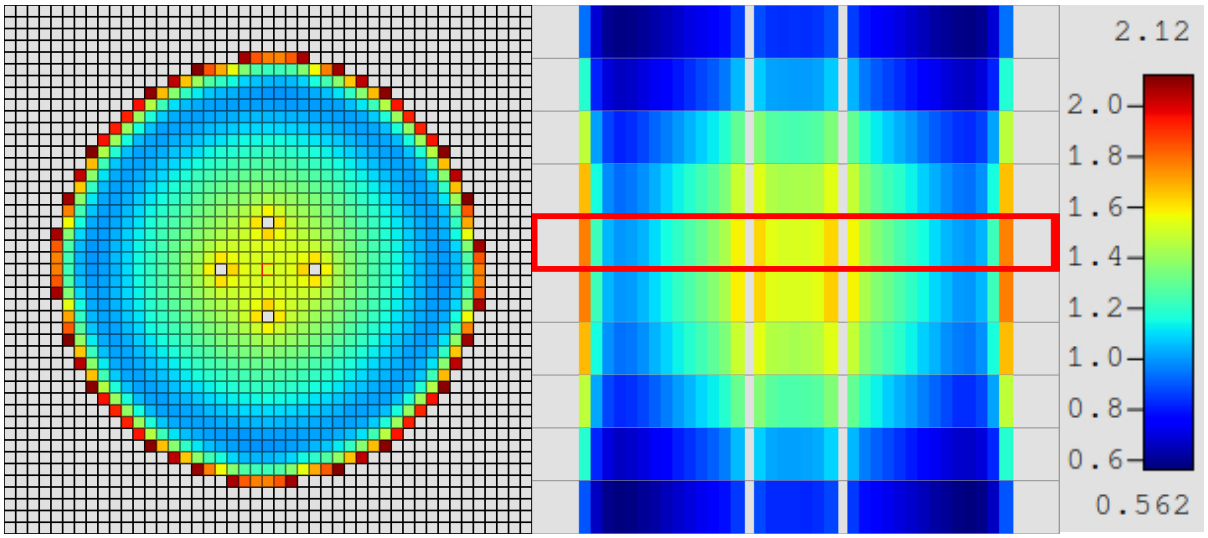

Figure B-9: KENO-VI radial (left) and axial (right) slices of fission rate distributions for Case 3.

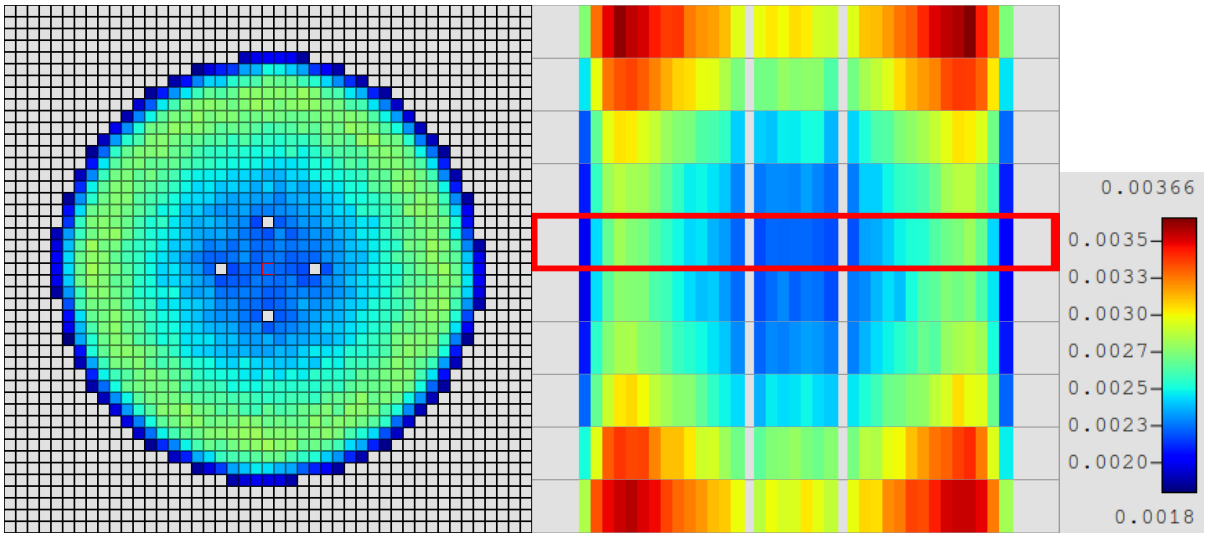

Figure B-10: KENO-VI radial (left) and axial (right) slices of fractional uncertainties for Case 3.

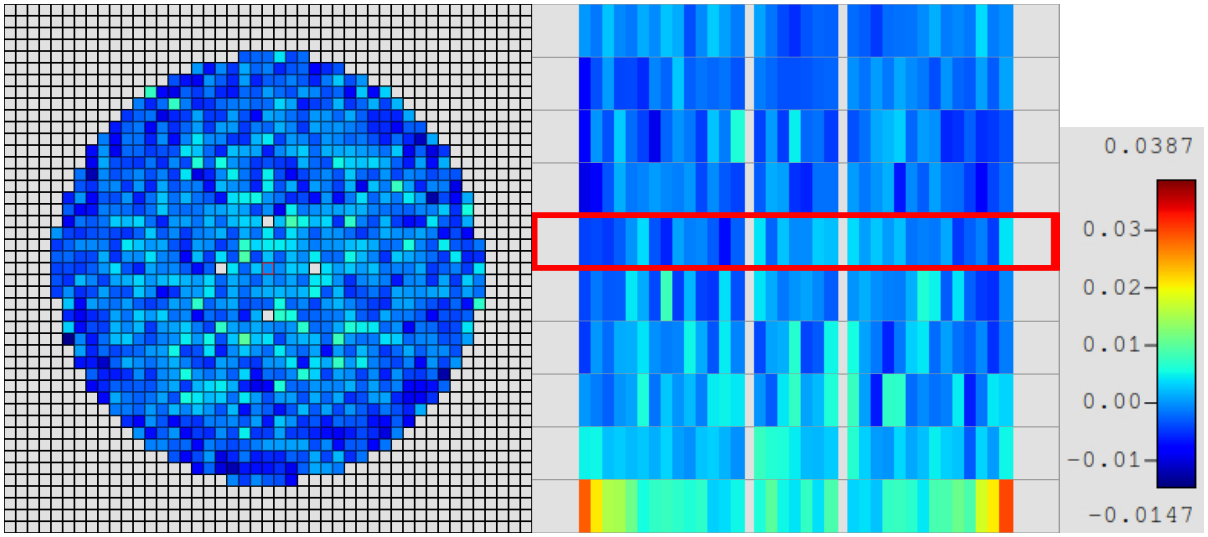

Figure B-11: Shift radial (left) and axial (right) slices of fission rate distribution differences for Case 3.

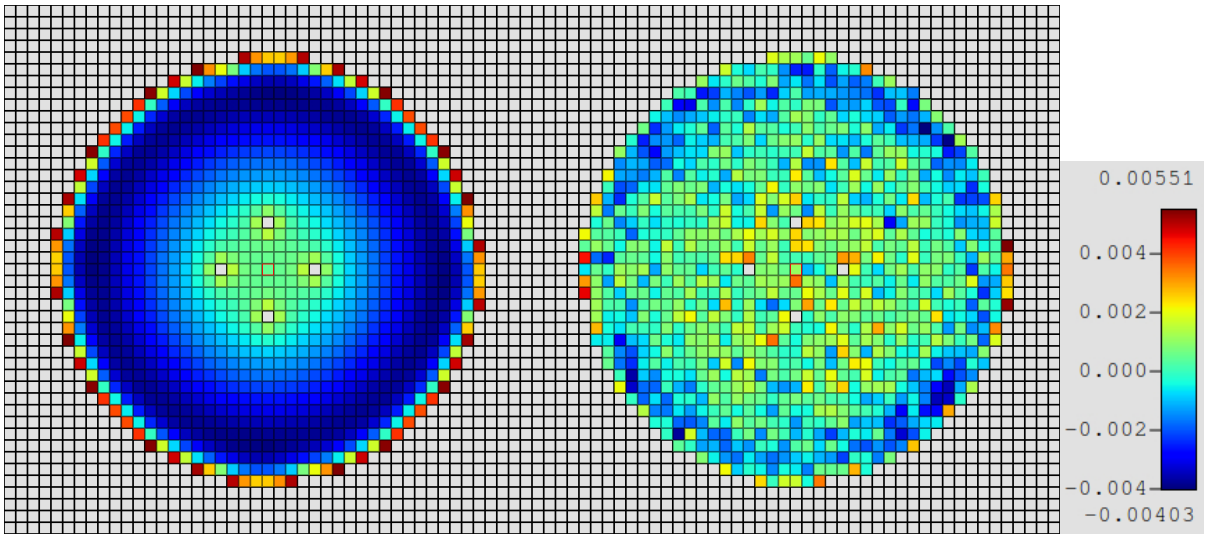

Figure B-12: KENO-VI radial fission rate distribution (left) and shift differences (right) for Case 3.

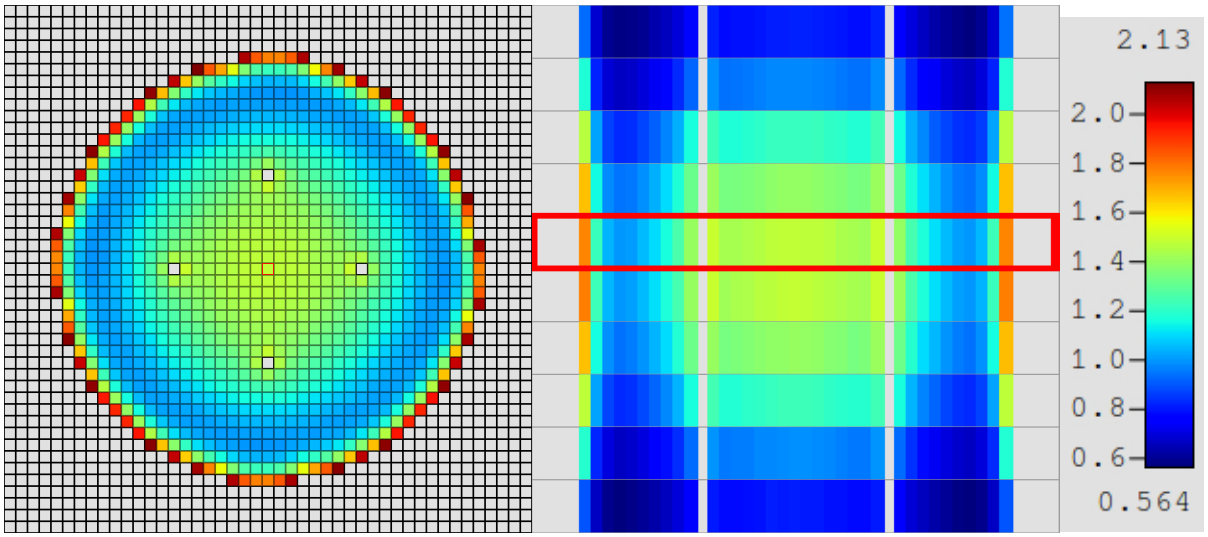

Figure B-13: KENO-VI radial (left) and axial (right) slices of fission rate distributions for Case 4.

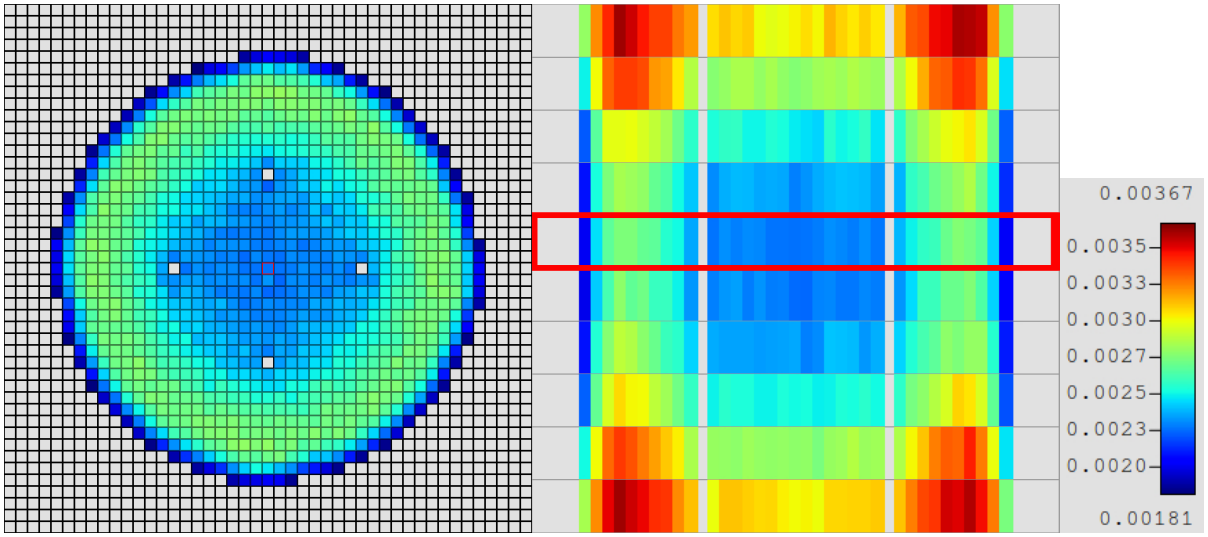

Figure B-14: KENO-VI radial (left) and axial (right) slices of fractional uncertainties for Case 4.

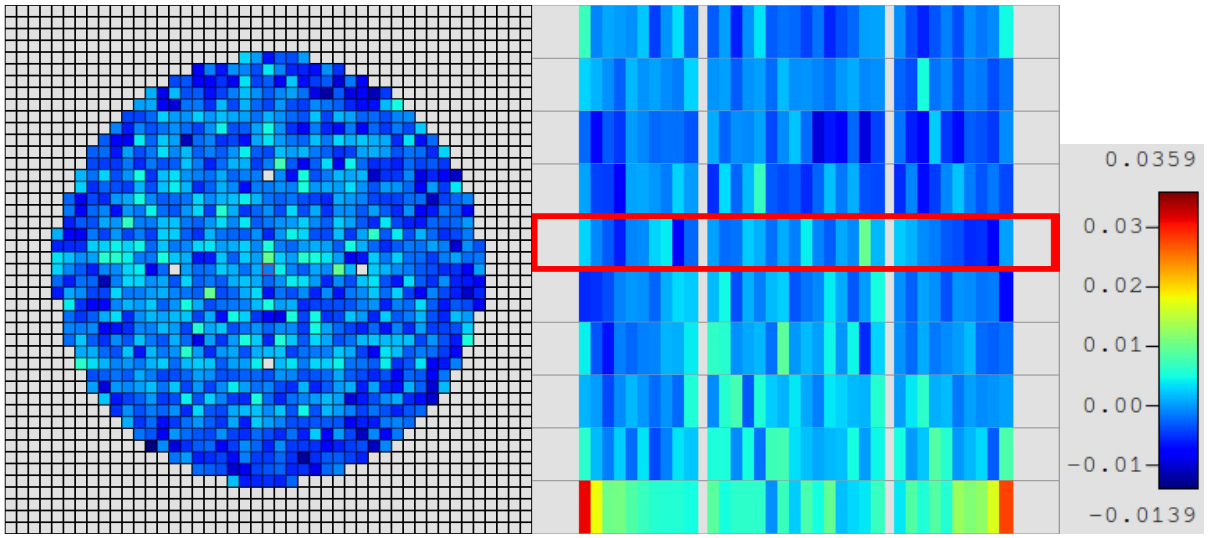

Figure B-15: Shift radial (left) and axial (right) slices of fission rate distribution differences for Case 4.

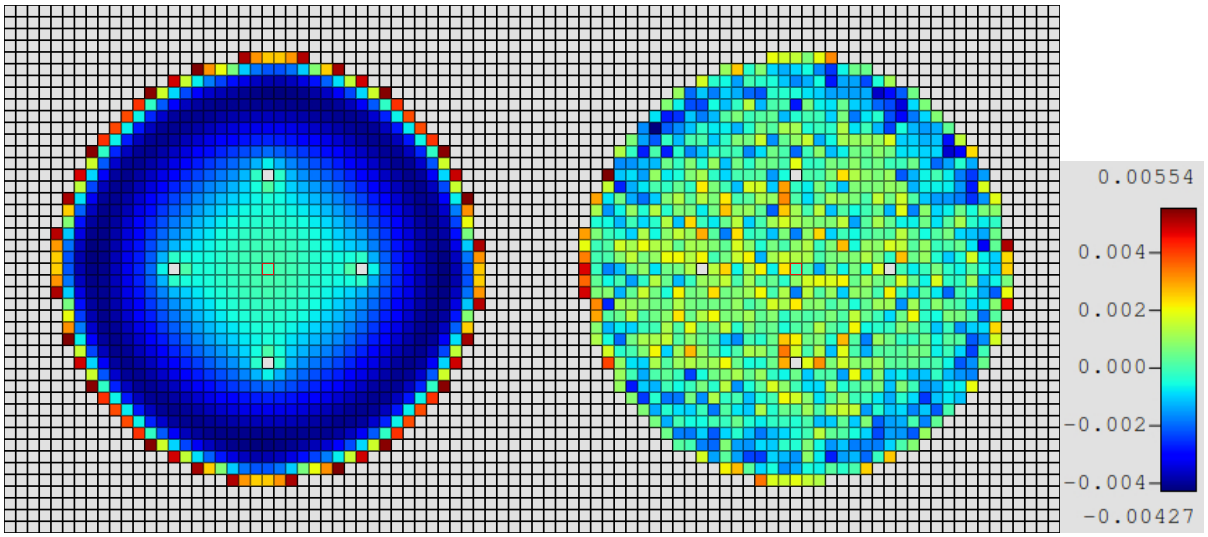

Figure B-16: KENO-VI radial fission rate distribution (left) and shift differences (right) for Case 4.

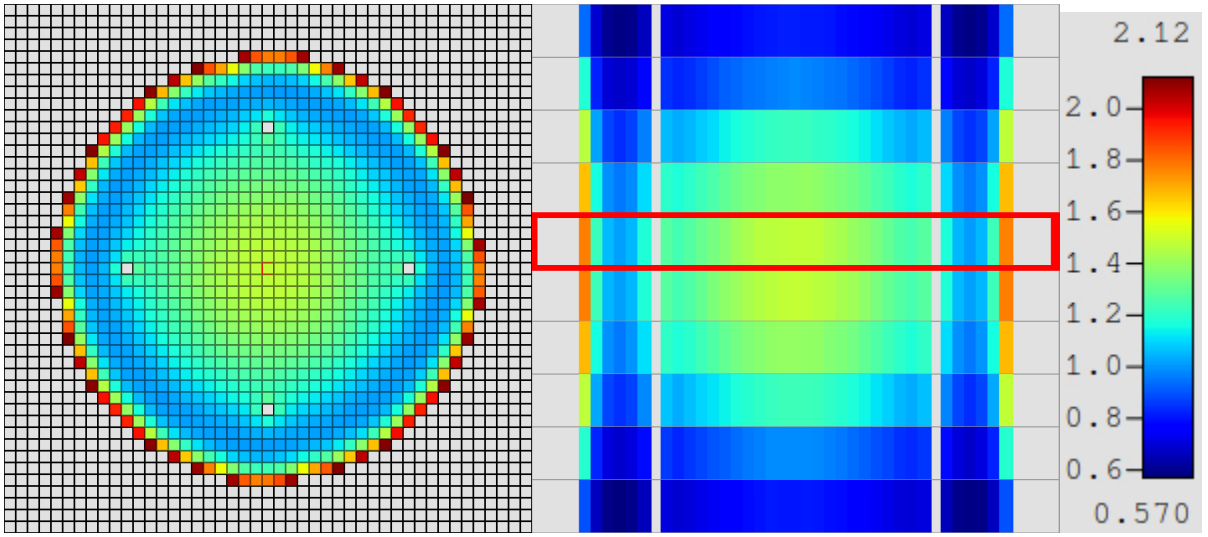

Figure B-17: KENO-VI radial (left) and axial (right) slices of fission rate distributions for Case 5.

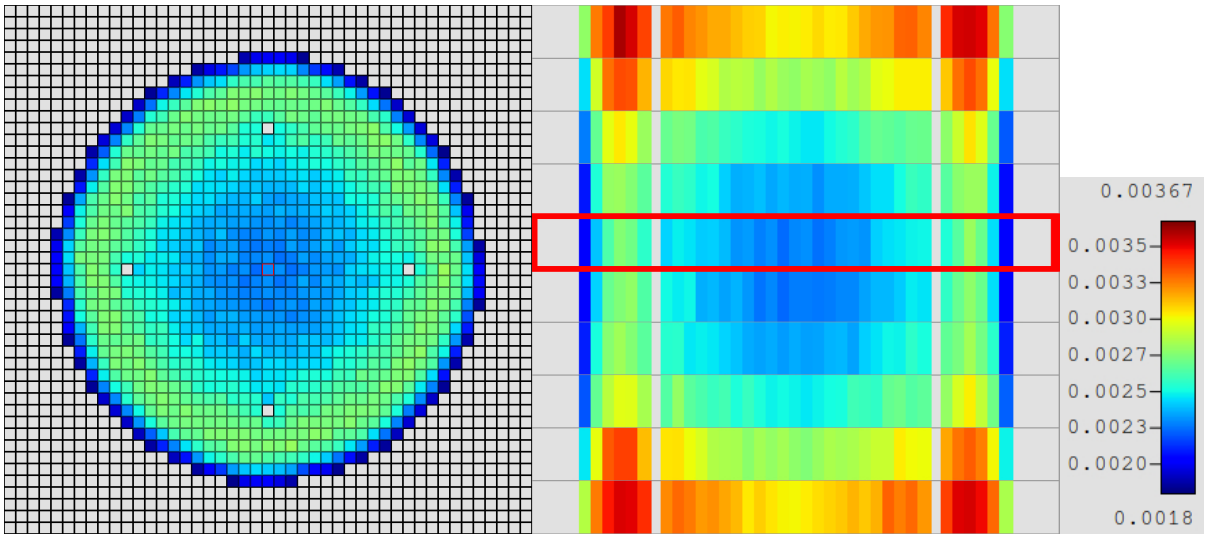

Figure B-18: KENO-VI radial (left) and axial (right) slices of fractional uncertainties for Case 5.

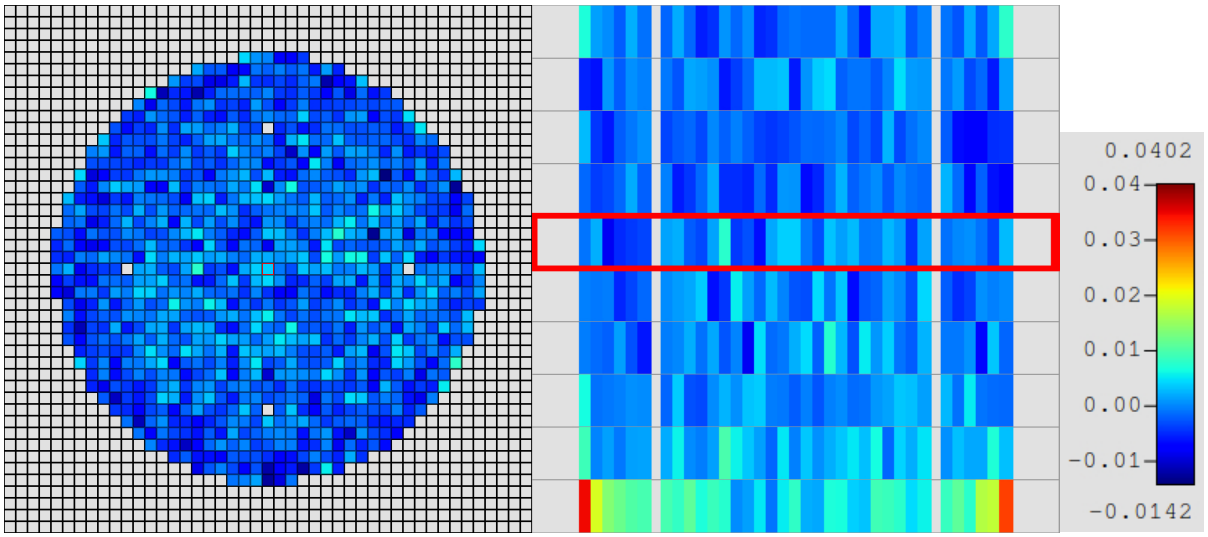

Figure B-19: Shift radial (left) and axial (right) slices of fission rate distribution differences for Case 5.

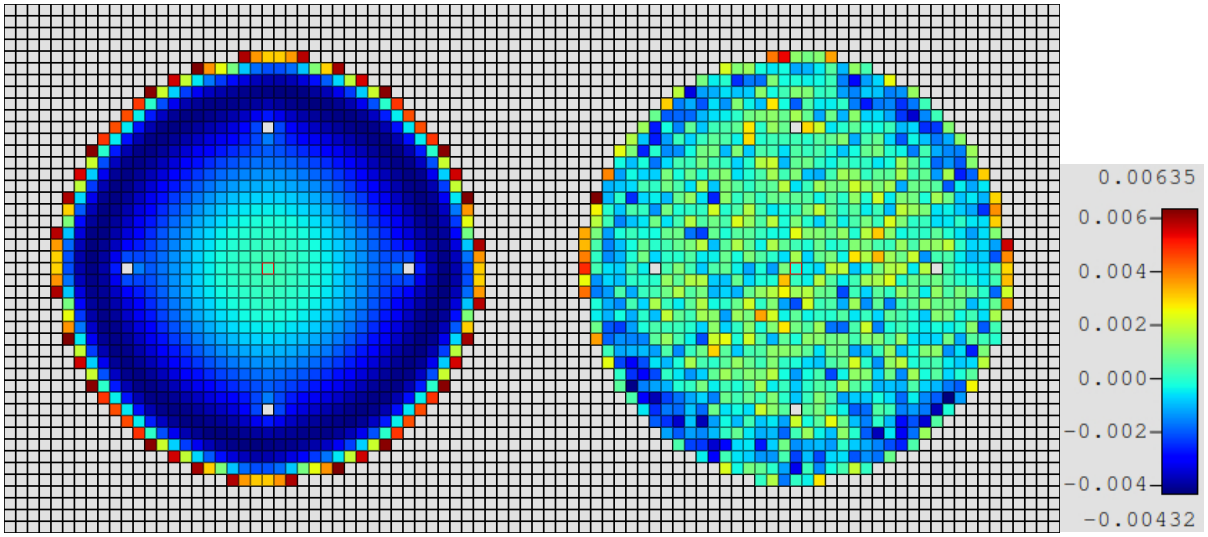

Figure B-20: KENO-VI radial fission rate distribution (left) and shift differences (right) for Case 5.

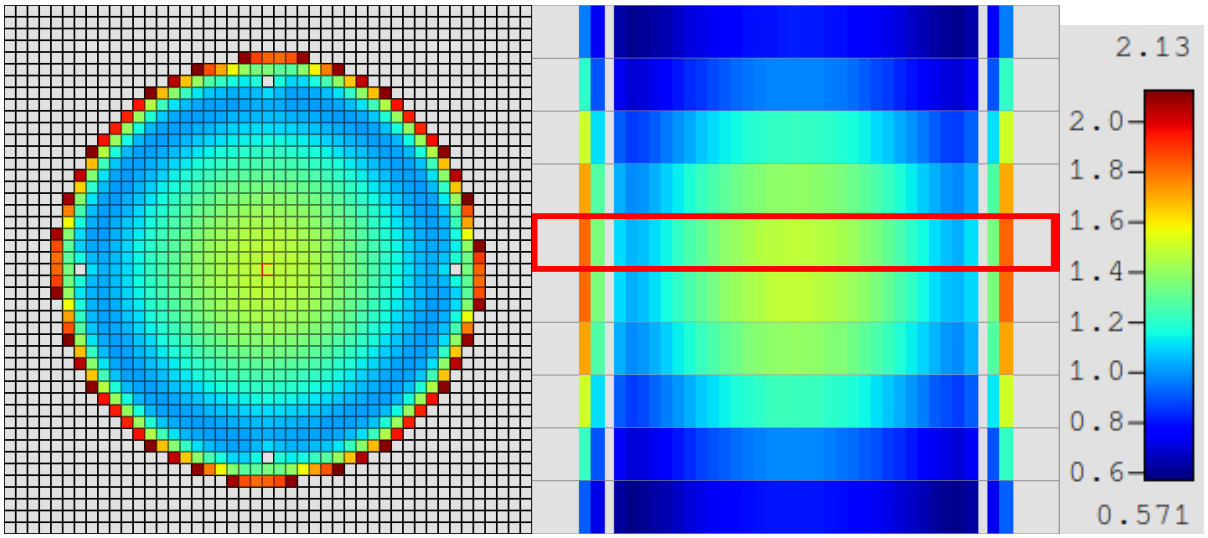

Figure B-21: KENO-VI radial (left) and axial (right) slices of fission rate distributions for Case 6.

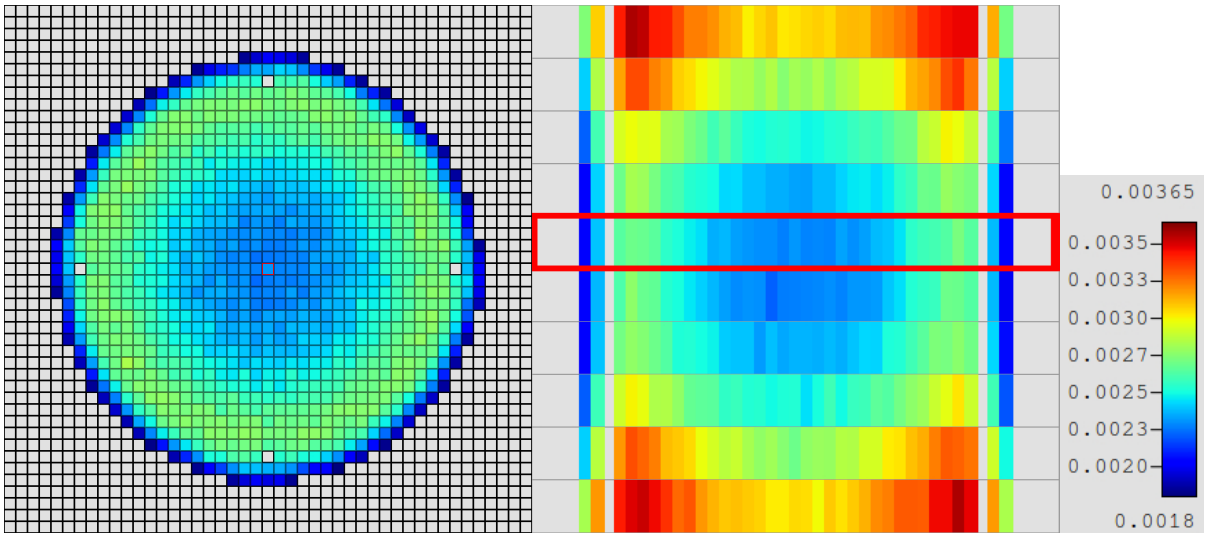

Figure B-22: KENO-VI radial (left) and axial (right) slices of fractional uncertainties for Case 6.

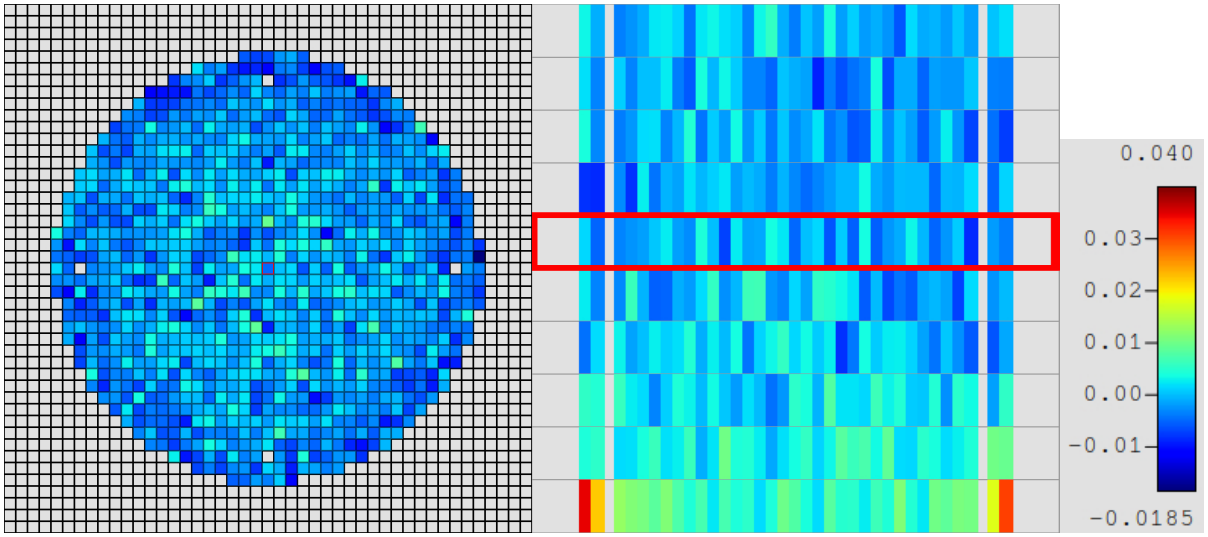

Figure B-23: Shift radial (left) and axial (right) slices of fission rate distribution differences for Case 6.

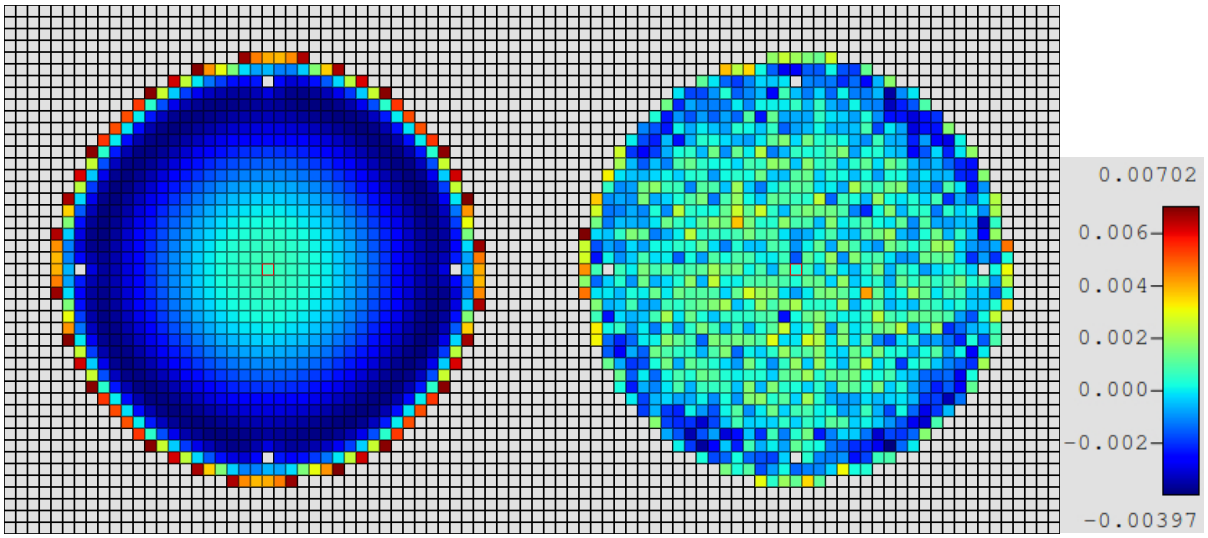

Figure B-24: KENO-VI radial fission rate distribution (left) and shift differences (right) for Case 6.

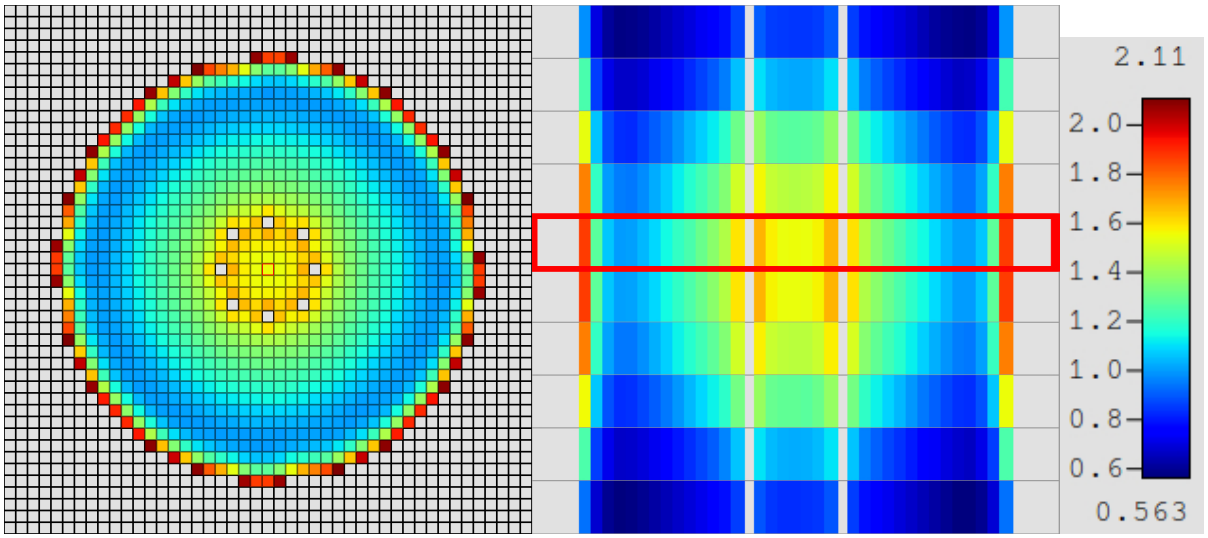

Figure B-25: KENO-VI radial (left) and axial (right) slices of fission rate distributions for Case 7.

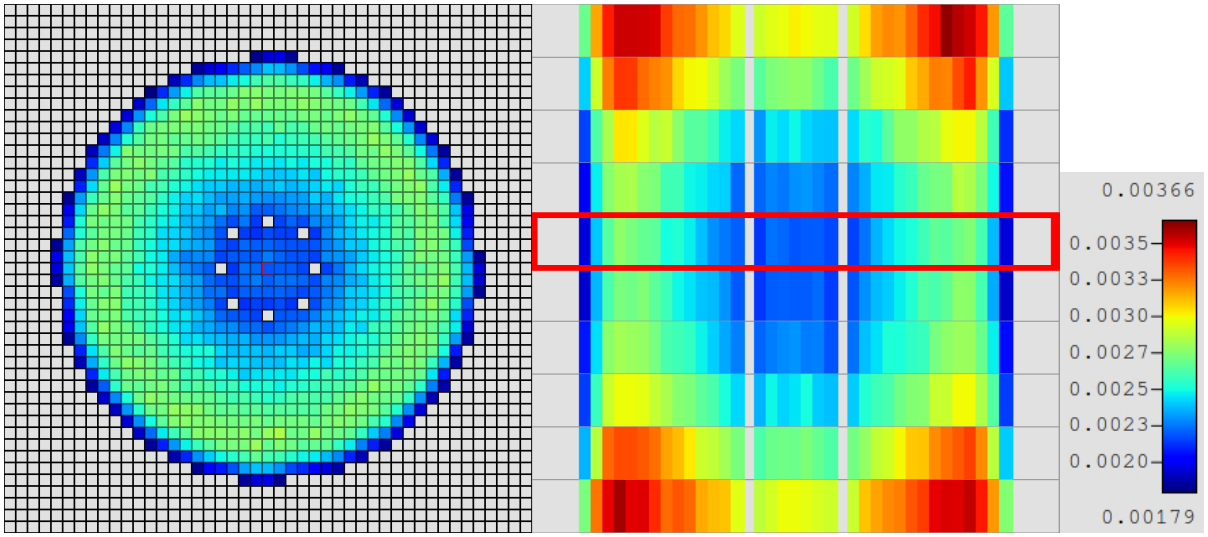

Figure B-26: KENO-VI radial (left) and axial (right) slices of fractional uncertainties for Case 7.

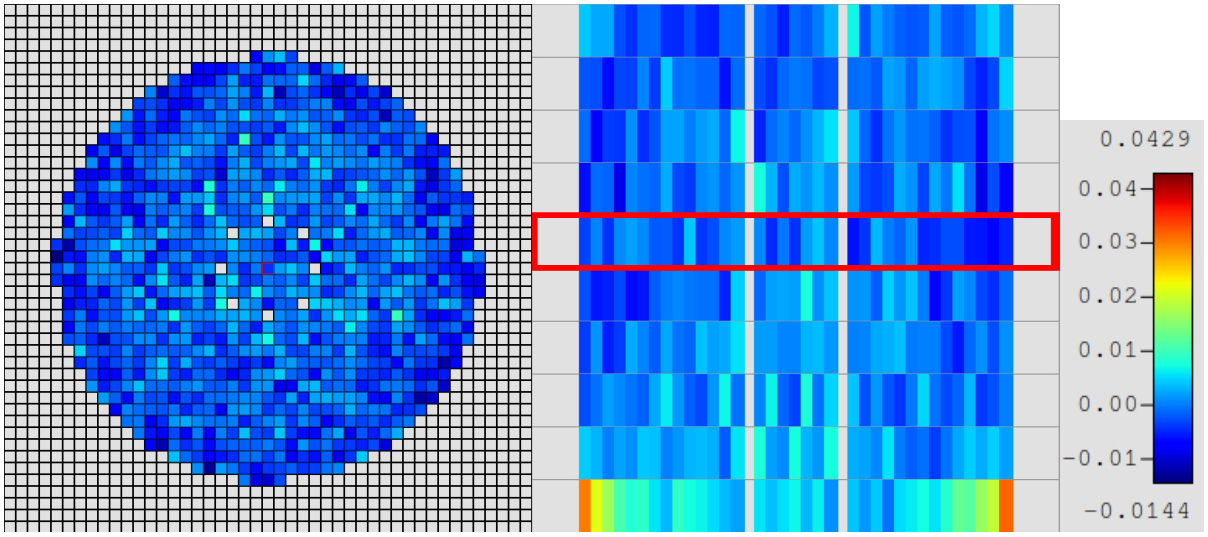

Figure B-27: Shift radial (left) and axial (right) slices of fission rate distribution differences for Case 7.

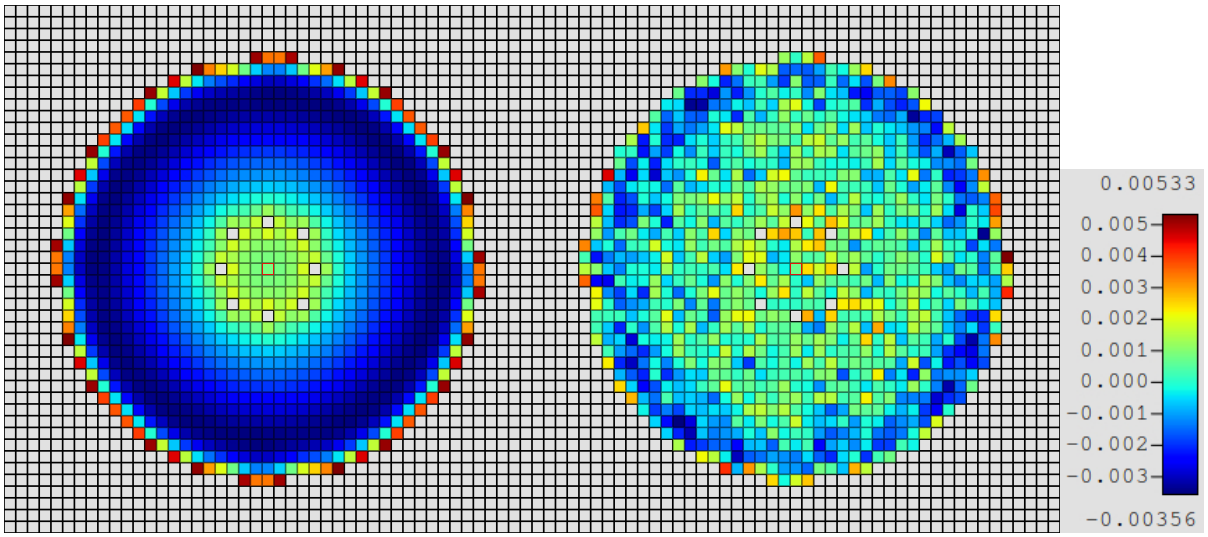

Figure B-28: KENO-VI radial fission rate distribution (left) and shift differences (right) for Case 7.

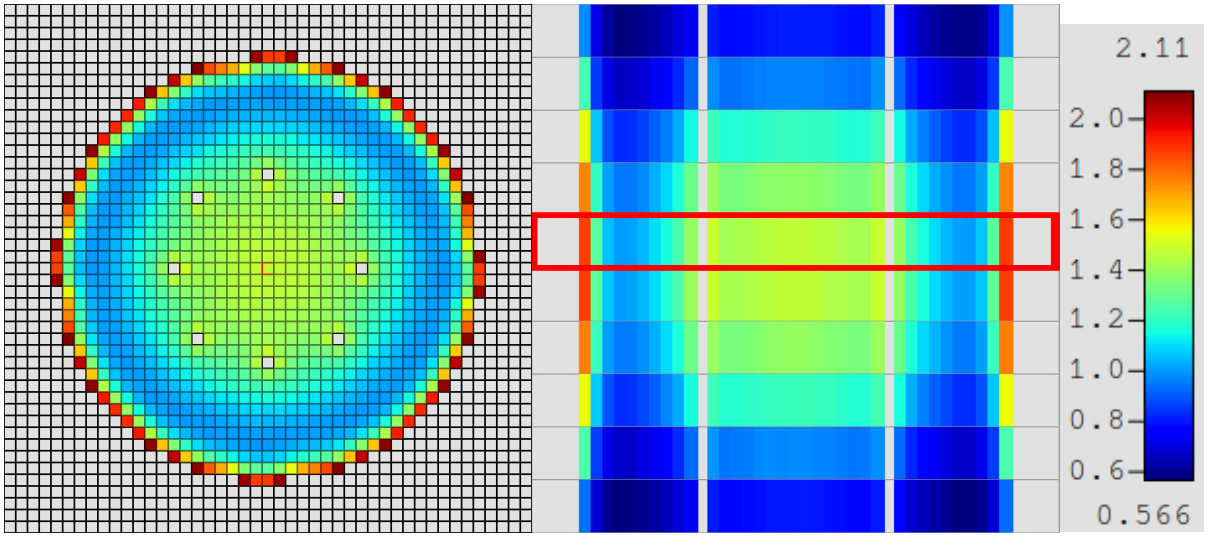

Figure B-29: KENO-VI radial (left) and axial (right) slices of fission rate distributions for Case 8.

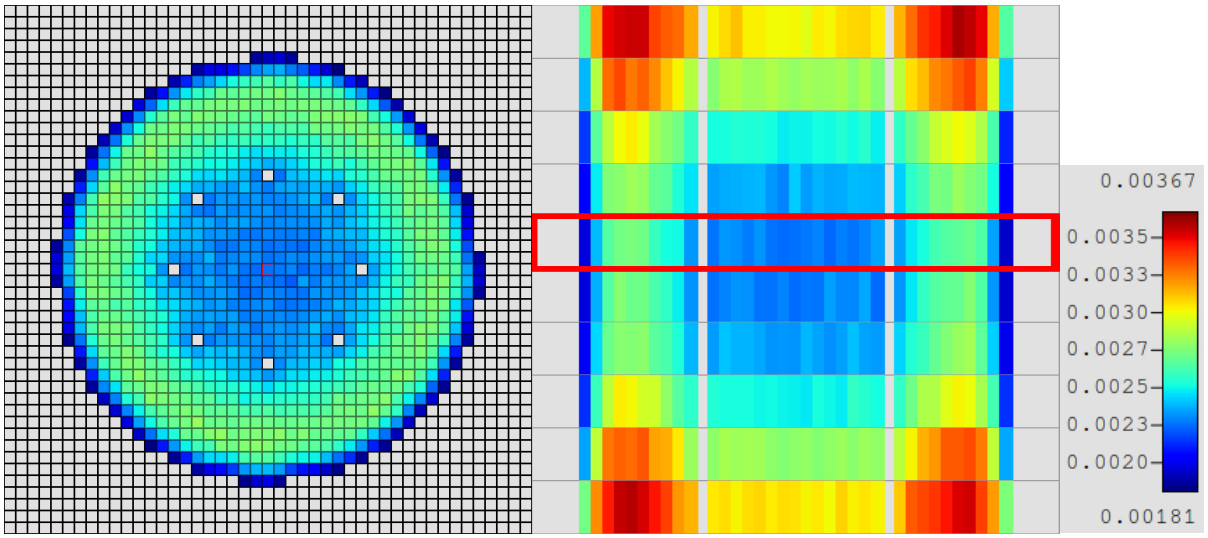

Figure B-30: KENO-VI radial (left) and axial (right) slices of fractional uncertainties for Case 8.

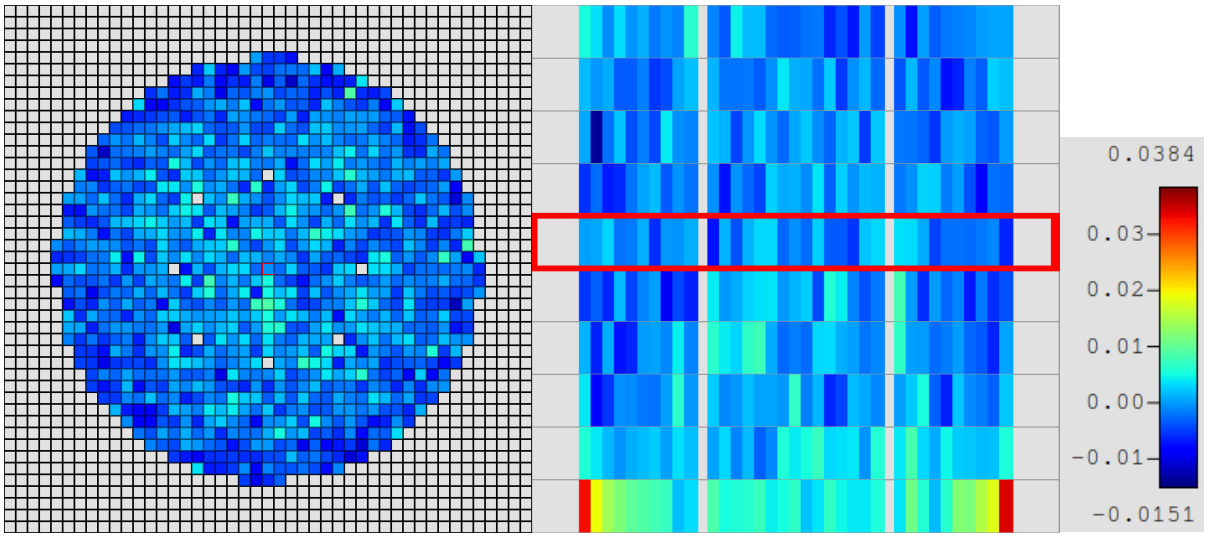

Figure B-31: Shift radial (left) and axial (right) slices of fission rate distribution differences for Case 8.

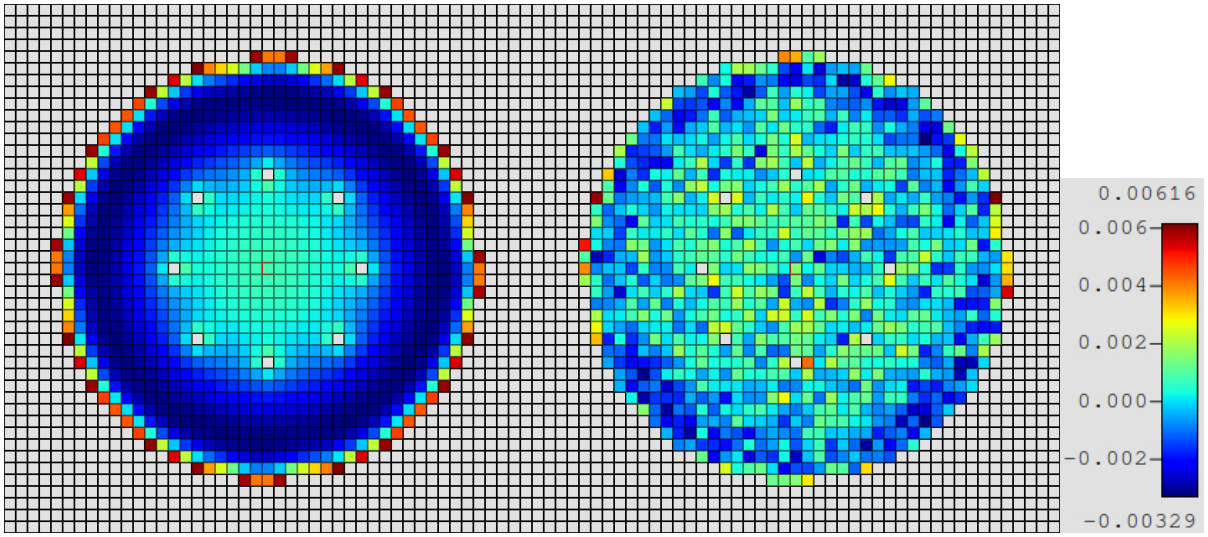

Figure B-32: KENO-VI radial fission rate distribution (left) and Shift differences (right) for Case 8.

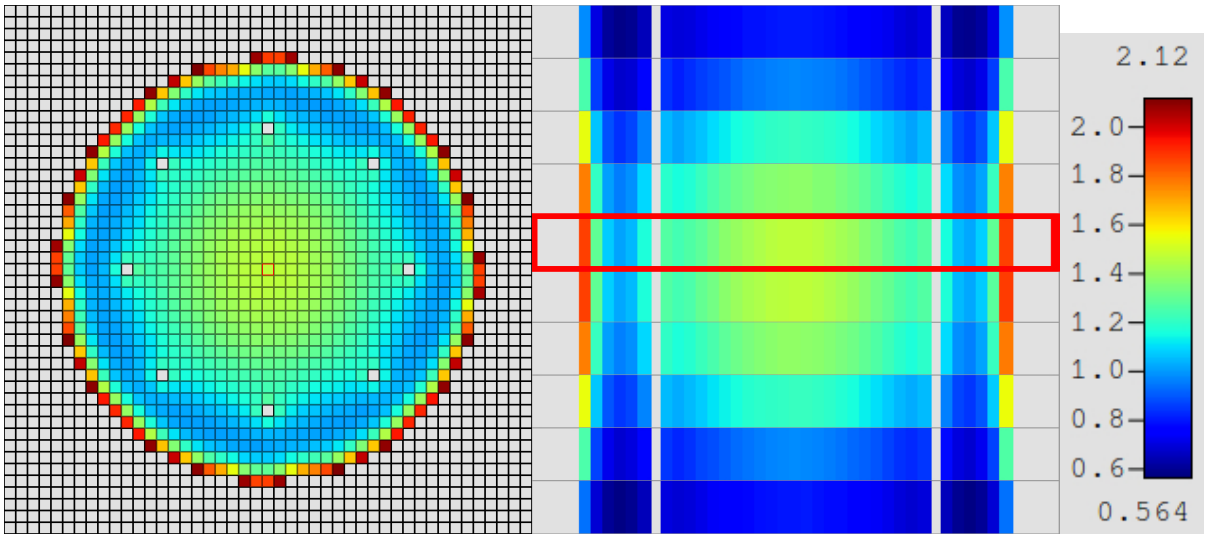

Figure B-33: KENO-VI radial (left) and axial (right) slices of fission rate distributions for Case 9.

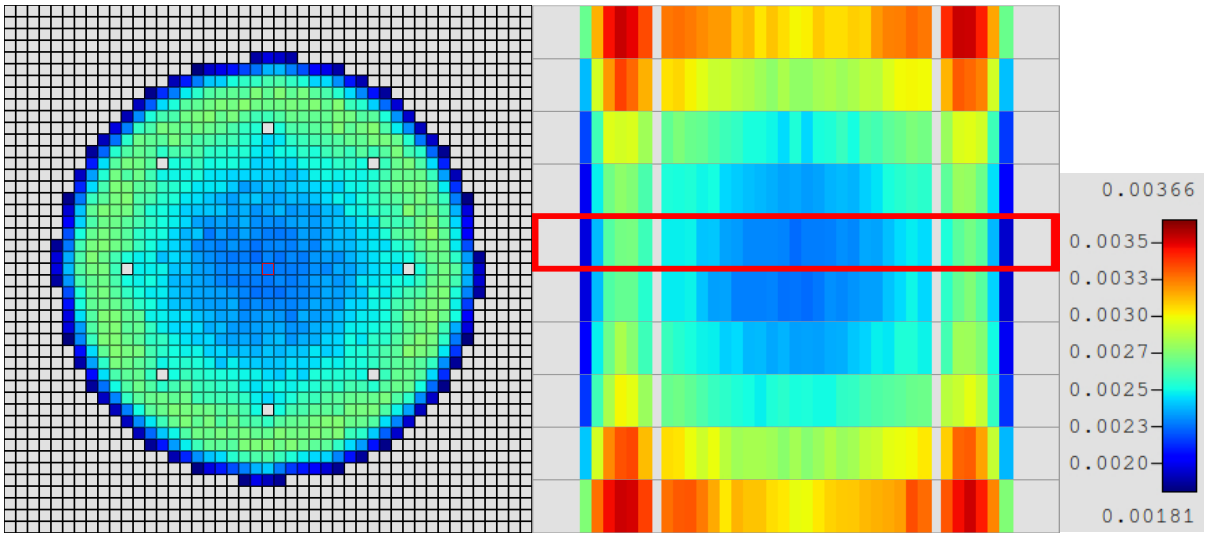

Figure B-34: KENO-VI radial (left) and axial (right) slices of fractional uncertainties for Case 9.

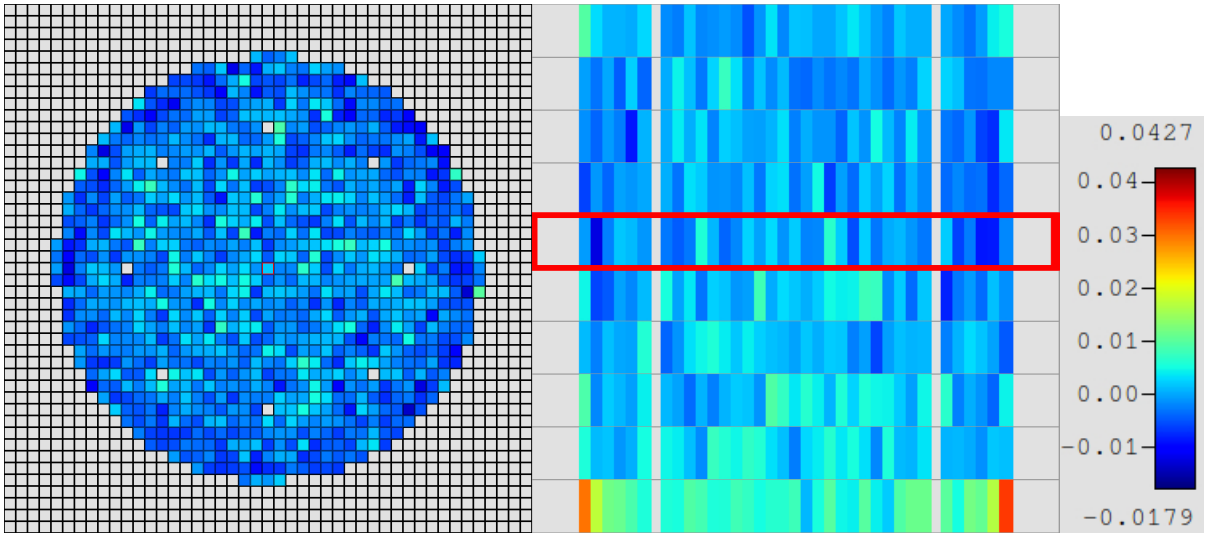

Figure B-35: Shift radial (left) and axial (right) slices of fission rate distribution differences for Case 9.

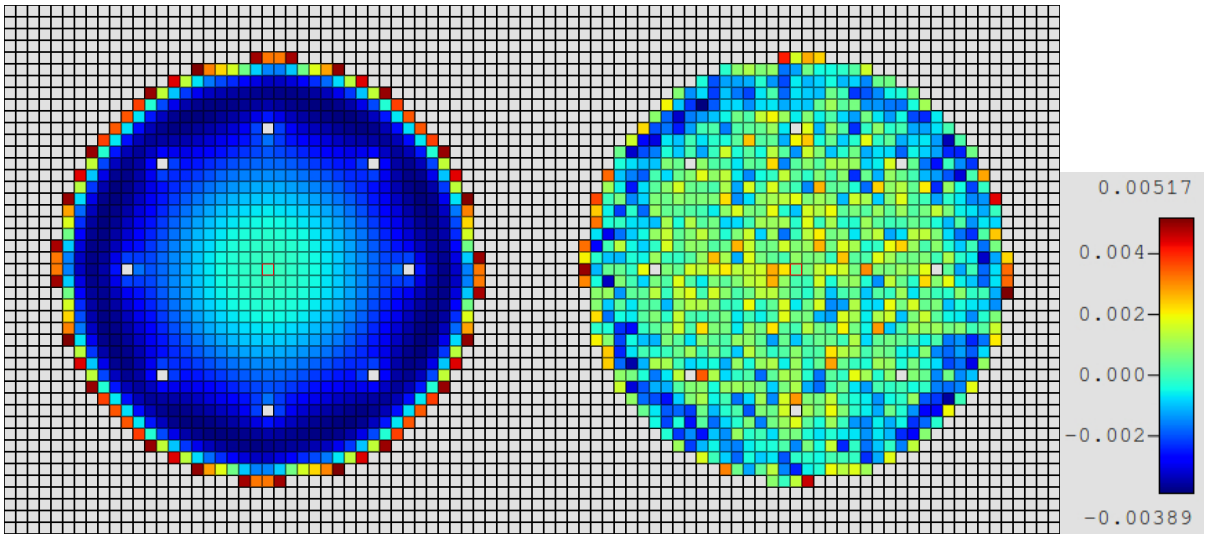

Figure B-36: KENO-VI radial fission rate distribution (left) and shift differences (right) for Case 9.

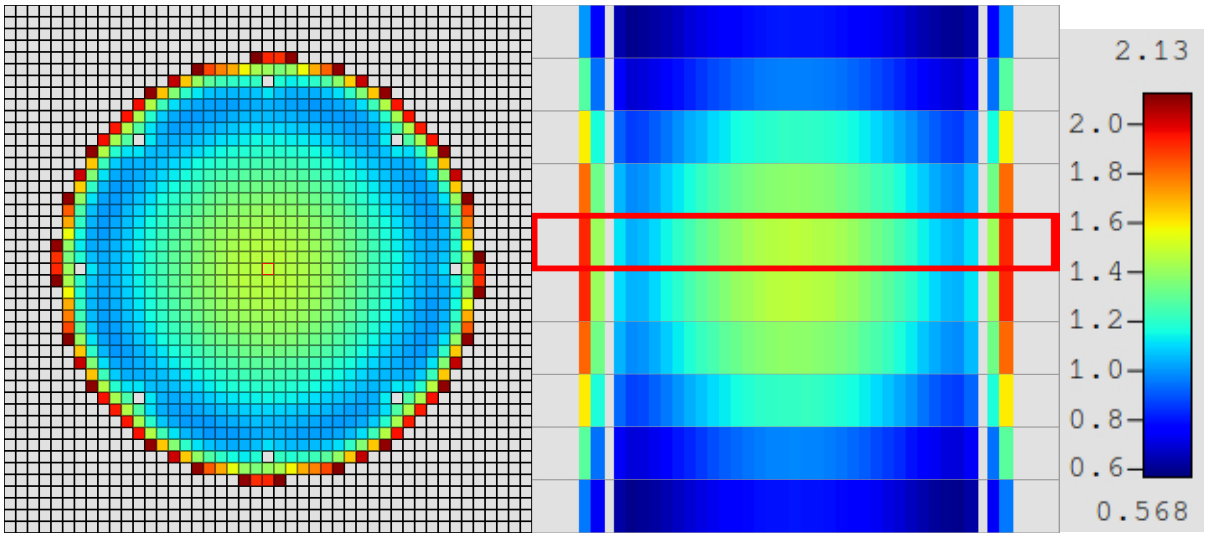

Figure B-37: KENO-VI radial (left) and axial (right) slices of fission rate distributions for Case 10.

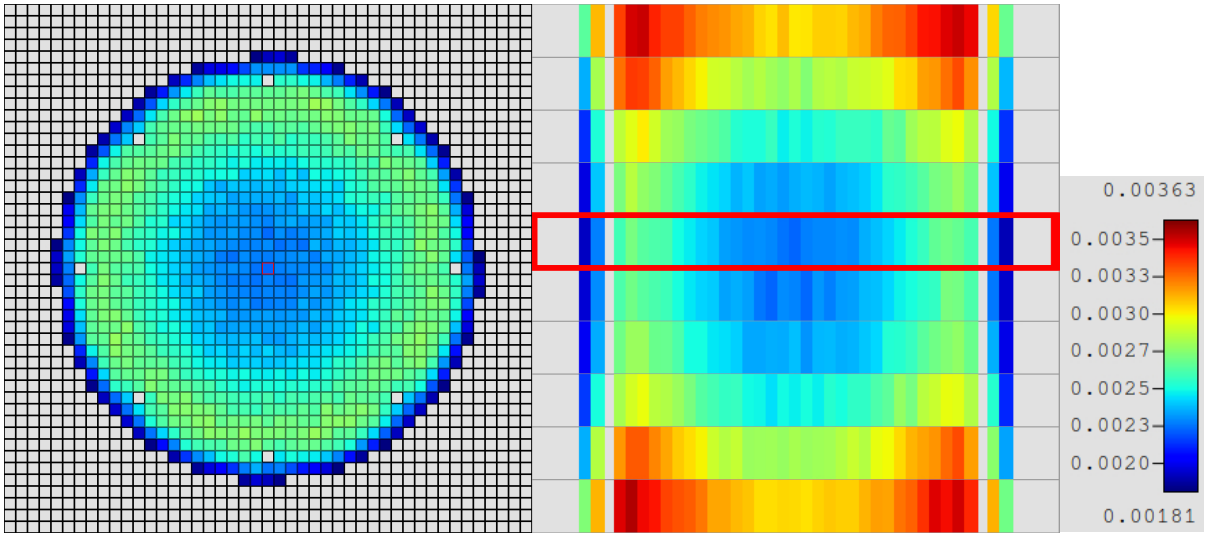

Figure B-38: KENO-VI radial (left) and axial (right) slices of fractional uncertainties for Case 10.

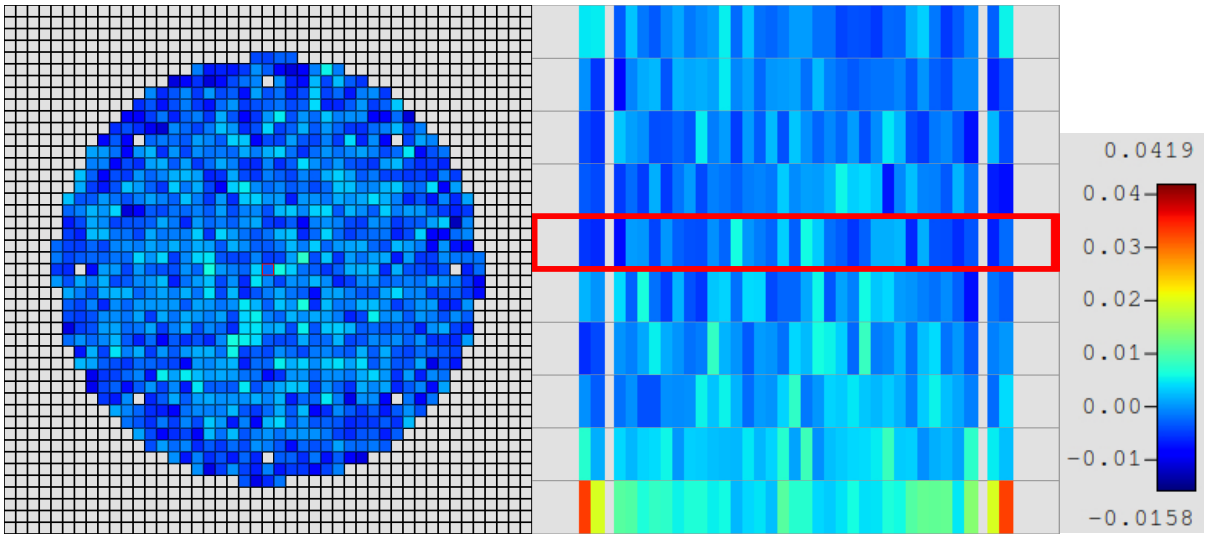

Figure B-39: Shift radial (left) and axial (right) slices of fission rate distribution differences for Case 10.

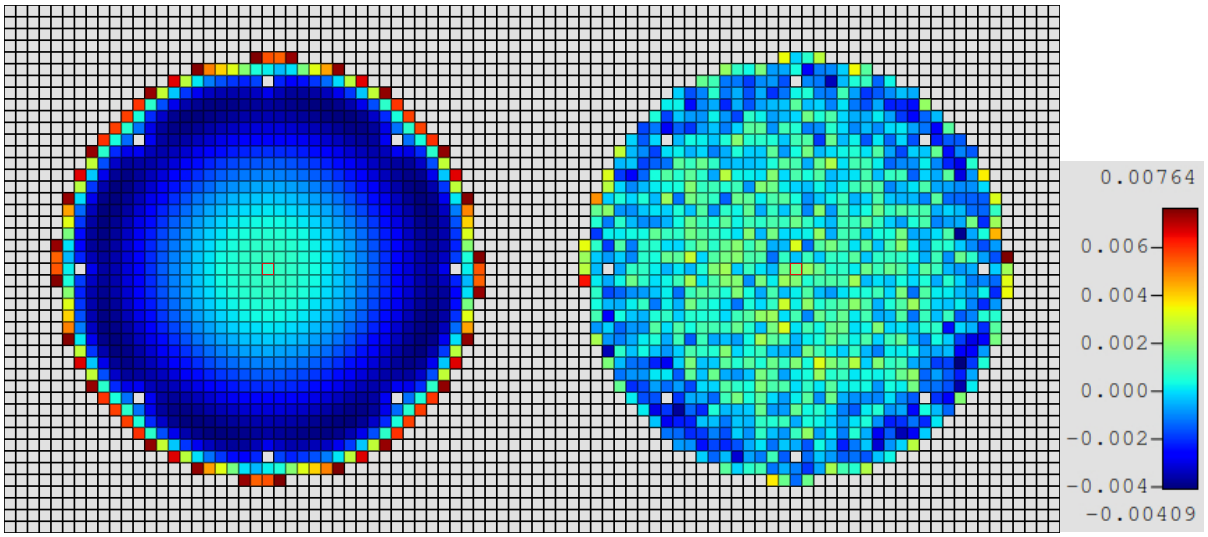

Figure B-40: KENO-VI radial fission rate distribution (left) and Shift differences (right) for Case 10.

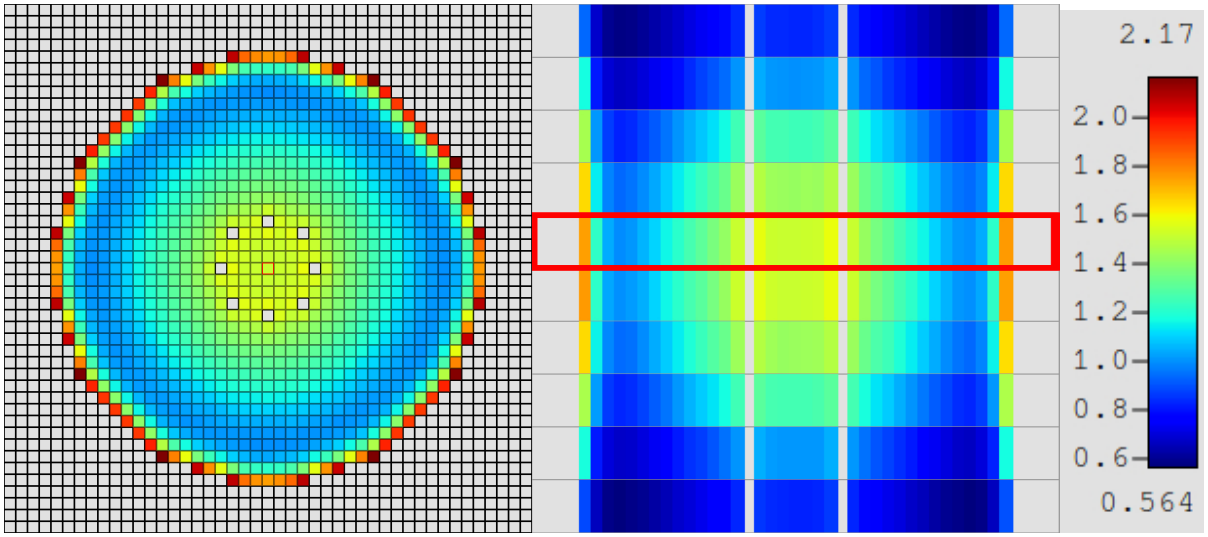

Figure B-41: KENO-VI radial (left) and axial (right) slices of fission rate distributions for Case 11.

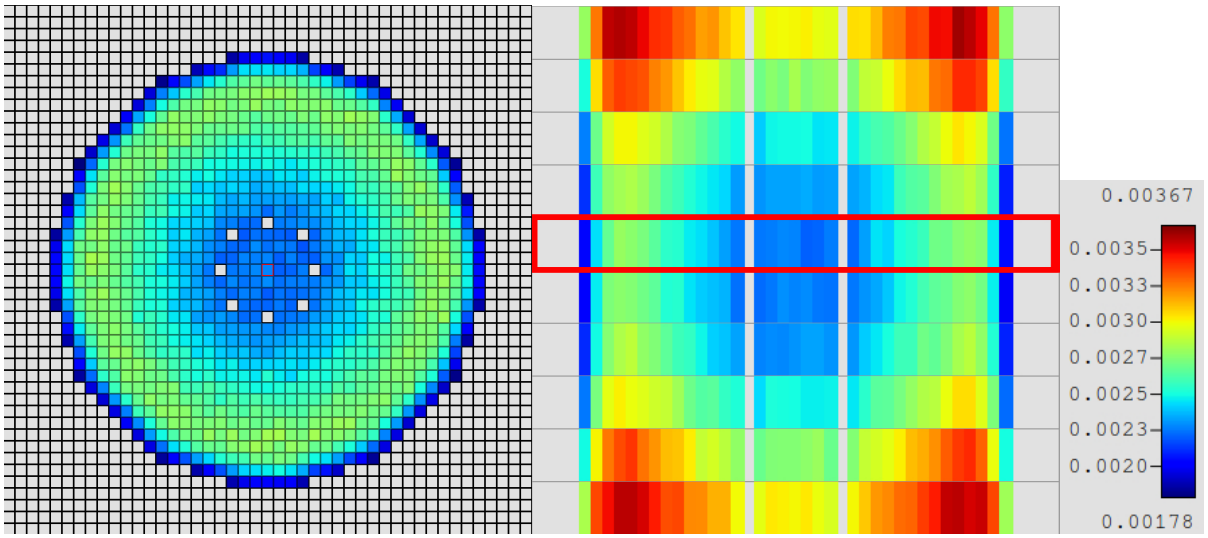

Figure B-42: KENO-VI radial (left) and axial (right) slices of fractional uncertainties for Case 11.

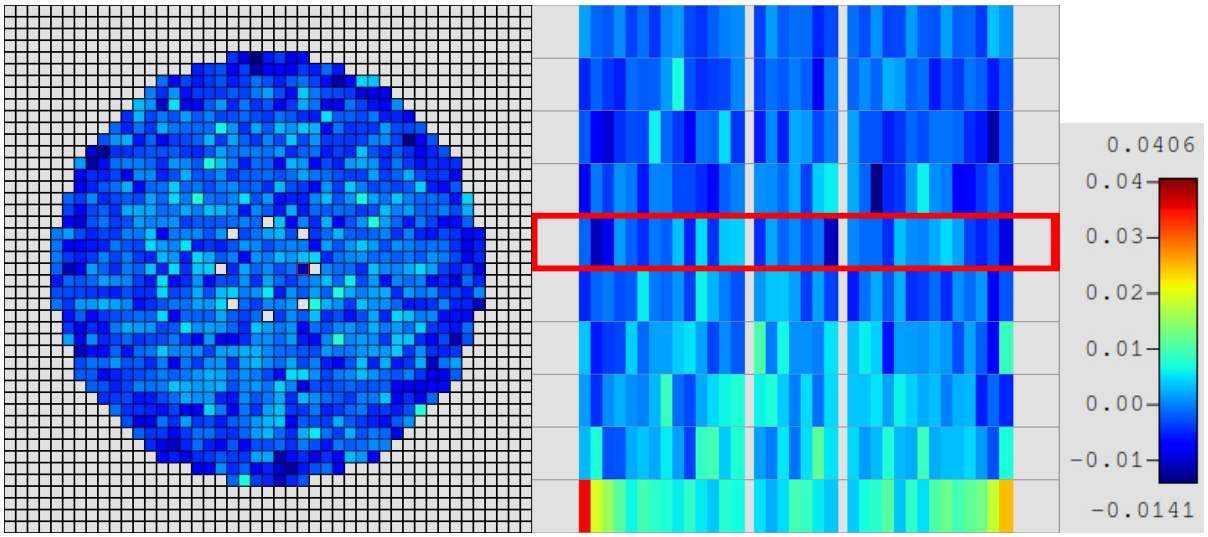

Figure B-43: Shift radial (left) and axial (right) slices of fission rate distribution differences for Case 11.

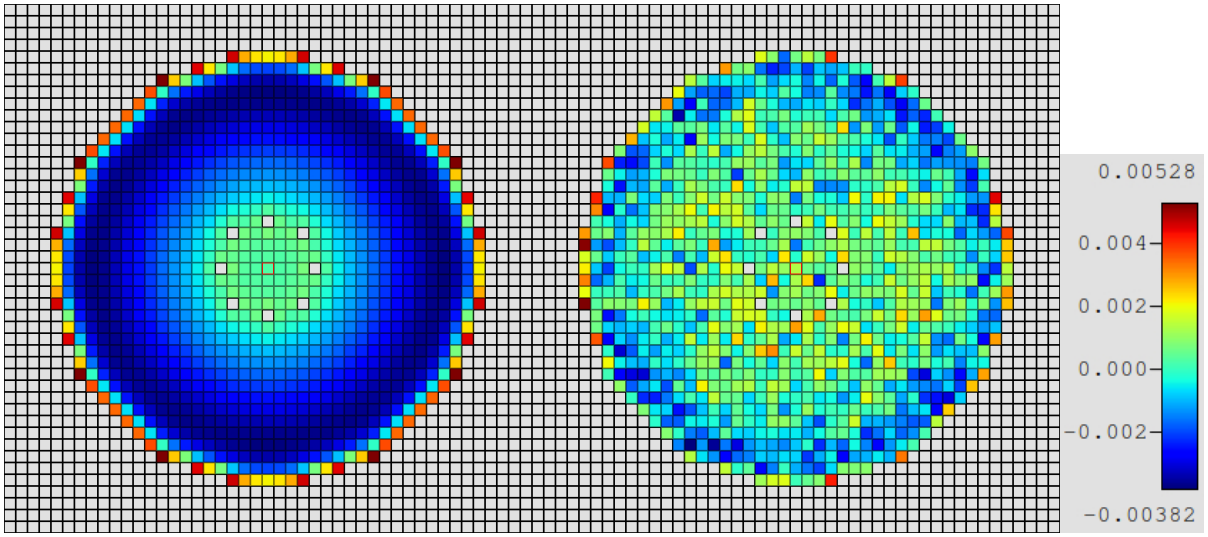

Figure B-44: KENO-VI radial fission rate distribution (left) and Shift differences (right) for Case 11.

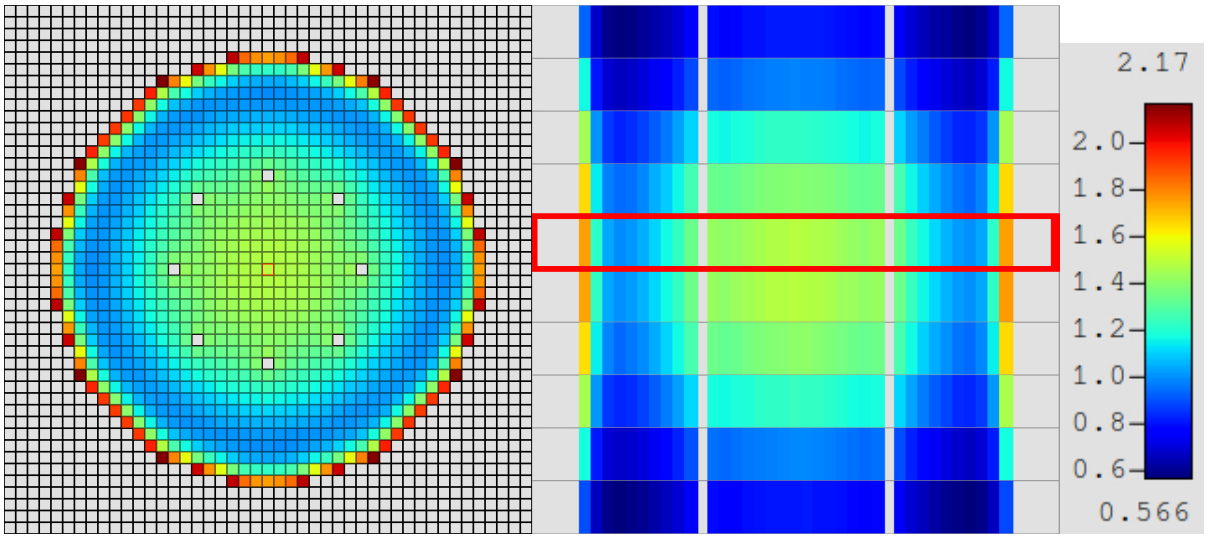

Figure B-45: KENO-VI radial (left) and axial (right) slices of fission rate distributions for Case 12.

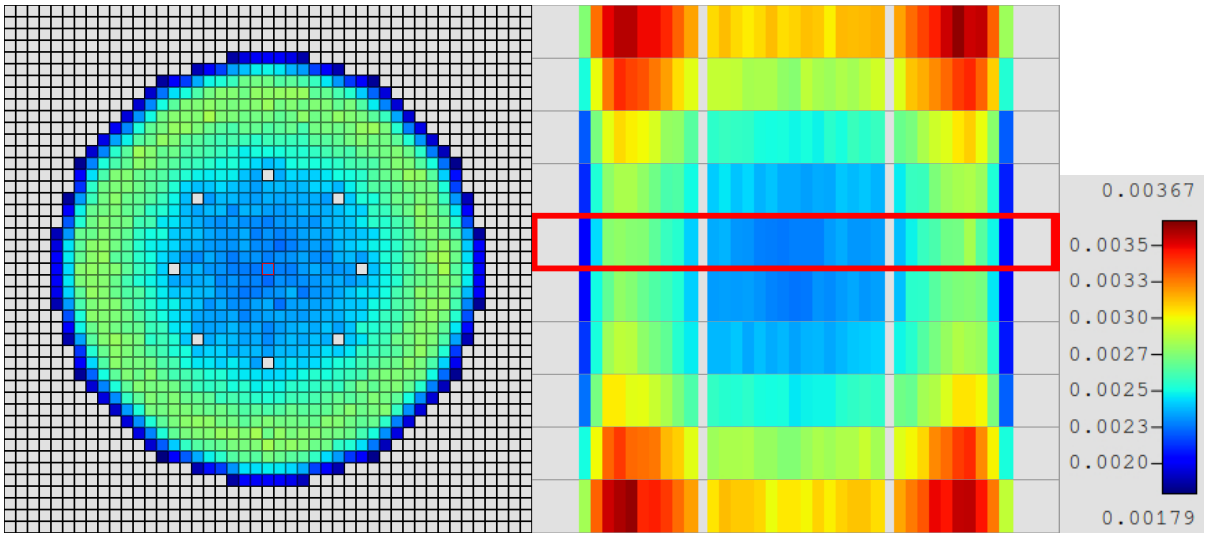

Figure B-46: KENO-VI radial (left) and axial (right) slices of fractional uncertainties for Case 12.

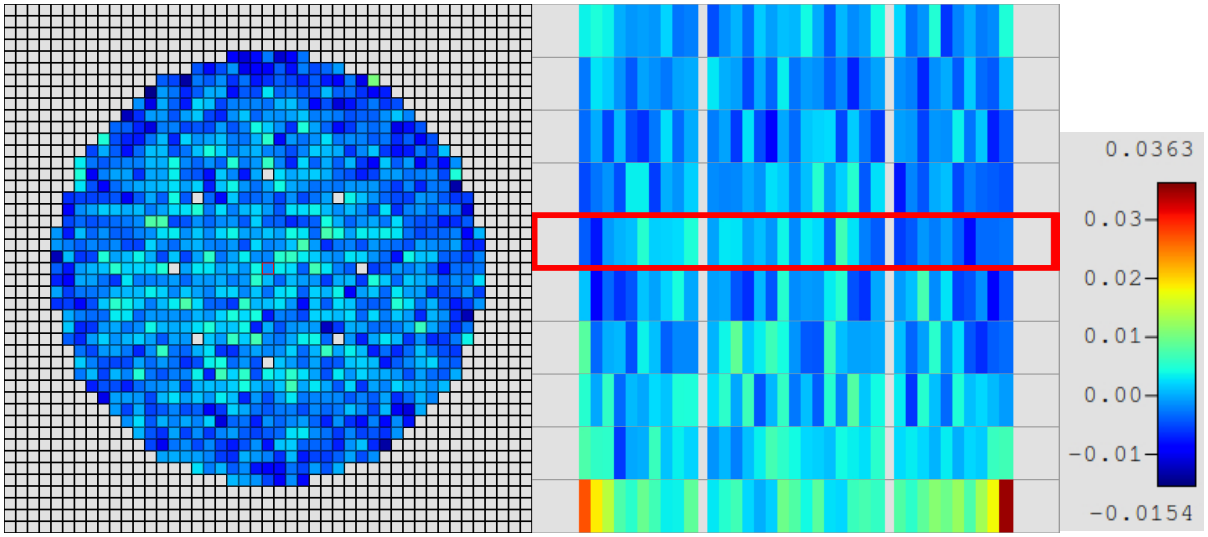

Figure B-47: Shift radial (left) and axial (right) slices of fission rate distribution differences for Case 12.

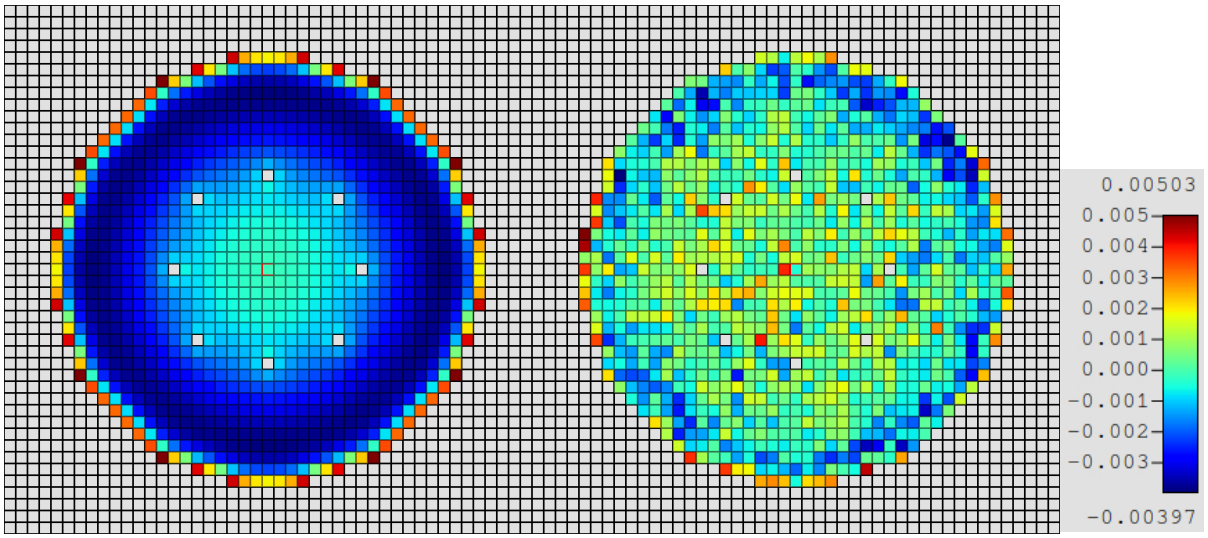

Figure B-48: KENO-VI radial fission rate distribution (left) and Shift differences (right) for Case 12.

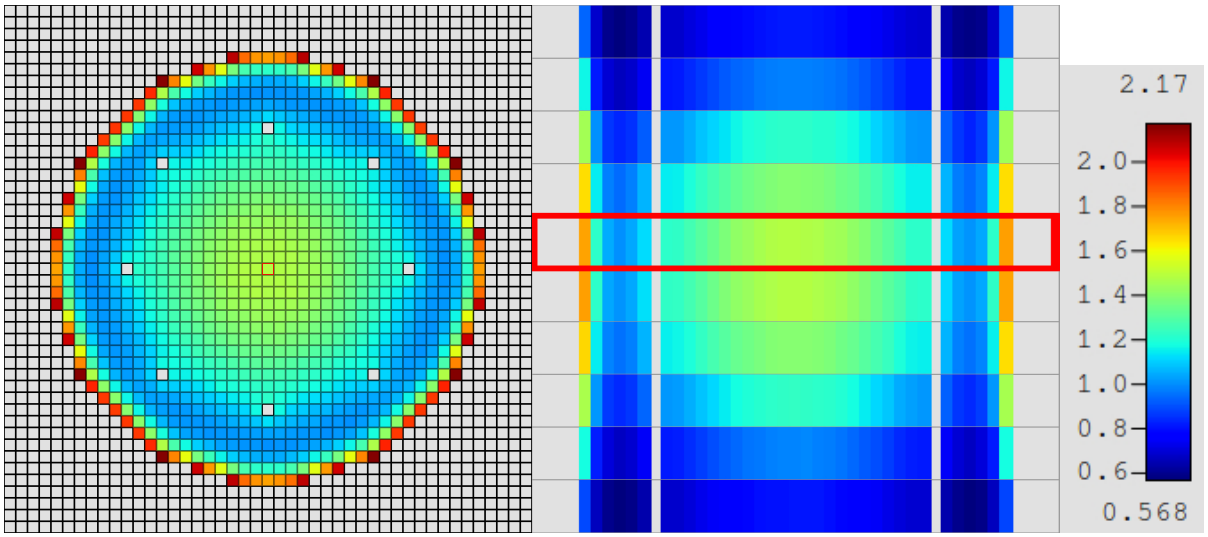

Figure B-49: KENO-VI radial (left) and axial (right) slices of fission rate distributions for Case 13.

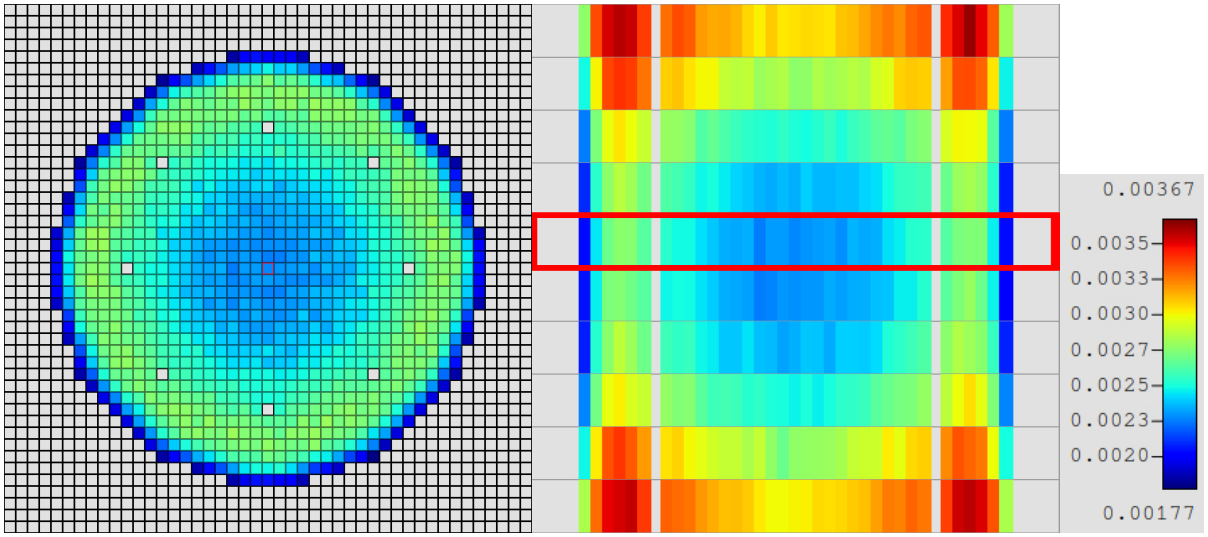

Figure B-50: KENO-VI radial (left) and axial (right) slices of fractional uncertainties for Case 13.

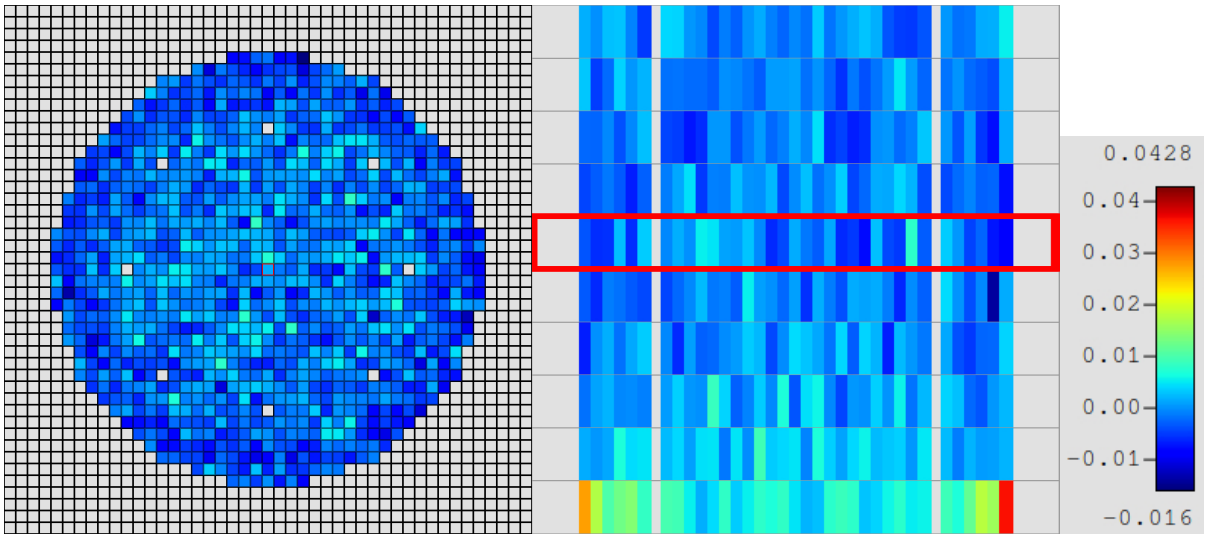

Figure B-51: Shift radial (left) and axial (right) slices of fission rate distribution differences for Case 13.

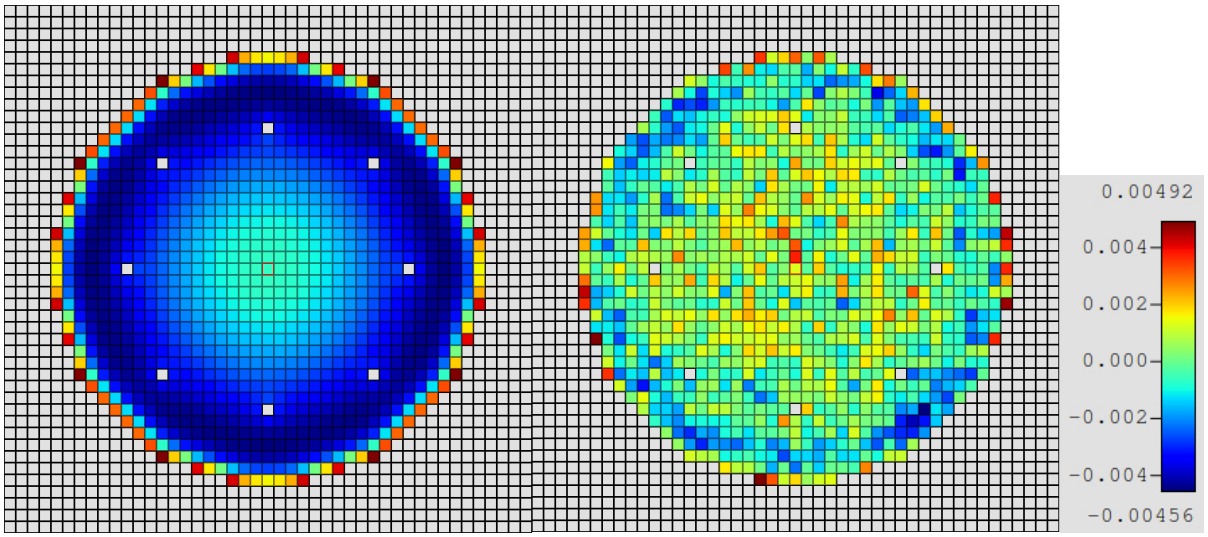

Figure B-52: KENO-VI radial fission rate distribution (left) and Shift differences (right) for Case 13.

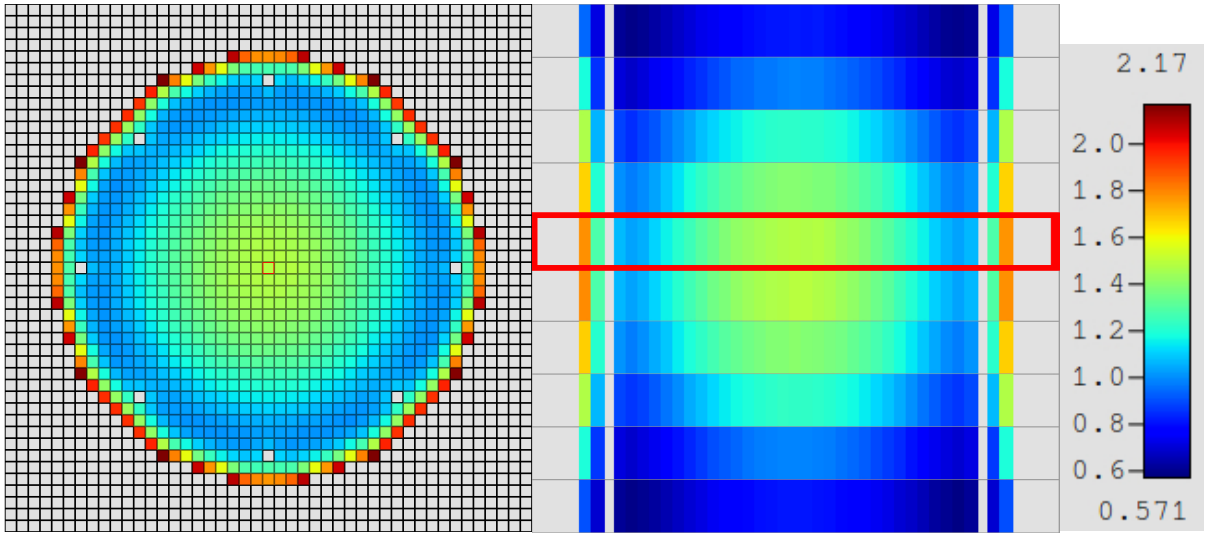

Figure B-53: KENO-VI radial (left) and axial (right) slices of fission rate distributions for Case 14.

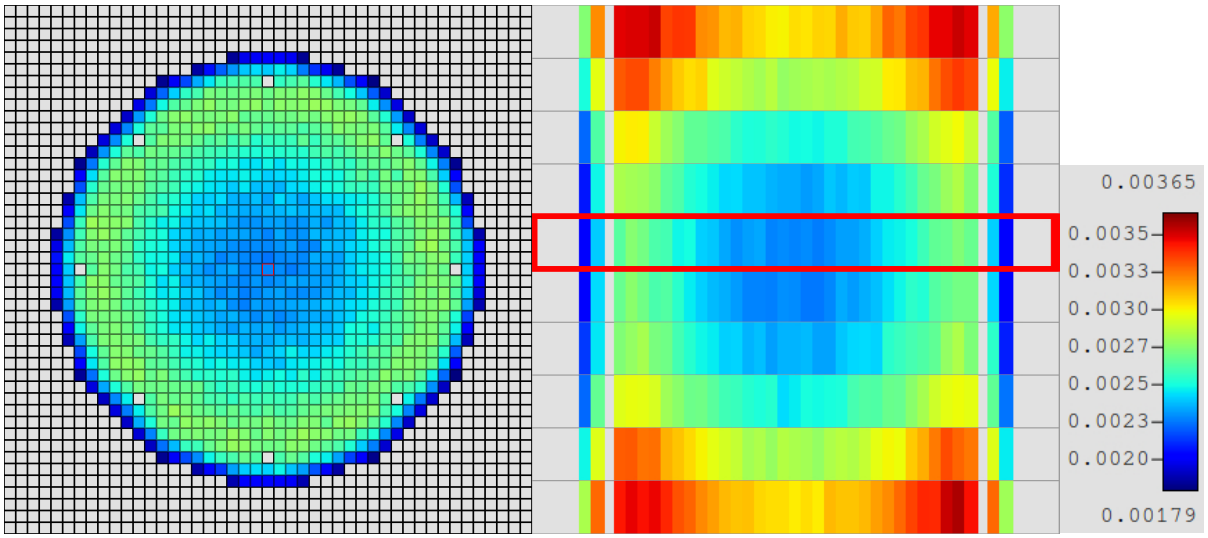

Figure B-54: KENO-VI radial (left) and axial (right) slices of fractional uncertainties for Case 14.

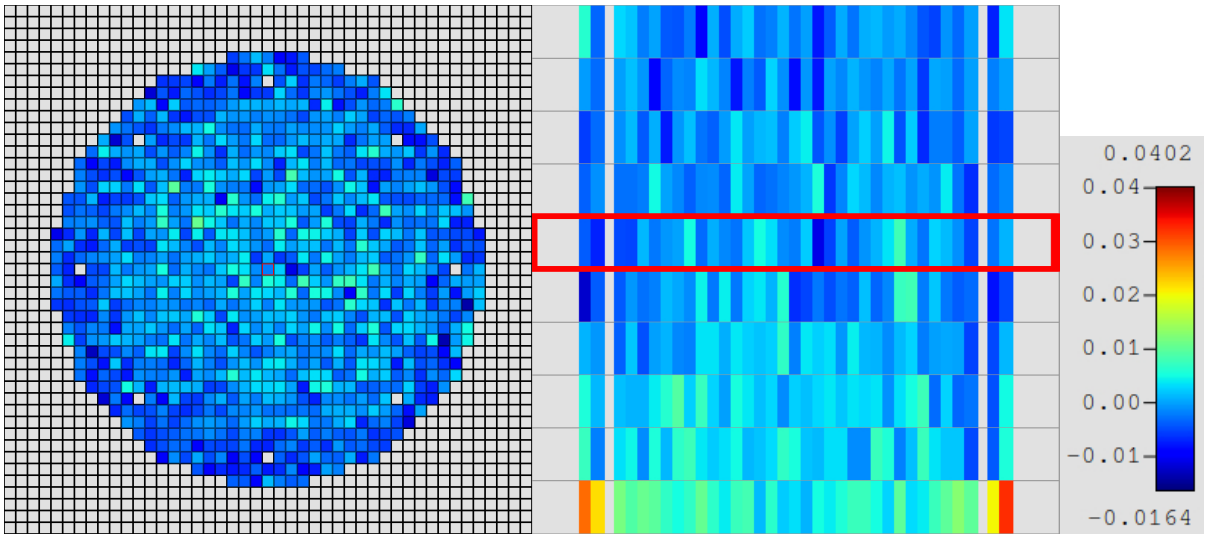

Figure B-55: Shift radial (left) and axial (right) slices of fission rate distribution differences for Case 14.

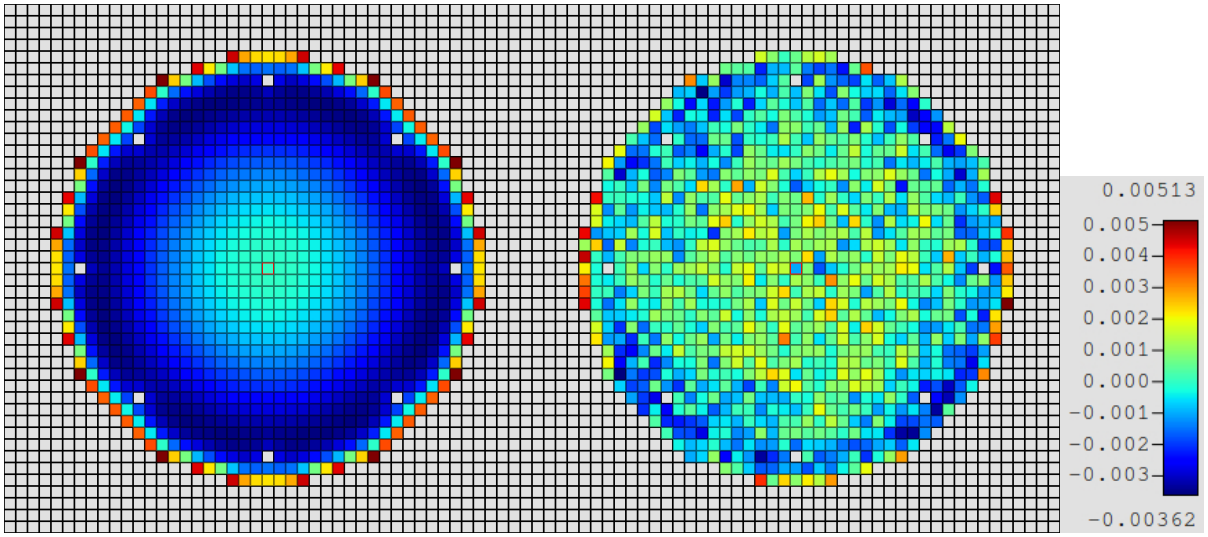

Figure B-56: KENO-VI radial fission rate distribution (left) and Shift differences (right) for Case 14.

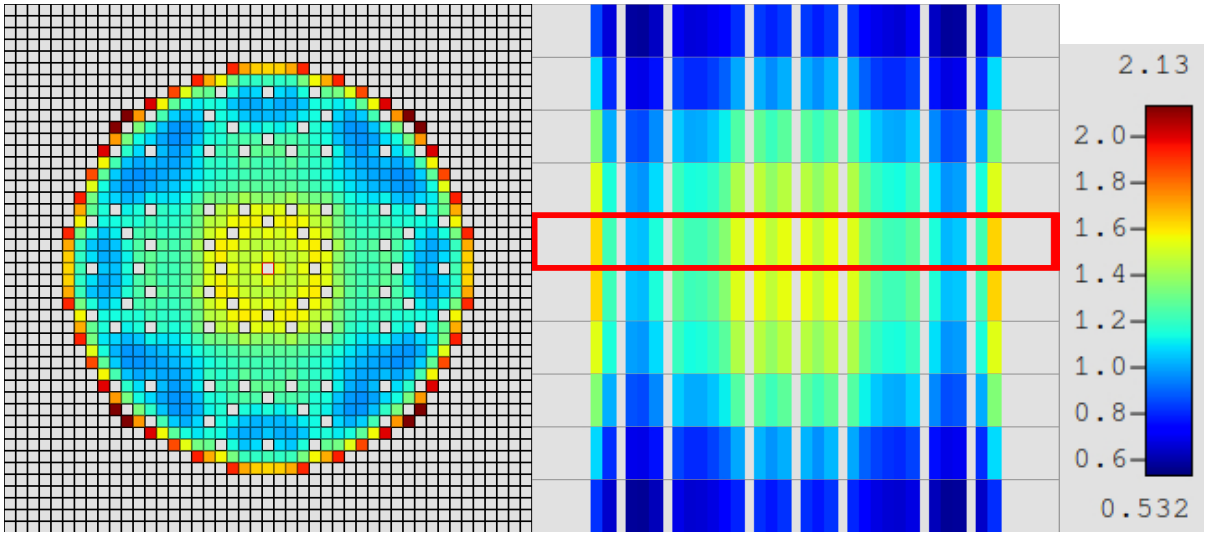

Figure B-57: KENO-VI radial (left) and axial (right) slices of fission rate distributions for Case 15.

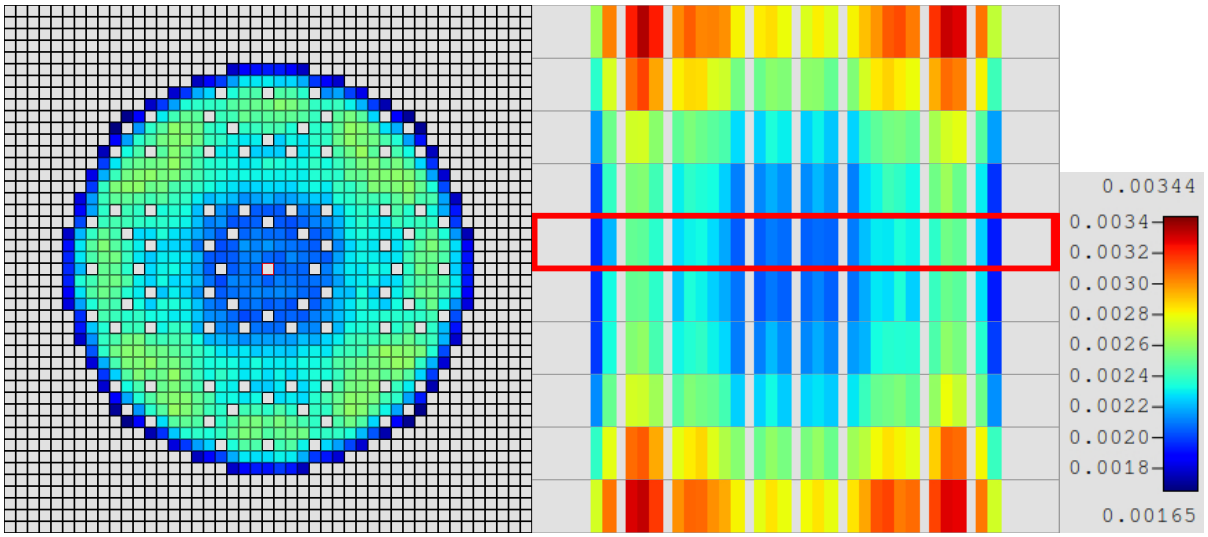

Figure B-58: KENO-VI radial (left) and axial (right) slices of fractional uncertainties for Case 15.

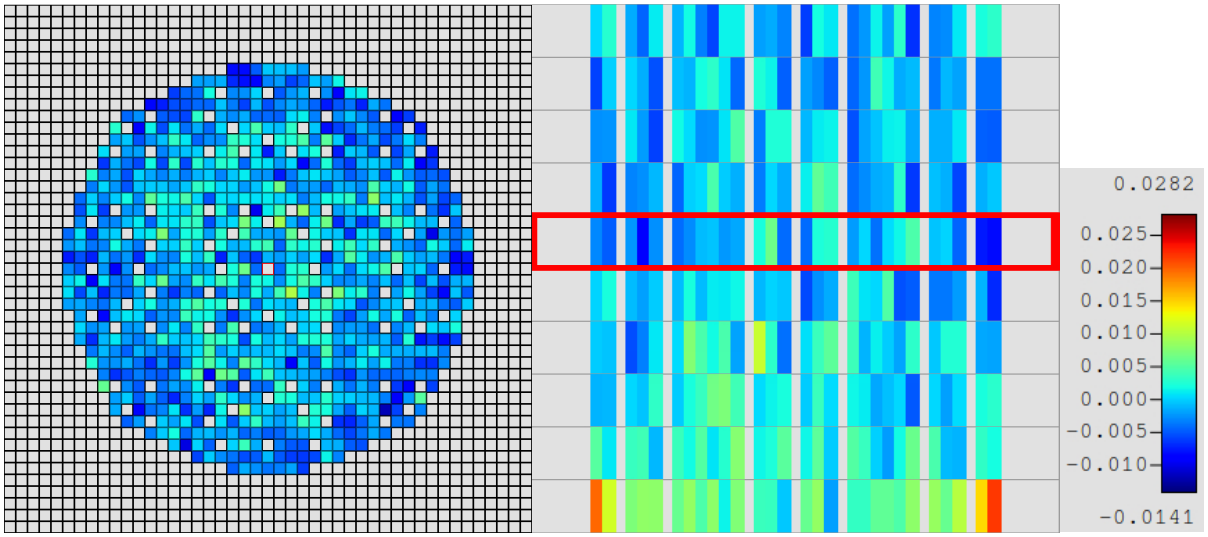

Figure B-59: Shift radial (left) and axial (right) slices of fission rate distribution differences for Case 15.

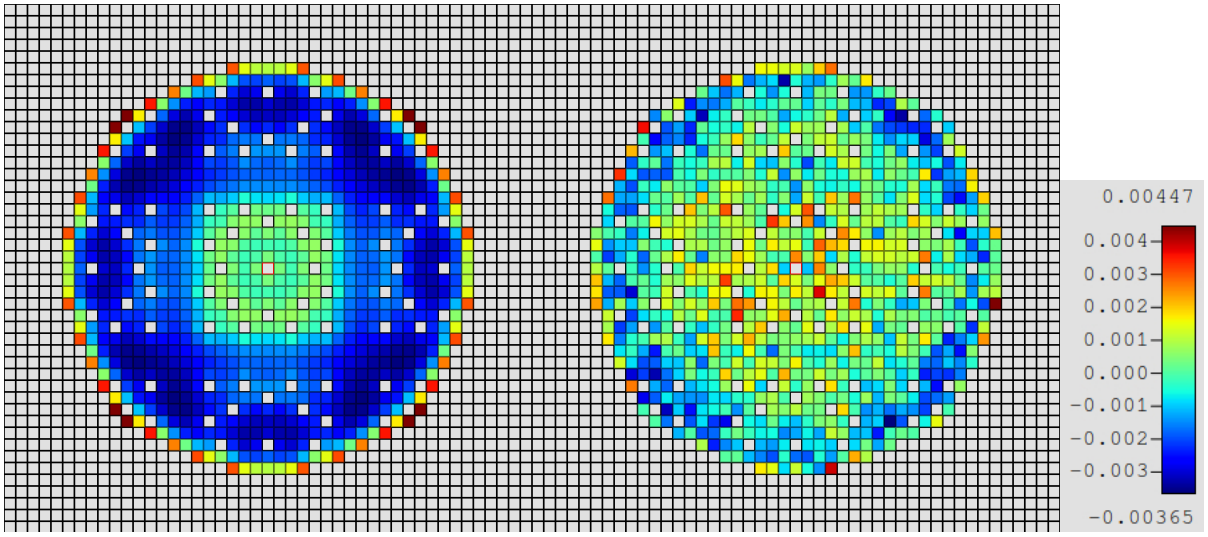

Figure B-60: KENO-VI radial fission rate distribution (left) and Shift differences (right) for Case 15.

APPENDIX C. Fission Rate Distribution Comparisons between MPACT and Shift

APPENDIX C. FISSION RATE DISTRIBUTION COMPARISONS BETWEEN MPACT AND SHIFT

The following results are comparisons of normalized fission rate distributions calculated for the 7uPCX experiment. The reference solutions are from Shift calculations using VERA 4.2 and CE ENDF/B-VII.1 data. The Shift results were generated with 10 billion active particle histories. The MPACT results are from VERA version 4.3RC7 and include both TCP_0 and P_2 scattering treatments. Tables C-1 and C-2 provide the overall statistical summaries; Figures C-1 through C-74 provide 2D color plots of the relevant results. For each case, the following are given:

- Shift normalized fission rate distribution, presented as radial and axial slices through the center of the experiment.
- Shift calculated percent relative uncertainty in the fission rate distribution, presented as radial and axial slices through the center of the experiment.
- Differences between MPACT and Shift normalized fission rate distributions, presented as radial and axial slices through the center of the experiment, where MPACT results are based on TCP_0 scattering.
- Differences between MPACT and Shift normalized fission rate distributions, presented as radial and axial slices through the center of the experiment, where MPACT results are based on P_2 scattering.
- Differences between MPACT and Shift radial (axially integrated) normalized total fission rate distributions for both TCP_0 and P_2 scattering.

Table C-1: Normalized Fission Rate Distribution Statistics, MPACT-Shift, TCP_0 Scattering

Case	k-eff Diff	3D RMS	3D Max	2D RMS	2D Max	AO Diff
1	130	1.03%	−3.15%	0.99%	−2.47%	−0.07%
2	130	1.03%	−3.61%	1.00%	−2.68%	−0.06%
3	129	1.04%	−3.26%	1.00%	−2.51%	−0.05%
4	131	1.03%	−2.98%	0.99%	−2.31%	−0.05%
5	131	1.01%	−3.12%	0.98%	−2.34%	−0.05%
6	133	1.01%	−2.97%	0.98%	−2.31%	−0.04%
7	129	1.06%	−3.50%	1.02%	−2.55%	−0.05%
8	133	1.03%	−2.85%	0.99%	−2.23%	−0.04%
9	133	1.01%	−2.97%	0.97%	−2.31%	−0.05%
10	136	1.00%	−2.99%	0.96%	−2.30%	−0.05%
11	123	1.06%	−3.06%	1.02%	−2.45%	−0.05%
12	126	1.04%	−3.00%	1.00%	−2.33%	−0.05%
13	130	1.02%	−3.11%	0.99%	−2.33%	−0.05%
14	129	1.01%	−2.92%	0.98%	−2.34%	−0.06%
15			failed			
Average	**130**	**1.03%**	**−2.90%**	**0.99%**	**−2.23%**	**−0.05%**
St Dev	**5**	**0.02%**	**0.83%**	**0.02%**	**0.63%**	**0.01%**

Table C-2. Normalized Fission Rate Distribution Statistics, MPACT-Shift, P_2 Scattering

Case	k-eff Diff	3D RMS	3D Max	2D RMS	2D Max	AO Diff
1	43	1.17%	3.06%	1.14%	2.55%	−0.07%
2	43	1.17%	−3.52%	1.15%	−2.57%	−0.06%
3	42	1.17%	−3.09%	1.14%	2.62%	−0.04%
4	45	1.18%	3.10%	1.15%	2.61%	−0.05%
5	45	1.17%	3.04%	1.14%	2.63%	−0.05%
6	46	1.17%	3.06%	1.14%	2.60%	−0.04%
7	46	1.20%	−3.20%	1.17%	2.69%	−0.04%
8	48	1.18%	3.04%	1.15%	2.67%	−0.04%
9	47	1.17%	3.30%	1.14%	2.71%	−0.05%
10	49	1.15%	3.07%	1.13%	2.74%	−0.05%
11	41	1.19%	2.95%	1.16%	2.54%	−0.05%
12	44	1.18%	3.01%	1.16%	2.60%	−0.06%
13	46	1.18%	−2.94%	1.15%	2.56%	−0.06%
14	42	1.16%	2.93%	1.13%	2.54%	−0.06%
15	48	1.14%	−2.89%	1.10%	2.36%	0.02%
Average	**45**	**1.17%**	**3.08%**	**1.14%**	**2.60%**	**−0.05%**
St Dev	**3**	**0.01%**	**0.16%**	**0.02%**	**0.09%**	**0.02%**

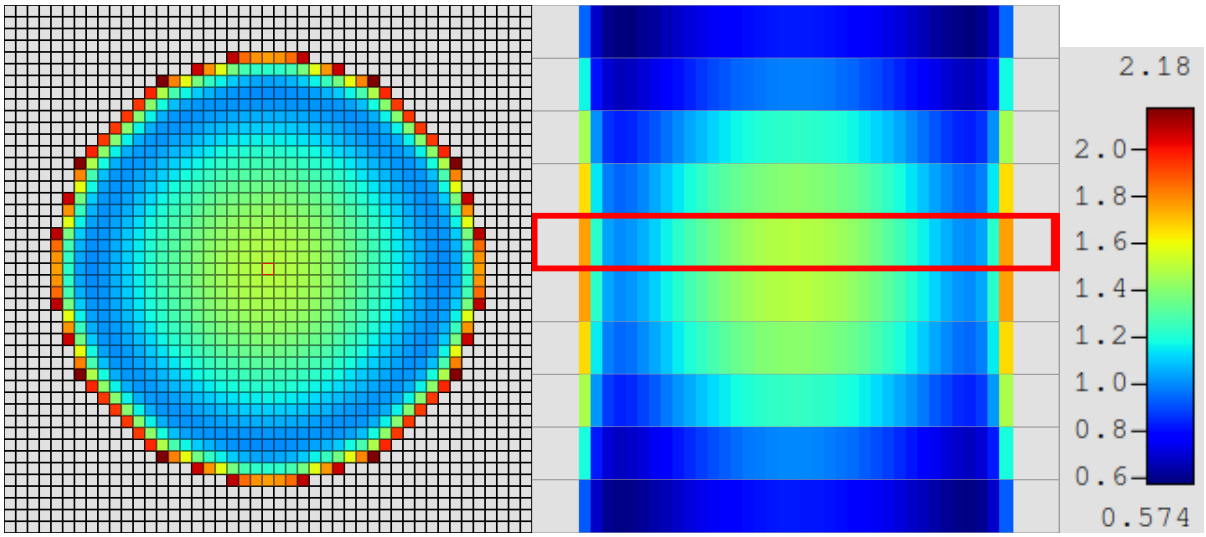

Figure C-1: Shift radial (left) and axial (right) slices of fission rate distributions for Case 1.

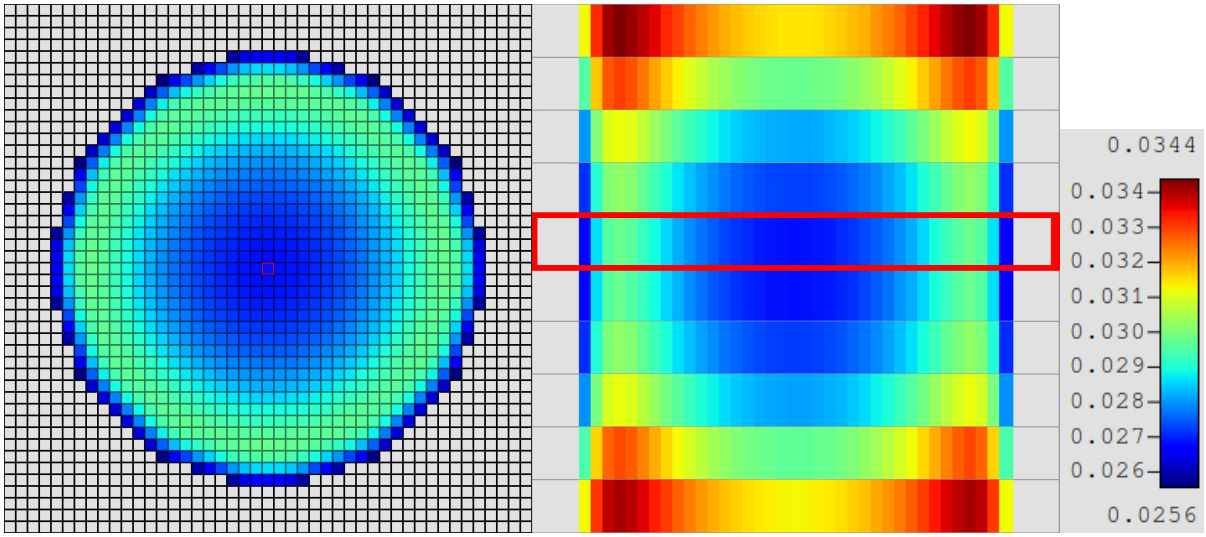

Figure C-2: Shift radial (left) and axial (right) slices of percent uncertainties for Case 1.

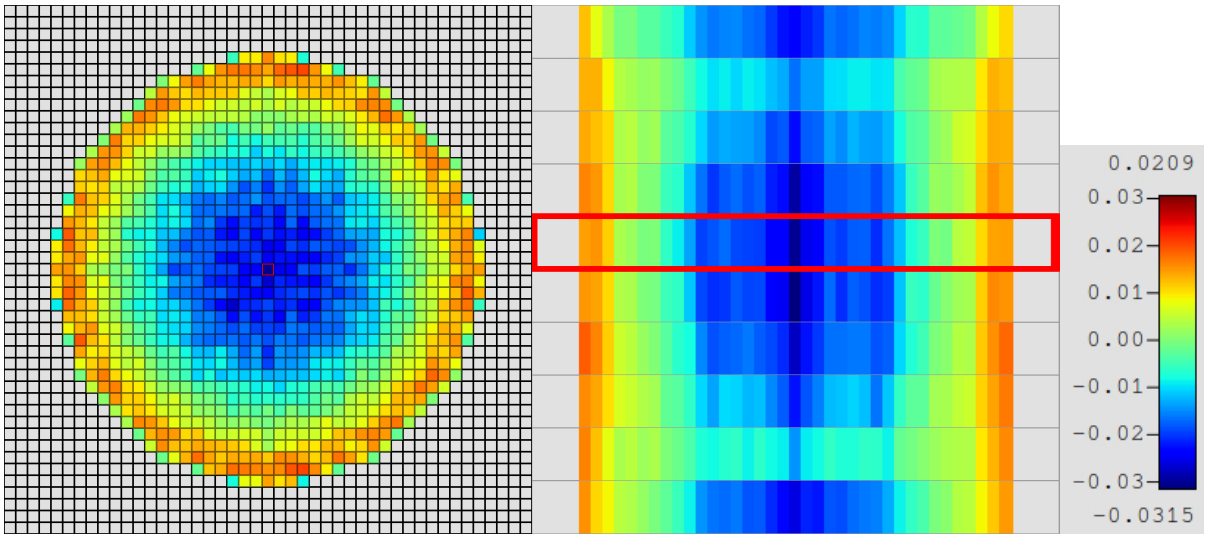

Figure C-3: MPACT radial (left) and axial (right) slices of fission rate differences for Case 1 (TCP0).

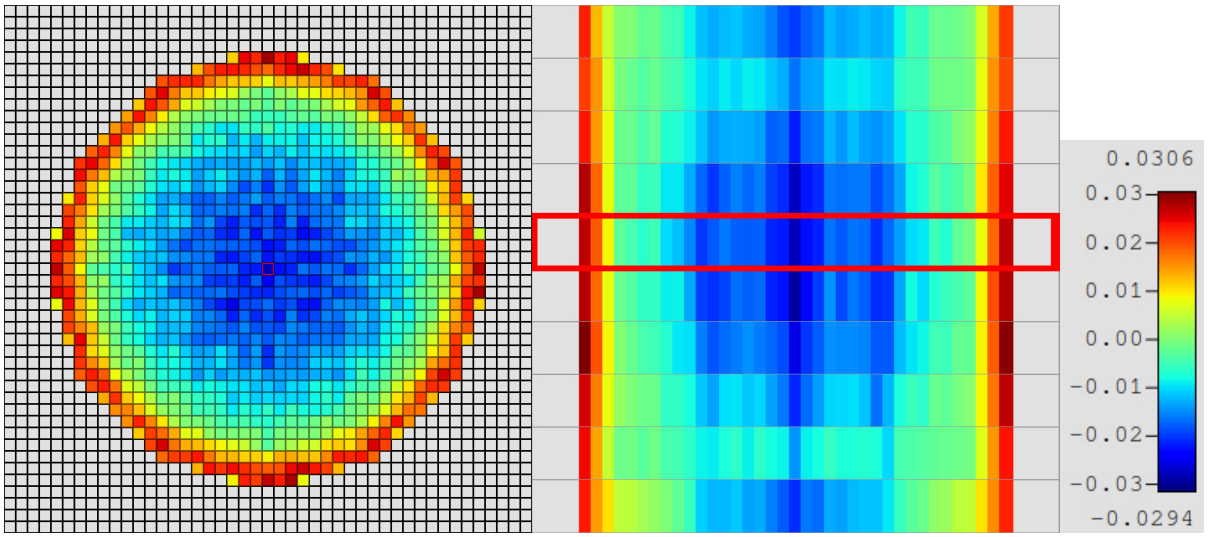

Figure C-4: MPACT radial (left) and axial (right) slices of fission rate differences for Case 1 (P2).

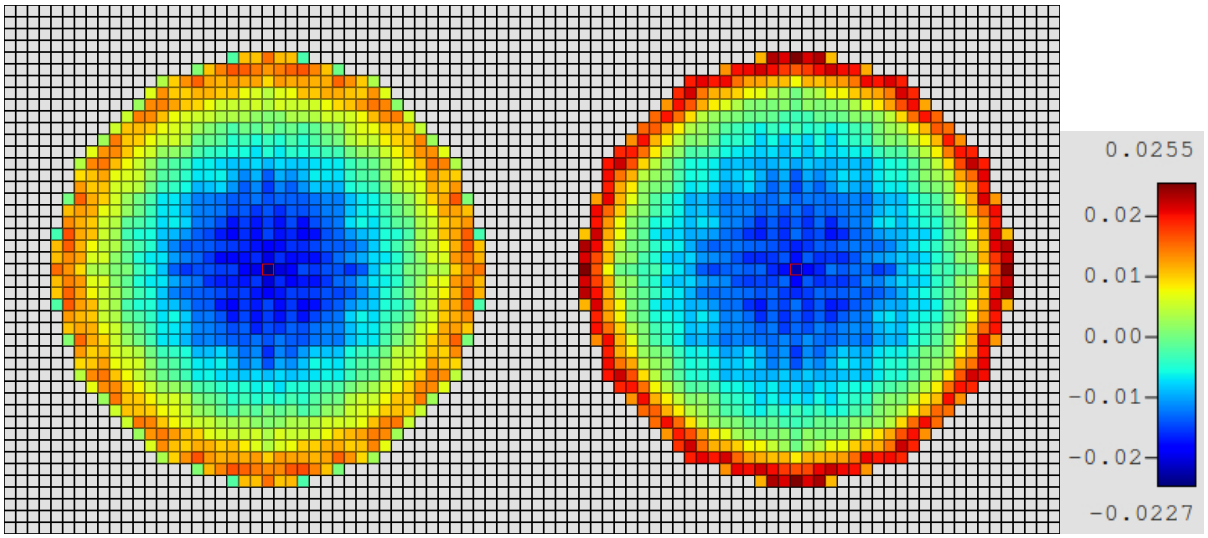

Figure C-5: MPACT radial fission rate differences using TCP0 (left) and P2 (right) scattering for Case 1.

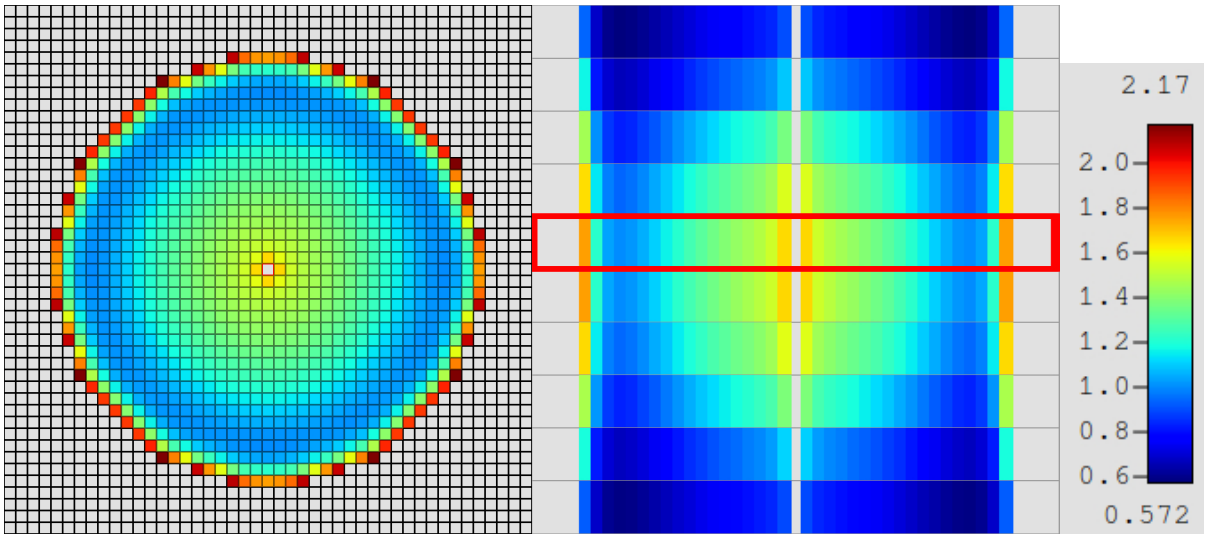

Figure C-6: Shift radial (left) and axial (right) slices of fission rate distributions for Case 2.

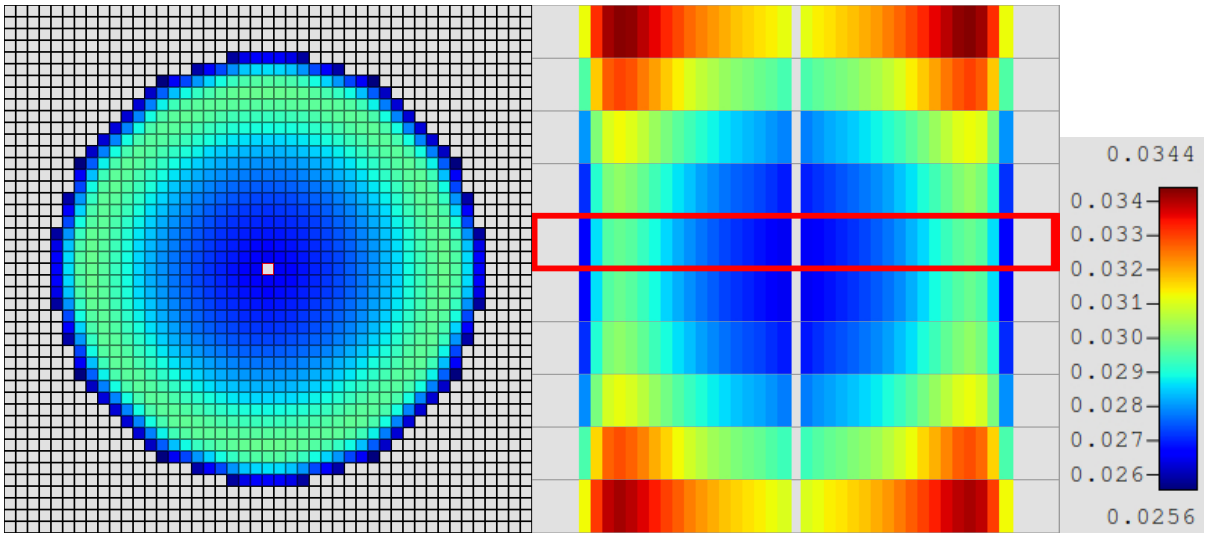

Figure C-7: Shift radial (left) and axial (right) slices of percent uncertainties for Case 2.

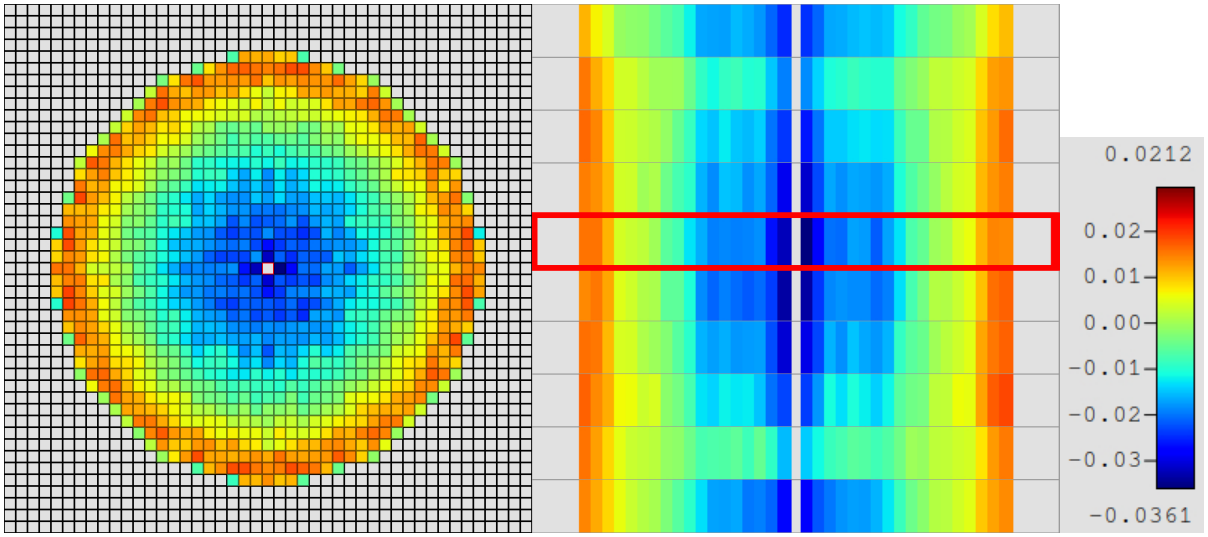

Figure C-8: MPACT radial (left) and axial (right) slices of fission rate differences for Case 2 (TCP0).

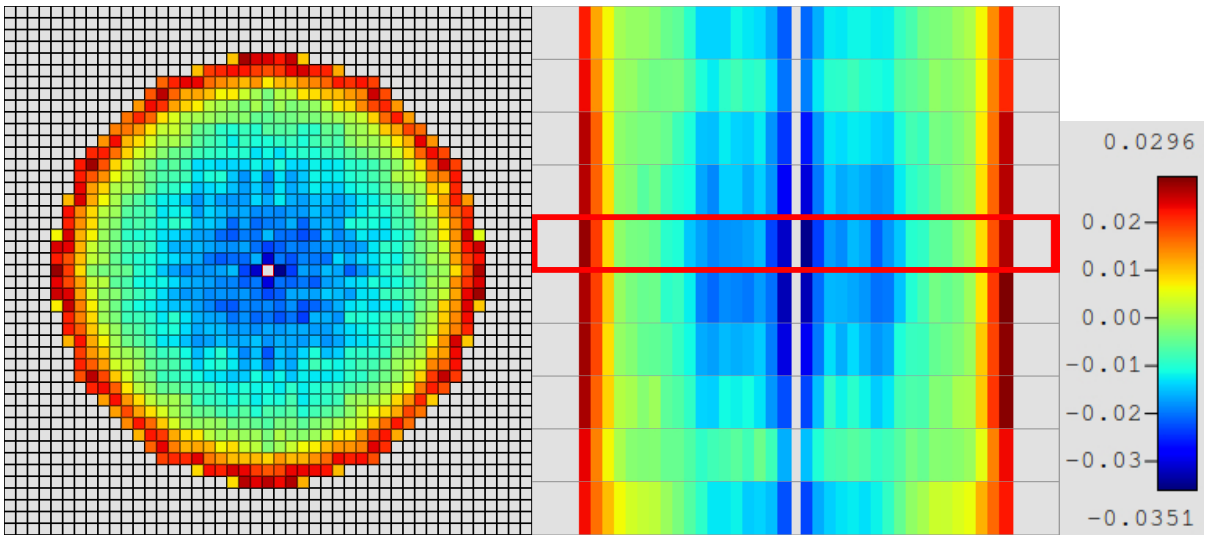

Figure C-9: MPACT radial (left) and axial (right) slices of fission rate differences for Case 2 (P2).

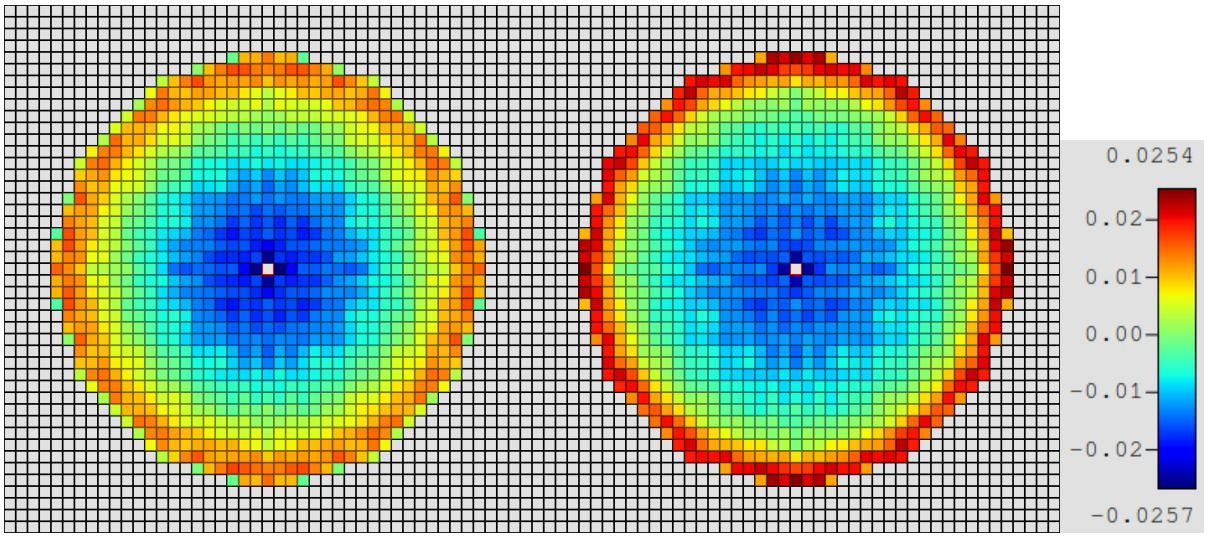

Figure C-10: MPACT radial fission rate differences using TCP0 (left) and P2 (right) scattering for Case 2.

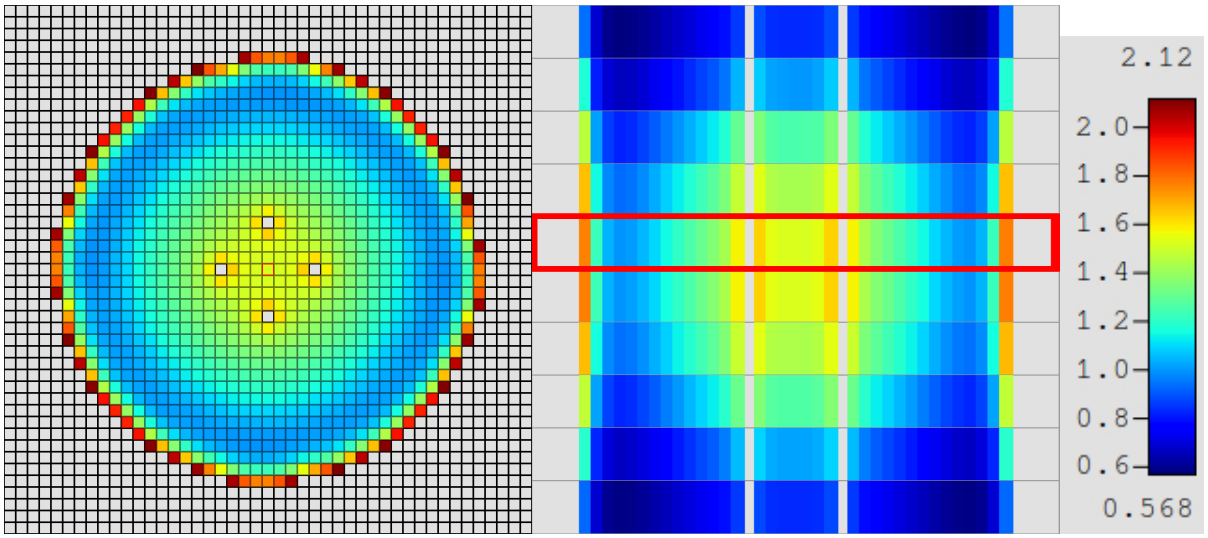

Figure C-11: Shift radial (left) and axial (right) slices of fission rate distributions for Case 3.

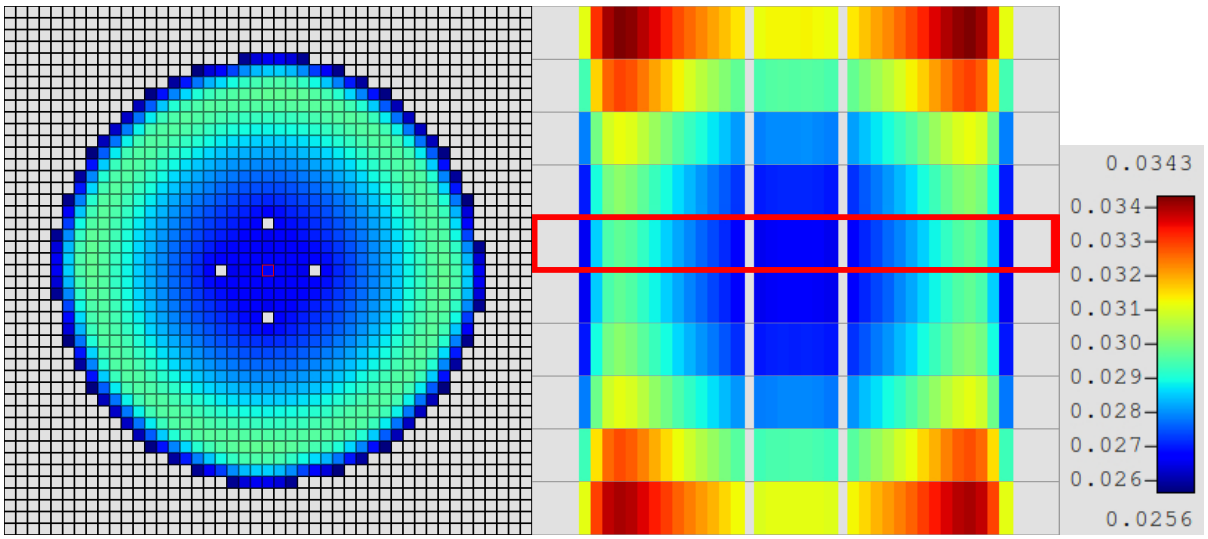

Figure C-12: Shift radial (left) and axial (right) slices of percent uncertainties for Case 3.

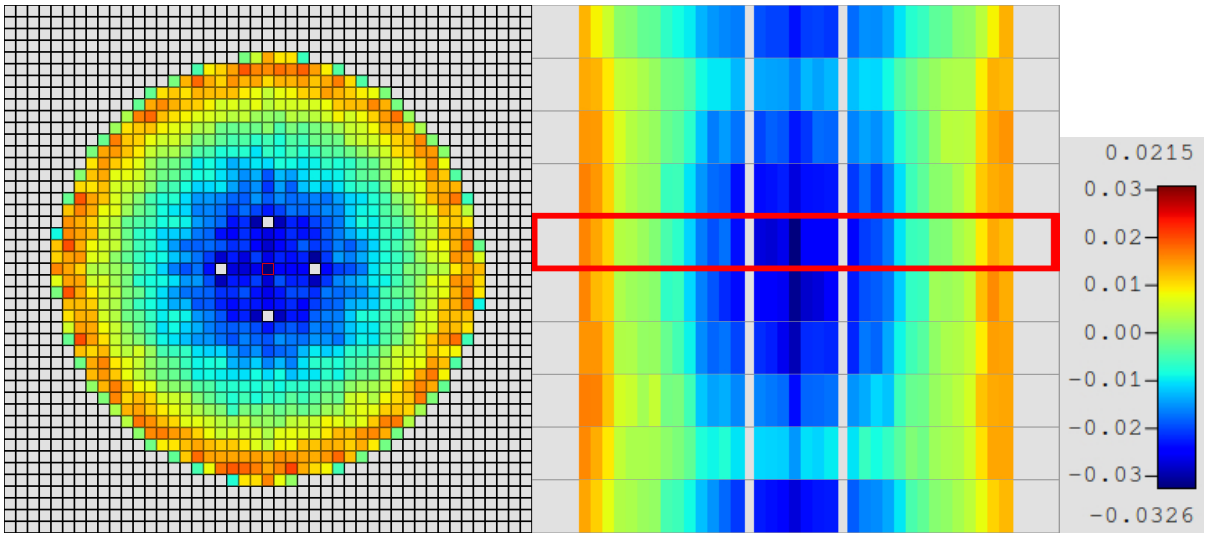

Figure C-13: MPACT radial (left) and axial (right) slices of fission rate differences for Case 3 (TCP0).

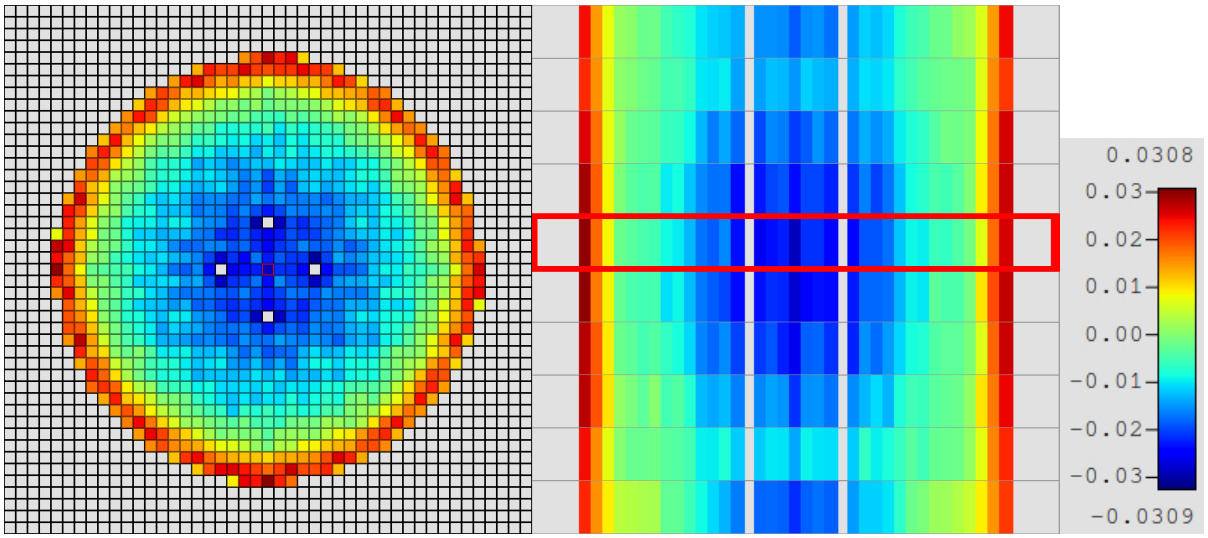

Figure C-14: MPACT radial (left) and axial (right) slices of fission rate differences for Case 3 (P2).

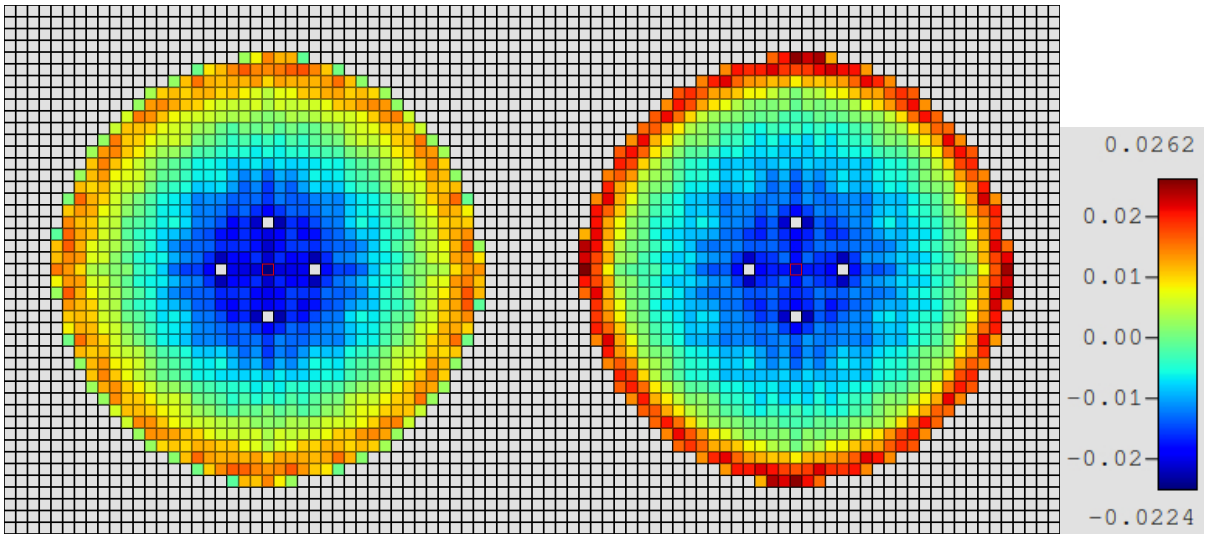

Figure C-15: MPACT radial fission rate differences using TCP0 (left) and P2 (right) scattering for Case 3.

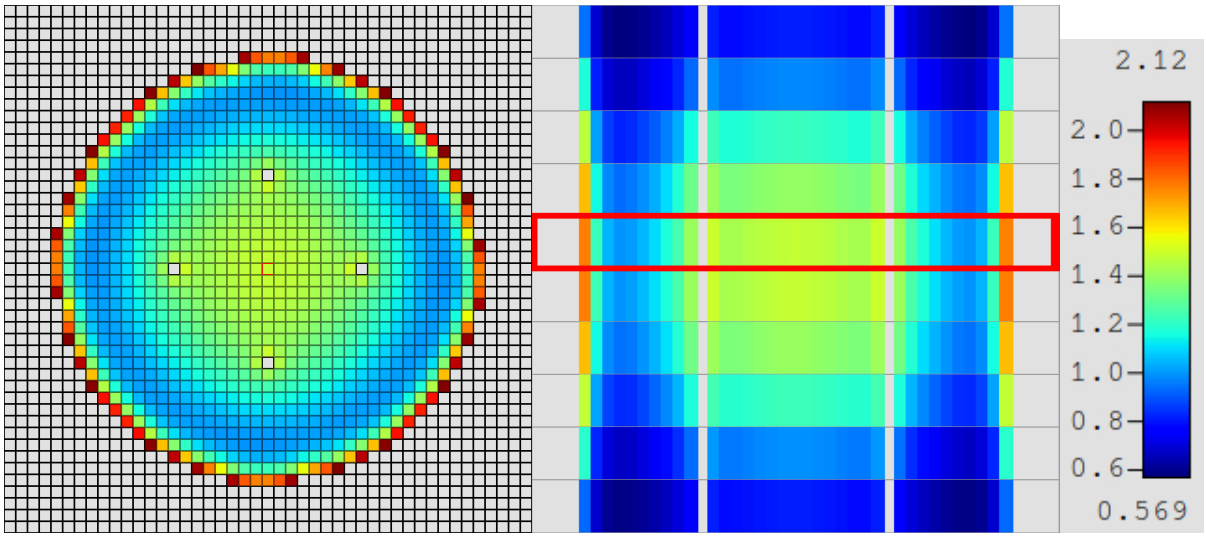

Figure C-16: Shift radial (left) and axial (right) slices of fission rate distributions for Case 4.

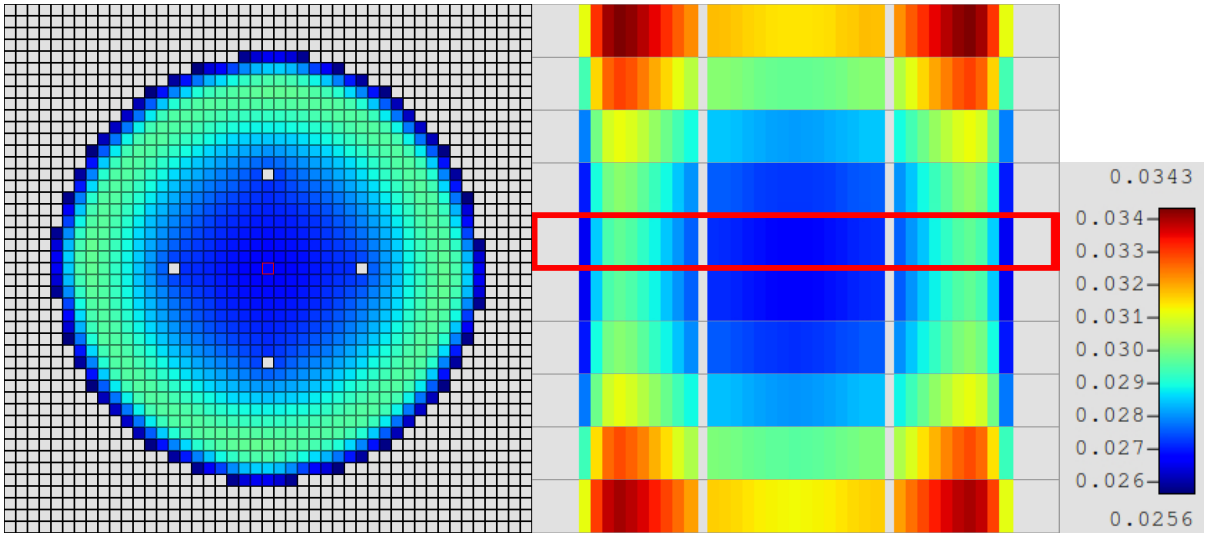

Figure C-17: Shift radial (left) and axial (right) slices of percent uncertainties for Case 4.

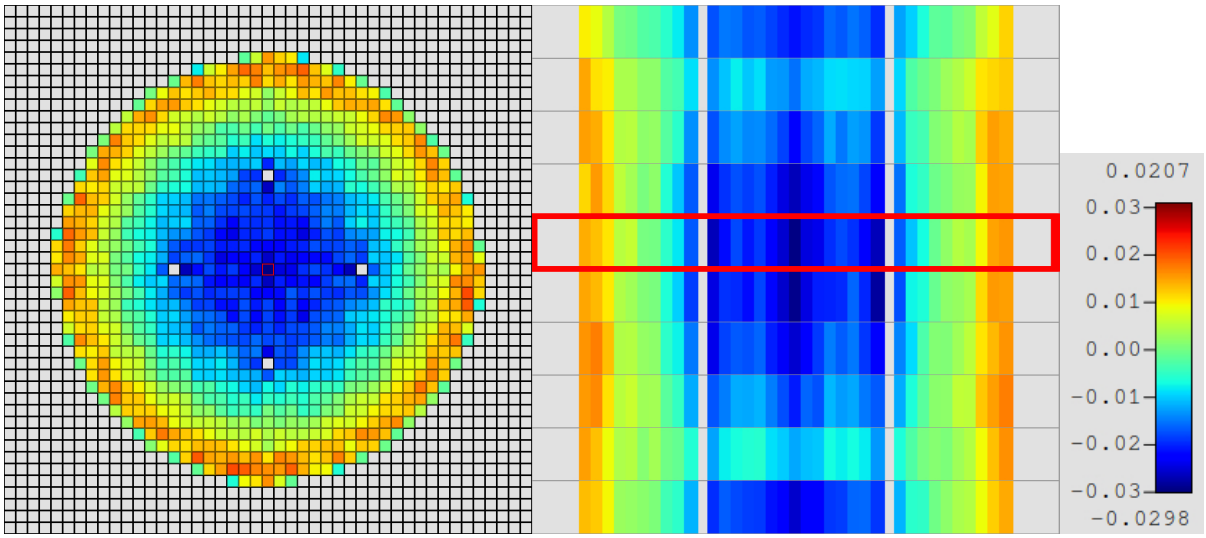

Figure C-18: MPACT radial (left) and axial (right) slices of fission rate differences for Case 4 (TCP0).

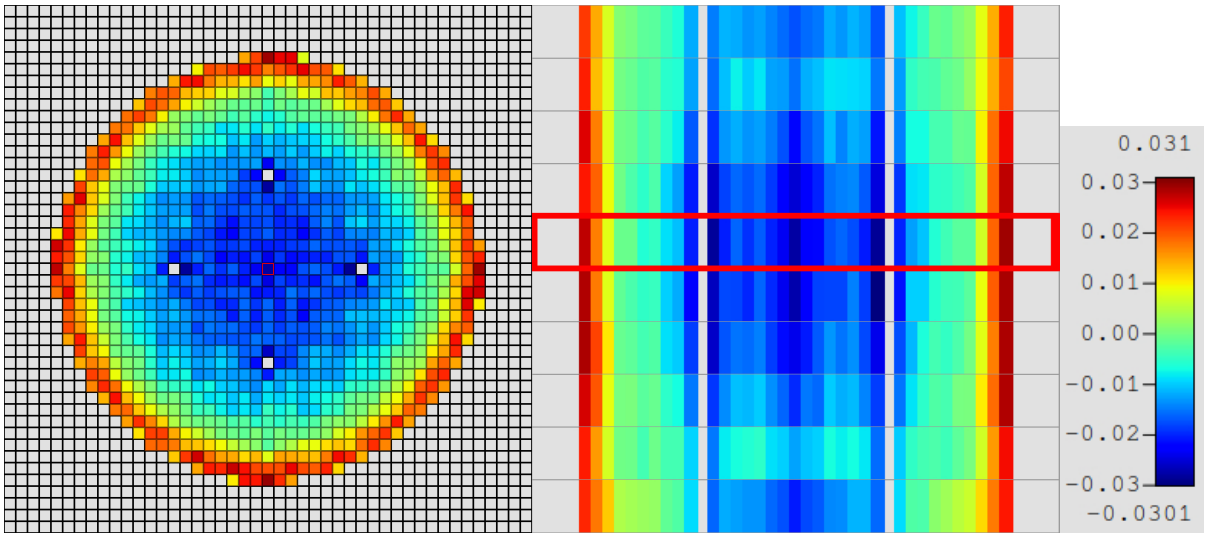

Figure C-19: MPACT radial (left) and axial (right) slices of fission rate differences for Case 4 (P2).

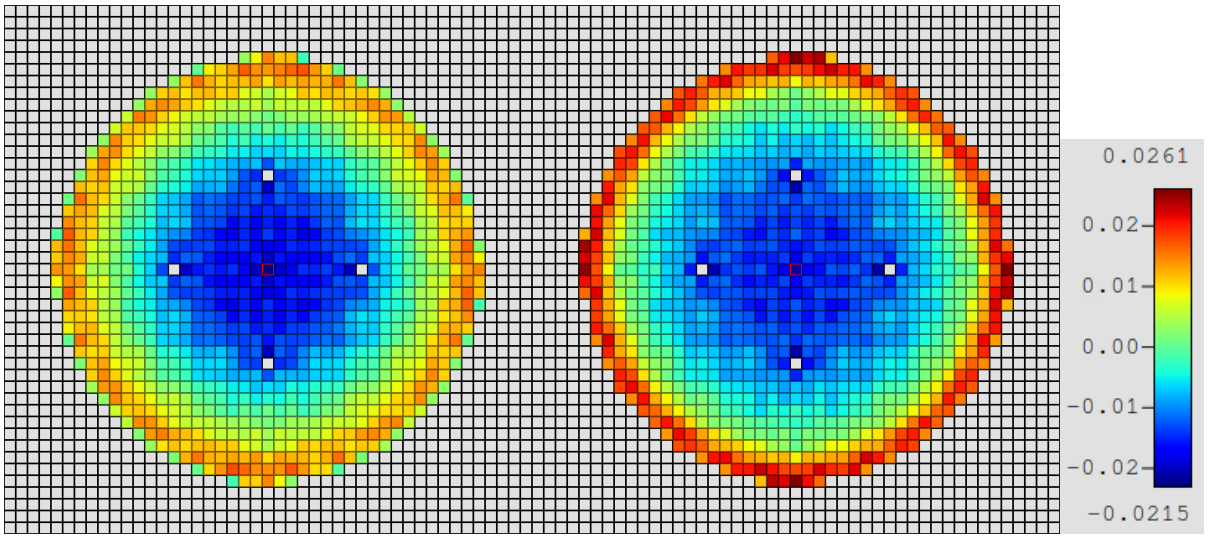

Figure C-20: MPACT radial fission rate differences using TCP0 (left) and P2 (right) scattering for Case 4.

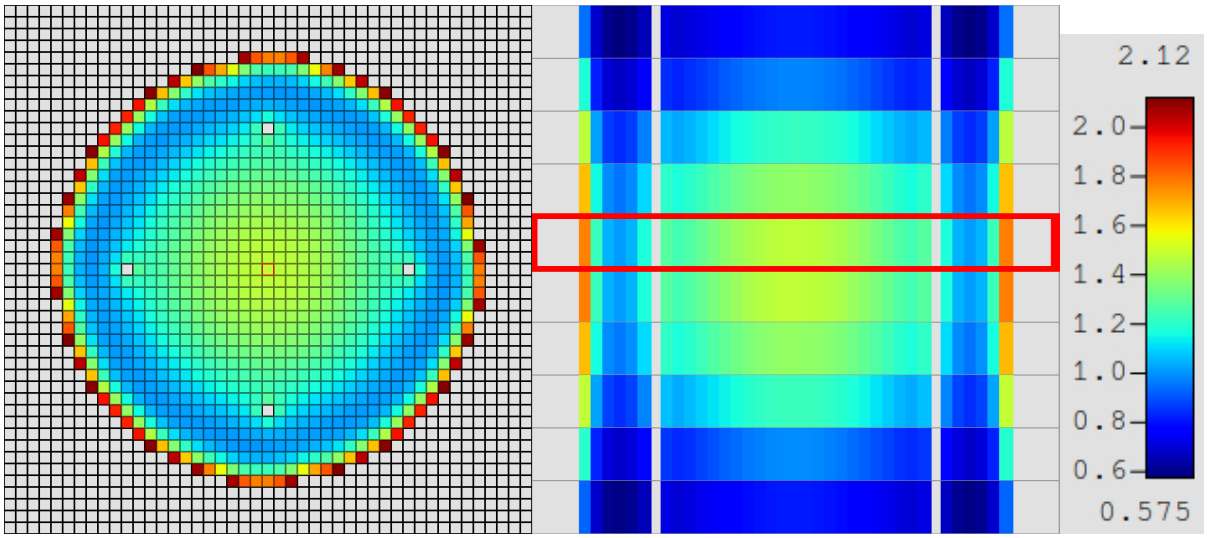

Figure C-21: Shift radial (left) and axial (right) slices of fission rate distributions for Case 5.

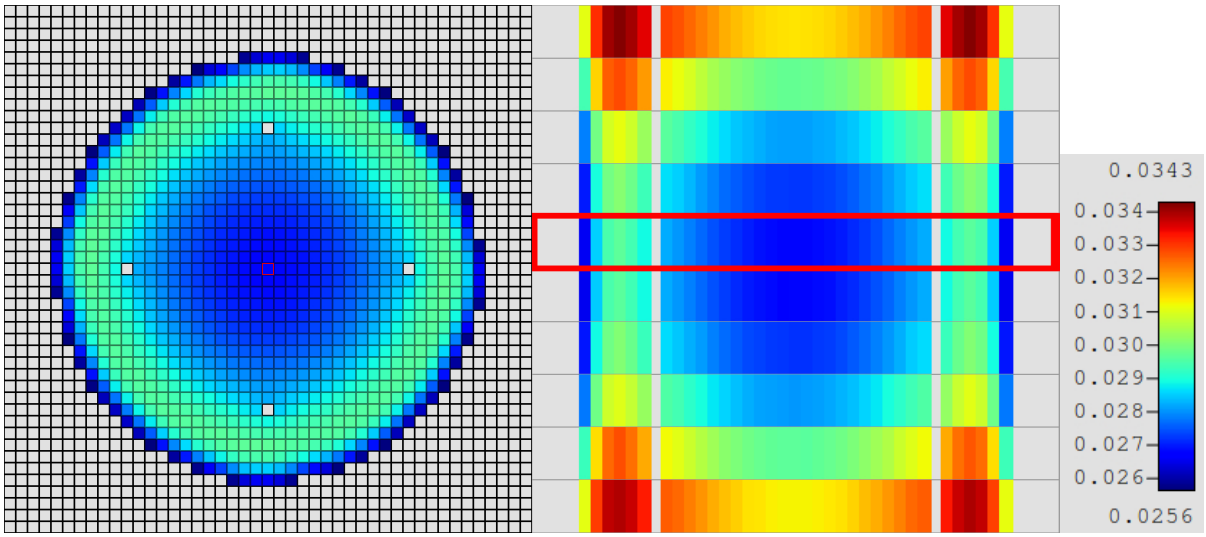

Figure C-22: Shift radial (left) and axial (right) slices of percent uncertainties for Case 5.

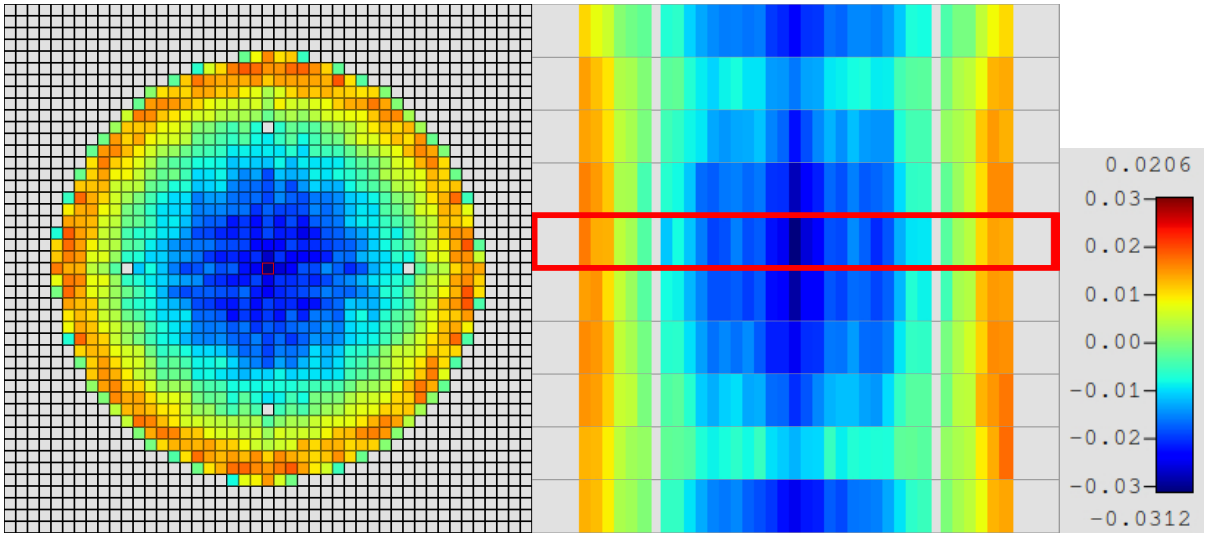

Figure C-23: MPACT radial (left) and axial (right) slices of fission rate differences for Case 5 (TCP0).

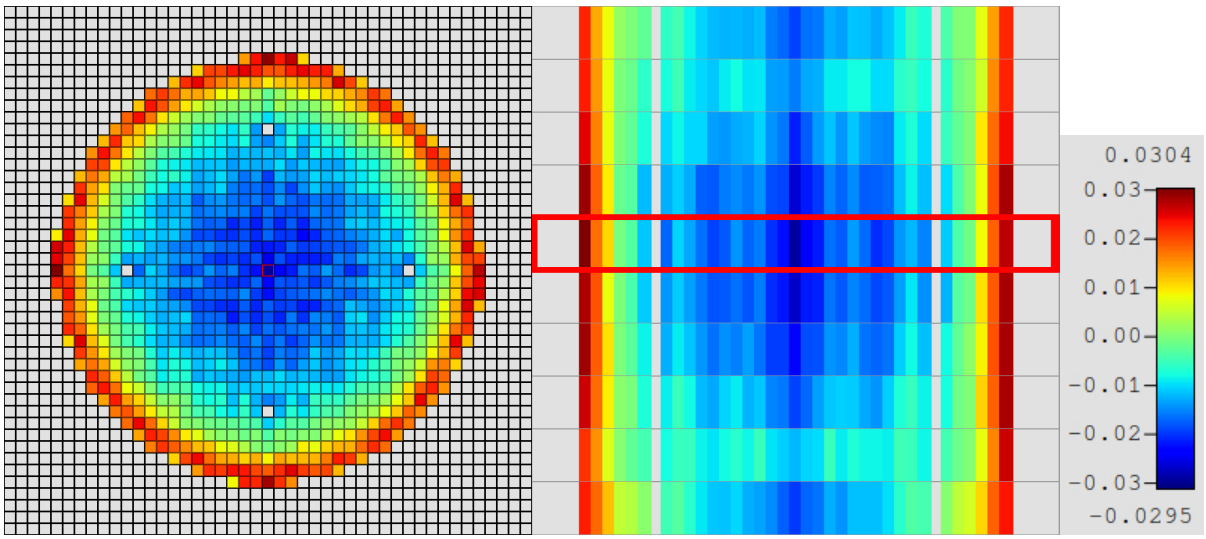

Figure C-24: MPACT radial (left) and axial (right) slices of fission rate differences for Case 5 (P2).

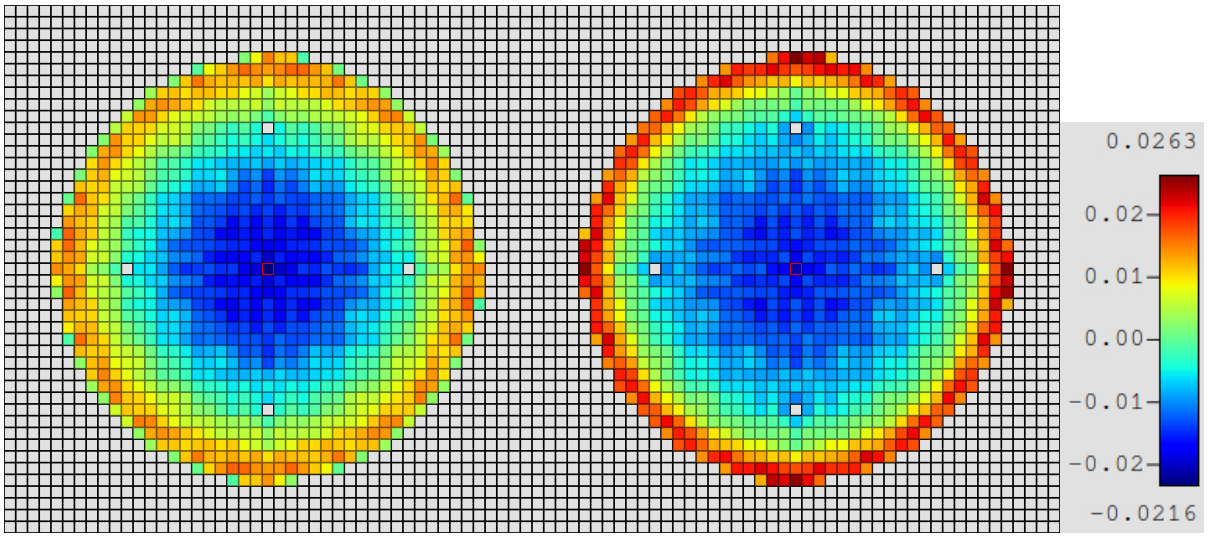

Figure C-25: MPACT radial fission rate differences using TCP0 (left) and P2 (right) scattering for Case 5.

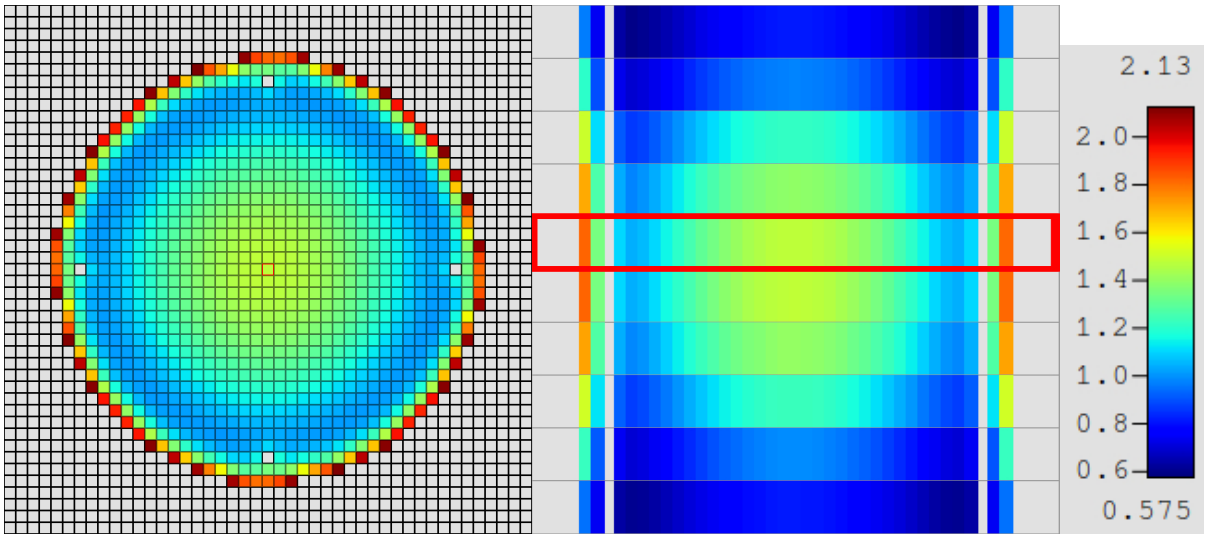

Figure C-26: Shift radial (left) and axial (right) slices of fission rate distributions for Case 6.

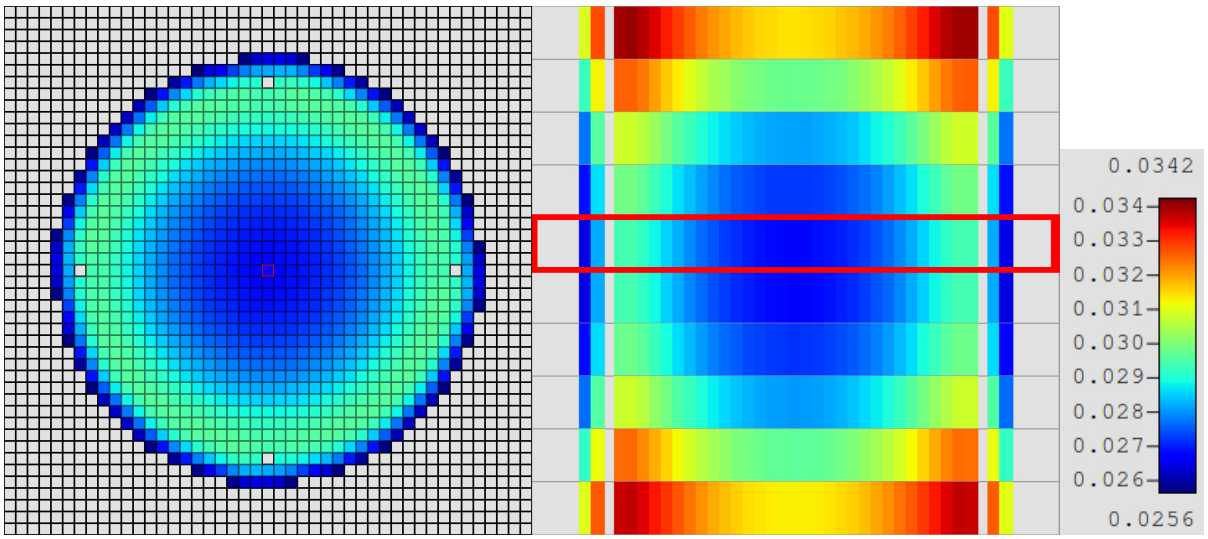

Figure C-27: Shift radial (left) and axial (right) slices of percent uncertainties for Case 6.

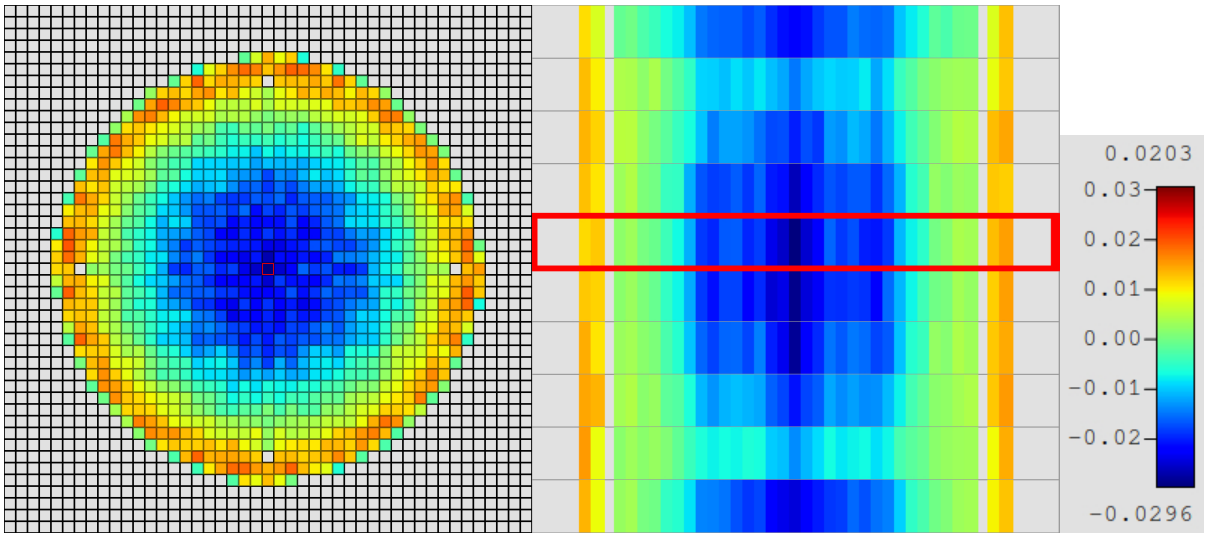

Figure C-28: MPACT radial (left) and axial (right) slices of fission rate differences for Case 6 (TCP0).

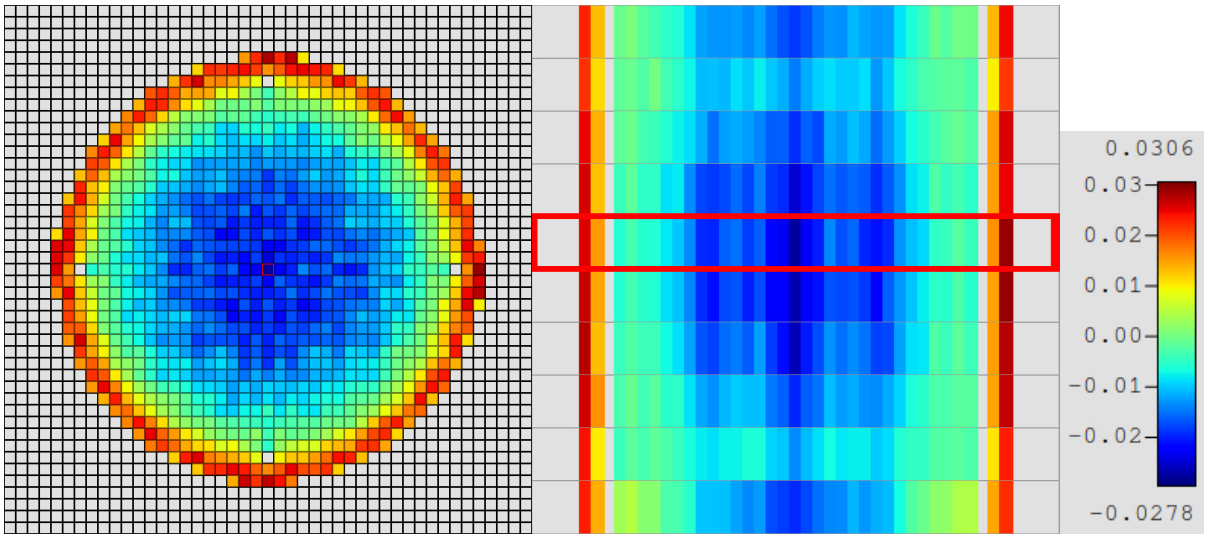

Figure C-29: MPACT radial (left) and axial (right) slices of fission rate differences for Case 6 (P2).

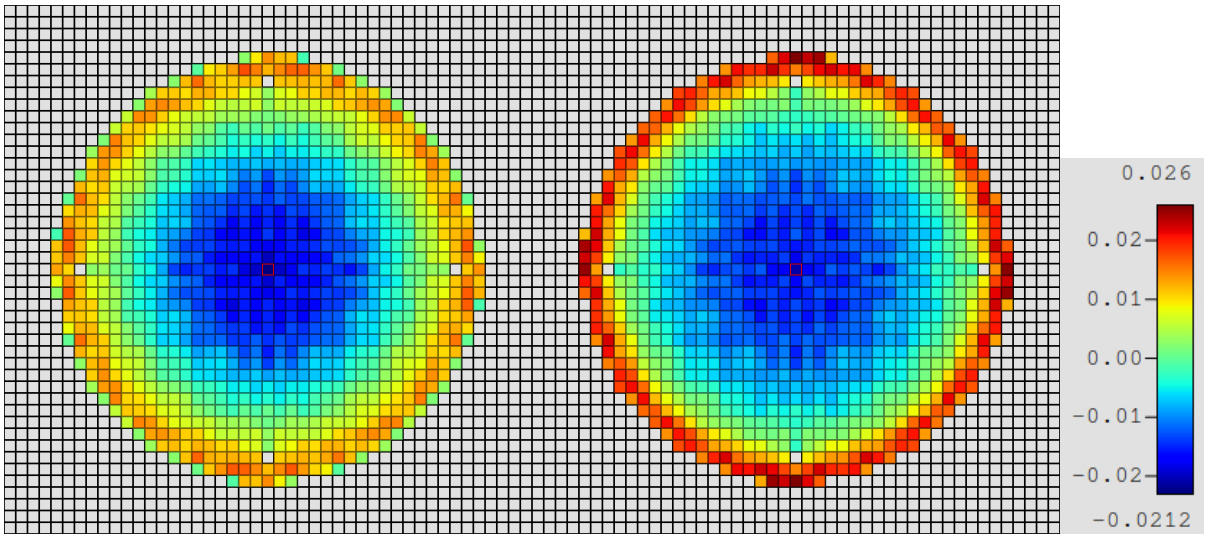

Figure C-30: MPACT radial fission rate differences using TCP0 (left) and P2 (right) scattering for Case 6.

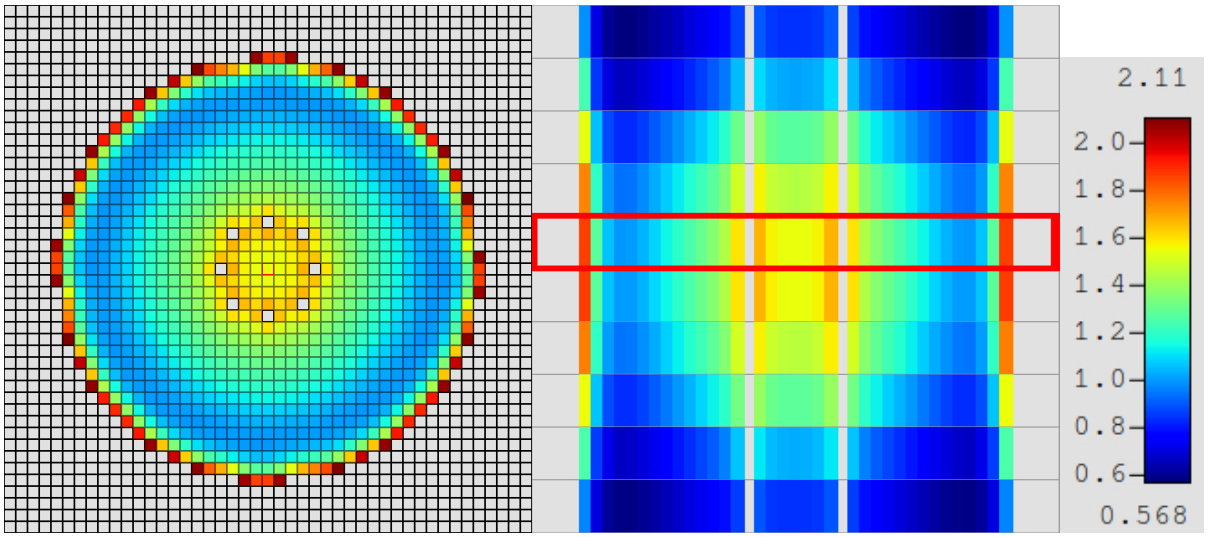

Figure C-31: Shift radial (left) and axial (right) slices of fission rate distributions for Case 7.

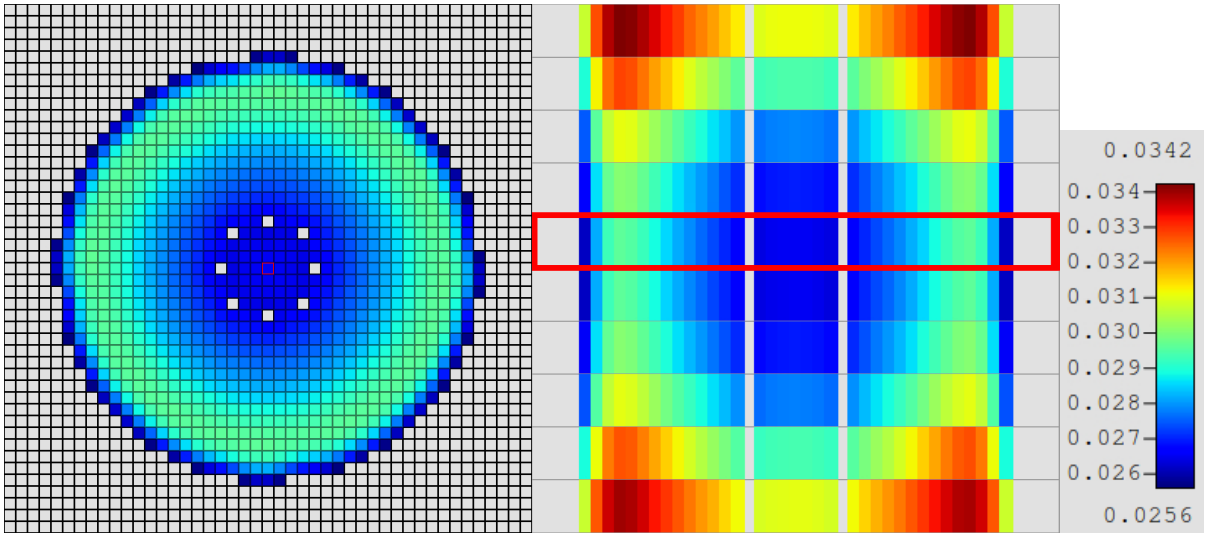

Figure C-32: Shift radial (left) and axial (right) slices of percent uncertainties for Case 7.

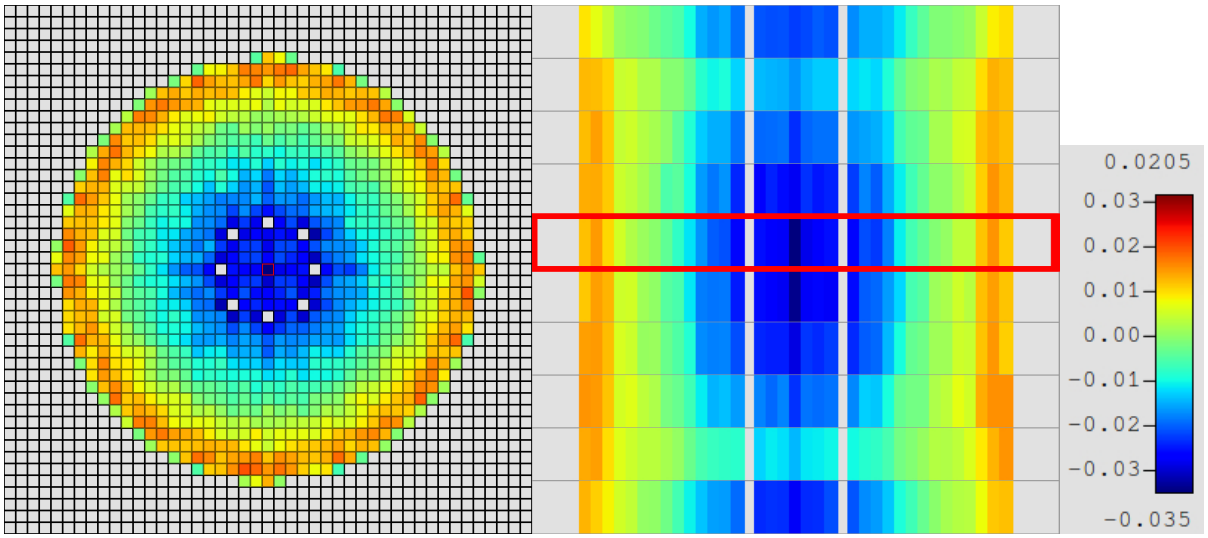

Figure C-33: MPACT radial (left) and axial (right) slices of fission rate differences for Case 7 (TCP0).

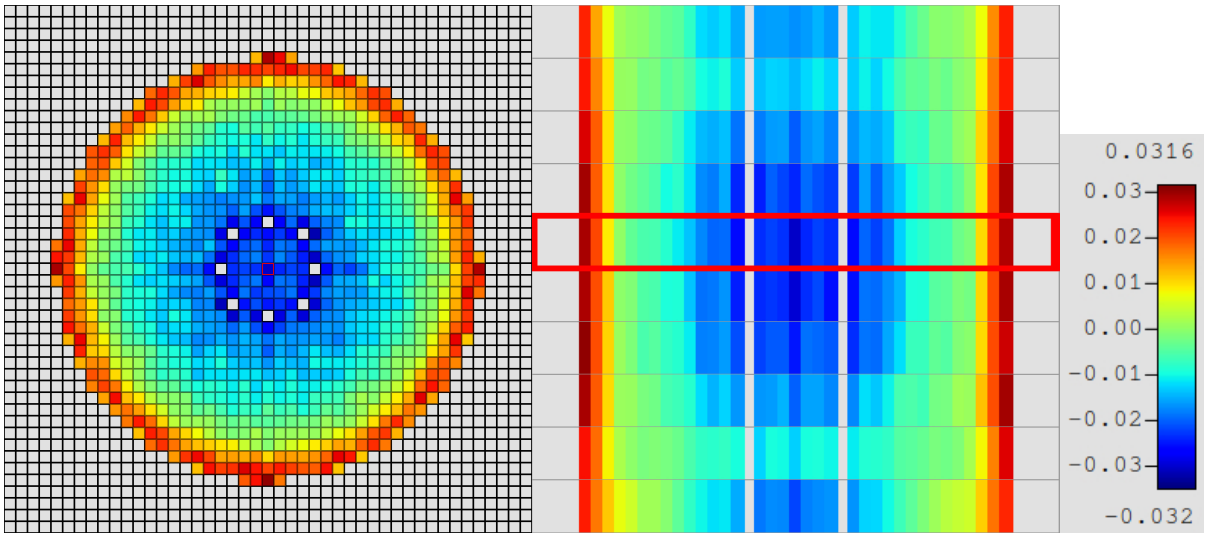

Figure C-34: MPACT radial (left) and axial (right) slices of fission rate differences for Case 7 (P2).

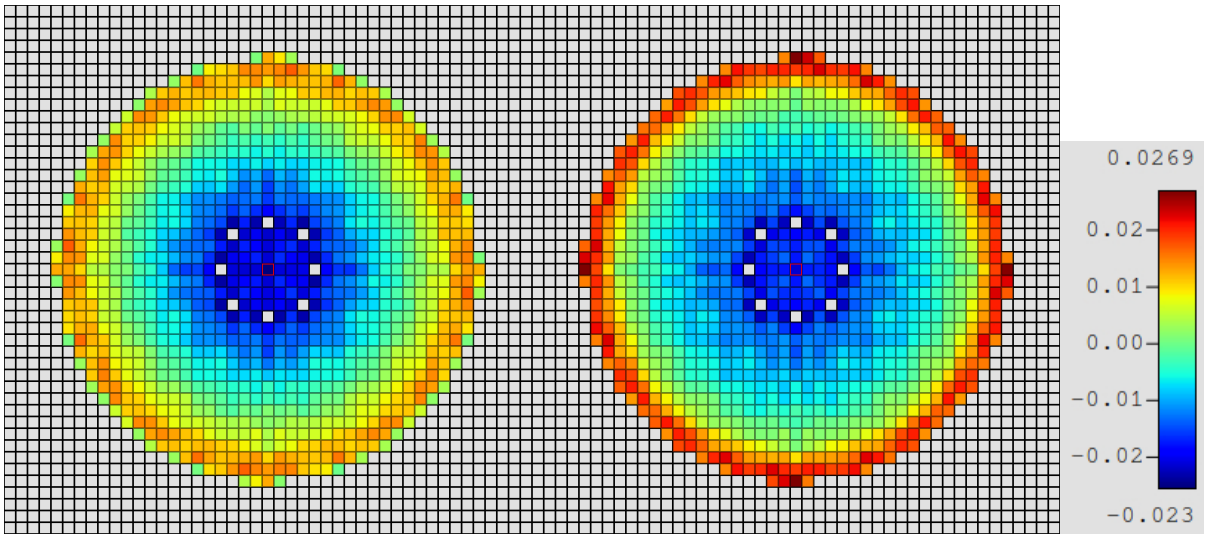

Figure C-35: MPACT radial fission rate differences using TCP0 (left) and P2 (right) scattering for Case 7.

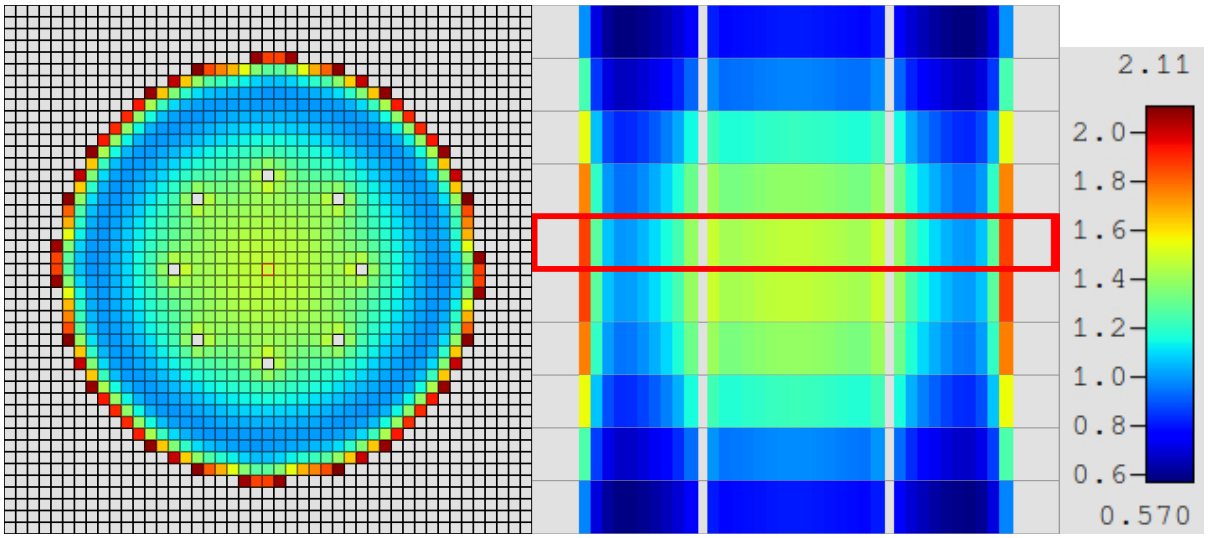

Figure C-36: Shift radial (left) and axial (right) slices of fission rate distributions for Case 8.

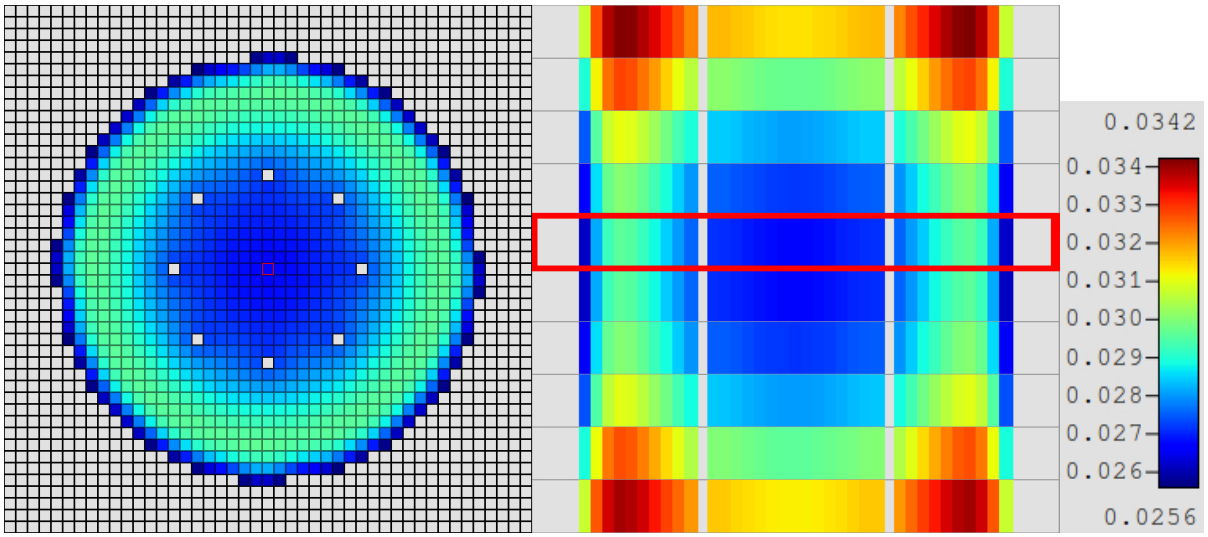

Figure C-37: Shift radial (left) and axial (right) slices of percent uncertainties for Case 8.

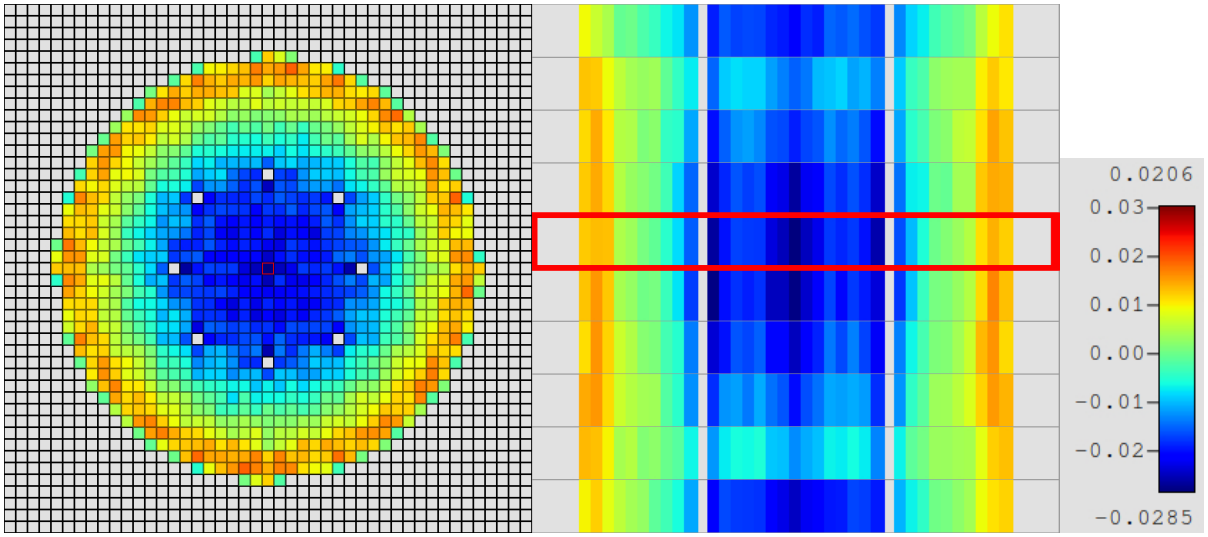

Figure C-38: MPACT radial (left) and axial (right) slices of fission rate differences for Case 8 (TCP0).

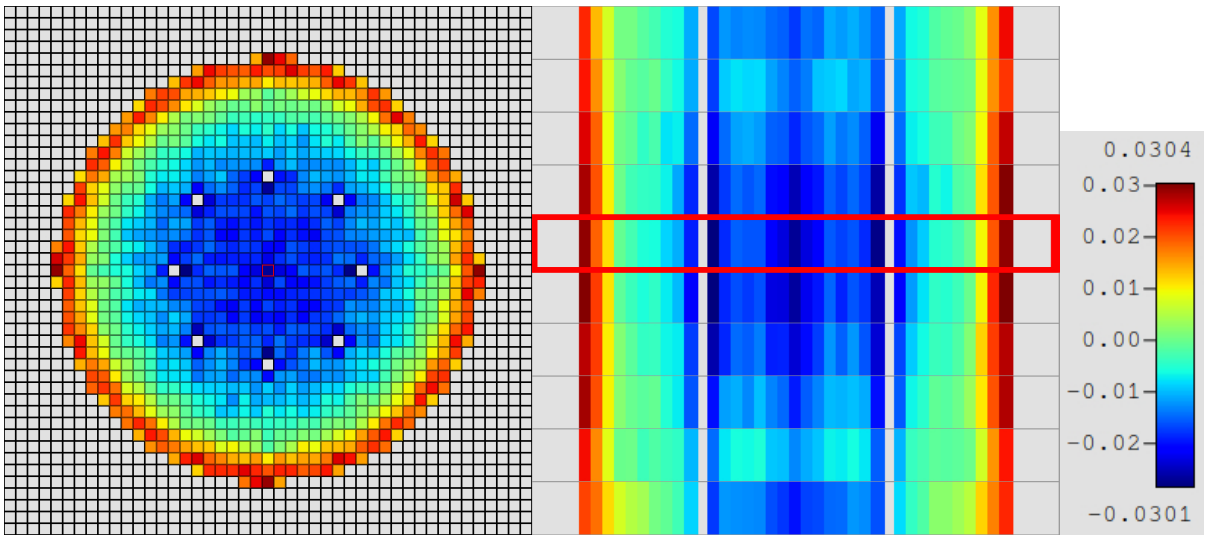

Figure C-39: MPACT radial (left) and axial (right) slices of fission rate differences for Case 8 (P2).

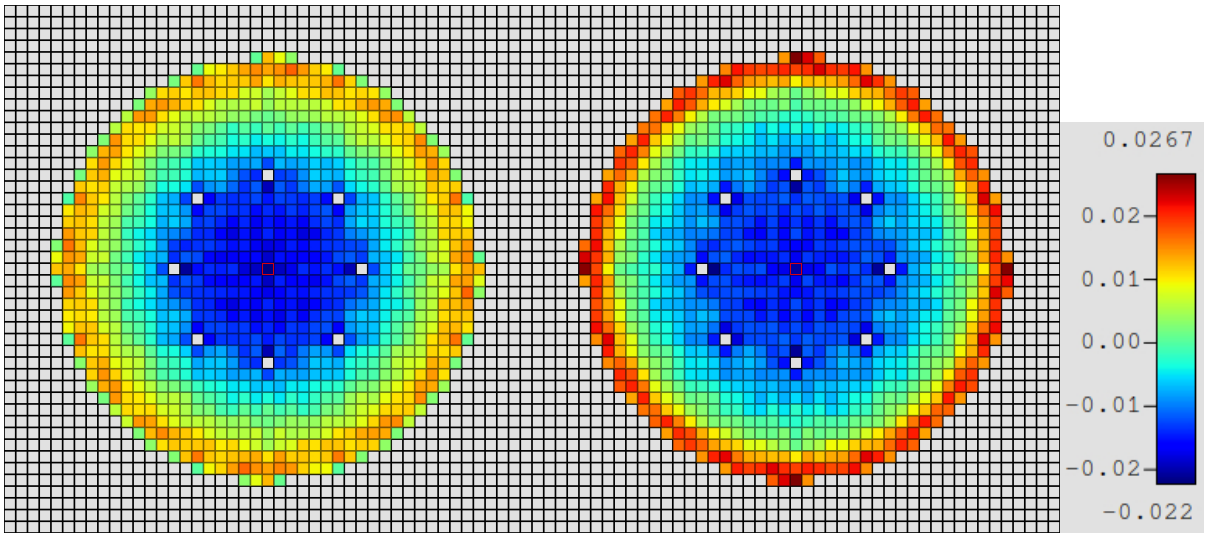

Figure C-40: MPACT radial fission rate differences using TCP0 (left) and P2 (right) scattering for Case 8.

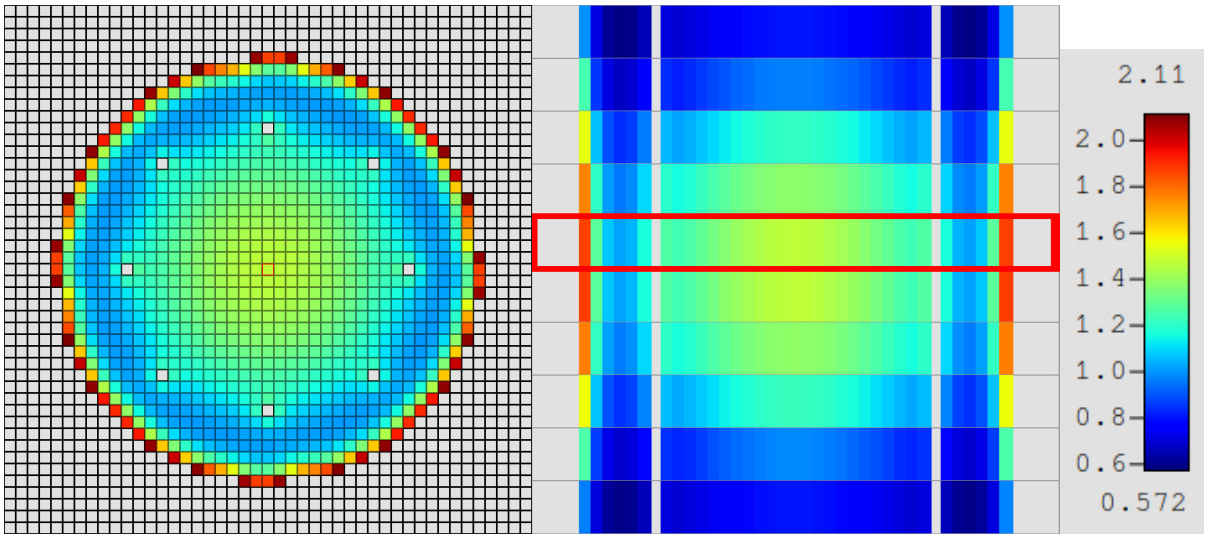

Figure C-41: Shift radial (left) and axial (right) slices of fission rate distributions for Case 9.

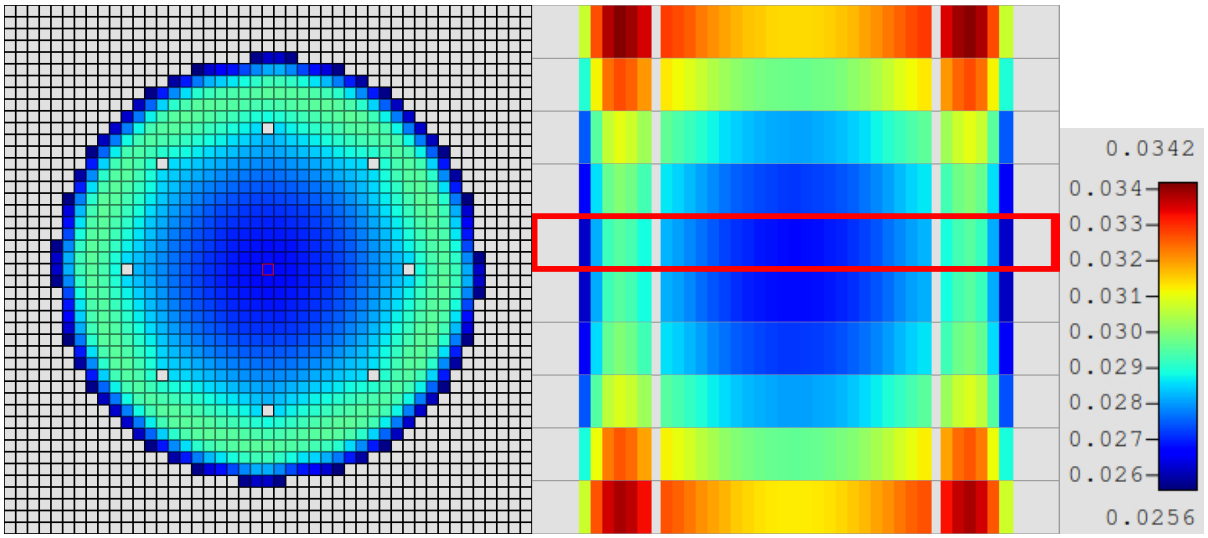

Figure C-42: Shift radial (left) and axial (right) slices of percent uncertainties for Case 9.

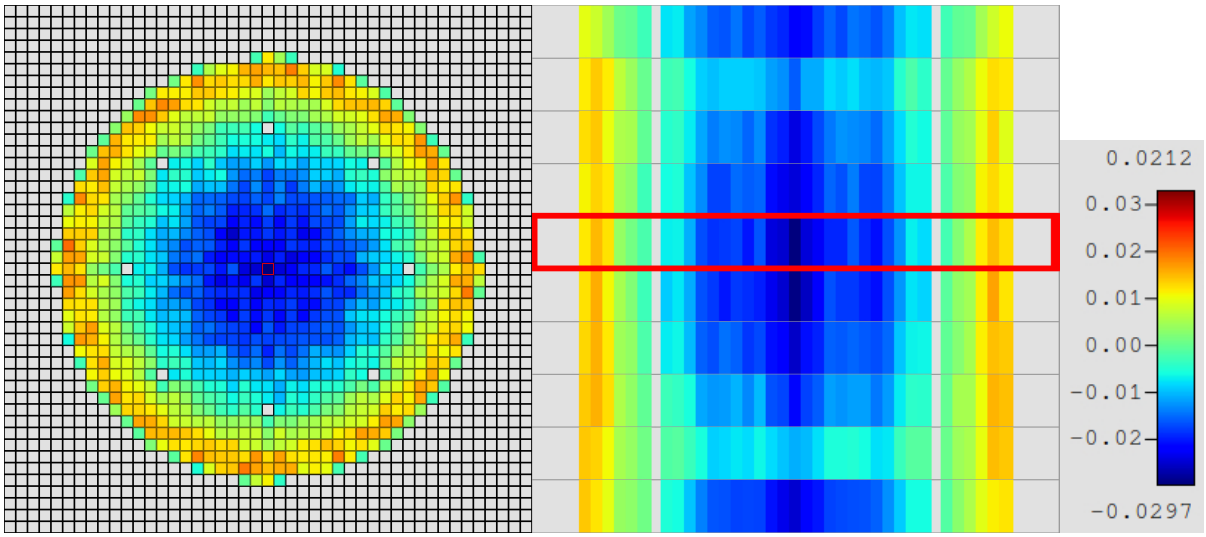

Figure C-43: MPACT radial (left) and axial (right) slices of fission rate differences for Case 9 (TCP0).

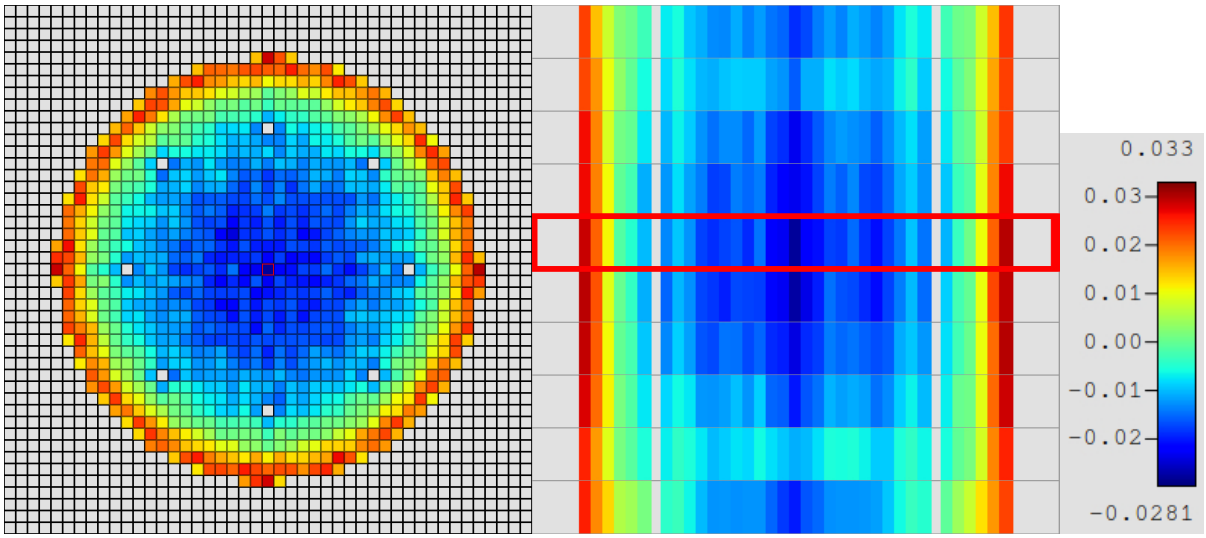

Figure C-44: MPACT radial (left) and axial (right) slices of fission rate differences for Case 9 (P2).

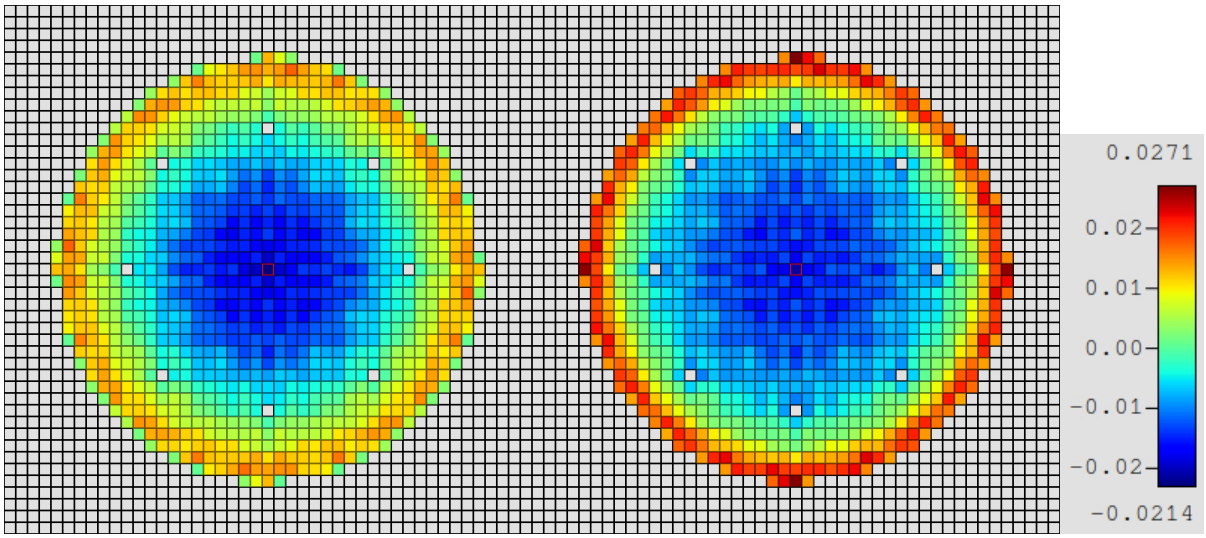

Figure C-45: MPACT radial fission rate differences using TCP0 (left) and P2 (right) scattering for Case 9.

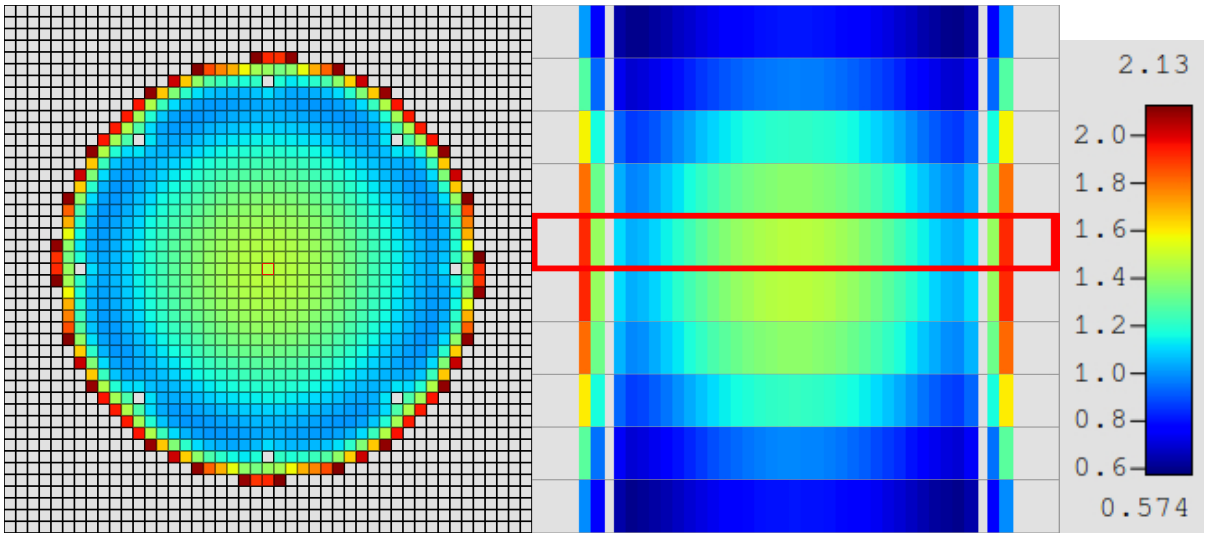

Figure C-46: Shift radial (left) and axial (right) slices of fission rate distributions for Case 10.

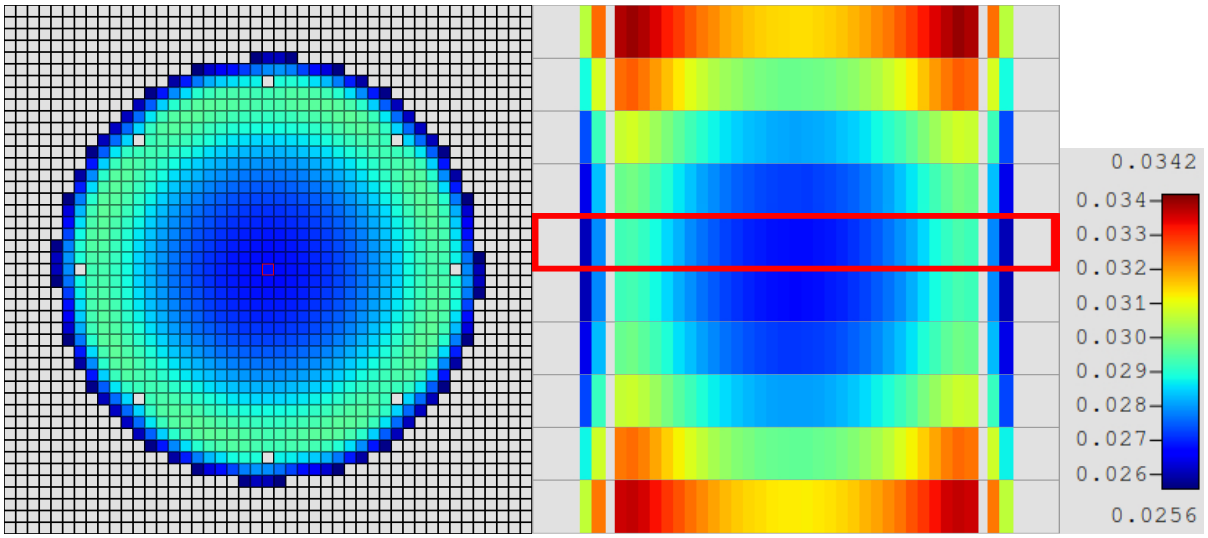

Figure C-47: Shift radial (left) and axial (right) slices of percent uncertainties for Case 10.

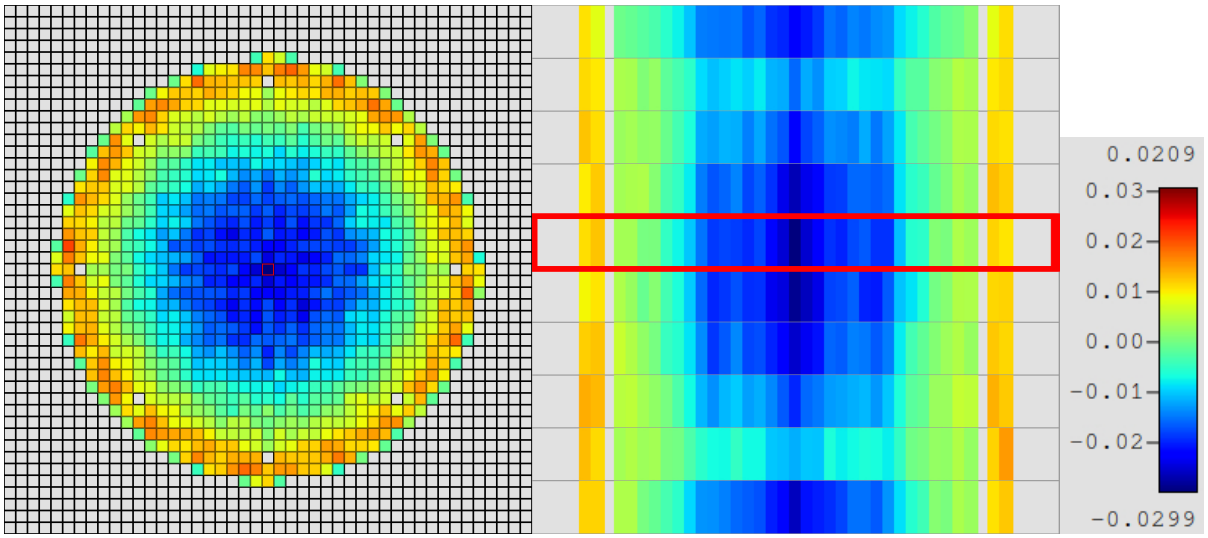

Figure C-48: MPACT radial (left) and axial (right) slices of fission rate differences for Case 10 (TCP0).

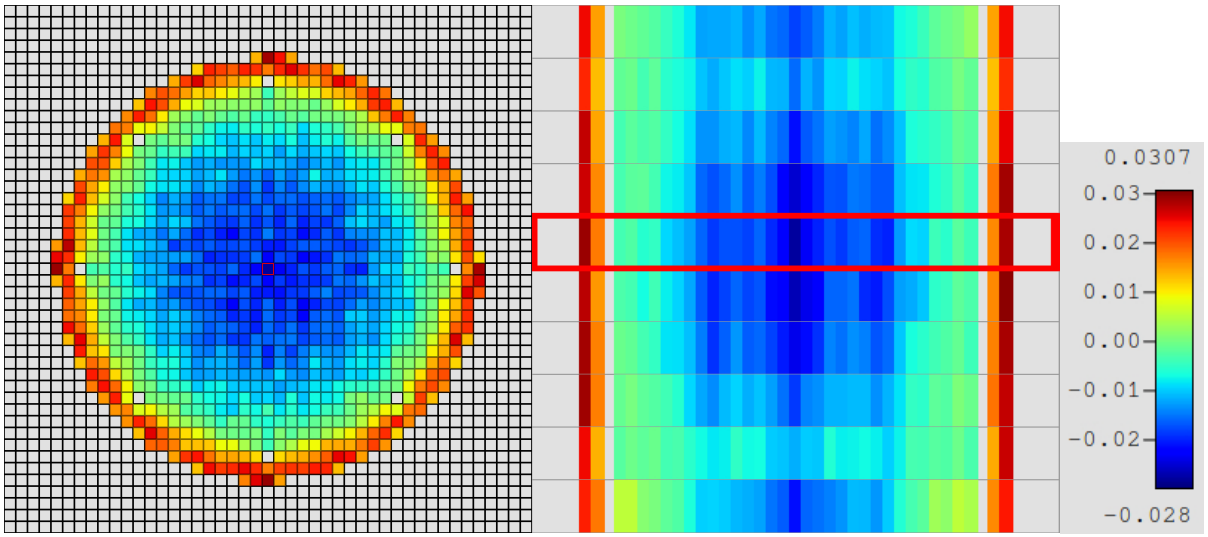

Figure C-49: MPACT radial (left) and axial (right) slices of fission rate differences for Case 10 (P2).

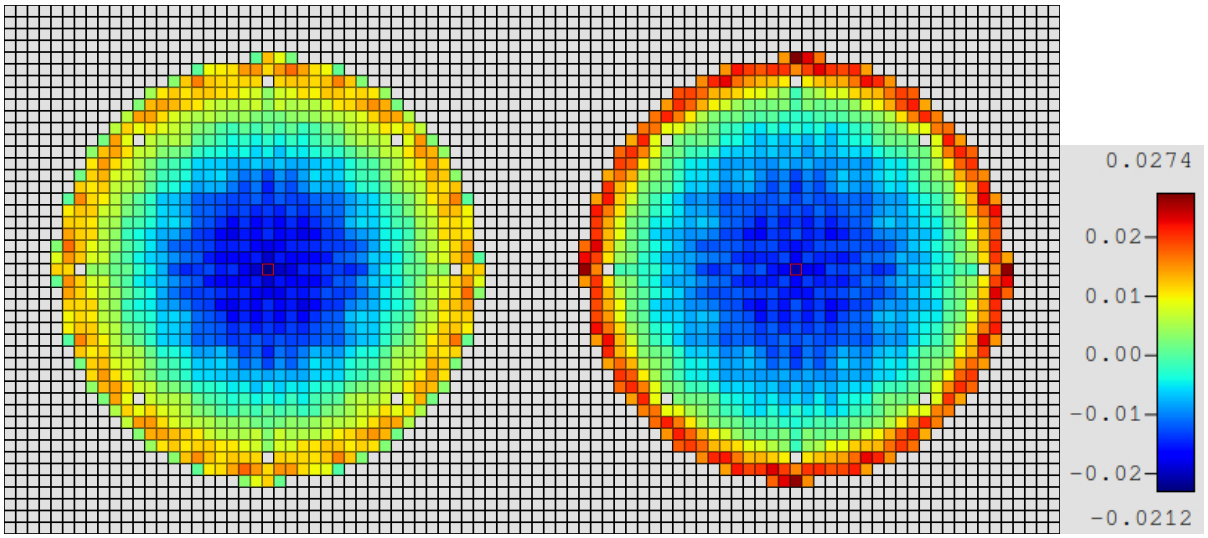

Figure C-50: MPACT radial fission rate differences using TCP0 (left) and P2 (right) scattering for Case 10.

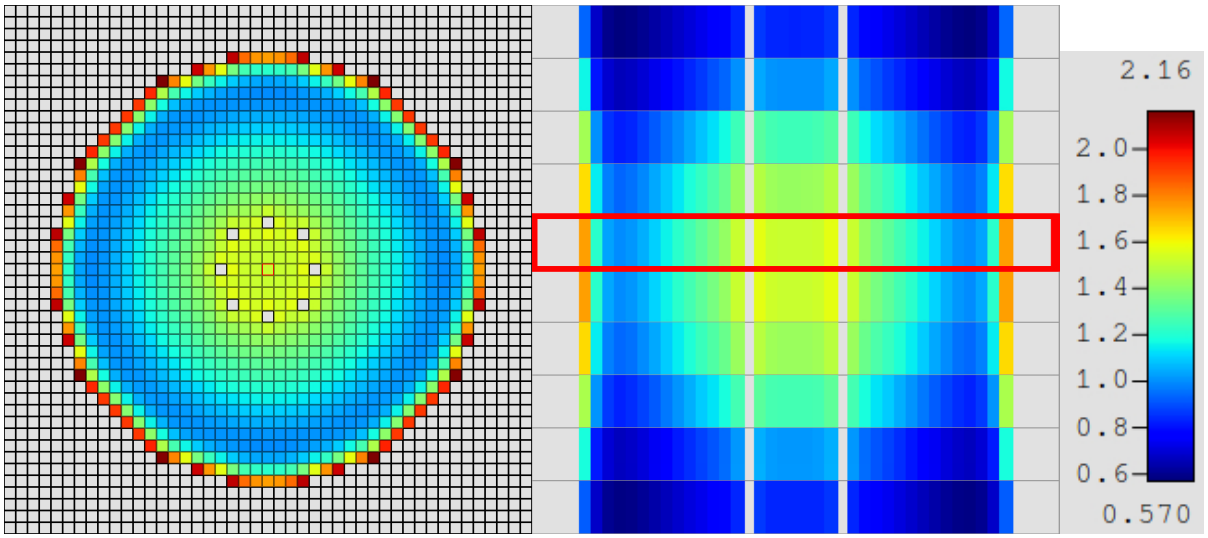

Figure C-51: Shift radial (left) and axial (right) slices of fission rate distributions for Case 11.

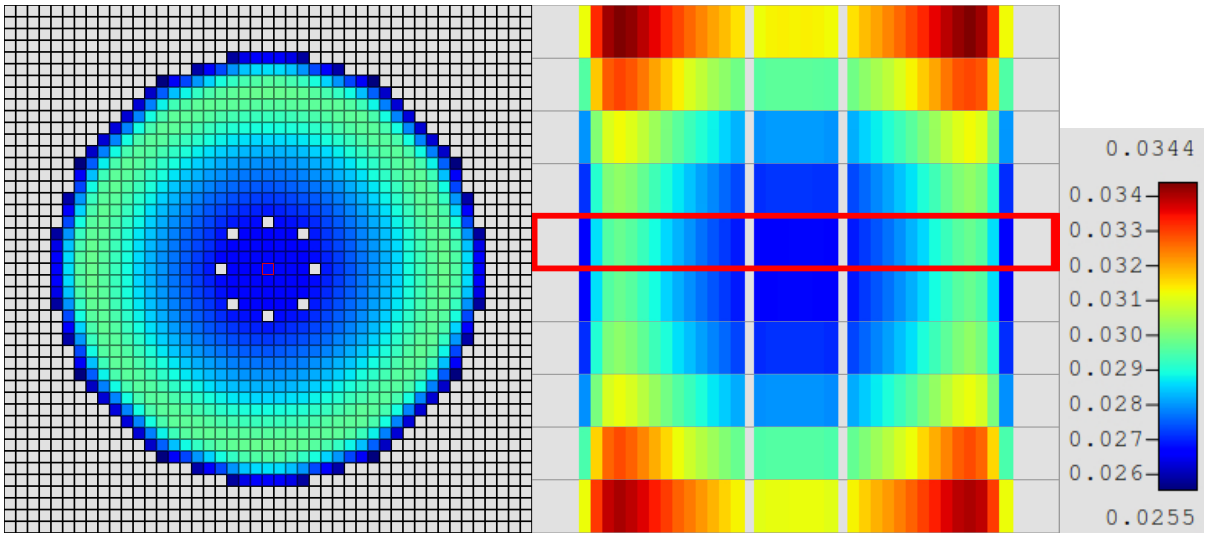

Figure C-52: Shift radial (left) and axial (right) slices of percent uncertainties for Case 11.

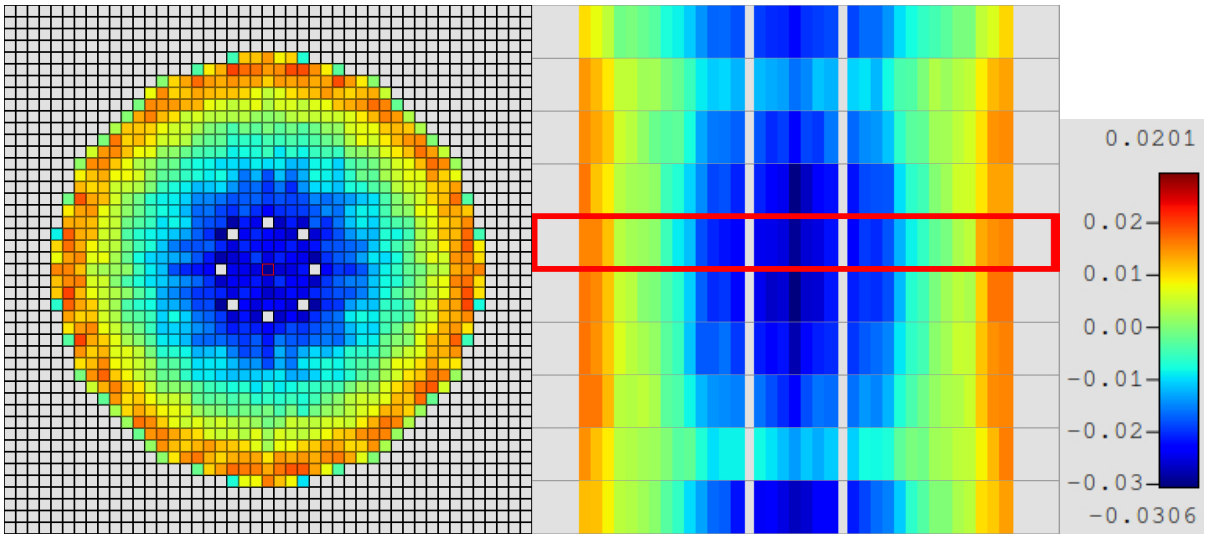

Figure C-53: MPACT radial (left) and axial (right) slices of fission rate differences for Case 11 (TCP0).

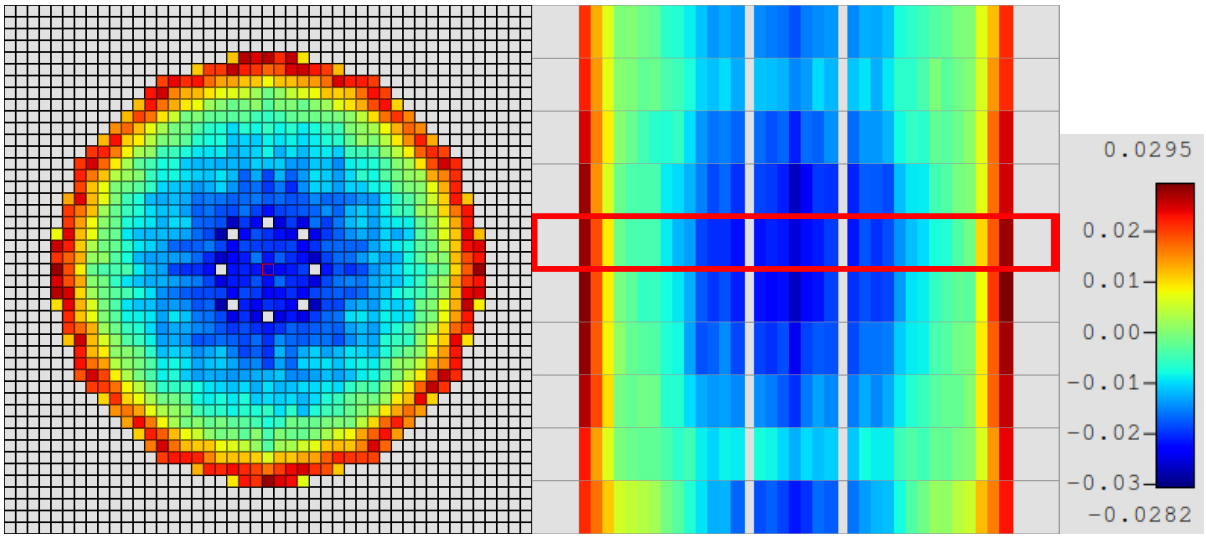

Figure C-54: MPACT radial (left) and axial (right) slices of fission rate differences for Case 11 (P2).

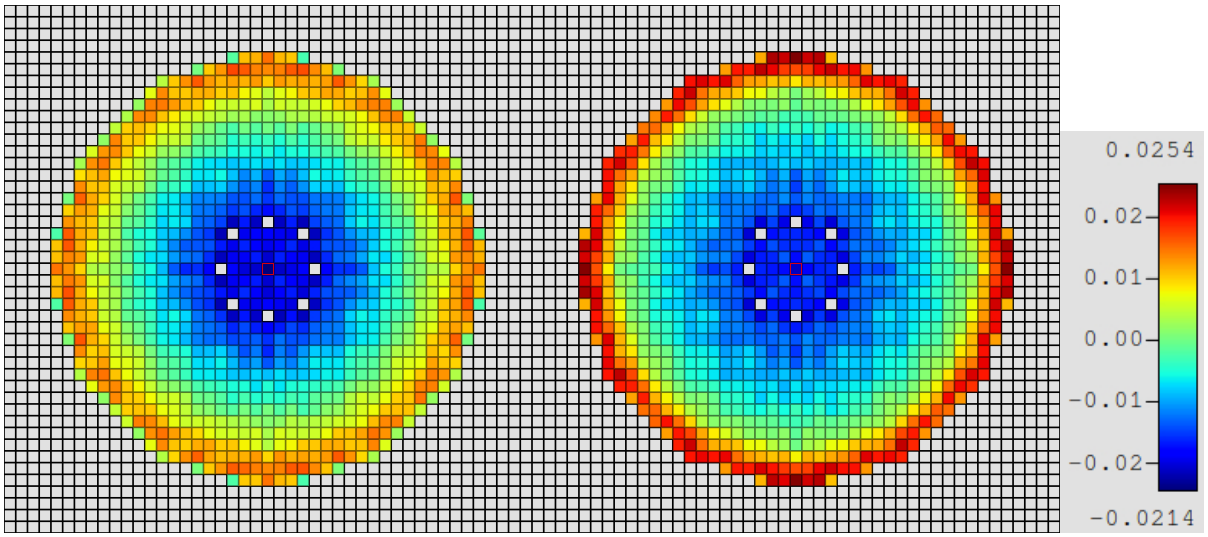

Figure C-55: MPACT radial fission rate differences using TCP0 (left) and P2 (right) scattering for Case 11.

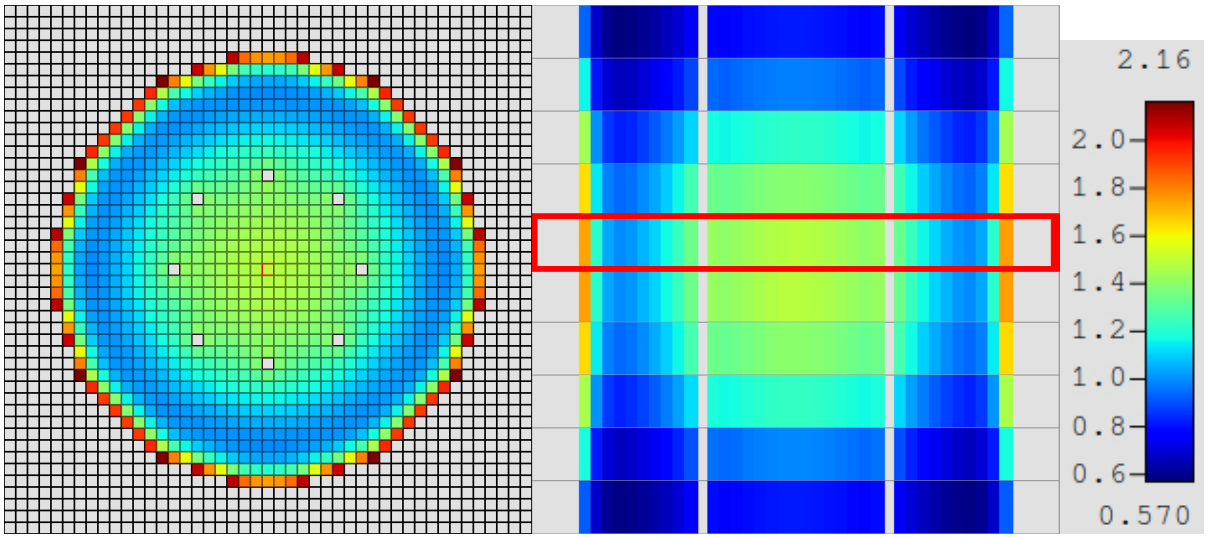

Figure C-56: Shift radial (left) and axial (right) slices of fission rate distributions for Case 12.

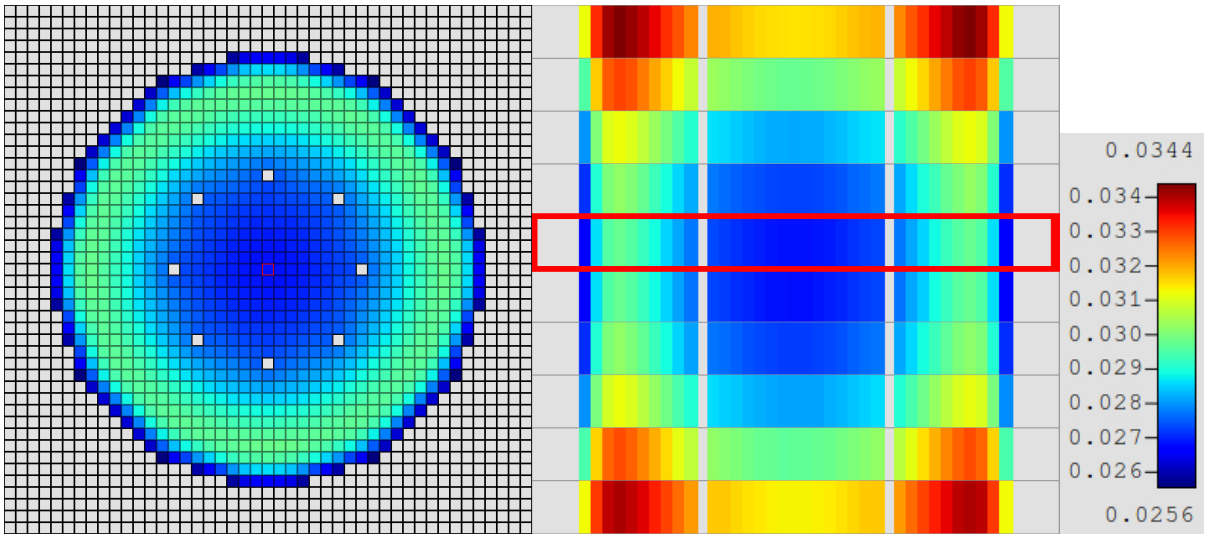

Figure C-57: Shift radial (left) and axial (right) slices of percent uncertainties for Case 12.

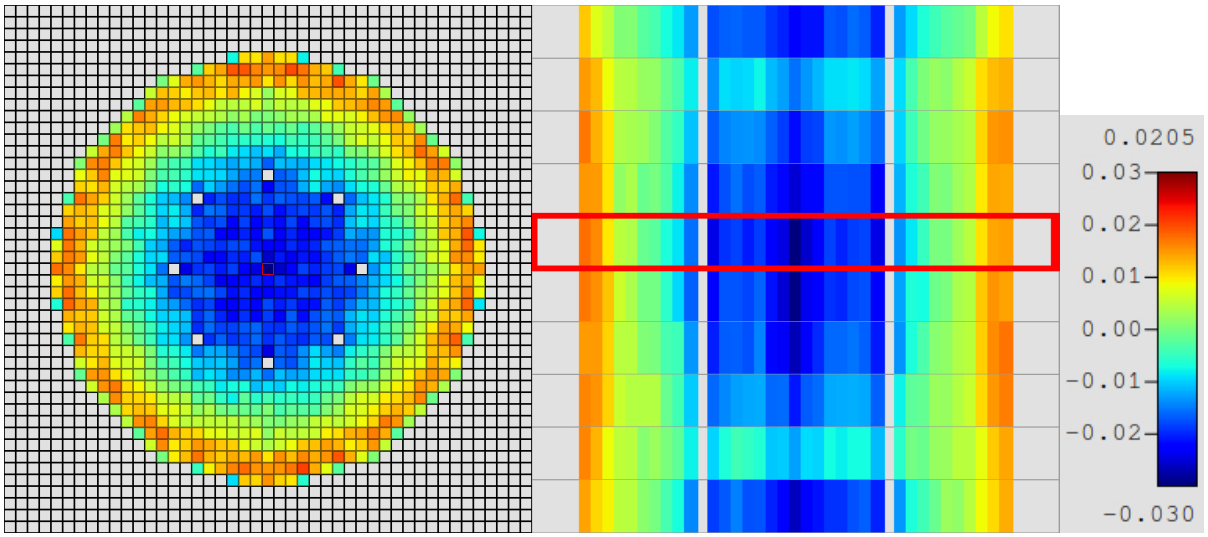

Figure C-58: MPACT radial (left) and axial (right) slices of fission rate differences for Case 12 (TCP0).

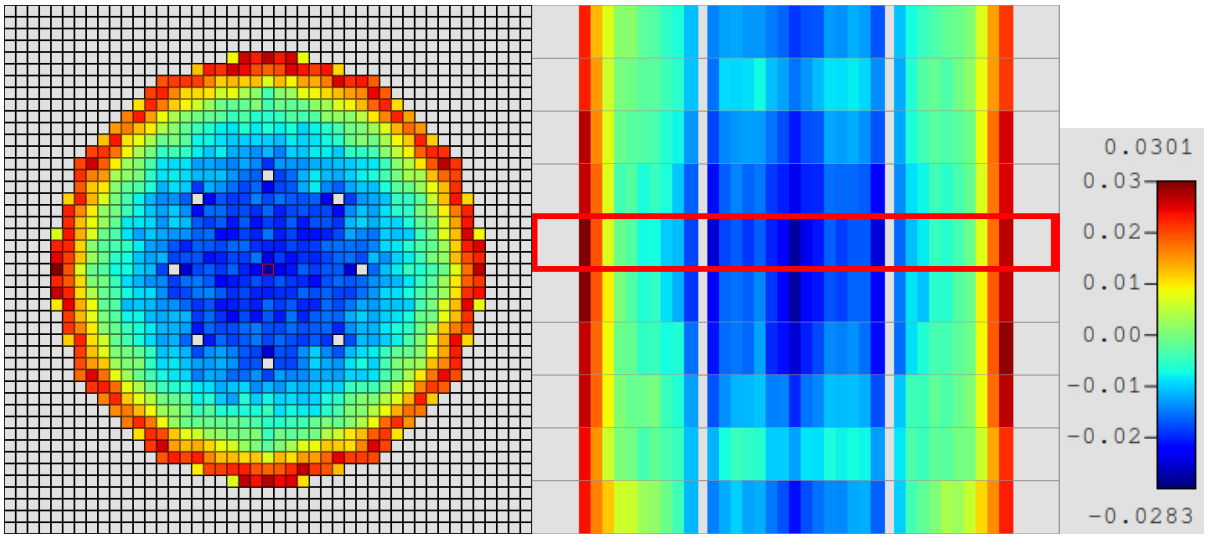

Figure C-59: MPACT radial (left) and axial (right) slices of fission rate differences for Case 12 (P2).

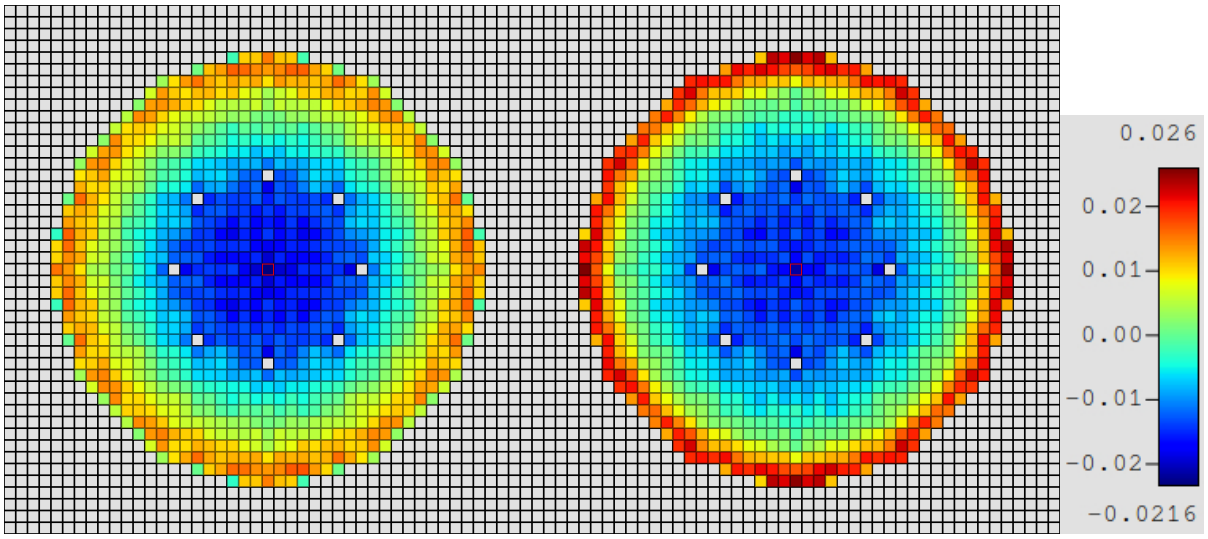

Figure C-60: MPACT radial fission rate differences using TCP0 (left) and P2 (right) scattering for Case 12.

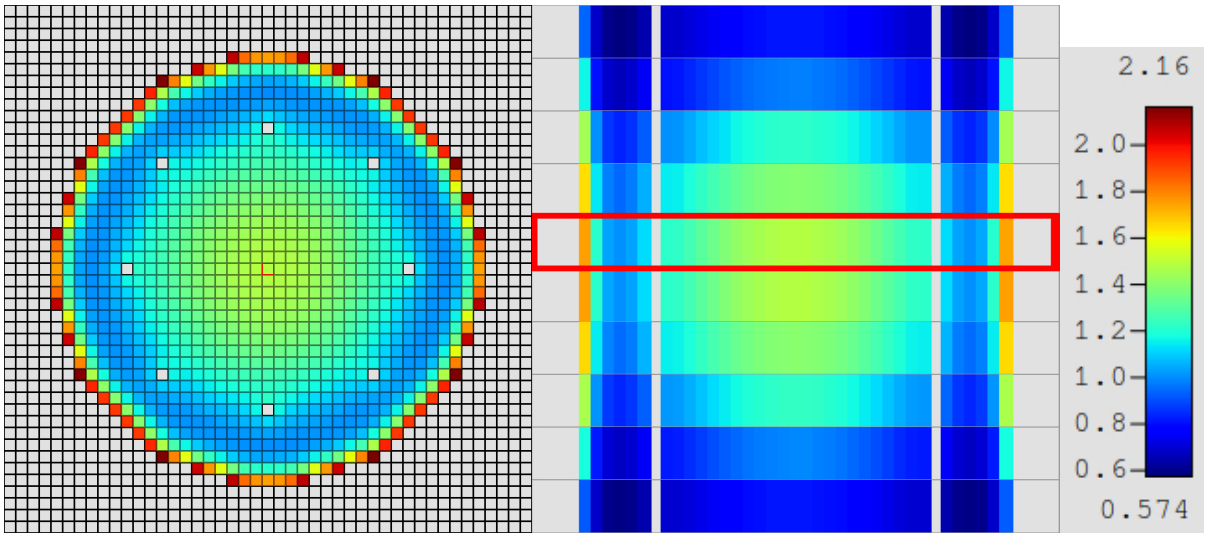

Figure C-61: Shift radial (left) and axial (right) slices of fission rate distributions for Case 13.

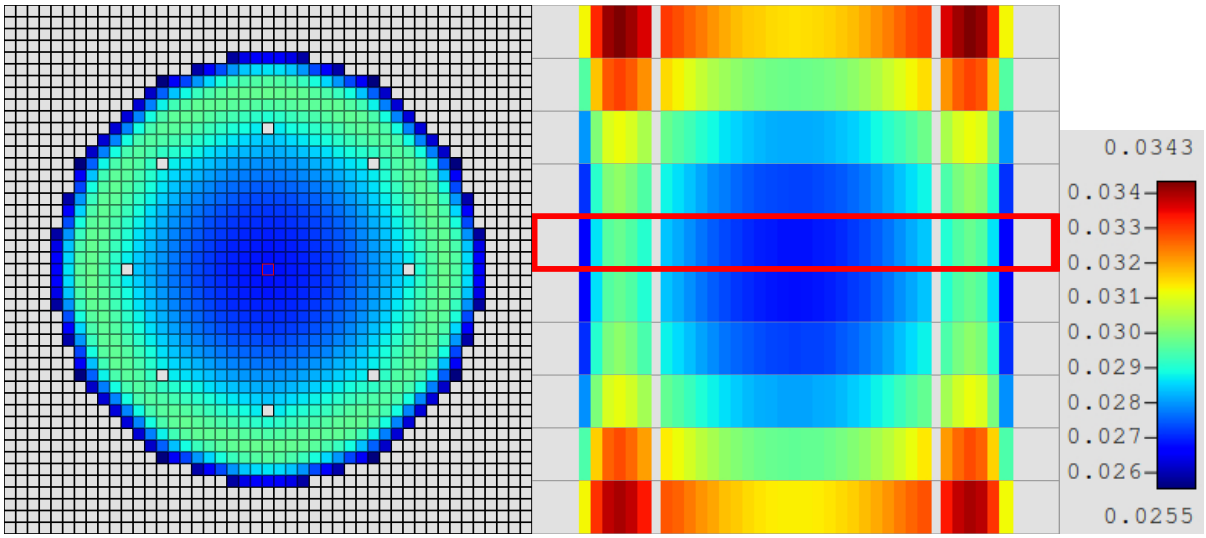

Figure C-62: Shift radial (left) and axial (right) slices of percent uncertainties for Case 13.

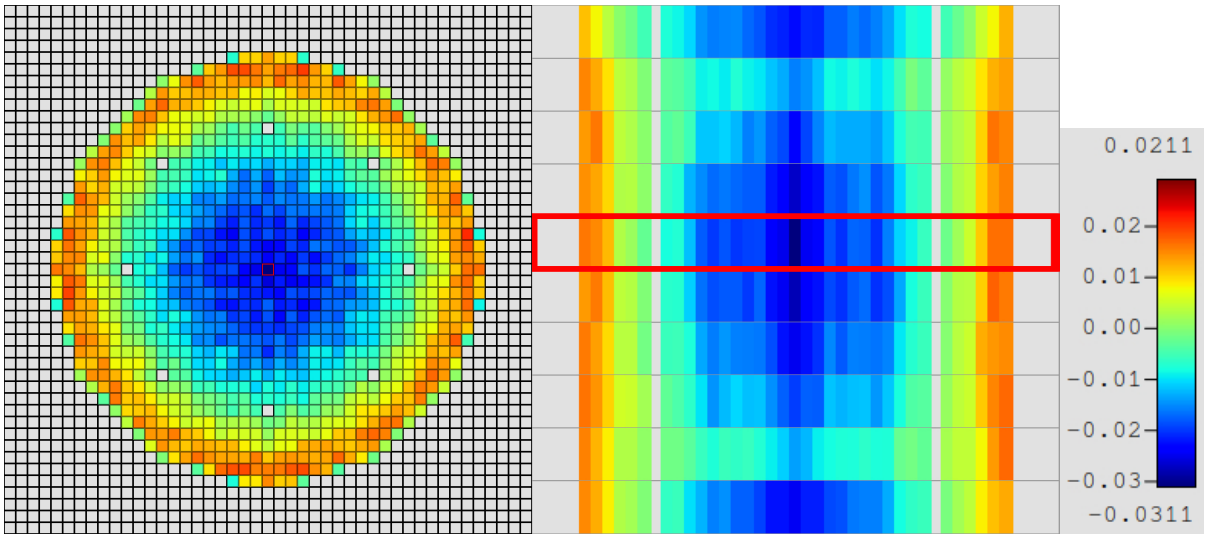

Figure C-63: MPACT radial (left) and axial (right) slices of fission rate differences for Case 13 (TCP0).

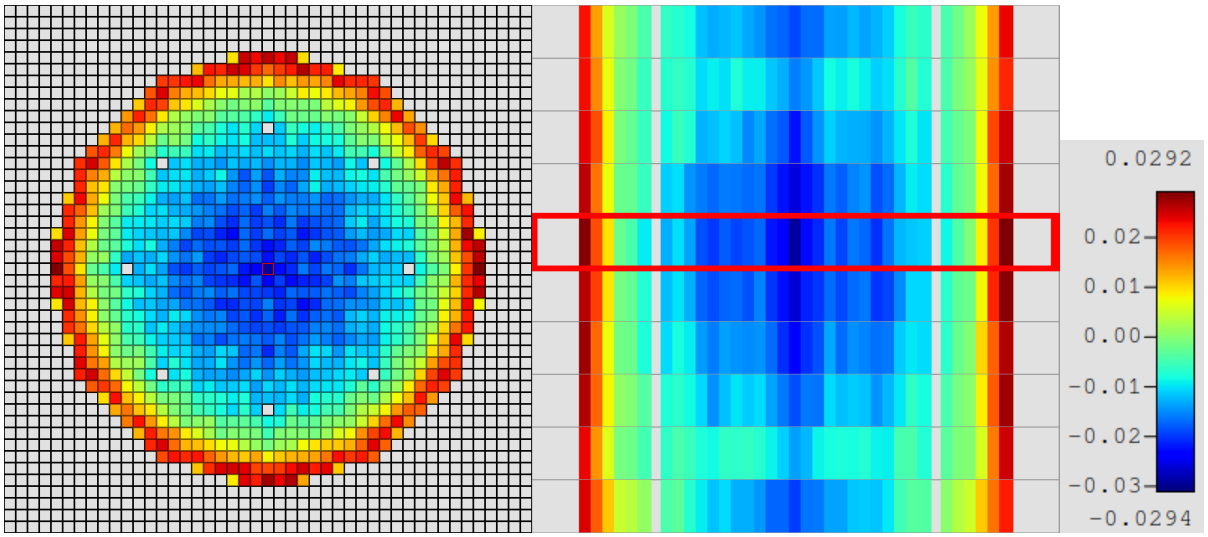

Figure C-64: MPACT radial (left) and axial (right) slices of fission rate differences for Case 13 (P2).

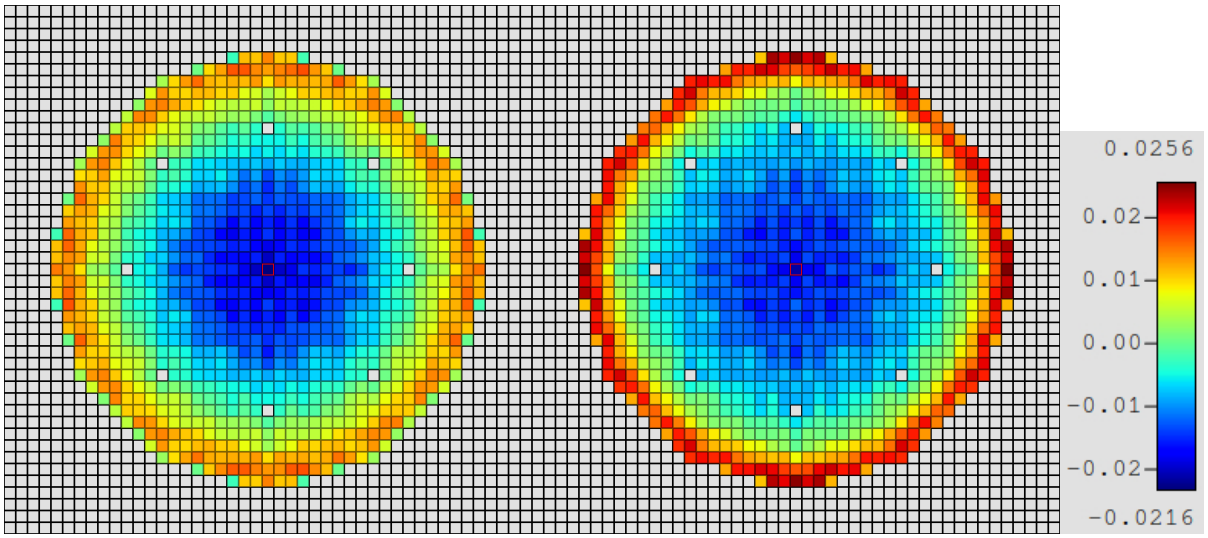

Figure C-65: MPACT radial fission rate differences using TCP0 (left) and P2 (right) scattering for Case 13.

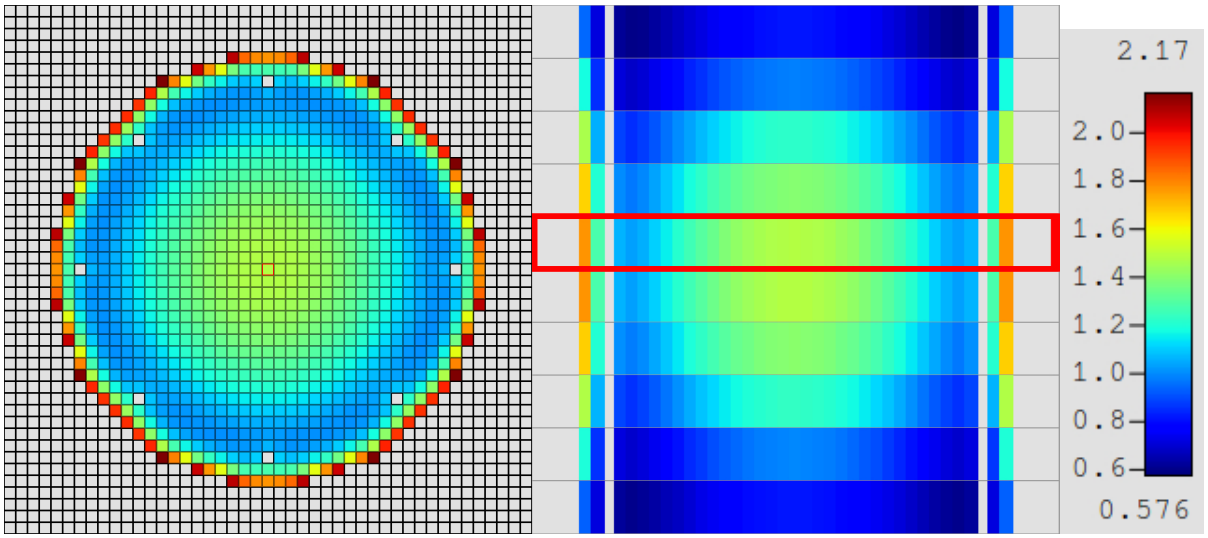

Figure C-66: Shift radial (left) and axial (right) slices of fission rate distributions for Case 14.

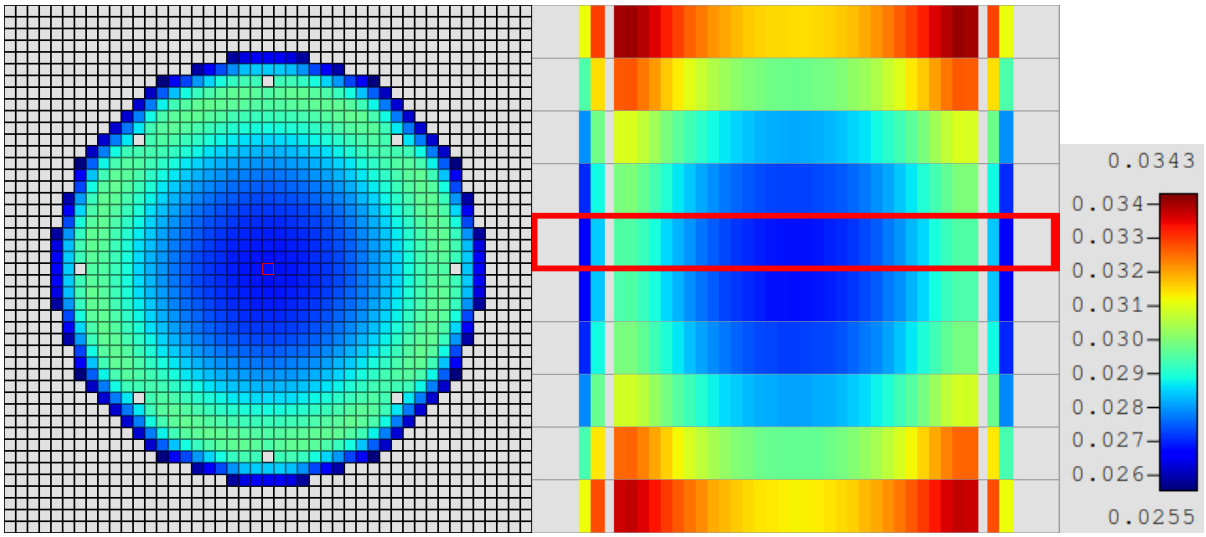

Figure C-67: Shift radial (left) and axial (right) slices of percent uncertainties for Case 14.

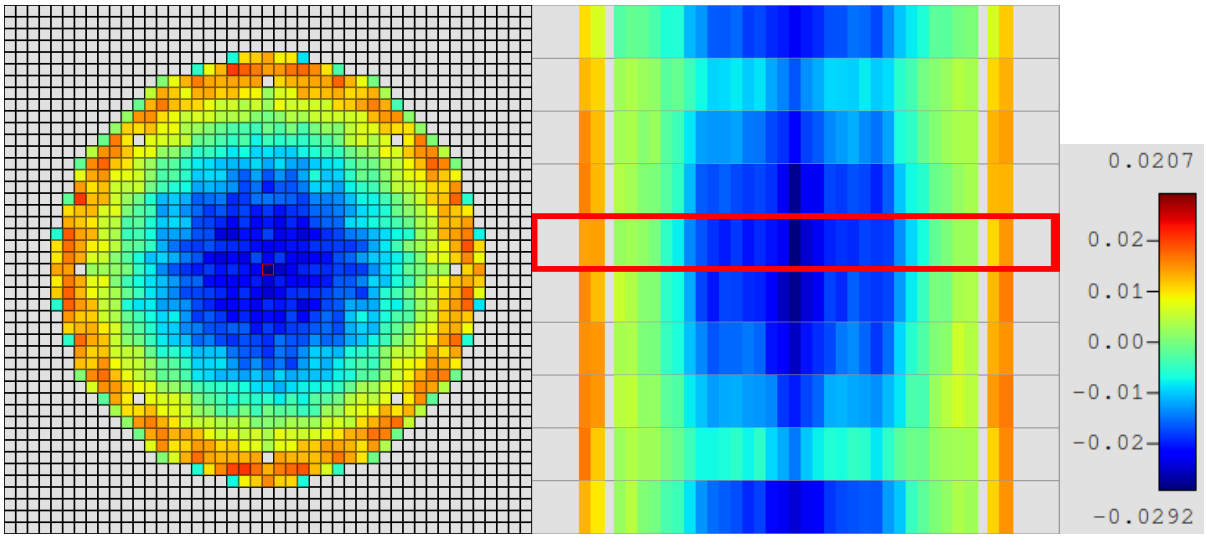

Figure C-68: MPACT radial (left) and axial (right) slices of fission rate differences for Case 14 (TCP0).

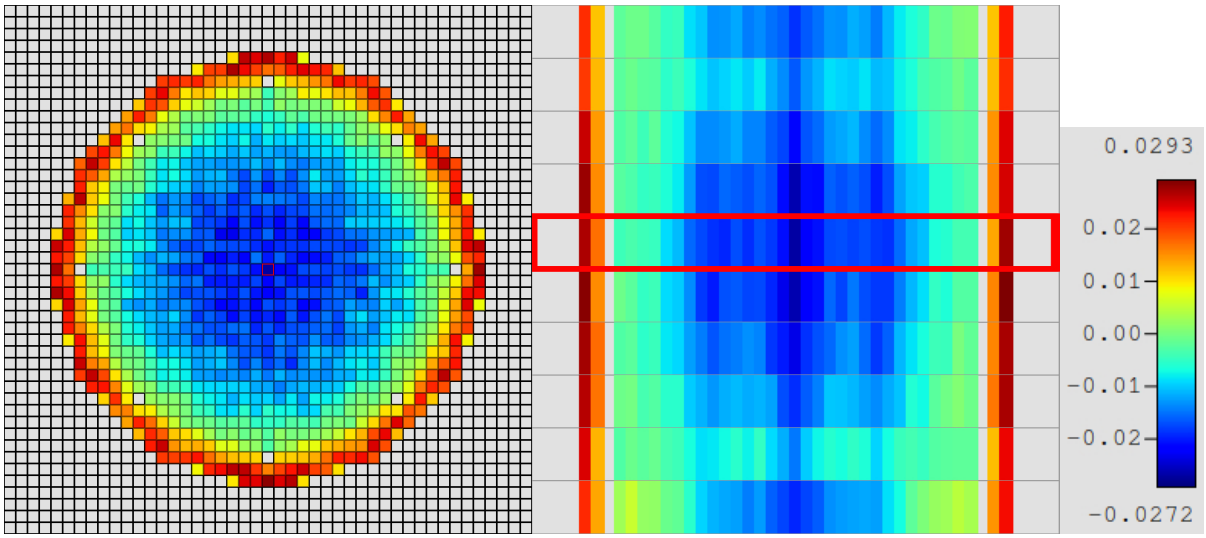

Figure C-69: MPACT radial (left) and axial (right) slices of fission rate differences for Case 14 (P2).

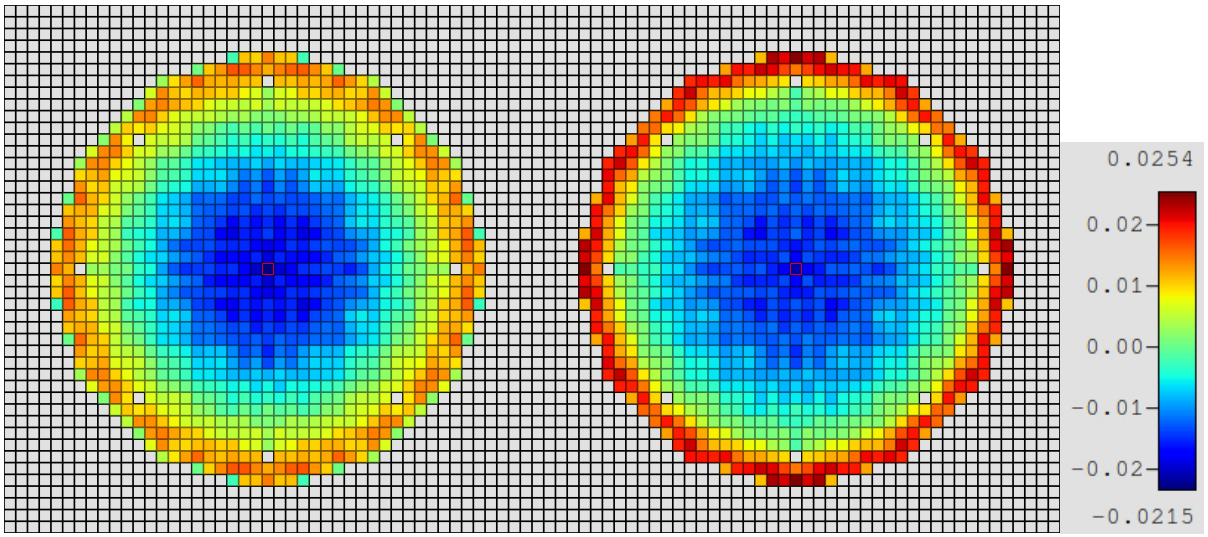

Figure C-70: MPACT radial fission rate differences using TCP0 (left) and P2 (right) scattering for Case 14.

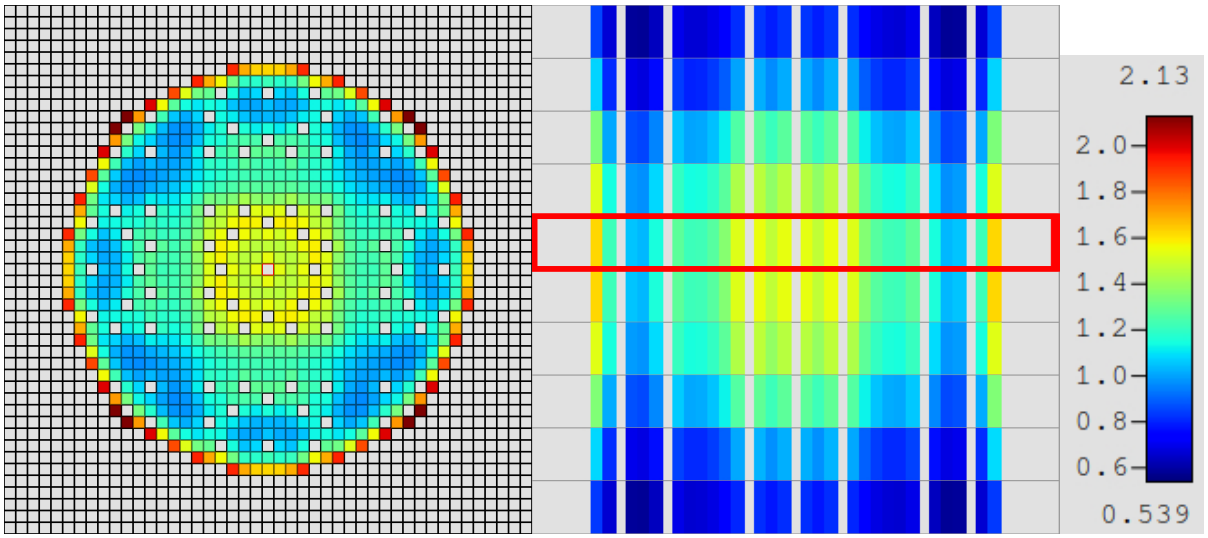

Figure C-71: Shift radial (left) and axial (right) slices of fission rate distributions for Case 15.

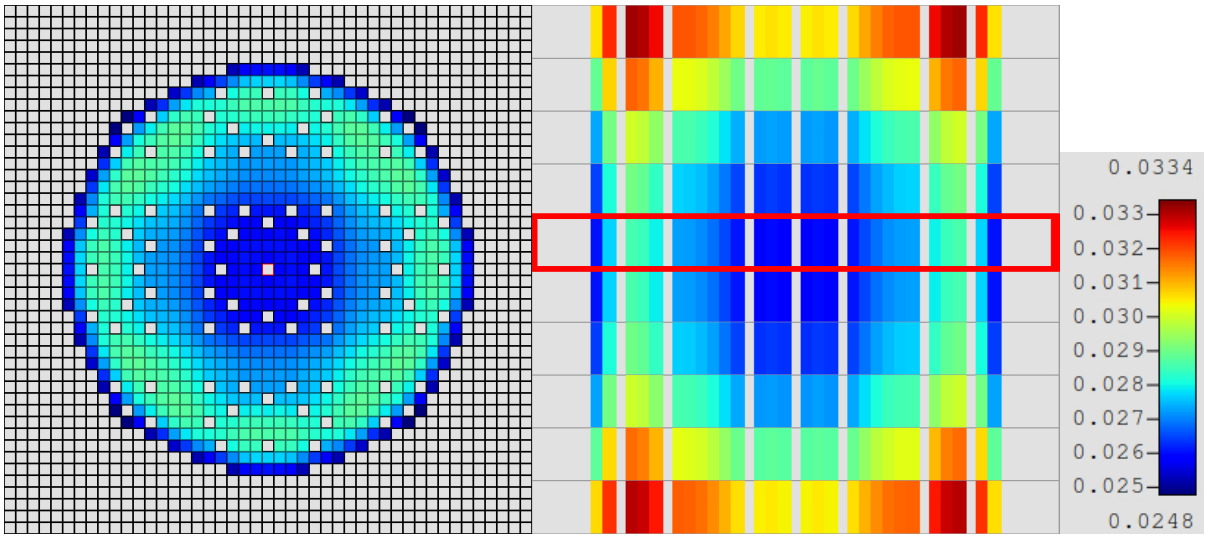

Figure C-72: Shift radial (left) and axial (right) slices of percent uncertainties for Case 15.

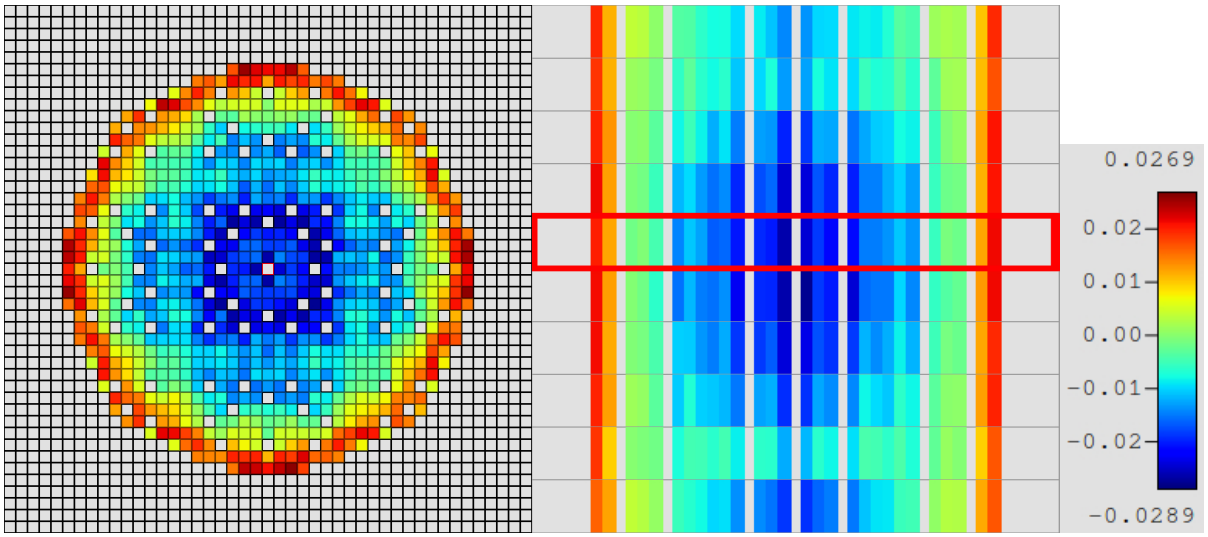

Figure C-73: MPACT radial (left) and axial (right) slices of fission rate differences for Case 15 (P2).

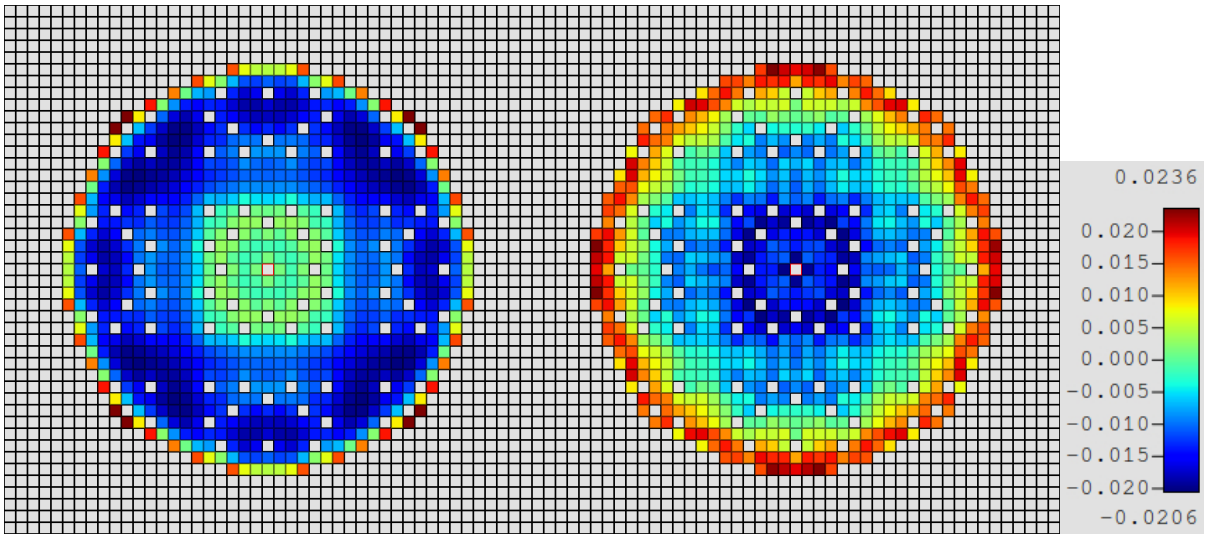

Figure C-74: SHIFT radial fission rate distribution (left) and MPACT differences using P2 scattering (right) for Case 15.

APPENDIX D. Particle History and Stochastic Uncertainty Analysis

APPENDIX D. PARTICLE HISTORY AND STOCHASTIC UNCERTAINTY ANALYSIS

In the application of a stochastic technique like Monte Carlo neutron transport, it is important to understand the calculated uncertainty that accompanies the calculated result, both in problem eigenvalue (in k-eigenvalue calculations) and reaction rate distributions. Monte Carlo uncertainty exists in the form of a standard deviation of a population about a calculated mean. The mean is the quantity of interest (eigenvalue, neutron flux, fission rate), whereas the standard deviation is calculated integrally with the solution and should continually reduce as the number of particle histories increases (theoretically as the square root of the total number of tallies, for instance). The magnitude of the standard deviation is simply limited by the computation resources and run time, which are inexorably tied to parallel efficiency of the Monte Carlo software in modern terms.

For application of the Monte Carlo tools KENO-VI and Shift (both CSAS-Shift and VERA Shift), the quantities of interest for the 7uPCX experiment are eigenvalue (which are measured), neutron flux distribution, and fission rate distribution. Reducing uncertainty to an acceptable level for the latter two requires sufficient particle histories as to result in very low eigenvalue uncertainty. For instance, the initial KENO-VI results for these models using the KENO-VI "sig" option resulted in a calculated uncertainty in eigenvalue of 10 pcm. These corresponded to approximately 8.3e7 active particle histories, on average. When the particle histories were increased to 2e9 active particle histories to reduce the local uncertainty in neutron flux, the uncertainty in eigenvalue was reduced to 2 pcm (~23× increase in particles produced 5× decrease in uncertainty). Since the measured uncertainty is reported in Harms and Miller [1] as 100 pcm, all of these amounts of particle histories are sufficient for comparison to the experiment reactivity results.

For the KENO-VI fission rate distribution, calculated with SCALE 6.3.0, the maximum calculated fractional uncertainty for the initial ~8.3e7 active particle history cases was 1.80%. This is based on a mesh tally where each mesh cell is $1/10^{th}$ of a fuel rod (the mesh aligns with the pin cells and is divided into ten uniform axial regions). A series of test cases based on Case 1 of the 7uPCX experiment were executed with increasing particle histories to choose a particle count for this analysis and to better understand the actual uncertainty in the stochastic results. KENO-VI is limited in its parallelism and was executed on a smaller, shared-computing cluster at ORNL, so an optimum number of particle histories was selected to minimize the local fission rate uncertainty while also not abusing the compute resource.

Table D-1 provides the KENO-VI results and runtimes for seven cases with increasing particle histories. The last case with 10 billion particle histories required nearly 13,000 core hours and is therefore the best reference solution for the other cases, even though it has its own uncertainty that cannot be precisely quantified. Based on the calculated uncertainty, local pin power errors of up to 0.8% may still be possible in the reference solution, with an average error of slightly less than 0.2%.

Table D-1: KENO-VI Particle History Results

Particles per Gen	Active Gens	Total Active Particles	k-eff	k-eff Sigma	Max Calc % Unc	k-eff Diff (pcm)	Pin Powers RMS Diff	Pin Powers Max Diff	Procs	Runtime (hours)	cpu-hours
4E4	2164	8.7E7	0.998184	9.9E-5	1.8%	6	1.3%	−6.8%	32	1.2	38
4E4	5E3	2E8	0.998183	6.6E-5	1.2%	6	0.9%	4.4%	64	1.7	107
2E5	5E3	1E9	0.998111	2.9E-5	0.5%	−1	0.4%	1.5%	160	5.2	832
4E5	**5E3**	**2E9**	**0.998155**	**2.0E-5**	**0.4%**	**3**	**0.3%**	**1.4%**	**320**	**6.1**	**1943**
8E5	5E3	4E9	0.998144	1.4E-5	0.3%	2	0.2%	1.0%	320	12.3	3922
1.6E6	5E3	8E9	0.998144	1.0E-5	0.2%	2	0.2%	0.9%	320	26.8	8562
2E6	5E3	1E10	0.998121	8.7E-6	0.2%	ref	ref	ref	480	26.5	12720

The maximum calculated percent statistical uncertainty is shown in the sixth column of Table D-1. Note that this value is approximately four times smaller than the calculated maximum differences in the ninth column, which is based on power distribution comparison to the largest case as a reference. For a normal distribution, 4σ includes 99.994% of the population, so in a population of ~10,000 tallies, a few deviations of 4σ are reasonable to expect.

Note that it becomes increasingly difficult to get the pin power agreement to fall far below 1%, possibly due to stochastic uncertainty in the reference solution. Therefore, 2 billion particles (row 4) was chosen as the optimum use of the available computing resources. The local pin uncertainty for these results is estimated as 0.3% rod average and up to 1.4% local maximum. Note that this estimate is based on comparison to the 10 billion particle reference solution, which required more than six times the computing resources.

Figure D-1 below compares the fission rate distribution differences between the 2 billion and 10 billion particle cases (rows 4 and 7 in Table D-1). On the left is a radial slice and the right is an axial slice, both through the core center. The locations of largest pin power differences appear very random and range from 1.4 to −1.4%. This should be kept in mind when comparing the other codes (Shift and MPACT) to the KENO-VI results, as further reduction of these statistical errors is impractical for all 15 cases.

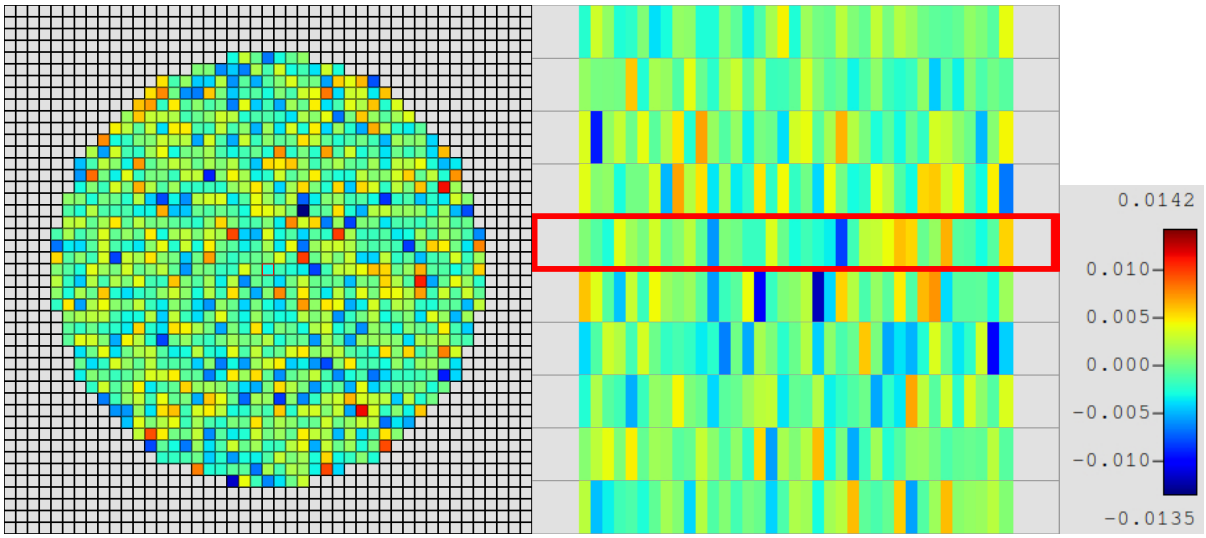

Figure D-1: Sample local pin fractional uncertainty in KENO-VI results.

For the Shift fission rate distribution, calculated with VERA 4.2, the maximum calculated fractional uncertainty for the initial eigenvalue cases with 1 billion active particle history cases was 0.061%. This is approximately 1/10 of the uncertainty reported by KENO-VI for the same number of particle histories. Another series of test cases based on Case 1 of the 7uPCX experiment were executed with Shift with increasing particle histories to assess the actual uncertainty in the stochastic results. Shift is much more parallel than KENO-VI and was executed on INL's Sawtooth, so more particles can be used compared to the KENO-VI results. However, an optimum number of particle histories still needed to be determined for Shift.

Table D-2 provides the Shift results and runtimes for three cases with increasing particle histories. The last case with 100 billion particle histories required nearly 18,000 core hours and is therefore the best reference solution for the other cases, even though it has its own uncertainty that cannot be precisely quantified. Based on the calculated uncertainty, local pin power errors of up to 0.3% may still be possible in the reference solution, with an average error of slightly less than 0.1%.

It is noted that a 1 trillion particle case was attempted with Shift but was unsuccessful, due to very large memory requirements. This is still being investigated.

Table D-2: Shift Particle History Results

Particles per Gen	Active Gens	Total Active Particles	k-eff	k-eff Sigma	Max Calc % Unc	k-eff Diff (pcm)	Pin Powers RMS Diff	Pin Powers Max Diff	Procs	Runtime (hours)	cpu-hours
5E5	2E3	1E9	0.998176	4.2E-5	0.061%	−8	0.29%	1.18%	480	0.4	190
5E6	**2E3**	**1E10**	**0.998255**	**1.3E-5**	**0.034%**	**0**	**0.10%**	**−0.57%**	**960**	**1.9**	**1812**
5E7	2E3	1E11	0.998255	4.1E-6	0.019%	ref	ref	ref	3840	4.6	17743

The maximum calculated percent statistical uncertainty is shown in the sixth column of Table D-2. Note that this value is approximately 20 times smaller than the calculated maximum differences in the ninth column, which is based on power distribution comparison to the largest case as a reference. For a normal distribution, the likelihood of a value occurring with a 20σ deviation is minuscule, and therefore the calculated uncertainty from Shift appears to be too low.

For the results in this analysis, the 10 billion particle case (row 2) was chosen as the optimum use of the available computing resources. The local pin uncertainty for these results is estimated as 0.1% on average and up to 0.6% local maximum. Note this estimate is based on comparison to the 100 billion particle reference solution, which required about ten times the computing resources.

Figure D-2 below compares the fission rate distribution differences between the 10 billion and 100 billion particle cases (rows 2 and 3 in Table D-2). On the left is a radial slice and the right is an axial slice, both through the core center. It is clear that the locations of largest pin power differences appear very random and range from 1.4 to -1.4%. This should be kept in mind when comparing the other codes (KENO-VI and MPACT) to the Shift results, as further reduction of these statistical errors is increasingly difficult for all 15 cases.

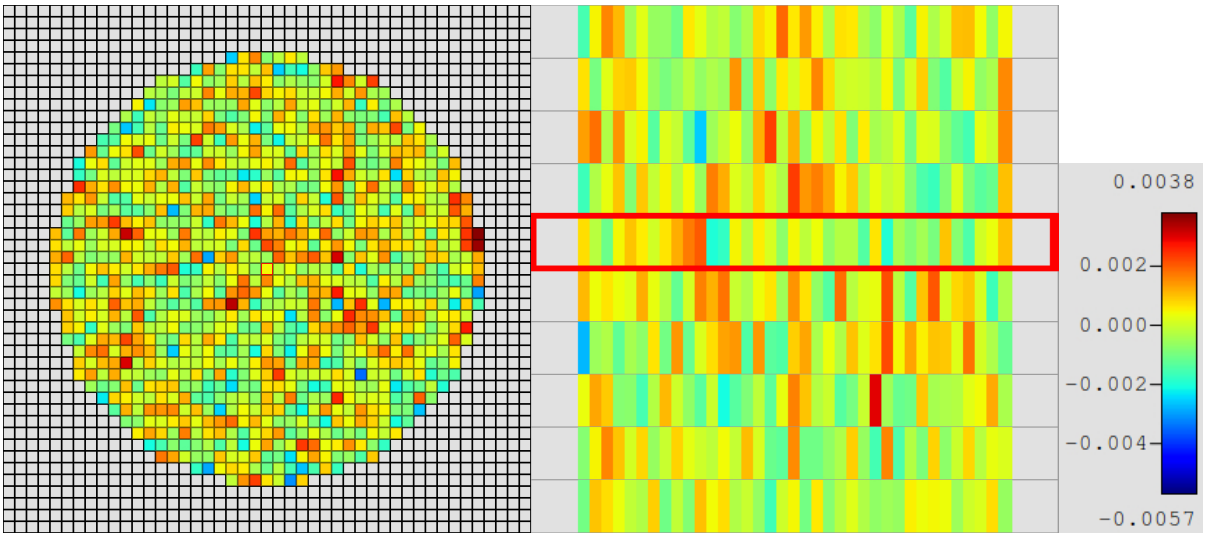

Figure D-2: Sample local pin fractional uncertainty in Shift results.

APPENDIX E. Sample VERA Input for Case 1

APPENDIX E. SAMPLE VERA INPUT FOR CASE 1

```
[CASEID]
 title 'Critical Experiment LEU-COMP-THERM-078 - Case 1'

[STATE]
 power 0.0
 flow 0.0
 tinlet 25 C
 tfuel 25 C
 modden 0.99705
 boron 0.0

 sym  full
 feedback off
 thexp off
 edit pin_flux_2g

[CORE]
 name LCT078
 size 3           ! assemblies across core - modeled as 3x3
 apitch 12.82446  ! 15 x pin pitch
 rated 0.01 0.01  ! MW, Mlbs/hr - dummy
 height 70.8152
 bc_sym mir

 core_shape
 1 1 1
 1 1 1
 1 1 1

 assm_map
 1 2 3
 4 5 6
 7 8 9

 vessel  mod 46.8376    ! tank IR (cm)
         al6061 47.4726 ! tank OR (cm)
         air 99         ! sufficiently large

 lower_ref mod 16.51 1.0 ! solid water beneath the lower grid

 mat al3003 0.0 Al-27 5.9668E-02 ! den=2.73
                Si-00 1.7561E-04
                Fe-00 1.0303E-04
                Mn-55 3.7407E-04
                Cu-63 2.23624E-05 ! Cu 3.2339E-05
                Cu-65 9.97658E-06
              ! Zn-00 1.2571E-05

 mat al6061 0.0 Al-27 5.8376E-02 ! den=2.70
                Si-00 4.1683E-04
                Fe-00 1.8051E-04
                Mn-55 2.6637E-05
                Mg-00 6.9574E-04
                Cr-00 6.2542E-05
                Ti-00 6.7918E-06
                V-00  3.1918E-06
                Cu-63 5.48498E-05 ! Cu 7.9320E-05
                Cu-65 2.44702E-05
              ! Zn-00 2.9839E-05

 mat poly 0.0   h-6  8.2755E-02 ! (H-1CH2)
                c-00 4.1377E-02 !
```

```
 mat ss304 0.0 Fe-00 1.2527E-02 ! 0.1923 g
               Cr-00 3.6455E-03
               Ni-00 1.5724E-03
               Mn-55 1.8160E-04
               C-00  3.3225E-05
               P-31  7.2471E-06
               S-00  4.6663E-06
               Si-00 1.7761E-04
               N-14  3.5613E-05

 mat he 0.17860E-03 he-4 1.0 ! SCALE 6.2

 mat air 1.189E-03 n-14 0.7649
                   o-16 0.2351

 mat xmod 0.0 1001 6.6676E-02 ! moderator for empty locations in the
              8016 3.3338E-02 ! upper grid plate so it doesn't smear it

[ASSEMBLY]
 npin 15
 ppitch 0.854964

 fuel uo2 0.0 0.0 / 0.0 U-234  6.5539E-06
                        U-236  1.4632E-05
                        U-238  2.1296E-02
                        O-1    4.5837E-02
                        B-00   2.3858E-07
                        Cd-00  1.2380E-08
                        Co-59  2.1620E-08
                        Cr-00  2.5100E-06
                        Fe-00  1.0311E-05
                        Mn-55  2.8372E-07
                        Mo-00  1.2443E-07
                        Ni-00  3.4989E-06
                        V-00   1.4813E-08
                        W-00   3.5998E-09
                        Ag-107 4.78572E-09 ! Ag 9.2319E-09
                        Ag-109 4.44617E-09
                        Cu-63  1.47400E-07 ! Cu 2.1316E-07
                        Cu-65  6.57599E-08

 cell F        0.262814 0.284519 0.317474 /      uo2 he al3003  ! fuel rod
 cell S 0.17526 0.22860 0.284519 0.317474 / he ss304 he al3003  ! ss spring
 cell A                          0.3192995 /             al6061  ! aluminum rods
 cell X                           0.317474 /               mod   ! no rod
 cell Y         0.26289 0.284519 0.317474 /     poly he al3003  ! polyethylene spacer

! each of the grid plate cells are designed to put homogenized grid spacer
! around in order to make the plate 'solid'

 cell M                            0.333375 /                 xmod ! no rod in up/lo grid plate
 cell Z 0.26289 0.284519 0.317474 0.333375 / al6061 he al3003 xmod ! aluminum spacer within upper
                                                                     grid plate
 cell E     0.317474 0.333375 /    al3003 xmod ! lower end cap within lower grid plate
 cell B    0.3192995 0.333375 /    al6061 xmod ! aluminum rods in lower grid plate
 cell G              0.333375 /         al6061 ! solid lower grid plate

 lattice FUEL1
  X X X X X X X X X X X X X X X  !
  X X X X X X X X X X X X X X X  ! lattices are names/numbered as:
  X X X X X X X X X X X X X X X  !
  X X X X X X X X X X X X X X X  !  1 2 3
  X X X X X X X X X X X X X X X  !  4 5 6
  X X X X X X X X X X X X X X X  !  7 8 9
  X X X X X X X X X X X X X F F
  X X X X X X X X X X X X F F F
  X X X X X X X X X X X F F F F
  X X X X X X X X X F F F F F
  X X X X X X X X F F F F F F
  X X X X X X X F F F F F F F
  X X X X X X F F F F F F F F
```

```
 X X X X X X F F F F F F F F
 X X X X X X F F F F F F F F

lattice FUEL2
 X X X X X X X X X X X X X X
 X X X X X X X X X X X X X X
 X X X X X X X X X X X X X X
 X X X X X X X X X X X X X X
 X X X X F F F F F F X X X X
 X F F F F F F F F F F F F X
 F F F F F F F F F F F F F F
 F F F F F F F F F F F F F F
 F F F F F F F F F F F F F F
 F F F F F F F F F F F F F F
 F F F F F F F F F F F F F F
 F F F F F F F F F F F F F F
 F F F F F F F F F F F F F F
 F F F F F F F F F F F F F F

lattice FUEL3
 X X X X X X X X X X X X X X
 X X X X X X X X X X X X X X
 X X X X X X X X X X X X X X
 X X X X X X X X X X X X X X
 X X X X X X X X X X X X X X
 X X X X X X X X X X X X X X
 F F X X X X X X X X X X X X
 F F F X X X X X X X X X X X
 F F F F X X X X X X X X X X
 F F F F F X X X X X X X X X
 F F F F F F X X X X X X X X
 F F F F F F F X X X X X X X
 F F F F F F F F X X X X X X
 F F F F F F F F F X X X X X
 F F F F F F F F F X X X X X

lattice FUEL4
 X X X X X F F F F F F F F F
 X X X X X F F F F F F F F F
 X X X X X F F F F F F F F F
 X X X X X F F F F F F F F F
 X X X X F F F F F F F F F F
 X X X X F F F F F F F F F F
 X X X X F F F F F F F F F F
 X X X X F F F F F F F F F F
 X X X X F F F F F F F F F F
 X X X X F F F F F F F F F F
 X X X X F F F F F F F F F F
 X X X X X F F F F F F F F F
 X X X X X F F F F F F F F F
 X X X X X F F F F F F F F F
 X X X X X F F F F F F F F F

lattice FUEL5
 F F F F F F F F F F F F F F
 F F F F F F F F F F F F F F
 F F F F F F F F F F F F F F
 F F F F F F F F F F F F F F
 F F F F F F F F F F F F F F
 F F F F F F F F F F F F F F
 F F F F F F F F F F F F F F
 F F F F F F F F F F F F F F
 F F F F F F F F F F F F F F
 F F F F F F F F F F F F F F
 F F F F F F F F F F F F F F
 F F F F F F F F F F F F F F
 F F F F F F F F F F F F F F
 F F F F F F F F F F F F F F
 F F F F F F F F F F F F F F
```

```
lattice FUEL6
 F F F F F F F F X X X X X X
 F F F F F F F F F X X X X X
 F F F F F F F F F X X X X X
 F F F F F F F F F X X X X X
 F F F F F F F F F F X X X X
 F F F F F F F F F F X X X X
 F F F F F F F F F F X X X X
 F F F F F F F F F F X X X X
 F F F F F F F F F F X X X X
 F F F F F F F F F F X X X X
 F F F F F F F F F F X X X X
 F F F F F F F F F F X X X X
 F F F F F F F F F F X X X X
 F F F F F F F F F F X X X X
 F F F F F F F F F F X X X X
 F F F F F F F F F F X X X X

lattice FUEL7
 X X X X X X F F F F F F F F
 X X X X X X F F F F F F F F
 X X X X X X X F F F F F F F
 X X X X X X X X F F F F F F
 X X X X X X X X X F F F F F
 X X X X X X X X X X F F F F
 X X X X X X X X X X X F F F
 X X X X X X X X X X X X F F
 X X X X X X X X X X X X X X
 X X X X X X X X X X X X X X
 X X X X X X X X X X X X X X
 X X X X X X X X X X X X X X
 X X X X X X X X X X X X X X
 X X X X X X X X X X X X X X
 X X X X X X X X X X X X X X

lattice FUEL8
 F F F F F F F F F F F F F F
 F F F F F F F F F F F F F F
 F F F F F F F F F F F F F F
 F F F F F F F F F F F F F F
 F F F F F F F F F F F F F F
 F F F F F F F F F F F F F F
 F F F F F F F F F F F F F F
 F F F F F F F F F F F F F F
 F F F F F F F F F F F F F F
 X F F F F F F F F F F F F X
 X X X X F F F F F F X X X X
 X X X X X X X X X X X X X X
 X X X X X X X X X X X X X X
 X X X X X X X X X X X X X X
 X X X X X X X X X X X X X X

lattice FUEL9
 F F F F F F F F X X X X X X
 F F F F F F F F F X X X X X
 F F F F F F F F X X X X X X
 F F F F F F F F X X X X X X
 F F F F F F F X X X X X X X
 F F F F F F X X X X X X X X
 F F F F F X X X X X X X X X
 F F F F X X X X X X X X X X
 F F F X X X X X X X X X X X
 F F X X X X X X X X X X X X
 X X X X X X X X X X X X X X
 X X X X X X X X X X X X X X
 X X X X X X X X X X X X X X
 X X X X X X X X X X X X X X
 X X X X X X X X X X X X X X

lattice SPRING1
 X X X X X X X X X X X X X X
 X X X X X X X X X X X X X X
```

```
 X X X X X X X X X X X X X X
 X X X X X X X X X X X X X X
 X X X X X X X X X X X X X X
 X X X X X X X X X X X X X X
 X X X X X X X X X X X X S S
 X X X X X X X X X X X S S S
 X X X X X X X X X X S S S S
 X X X X X X X X X S S S S S
 X X X X X X X X S S S S S S
 X X X X X X X S S S S S S S
 X X X X X X X S S S S S S S
 X X X X X X S S S S S S S S
 X X X X X S S S S S S S S S
 X X X X X S S S S S S S S S
```

lattice SPRING2

```
 X X X X X X X X X X X X X X
 X X X X X X X X X X X X X X
 X X X X X X X X X X X X X X
 X X X X X X X X X X X X X X
 X X X X S S S S S S X X X X
 X S S S S S S S S S S S S X
 S S S S S S S S S S S S S S
 S S S S S S S S S S S S S S
 S S S S S S S S S S S S S S
 S S S S S S S S S S S S S S
 S S S S S S S S S S S S S S
 S S S S S S S S S S S S S S
 S S S S S S S S S S S S S S
 S S S S S S S S S S S S S S
```

lattice SPRING3

```
 X X X X X X X X X X X X X X
 X X X X X X X X X X X X X X
 X X X X X X X X X X X X X X
 X X X X X X X X X X X X X X
 X X X X X X X X X X X X X X
 X X X X X X X X X X X X X X
 S S X X X X X X X X X X X X
 S S S X X X X X X X X X X X
 S S S S X X X X X X X X X X
 S S S S S X X X X X X X X X
 S S S S S S X X X X X X X X
 S S S S S S S X X X X X X X
 S S S S S S S S X X X X X X
 S S S S S S S S S X X X X X
 S S S S S S S S S S X X X X
```

lattice SPRING4

```
 X X X X X X S S S S S S S S
 X X X X X S S S S S S S S S
 X X X X X S S S S S S S S S
 X X X X X S S S S S S S S S
 X X X X S S S S S S S S S S
 X X X X S S S S S S S S S S
 X X X X S S S S S S S S S S
 X X X X S S S S S S S S S S
 X X X X S S S S S S S S S S
 X X X X S S S S S S S S S S
 X X X X S S S S S S S S S S
 X X X X X S S S S S S S S S
 X X X X X S S S S S S S S S
 X X X X X S S S S S S S S S
 X X X X X X S S S S S S S S
```

lattice SPRING5

```
 S S S S S S S S S S S S S S
 S S S S S S S S S S S S S S
 S S S S S S S S S S S S S S
 S S S S S S S S S S S S S S
 S S S S S S S S S S S S S S
```

```
 S S S S S S S S S S S S S S
 S S S S S S S S S S S S S S
 S S S S S S S S S S S S S S
 S S S S S S S S S S S S S S
 S S S S S S S S S S S S S S
 S S S S S S S S S S S S S S
 S S S S S S S S S S S S S S
 S S S S S S S S S S S S S S
 S S S S S S S S S S S S S S
 S S S S S S S S S S S S S S

lattice SPRING6
 S S S S S S S S S X X X X X
 S S S S S S S S S S X X X X X
 S S S S S S S S S S X X X X X
 S S S S S S S S S S X X X X X
 S S S S S S S S S S S X X X X
 S S S S S S S S S S S X X X X
 S S S S S S S S S S S X X X X
 S S S S S S S S S S S X X X X
 S S S S S S S S S S S X X X X
 S S S S S S S S S S S X X X X
 S S S S S S S S S S S X X X X
 S S S S S S S S S S X X X X X
 S S S S S S S S S S X X X X X
 S S S S S S S S S S X X X X X

lattice SPRING7
 X X X X X X S S S S S S S S S
 X X X X X X S S S S S S S S S
 X X X X X X X S S S S S S S S
 X X X X X X X X S S S S S S S
 X X X X X X X X X S S S S S S
 X X X X X X X X X X S S S S S
 X X X X X X X X X X X S S S S
 X X X X X X X X X X X X S S S
 X X X X X X X X X X X X X S S
 X X X X X X X X X X X X X X X
 X X X X X X X X X X X X X X X
 X X X X X X X X X X X X X X X
 X X X X X X X X X X X X X X X
 X X X X X X X X X X X X X X X
 X X X X X X X X X X X X X X X

lattice SPRING8
 S S S S S S S S S S S S S S S
 S S S S S S S S S S S S S S S
 S S S S S S S S S S S S S S S
 S S S S S S S S S S S S S S S
 S S S S S S S S S S S S S S S
 S S S S S S S S S S S S S S S
 S S S S S S S S S S S S S S S
 S S S S S S S S S S S S S S S
 S S S S S S S S S S S S S S S
 X S S S S S S S S S S S S S X
 X X X X S S S S S S S X X X X
 X X X X X X X X X X X X X X X
 X X X X X X X X X X X X X X X
 X X X X X X X X X X X X X X X
 X X X X X X X X X X X X X X X

lattice SPRING9
 S S S S S S S S S X X X X X X
 S S S S S S S S S X X X X X X
 S S S S S S S S S X X X X X X
 S S S S S S S S X X X X X X X
 S S S S S S S X X X X X X X X
 S S S S S S X X X X X X X X X
 S S S S S X X X X X X X X X X
 S S S S X X X X X X X X X X X
 S S S X X X X X X X X X X X X
```

```
 S S X X X X X X X X X X X X X
 X X X X X X X X X X X X X X X
 X X X X X X X X X X X X X X X
 X X X X X X X X X X X X X X X
 X X X X X X X X X X X X X X X
 X X X X X X X X X X X X X X X
 X X X X X X X X X X X X X X X

lattice POLY1
 X X X X X X X X X X X X X X X
 X X X X X X X X X X X X X X X
 X X X X X X X X X X X X X X X
 X X X X X X X X X X X X X X X
 X X X X X X X X X X X X X X X
 X X X X X X X X X X X X X X X
 X X X X X X X X X X X X X Y Y
 X X X X X X X X X X X X Y Y Y
 X X X X X X X X X X X Y Y Y Y
 X X X X X X X X X X Y Y Y Y Y
 X X X X X X X X X Y Y Y Y Y Y
 X X X X X X X X Y Y Y Y Y Y Y
 X X X X X X X Y Y Y Y Y Y Y Y
 X X X X X X Y Y Y Y Y Y Y Y Y
 X X X X X Y Y Y Y Y Y Y Y Y Y

lattice POLY2
 X X X X X X X X X X X X X X X
 X X X X X X X X X X X X X X X
 X X X X X X X X X X X X X X X
 X X X X X X X X X X X X X X X
 X X X X Y Y Y Y Y Y Y X X X X
 X Y Y Y Y Y Y Y Y Y Y Y Y Y X
 Y Y Y Y Y Y Y Y Y Y Y Y Y Y Y
 Y Y Y Y Y Y Y Y Y Y Y Y Y Y Y
 Y Y Y Y Y Y Y Y Y Y Y Y Y Y Y
 Y Y Y Y Y Y Y Y Y Y Y Y Y Y Y
 Y Y Y Y Y Y Y Y Y Y Y Y Y Y Y
 Y Y Y Y Y Y Y Y Y Y Y Y Y Y Y
 Y Y Y Y Y Y Y Y Y Y Y Y Y Y Y
 Y Y Y Y Y Y Y Y Y Y Y Y Y Y Y
 Y Y Y Y Y Y Y Y Y Y Y Y Y Y Y

lattice POLY3
 X X X X X X X X X X X X X X X
 X X X X X X X X X X X X X X X
 X X X X X X X X X X X X X X X
 X X X X X X X X X X X X X X X
 X X X X X X X X X X X X X X X
 X X X X X X X X X X X X X X X
 Y Y X X X X X X X X X X X X X
 Y Y Y X X X X X X X X X X X X
 Y Y Y Y X X X X X X X X X X X
 Y Y Y Y Y X X X X X X X X X X
 Y Y Y Y Y Y X X X X X X X X X
 Y Y Y Y Y Y Y X X X X X X X X
 Y Y Y Y Y Y Y Y X X X X X X X
 Y Y Y Y Y Y Y Y Y X X X X X X
 Y Y Y Y Y Y Y Y Y Y X X X X X

lattice POLY4
 X X X X X Y Y Y Y Y Y Y Y Y Y
 X X X X X Y Y Y Y Y Y Y Y Y Y
 X X X X X Y Y Y Y Y Y Y Y Y Y
 X X X X X Y Y Y Y Y Y Y Y Y Y
 X X X X Y Y Y Y Y Y Y Y Y Y Y
 X X X X Y Y Y Y Y Y Y Y Y Y Y
 X X X X Y Y Y Y Y Y Y Y Y Y Y
 X X X X Y Y Y Y Y Y Y Y Y Y Y
 X X X X Y Y Y Y Y Y Y Y Y Y Y
 X X X X Y Y Y Y Y Y Y Y Y Y Y
 X X X X Y Y Y Y Y Y Y Y Y Y Y
```

```
 X X X X X Y Y Y Y Y Y Y Y Y
 X X X X X Y Y Y Y Y Y Y Y Y
 X X X X X Y Y Y Y Y Y Y Y Y
 X X X X X X Y Y Y Y Y Y Y Y

lattice POLY5
 Y Y Y Y Y Y Y Y Y Y Y Y Y Y
 Y Y Y Y Y Y Y Y Y Y Y Y Y Y
 Y Y Y Y Y Y Y Y Y Y Y Y Y Y
 Y Y Y Y Y Y Y Y Y Y Y Y Y Y
 Y Y Y Y Y Y Y Y Y Y Y Y Y Y
 Y Y Y Y Y Y Y Y Y Y Y Y Y Y
 Y Y Y Y Y Y Y Y Y Y Y Y Y Y
 Y Y Y Y Y Y Y Y Y Y Y Y Y Y
 Y Y Y Y Y Y Y Y Y Y Y Y Y Y
 Y Y Y Y Y Y Y Y Y Y Y Y Y Y
 Y Y Y Y Y Y Y Y Y Y Y Y Y Y
 Y Y Y Y Y Y Y Y Y Y Y Y Y Y
 Y Y Y Y Y Y Y Y Y Y Y Y Y Y
 Y Y Y Y Y Y Y Y Y Y Y Y Y Y
 Y Y Y Y Y Y Y Y Y Y Y Y Y Y

lattice POLY6
 Y Y Y Y Y Y Y Y X X X X X X
 Y Y Y Y Y Y Y Y Y X X X X X
 Y Y Y Y Y Y Y Y Y Y X X X X
 Y Y Y Y Y Y Y Y Y Y X X X X
 Y Y Y Y Y Y Y Y Y Y Y X X X
 Y Y Y Y Y Y Y Y Y Y Y X X X
 Y Y Y Y Y Y Y Y Y Y Y X X X
 Y Y Y Y Y Y Y Y Y Y Y X X X
 Y Y Y Y Y Y Y Y Y Y Y X X X
 Y Y Y Y Y Y Y Y Y Y Y X X X
 Y Y Y Y Y Y Y Y Y Y Y X X X
 Y Y Y Y Y Y Y Y Y Y Y X X X
 Y Y Y Y Y Y Y Y Y Y Y X X X
 Y Y Y Y Y Y Y Y Y Y Y X X X
 Y Y Y Y Y Y Y Y Y Y Y X X X

lattice POLY7
 X X X X X X Y Y Y Y Y Y Y Y
 X X X X X X Y Y Y Y Y Y Y Y
 X X X X X X X Y Y Y Y Y Y Y
 X X X X X X X X Y Y Y Y Y Y
 X X X X X X X X X Y Y Y Y Y
 X X X X X X X X X X Y Y Y Y
 X X X X X X X X X X X Y Y Y
 X X X X X X X X X X X X Y Y
 X X X X X X X X X X X X X X
 X X X X X X X X X X X X X X
 X X X X X X X X X X X X X X
 X X X X X X X X X X X X X X
 X X X X X X X X X X X X X X
 X X X X X X X X X X X X X X

lattice POLY8
 Y Y Y Y Y Y Y Y Y Y Y Y Y Y
 Y Y Y Y Y Y Y Y Y Y Y Y Y Y
 Y Y Y Y Y Y Y Y Y Y Y Y Y Y
 Y Y Y Y Y Y Y Y Y Y Y Y Y Y
 Y Y Y Y Y Y Y Y Y Y Y Y Y Y
 Y Y Y Y Y Y Y Y Y Y Y Y Y Y
 Y Y Y Y Y Y Y Y Y Y Y Y Y Y
 Y Y Y Y Y Y Y Y Y Y Y Y Y Y
 Y Y Y Y Y Y Y Y Y Y Y Y Y Y
 X Y Y Y Y Y Y Y Y Y Y Y Y X
 X X X X Y Y Y Y Y Y Y X X X
 X X X X X X X X X X X X X X
 X X X X X X X X X X X X X X
 X X X X X X X X X X X X X X
```

```
 X X X X X X X X X X X X X X

lattice POLY9
 Y Y Y Y Y Y Y Y X X X X X X
 Y Y Y Y Y Y Y Y X X X X X X
 Y Y Y Y Y Y Y X X X X X X X
 Y Y Y Y Y Y X X X X X X X X
 Y Y Y Y Y Y X X X X X X X X
 Y Y Y Y Y X X X X X X X X X
 Y Y Y Y X X X X X X X X X X
 Y Y Y X X X X X X X X X X X
 Y Y X X X X X X X X X X X X
 X X X X X X X X X X X X X X
 X X X X X X X X X X X X X X
 X X X X X X X X X X X X X X
 X X X X X X X X X X X X X X
 X X X X X X X X X X X X X X
 X X X X X X X X X X X X X X

lattice UPGRID1
 M M M M M M M M M M M M M M
 M M M M M M M M M M M M M M
 M M M M M M M M M M M M M M
 M M M M M M M M M M M M M M
 M M M M M M M M M M M M M M
 M M M M M M M M M M M M M M
 M M M M M M M M M M M M Z Z
 M M M M M M M M M M M Z Z Z
 M M M M M M M M M M Z Z Z Z
 M M M M M M M M M Z Z Z Z Z
 M M M M M M M M Z Z Z Z Z Z
 M M M M M M M Z Z Z Z Z Z Z
 M M M M M M Z Z Z Z Z Z Z Z
 M M M M M M Z Z Z Z Z Z Z Z
 M M M M M M Z Z Z Z Z Z Z Z

lattice UPGRID2
 M M M M M M M M M M M M M M
 M M M M M M M M M M M M M M
 M M M M M M M M M M M M M M
 M M M M M M M M M M M M M M
 M M M M Z Z Z Z Z Z M M M M
 M Z Z Z Z Z Z Z Z Z Z Z Z M
 Z Z Z Z Z Z Z Z Z Z Z Z Z Z
 Z Z Z Z Z Z Z Z Z Z Z Z Z Z
 Z Z Z Z Z Z Z Z Z Z Z Z Z Z
 Z Z Z Z Z Z Z Z Z Z Z Z Z Z
 Z Z Z Z Z Z Z Z Z Z Z Z Z Z
 Z Z Z Z Z Z Z Z Z Z Z Z Z Z
 Z Z Z Z Z Z Z Z Z Z Z Z Z Z
 Z Z Z Z Z Z Z Z Z Z Z Z Z Z

lattice UPGRID3
 M M M M M M M M M M M M M M
 M M M M M M M M M M M M M M
 M M M M M M M M M M M M M M
 M M M M M M M M M M M M M M
 M M M M M M M M M M M M M M
 M M M M M M M M M M M M M M
 Z Z M M M M M M M M M M M M
 Z Z Z M M M M M M M M M M M
 Z Z Z Z M M M M M M M M M M
 Z Z Z Z Z M M M M M M M M M
 Z Z Z Z Z Z M M M M M M M M
 Z Z Z Z Z Z Z M M M M M M M
 Z Z Z Z Z Z Z Z M M M M M M
 Z Z Z Z Z Z Z Z Z M M M M M
 Z Z Z Z Z Z Z Z Z M M M M M
```

```
lattice UPGRID4
 M M M M M Z Z Z Z Z Z Z Z Z
 M M M M M Z Z Z Z Z Z Z Z Z
 M M M M M Z Z Z Z Z Z Z Z Z
 M M M M M Z Z Z Z Z Z Z Z Z
 M M M M Z Z Z Z Z Z Z Z Z Z
 M M M M Z Z Z Z Z Z Z Z Z Z
 M M M M Z Z Z Z Z Z Z Z Z Z
 M M M M Z Z Z Z Z Z Z Z Z Z
 M M M M Z Z Z Z Z Z Z Z Z Z
 M M M M Z Z Z Z Z Z Z Z Z Z
 M M M M Z Z Z Z Z Z Z Z Z Z
 M M M M Z Z Z Z Z Z Z Z Z Z
 M M M M M Z Z Z Z Z Z Z Z Z
 M M M M M Z Z Z Z Z Z Z Z Z
 M M M M M Z Z Z Z Z Z Z Z Z
 M M M M M M Z Z Z Z Z Z Z Z

lattice UPGRID5
 Z Z Z Z Z Z Z Z Z Z Z Z Z Z
 Z Z Z Z Z Z Z Z Z Z Z Z Z Z
 Z Z Z Z Z Z Z Z Z Z Z Z Z Z
 Z Z Z Z Z Z Z Z Z Z Z Z Z Z
 Z Z Z Z Z Z Z Z Z Z Z Z Z Z
 Z Z Z Z Z Z Z Z Z Z Z Z Z Z
 Z Z Z Z Z Z Z Z Z Z Z Z Z Z
 Z Z Z Z Z Z Z Z Z Z Z Z Z Z
 Z Z Z Z Z Z Z Z Z Z Z Z Z Z
 Z Z Z Z Z Z Z Z Z Z Z Z Z Z
 Z Z Z Z Z Z Z Z Z Z Z Z Z Z
 Z Z Z Z Z Z Z Z Z Z Z Z Z Z
 Z Z Z Z Z Z Z Z Z Z Z Z Z Z
 Z Z Z Z Z Z Z Z Z Z Z Z Z Z

lattice UPGRID6
 Z Z Z Z Z Z Z Z Z M M M M M M
 Z Z Z Z Z Z Z Z Z Z M M M M M
 Z Z Z Z Z Z Z Z Z Z M M M M M
 Z Z Z Z Z Z Z Z Z Z M M M M M
 Z Z Z Z Z Z Z Z Z Z Z M M M M
 Z Z Z Z Z Z Z Z Z Z Z M M M M
 Z Z Z Z Z Z Z Z Z Z Z M M M M
 Z Z Z Z Z Z Z Z Z Z Z M M M M
 Z Z Z Z Z Z Z Z Z Z Z M M M M
 Z Z Z Z Z Z Z Z Z Z Z M M M M
 Z Z Z Z Z Z Z Z Z Z Z M M M M
 Z Z Z Z Z Z Z Z Z Z Z M M M M
 Z Z Z Z Z Z Z Z Z Z Z M M M M
 Z Z Z Z Z Z Z Z Z Z Z M M M M

lattice UPGRID7
 M M M M M M Z Z Z Z Z Z Z Z Z
 M M M M M M M Z Z Z Z Z Z Z Z
 M M M M M M M M Z Z Z Z Z Z Z
 M M M M M M M M M Z Z Z Z Z Z
 M M M M M M M M M M Z Z Z Z Z
 M M M M M M M M M M M Z Z Z Z
 M M M M M M M M M M M M Z Z Z
 M M M M M M M M M M M M M Z Z
 M M M M M M M M M M M M M M M
 M M M M M M M M M M M M M M M
 M M M M M M M M M M M M M M M
 M M M M M M M M M M M M M M M
 M M M M M M M M M M M M M M M
 M M M M M M M M M M M M M M M

lattice UPGRID8
 Z Z Z Z Z Z Z Z Z Z Z Z Z Z
 Z Z Z Z Z Z Z Z Z Z Z Z Z Z
```

```
 Z Z Z Z Z Z Z Z Z Z Z Z Z Z
 Z Z Z Z Z Z Z Z Z Z Z Z Z Z
 Z Z Z Z Z Z Z Z Z Z Z Z Z Z
 Z Z Z Z Z Z Z Z Z Z Z Z Z Z
 Z Z Z Z Z Z Z Z Z Z Z Z Z Z
 Z Z Z Z Z Z Z Z Z Z Z Z Z Z
 Z Z Z Z Z Z Z Z Z Z Z Z Z Z
 M Z Z Z Z Z Z Z Z Z Z Z Z M
 M M M M Z Z Z Z Z Z Z M M M M
 M M M M M M M M M M M M M M
 M M M M M M M M M M M M M M
 M M M M M M M M M M M M M M
 M M M M M M M M M M M M M M
```

lattice UPGRID9

```
 Z Z Z Z Z Z Z Z Z M M M M M
 Z Z Z Z Z Z Z Z Z M M M M M
 Z Z Z Z Z Z Z Z M M M M M M
 Z Z Z Z Z Z Z M M M M M M M
 Z Z Z Z Z Z M M M M M M M M
 Z Z Z Z Z M M M M M M M M M
 Z Z Z Z M M M M M M M M M M
 Z Z Z M M M M M M M M M M M
 Z Z M M M M M M M M M M M M
 M M M M M M M M M M M M M M
 M M M M M M M M M M M M M M
 M M M M M M M M M M M M M M
 M M M M M M M M M M M M M M
 M M M M M M M M M M M M M M
 M M M M M M M M M M M M M M
```

lattice LOGRID1

```
 M M M M M M M M M M M M M M
 M M M M M M M M M M M M M M
 M M M M M M M M M M M M M M
 M M M M M M M M M M M M M M
 M M M M M M M M M M M M M M
 M M M M M M M M M M M M M M
 M M M M M M M M M M M M E E
 M M M M M M M M M M M E E E
 M M M M M M M M M M E E E E
 M M M M M M M M M M E E E E
 M M M M M M M M M E E E E E
 M M M M M M M M E E E E E E
 M M M M M M M E E E E E E E
 M M M M M M E E E E E E E E
 M M M M M M E E E E E E E E
```

lattice LOGRID2

```
 M M M M M M M M M M M M M M
 M M M M M M M M M M M M M M
 M M M M M M M M M M M M M M
 M M M M M M M M M M M M M M
 M M M M E E E E E E M M M M
 M E E E E E E E E E E E E M
 E E E E E E E E E E E E E E
 E E E E E E E E E E E E E E
 E E E E E E E E E E E E E E
 E E E E E E E E E E E E E E
 E E E E E E E E E E E E E E
 E E E E E E E E E E E E E E
 E E E E E E E E E E E E E E
 E E E E E E E E E E E E E E
```

lattice LOGRID3

```
 M M M M M M M M M M M M M M
 M M M M M M M M M M M M M M
 M M M M M M M M M M M M M M
 M M M M M M M M M M M M M M
 M M M M M M M M M M M M M M
```

```
 M M M M M M M M M M M M M M
 E E M M M M M M M M M M M M
 E E E M M M M M M M M M M M
 E E E E M M M M M M M M M M
 E E E E E M M M M M M M M M
 E E E E E E M M M M M M M M
 E E E E E E E M M M M M M M
 E E E E E E E E M M M M M M
 E E E E E E E E E M M M M M
 E E E E E E E E E E M M M M
 E E E E E E E E E E E M M M

lattice LOGRID4
 M M M M M M E E E E E E E E
 M M M M M E E E E E E E E E
 M M M M M E E E E E E E E E
 M M M M M E E E E E E E E E
 M M M M E E E E E E E E E E
 M M M M E E E E E E E E E E
 M M M M E E E E E E E E E E
 M M M M E E E E E E E E E E
 M M M M E E E E E E E E E E
 M M M M E E E E E E E E E E
 M M M M M E E E E E E E E E
 M M M M M E E E E E E E E E
 M M M M M E E E E E E E E E
 M M M M M M E E E E E E E E

lattice LOGRID5
 E E E E E E E E E E E E E E
 E E E E E E E E E E E E E E
 E E E E E E E E E E E E E E
 E E E E E E E E E E E E E E
 E E E E E E E E E E E E E E
 E E E E E E E E E E E E E E
 E E E E E E E E E E E E E E
 E E E E E E E E E E E E E E
 E E E E E E E E E E E E E E
 E E E E E E E E E E E E E E
 E E E E E E E E E E E E E E
 E E E E E E E E E E E E E E
 E E E E E E E E E E E E E E
 E E E E E E E E E E E E E E

lattice LOGRID6
 E E E E E E E E M M M M M M
 E E E E E E E E E M M M M M
 E E E E E E E E E M M M M M
 E E E E E E E E E M M M M M
 E E E E E E E E E E M M M M
 E E E E E E E E E E M M M M
 E E E E E E E E E E M M M M
 E E E E E E E E E E M M M M
 E E E E E E E E E E M M M M
 E E E E E E E E E E M M M M
 E E E E E E E E E E M M M M
 E E E E E E E E E E M M M M
 E E E E E E E E E E M M M M
 E E E E E E E E E E M M M M

lattice LOGRID7
 M M M M M M E E E E E E E E
 M M M M M M E E E E E E E E
 M M M M M M M E E E E E E E
 M M M M M M M M E E E E E E
 M M M M M M M M M E E E E E
 M M M M M M M M M M E E E E
 M M M M M M M M M M M E E E
```

```
 M M M M M M M M M M M M E E
 M M M M M M M M M M M M M M
 M M M M M M M M M M M M M M
 M M M M M M M M M M M M M M
 M M M M M M M M M M M M M M
 M M M M M M M M M M M M M M
 M M M M M M M M M M M M M M

lattice LOGRID8
 E E E E E E E E E E E E E E
 E E E E E E E E E E E E E E
 E E E E E E E E E E E E E E
 E E E E E E E E E E E E E E
 E E E E E E E E E E E E E E
 E E E E E E E E E E E E E E
 E E E E E E E E E E E E E E
 E E E E E E E E E E E E E E
 E E E E E E E E E E E E E E
 M E E E E E E E E E E E E M
 M M M M E E E E E E M M M M
 M M M M M M M M M M M M M M
 M M M M M M M M M M M M M M
 M M M M M M M M M M M M M M
 M M M M M M M M M M M M M M

lattice LOGRID9
 E E E E E E E E M M M M M M
 E E E E E E E E M M M M M M
 E E E E E E E E M M M M M M
 E E E E E E E M M M M M M M
 E E E E E E M M M M M M M M
 E E E E E M M M M M M M M M
 E E E E M M M M M M M M M M
 E E E M M M M M M M M M M M
 E E M M M M M M M M M M M M
 M M M M M M M M M M M M M M
 M M M M M M M M M M M M M M
 M M M M M M M M M M M M M M
 M M M M M M M M M M M M M M
 M M M M M M M M M M M M M M
 M M M M M M M M M M M M M M

lattice PGRID
  225*G

axial 1 0.0 PGRID 1.27 LOGRID1 2.54 FUEL1 51.32 SPRING1 53.0352 UPGRID1 55.5752 POLY1 70.8152
axial 2 0.0 PGRID 1.27 LOGRID2 2.54 FUEL2 51.32 SPRING2 53.0352 UPGRID2 55.5752 POLY2 70.8152
axial 3 0.0 PGRID 1.27 LOGRID3 2.54 FUEL3 51.32 SPRING3 53.0352 UPGRID3 55.5752 POLY3 70.8152
axial 4 0.0 PGRID 1.27 LOGRID4 2.54 FUEL4 51.32 SPRING4 53.0352 UPGRID4 55.5752 POLY4 70.8152
axial 5 0.0 PGRID 1.27 LOGRID5 2.54 FUEL5 51.32 SPRING5 53.0352 UPGRID5 55.5752 POLY5 70.8152
axial 6 0.0 PGRID 1.27 LOGRID6 2.54 FUEL6 51.32 SPRING6 53.0352 UPGRID6 55.5752 POLY6 70.8152
axial 7 0.0 PGRID 1.27 LOGRID7 2.54 FUEL7 51.32 SPRING7 53.0352 UPGRID7 55.5752 POLY7 70.8152
axial 8 0.0 PGRID 1.27 LOGRID8 2.54 FUEL8 51.32 SPRING8 53.0352 UPGRID8 55.5752 POLY8 70.8152
axial 9 0.0 PGRID 1.27 LOGRID9 2.54 FUEL9 51.32 SPRING9 53.0352 UPGRID9 55.5752 POLY9 70.8152

grid XXX al6061 2.54 588.4323 ! (ppitch^2-pi/4*0.66675^2)*2.54*15*15*2.6967
grid_axial
    XXX 1.27
    XXX 54.3052

[EDITS]
  axial_edit_bounds
    2.54
    7.418
   12.296
   17.174
   22.052
   26.93
   31.808
   36.686
   41.564
```

```
   46.442
   51.32

[MPACT]
 nodal_method p3    ! help convergence
 nodal_group_loop 20
 nodal_group_start 1
 nodal_inners 20
 nodal_inner_tol 1e-5
 nodal_group_tol 1e-5
 nodal_relax_negative true

 mesh cell_A 2 / 2*8 8  ! set number of radial meshes for each non-fuel rod type
 mesh cell_X 2 / 2*8 8
 mesh cell_S 2 1 1 1 / 2*8 8 8 8 8
 mesh cell_Y 2 1 1 / 2*8 8 8 8
 mesh cell_M 2 / 2*8 8
 mesh cell_Z 2 1 1 1 / 2*8 8 8 8 8
 mesh cell_E 2 1 / 2*8 8 8
 mesh cell_G 2 / 2*8 8
 mesh cell_G 2 1 / 2*8 8 8

 refl_assembly_layers 1
 grid_treatment homogenize
 num_space 162
 meshing_method useraxialmesh
 axial_mesh
  8.26
  8.25
  1.27
  1.27
  4.878
  4.878
  4.878
  4.878
  4.878
  4.878
  4.878
  4.878
  4.878
  4.878
  1.7152
  2.54
  7.62
  7.62

[SHIFT]
 num_cycles 2500
 num_inactive_cycles 500
 Np 5000000
 problem_mode eigenvalue
 broaden_xs true
 dbrc false
 global_log diagnostic

[RUN]
 walltime 0.5
```

Because Shift uses the CE SCALE library, the isotopic names available on the Shift data library are slightly different than those on the MPACT 51-group library, and many of the elements are not available and must be input as individual isotopes. The material inputs used for Shift for both fuel and non-fuel are also provided below.

```
[CORE]
 mat al3003 0.0 cu-63  2.23624E-05 ! 29063 ! den=2.73
                cu-65  9.97658E-06 ! 29065
                fe-54  6.02210E-06 ! 26054
                fe-56  9.45341E-05 ! 26056
                fe-57  2.18321E-06 ! 26057
```

```
               fe-58  2.90545E-07 ! 26058
               mn-55  3.74070E-04 ! 25055
               al-27  5.96680E-02 ! 13027
               si-28  1.61953E-04 ! 14028
               si-29  8.22733E-06 ! 14029
               si-30  5.42986E-06 ! 14030
               zn-nat 1.25710E-05 ! 30000

mat al6061 0.0 cr-50  2.71745E-06 ! 24050 ! den=2.70
               cr-52  5.24033E-05 ! 24052
               cr-53  5.94212E-06 ! 24053
               cr-54  1.47912E-06 ! 24054
               cu-63  5.48498E-05 ! 29063
               cu-65  2.44702E-05 ! 29065
               fe-54  1.05508E-05 ! 26054
               fe-56  1.65625E-04 ! 26056
               fe-57  3.82501E-06 ! 26057
               fe-58  5.09038E-07 ! 26058
               mn-55  2.66370E-05 ! 25055
               v-nat  3.19180E-06 ! 23000
               al-27  5.83760E-02 ! 13027
               si-28  3.84413E-04 ! 14028
               si-29  1.95285E-05 ! 14029
               si-30  1.28884E-05 ! 14030
               zn-nat 2.98390E-05 ! 30000
               mg-24  5.49565E-04 ! 12024
               mg-25  6.95740E-05 ! 12025
               mg-26  7.66010E-05 ! 12026
               ti-46  5.60323E-07 ! 22046
               ti-47  5.05310E-07 ! 22047
               ti-48  5.00691E-06 ! 22048
               ti-49  3.67436E-07 ! 22049
               ti-50  3.51815E-07 ! 22050

mat poly 0.0  h-1   8.27550E-02 ! 1901 ! den=0.96373 h_ch2
              c-nat 4.13770E-02 ! 6000

mat ss304 0.0 cr-50 1.58397E-04 ! 24050 ! den=1.6566
              cr-52 3.05453E-03 ! 24052
              cr-53 3.46359E-04 ! 24053
              cr-54 8.62161E-05 ! 24054
              fe-54 7.32203E-04 ! 26054
              fe-56 1.14940E-02 ! 26056
              fe-57 2.65447E-04 ! 26057
              fe-58 3.53261E-05 ! 26058
              mn-55 1.81600E-04 ! 25055
              ni-58 1.07044E-03 ! 28058
              ni-60 4.12332E-04 ! 28060
              ni-61 1.79238E-05 ! 28061
              ni-62 5.71489E-05 ! 28062
              ni-64 1.45541E-05 ! 28064
              si-28 1.63797E-04 ! 14028
              si-29 8.32103E-06 ! 14029
              si-30 5.49170E-06 ! 14030
              c-nat 3.32250E-05 ! 6000
              p-31  7.24710E-06 ! 15031
              s-32  4.43252E-06 ! 16032
              s-33  3.49972E-08 ! 16033
              s-34  1.98318E-07 ! 16034
              s-36  4.66630E-10 ! 16036
              n-14  3.56130E-05 ! 7014

mat he 0.17860E-03 he-4 1.0 ! SCALE 6.2

mat air 1.189E-03 n-14 0.7649
                  o-16 0.2351

mat xmod 0.0 h-1  6.667613488295485E-02
             o-16 3.333806744147742E-02
```

```
[ASSEMBLY]
 fuel uo2 0.0 0.0 / 0.0 u-234  6.55390E-06 ! 92234 ! den=10.270
                        u-235  1.60100E-03 ! 92235
                        u-236  1.46320E-05 ! 92236
                        u-238  2.12960E-02 ! 92238
                        o-16   4.58370E-02 ! 8016
                        ag-107 4.78572E-09 ! 47107
                        ag-109 4.44617E-09 ! 47109
                        b-10   4.74774E-08 ! 5010
                        b-11   1.91103E-07 ! 5011
                        cd-106 1.54750E-10 ! 48106
                        cd-108 1.10182E-10 ! 48108
                        cd-110 1.54626E-09 ! 48110
                        cd-111 1.58464E-09 ! 48111
                        cd-112 2.98729E-09 ! 48112
                        cd-113 1.51284E-09 ! 48113
                        cd-114 3.55677E-09 ! 48114
                        cd-116 9.27262E-10 ! 48116
                        co-59  2.16200E-08 ! 27059
                        cr-50  1.09059E-07 ! 24050
                        cr-52  2.10310E-06 ! 24052
                        cr-53  2.38475E-07 ! 24053
                        cr-54  5.93615E-08 ! 24054
                        cu-63  1.47400E-07 ! 29063
                        cu-65  6.57599E-08 ! 29065
                        fe-54  6.02678E-07 ! 26054
                        fe-56  9.46075E-06 ! 26056
                        fe-57  2.18490E-07 ! 26057
                        fe-58  2.90770E-08 ! 26058
                        mn-55  2.83720E-07 ! 25055
                        mo-92  1.83783E-08 ! 42092
                        mo-94  1.14849E-08 ! 42094
                        mo-95  1.97844E-08 ! 42095
                        mo-96  2.07549E-08 ! 42096
                        mo-97  1.18955E-08 ! 42097
                        mo-98  3.00996E-08 ! 42098
                        mo-100 1.20324E-08 ! 42100
                        ni-58  2.38194E-06 ! 28058
                        ni-60  9.17520E-07 ! 28060
                        ni-61  3.98840E-08 ! 28061
                        ni-62  1.27168E-07 ! 28062
                        ni-64  3.23858E-08 ! 28064
                        v-nat  1.48130E-08 ! 23000
                        w-180  4.31976e-12 ! 74180
                        w-182  9.53947E-10 ! 74182
                        w-183  5.15131E-10 ! 74183
                        w-184  1.10298E-09 ! 74184
                        w-186  1.02342E-09 ! 74186
```

Note that natural zinc is not available on the MPACT 51-group cross section library.